2018-01-01

A Mixed Finite Element Method for the Coupling of Linear Elasticity and Stokes Flow

Maranda Bean
University of Texas at El Paso, maranda.bean@gmail.com

A MIXED FINITE ELEMENT METHOD FOR THE COUPLING OF LINEAR ELASTICITY AND STOKES FLOW

MARANDA LEE BEAN

Doctoral Program in Computational Science

APPROVED:

Son-Young Yi, Ph.D., Chair

Konstantin Lipnikov, Ph.D.

Natasha Sharma, Ph.D.

Vinod Kumar, Ph.D.

Charles H. Ambler, Ph.D.
Dean of the Graduate School

A MIXED FINITE ELEMENT METHOD FOR THE COUPLING OF LINEAR ELASTICITY AND STOKES FLOW

by

MARANDA LEE BEAN, B.S., M.S.

DISSERTATION

Presented to the Faculty of the Graduate School of

The University of Texas at El Paso

in Partial Fulfillment

of the Requirements

for the Degree of

DOCTOR OF PHILOSOPHY

Computational Science Program

THE UNIVERSITY OF TEXAS AT EL PASO

December 2018

Acknowledgements

My deepest thanks go out to my advisor, Dr. Son-Young Yi of the Department of Mathematics at UTEP. Her willingness to answer and re-answer my questions and her enthusiasm for research are a constant source of inspiration. I am very fortunate that she to provided patient guidance.

I'd also like to thank Dr. Konstantin Lipnikov, Dr. Natasha Sharma, and Dr. Vinod Kumar for finding the time be on my committee and provide so many helpful comments. They have all help me immensely and improved this work greatly.

Additionally, I'd like to express my gratitude to all of the faculty at UTEP who have taught me things I needed to know to complete this project and to the staff at UTEP. I deeply appreciate your dedication.

I'd like to acknowledge the Texas Advanced Computing Center (TACC) at The University of Texas at Austin for providing HPC resources that have contributed to the research results reported within this dissertation. URL: http://www.tacc.utexas.edu

Finally, I need to thank my family for supporting me, putting up with me and pushing me. Without their constant support this task would have been insurmountable.

Abstract

The complex interaction between fluids and structures require the coupling the laws concerning structure mechanics and fluid dynamics and are of vital importance to many scientific and engineering fields. We propose a method for modeling the coupling of a linearly elastic solid and slow fluid flow modeled by Stokes equations. The model equations are expressed in terms of displacement, velocity and stress. With these primary variables, we use a single mixed finite element space based on the Hellinger-Reissner variational principle for linear elasticity to discretize the resulting system spatially. This results in more accurate approximations for stress than those obtained by using standard finite element methods followed by post processing and simple imposition of the interface conditions. Although the solid and fluid subproblems using this mixed form have been studied separately, to our knowledge, a fluid-structure interaction (FSI) problem has not been studied using these models.

In this dissertation, we first discuss the linear elasticity and fluid flow models separately. This includes an improvement to the proved convergence rate of a nonconforming mixed finite element method originally discovered by Arnold and Winther [MATHEMATICAL MODELS & METHODS IN APPLIED SCIENCES,**13** ,3, March 2003] for the steady state problem with certain boundary conditions. Also a description of the special attention required to obtain approximations to the initial conditions for the fluid model is required to make use of a second order in time discretization.

A fully discrete implicit in time model is presented for the complete FSI problem. A priori error estimates are derived for all primary variables. These error estimate show a unfavorable effect caused by the presence of an interface. However, this effect may be not be noticeable when compared with the approximation properties of the mixed finite element space chosen for spatial discretization of the problem. Numerical results using conforming and nonconforming finite element spaces are provided for the interaction problem.

Table of Contents

List of Tables

List of Figures

Chapter 1

Introduction

Considering the interaction between a fluid and a deformable solid is crucial in many engineering applications and scientific fields. These so called fluid-structure interaction (FSI) problems require the coupling of laws concerning structure mechanics and fluid dynamics. Therefore these problems are often complex.

The specific solids and fluids considered can vary greatly by application. For example, in civil engineering, the solids considered may include bridges or high-rise buildings, while the fluid of interest is wind [60, 97]. In aerodynamics, the study of the movement of air and its interaction with solid objects moving through it, the solids may be parts of aircraft [39, 41] or parachutes [68], while the fluid is the surrounding air. Similarly, the motion of a ship's hull through water is of interest in hydrodynamics [94]. Sedimentation studies the motion of solid particles, such as sand or rocks, as they fall through a fluid, such as water, under their own weight [74, 90]. The interaction between a fluid and solid also has application to the biomechanical engineering field. For example, in [37, 57] the interaction between a viscous fluid, such as blood, and solids such as blood vessels or various parts of the heart are considered and in [14] applications to cerebral hemorrhages are considered.

Neglecting to consider the interaction can lead to unintended consequences. One famous example of this is the collapse of the Tacoma Narrows bridge in 1940 [76]. This failure was due to an interaction with wind that caused resonance in the bridge. Other failures are possible when fluid-structure interactions are not considered. For example, wear on the structure due to the the fluid-structure interaction may cause failures.

Since the interactions between different fluids and structures are often very complex, laboratory experiments may be limited by expense and practicality. Therefore, to study

these interactions, mathematical model equations are written to describe the movement of the solid material and the fluid and the interaction between them as partial differential equations. Analytic solutions to the resulting systems are rarely available. Therefore good computational algorithms are crucial to understanding physical phenomena and improving designs.

The remainder of this introduction begins with a brief explanation of model equations for the fluid and solid to be considered in this dissertation. This is followed by an overview of the current methods used to solve FSI problems. Finally, there is a synopsis of the method studied in this dissertation and an outline of the remaining chapters.

1.1 Fluid-Structure Interaction Model

The FSI model in this dissertation will be described by considering the solid and fluid subdomains first, then including some coupling conditions. Let Ω_f be a fluid domain in $\mathcal{R}^2$ and Ω_s be a solid domain in $\mathcal{R}^2$. The common boundary shared by the solid and fluid subdomains is referred to as the interface, which we denote as Γ. Figure 1.1 shows a simple representation of this domain.

In the solid subdomain, we will be considering an isotropic linearly elastic structure. These linear assumptions are that the material will undergo only small deformations and will not yield or break. The elastodynamic, or time dependent, behavior of these objects will be considered. A detailed description of the physical derivation of the model equations for elasticity is provided in Chapter 2.

For the fluid, we will consider the slow flow of a viscous fluid. This flow is described by the time-dependent Stokes equations. More details about the physical derivation of this model are provided in Chapter 3. Along the interface, we enforce the continuity of velocity and the normal component of stress between the solid and fluid subdomains.

As the interface conditions involve stress, the model equations in both subdomains will be written so that stress is a primary variable. For the elasticity subdomain, the numerical

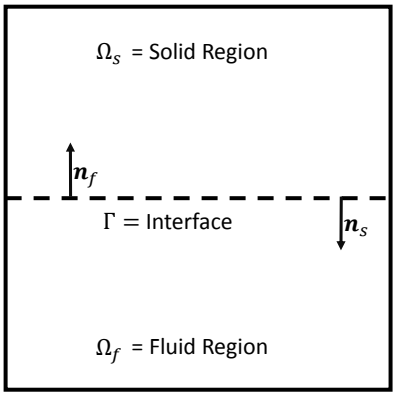

Figure 1.1: Model domain.

method is based on the Hellinger-Reissner principle. For the fluid subdomain, the work of Carstensen et. al [27], which uses the stationary Stokes equations, is extended. The authors note that the Stokes equations are a limit case of the elasticity equations when expressed in a particular way. Therefore, mixed finite element methods (MFEMs) developed for the linear elasticity equations can also be used with the Stokes problem. That is, we can use the same MFEM in the entire domain. Additionally, using a MFEM results in more accurate approximations for stress than would be obtained by using a standard finite element method and post processing.

Below, the mathematical model is expressed while details on how this model is derived from the traditional forms will be withheld until later in Chapters 2 and 3. Consider the system

$$\rho_s \boldsymbol{u}_{tt} - \nabla \cdot \boldsymbol{\sigma}_s = \boldsymbol{f}_s \quad \text{in } \Omega_s, \tag{1.1a}$$

$$\mathcal{A}\boldsymbol{\sigma}_s - \boldsymbol{\epsilon}(\boldsymbol{u}) = 0 \quad \text{in } \Omega_s, \tag{1.1b}$$

$$\rho_f \boldsymbol{v}_t - \nabla \cdot \boldsymbol{\sigma}_f = \boldsymbol{f}_f \quad \text{in } \Omega_f, \tag{1.1c}$$

$$\mathcal{A}_\infty \boldsymbol{\sigma}_f - \boldsymbol{\epsilon}(\boldsymbol{v}) = 0 \quad \text{in } \Omega_f, \tag{1.1d}$$

where $\boldsymbol{u}$ is the solid displacement, $\boldsymbol{v}$ is the fluid velocity, $\boldsymbol{\sigma}_s$ is the solid stress, and $\boldsymbol{\sigma}_f$ is the fluid stress. Here and throughout this work, $\boldsymbol{\epsilon}(\boldsymbol{u}) = \frac{1}{2}\left[\nabla \boldsymbol{u} + (\nabla \boldsymbol{u})^T\right]$, $\mathcal{A}$ is a symmetric fourth order bounded and positive definite elasticity tensor and $\mathcal{A}_\infty$ is the deviatoric stress tensor. The tensors $\mathcal{A}$ and $\mathcal{A}_\infty$ are associated with elasticity and fluid flow and will be explained in greater detail in later chapters. Note that equations (1.1a) and (1.1b) describe the elastic solid and will be discussed in detail in Chapter 2, while equations (1.1c) and (1.1d) describe the fluid flow and will be discussed in Chapter 3.

Along the interface Γ the following no-slip conditions will be imposed

$$\begin{aligned} \boldsymbol{u}_t &= \boldsymbol{v} && \text{on } \Gamma \\ \boldsymbol{\sigma}_s \cdot \boldsymbol{n}_s &= -\boldsymbol{\sigma}_f \cdot \boldsymbol{n}_f && \text{on } \Gamma. \end{aligned}$$

where $\boldsymbol{n}_s$ is a unit vector normal to the interface directed out of the solid domain and similarly $\boldsymbol{n}_f$ is the unit normal vector directed out of the fluid domain. Alternatively, some authors consider slip boundary conditions in which the fluid is allowed to slip over the surface, see for example [11, 70].

1.2 Overview of Numerical Methods for Fluid-Structure Interaction Problems

As analytic solutions to the model equations for complex FSI problems are rarely available, numerical procedures for solving FSI problems have been extensively studied. Overviews of methods available can be found, for example, in [22, 42, 56, 92]. These numerical solutions are often classified in several ways. They are classified based on the solution approach as partitioned or monolithic. This distinction is described in more detail in the following section.

FSI solution procedures may also be classified based on their treatment of meshes as conforming mesh, which may also be called body fitted, or nonconforming mesh, which may also be called not body fitted [56]. In the body fitted mesh case, the interface is considered

to be a physical boundary between the fluid and solid. Therefore the mesh must conform to this boundary and no mesh element will contain both fluid and solid parts. This tracks the motion of the interface and may require remeshing as time advances. However, this method is convenient for partitioned methods discussed below. On the other hand, in thenot body fitted mesh case, the interface location and interface conditions are considered to be constraints to the model equations. In this case, the interface can fall inside an element. This may not require remeshing. However, as these method can be derived from the the theorem of Lagrange multipliers [50, 56], they require the use of Lagrange multiplies. We have restricted our study to the use of body fitted meshes, however an overview of methods that use nonconforming meshes can be found in [56] and the references within.

1.2.1 Classification by Approach

Numerical procedures for FSI problems are divided based on approach into two categories: partitioned or monolithic. Partitioned approaches treat the solid and fluid domains separately. The interface conditions are used to pass information between the subdomains in such cases. For a given time step, these methods will first solve in one subdomain, say for example, the fluid domain. These results will be used along with the interface conditions as a boundary condition on the second domain, in this case the solid domain. Then the time step is advanced and the process is repeated for the next time step. This is referred to as a loosely or one-way coupled approach. In some cases, the approximation from the solid domain may be used to find a new boundary condition for the fluid domain and the process is repeated until some convergence condition is satisfied. Once suitable approximations are found in each subdomain, then the time step is advanced. This is referred to as strongly coupled.

Partitioned methods have the possible advantage of being able to reuse numerical methods and codes designed for only the fluid or solid subdomain. However, as the codes are often developed by different authors with different goals in mind, changes to each code may be required [56]. Furthermore, these methods are generally not stable and may require

extra conditions on the interface.

Many partitioned and stabilized approaches have been studied. Some examples are stated here. In the case of aerodynamics, Farhat et al. [41] develop partitioned algorithms that are proved to be second order accurate. However, in some cases and under certain physical parameters, such as when the density of the fluid and the solid are comparable, convergence issues have been observed, see for example [79]. Explanations of the causes of these instabilities can be found in [30, 44] and are often referred to as added mass effects. Therefore other authors have developed stabilized approaches. In [12], Banks et.al. study a class of FSI problems involving light structures which have suffered from stability issues. The authors alter the traditional partition, where the velocity of the solid is used as a boundary condition for the fluid and the traction from the fluid is used on the solid, by considering added mass predictors on certain variables. Burman and Fernández [23] study a similar class of problems that suffer when the densities of the fluid and solid are similar. The authors stabilized their approach using Nische's method and a time penalty term at the interface. Another method of partitioning the FSI problem is studied by Kurberry and Lee [67], where the authors formulate the problem as a least squares problem. At the interface, the authors find the stress, then minimize the jump between the fluid and structure velocities. Other examples of partitioned methods can be found in the references within these examples.

Monolithic approaches, on the other hand, are designed to obtain an approximation of the entire domain in one step. This type of coupling has been studied, for example, in [57, 95]. These methods impose the interface conditions strongly at each step to avoid instabilities. That is, the equations in the solid and fluid domains are solved simultaneously with the interface conditions. However, these methods often require the solution of large systems which can be computationally expensive, and require specialized codes be written. Some comparisons between partitioned and monolithic approaches can be found in [16, 73]. Both of these deal with one dimensional problems.

Finally, semi-implicit methods, like those studied in [9, 77], attempt to find a balance

between the implicit and explicit methods. Here we will consider a monolithic method as we wish to find a rigorous error estimate.

1.3 Numerical Methods and Error Estimates

In this dissertation, we will use a monolithic approach to find an approximate solution to the model equations (1.1). We will use a method similar to the so called method of lines [49, 82]. For this method we use some MFEM to discretize the entire domain spatially, then use some finite difference time stepping scheme such as the Euler or Crank-Nicholson method, see for example [31], to discretize in time. This procedure is detailed in Chapter 4.

Solving the resulting system requires a pair of finite element spaces which satisfy certain stability conditions for mixed methods [19]. Although there are several known stable spaces for scalar second order elliptic problems, where the unknowns are a scalar and a vector, the extension of these spaces to the vector and tensor pair has been difficult, see for example [19, 45, 71] and the references within. Specifically, the need for both symmetry and continuity conditions in the stress tensor field has presented a significant difficultly in developing stable mixed finite element pairs. In this dissertation we focus only on conforming methods, in which the required continuity conditions are satisfied, and nonconforming methods, in which the conformity requirement is relaxed.

Conforming element spaces have the benefit of satisfying the continuity conditions in the stress tensor field. However, these may involve a large number of degrees of freedom and thus require large matrix systems to be solved. Additionally, when using polynomial shape functions, conforming methods must include vertex degrees of freedom for stress [7]. This implies continuity of stress at the vertices which is not required by the weak formulation, and may not be desirable. On the other hand, nonconforming spaces do not satisfying the continuity conditions in the stress tensor field. These spaces may require fewer degrees of freedom, but must be formed careful to ensure convergence. More information about

existing MFEMs for linear elasticity are discussed in Chapter 2

We also consider the fixed reference domains for the fluid and solid. In [43], the types of situations in which this is a suitable simplification is discussed in the context of hemodynamics. These simplifications are valid for smaller blood vessels particularly when the displacement of the structure is small. Furthermore, many characteristics of flow are captured using this simplification even when larger displacements are considered. In [21], a similar fixed domain assumption is made for a fluid and poroelastic structure interaction problem, where the equations for the solid are modeling a geomechanical structure. The article further claims that although simplified, this simplification is suitable for small displacement and shares many of the difficulties with other fluid-structure interactions problem. Finally in [20], results using a moving mesh are compared to those obtained using a fixed mesh, on a benchmark problem, to assess the impact of the simplification in the small displacement case. The authors observe similar results in both cases.

We find a priori error estimates for this model. Much work has been done analyzing these types of equations. Specifically, in [36], an analytic tool called asymptotic projection is used to obtain results considering a high-order MFEM. Additionally in [72], Makridakis considers rational approximations to cosine to discretize the elastodynamics problem in time. However, we would like to use the method of lines with finite differences to discretize in time. To this end we note that several researchers have studied error estimates for second order hyperbolic equations in conjunction with MFEMs. For example, in [61] Jenkins et al. develop and analyze an explicit-in-time method for wave equations. In [35], Cowsar et al. develop a priori error estimates for a stress-displacement second order hyperbolic equation using both explicit and implicit time stepping.

1.4 Outline

The remainder of this dissertation will be organized as follows. In Chapter 2, details related to the solid subdomain will be discussed. First, there is some information on the derivation

of the linear elasticity equation used. After some notations are introduced, the stationary linear elasticity equations are discussed. Applicable MFEMs are discussed including an improvement to the analysis for a particular MFEM originally proposed by Arnold and Winther [8]. Some numerical results are shown for the elastostatic case. We then discuss the elastodynamic case as an extension of the static case. This includes forming a fully discrete model using the method of lines. Finally, numerical results are provided for the dynamic case.

In Chapter 3, details related to the fluid subdomain will be discussed. First, since we know we wish to express the Stokes flow equations in terms of velocity and stress in a manner similar to the elasticity equations, the model equations are derived as a limit case of the elasticity equations. We also show how the traditional form of these equations is related to the stress-velocity model. Next, a fully discrete model is formed for the nonstationary Stokes equations. This includes a discussion on how the initial conditions are approximated. Finally, some numerical results are provided for our model.

In Chapter 4, the FSI model based on the models for elasticity and fluid flow will be introduced and discussed. The domain and interface conditions are first introduced and described. Then the fully discrete model is formed. Next, an a priori error estimate will be derived for all variables. Finally numerical results are provided.

Chapter 2

Mixed Finite Element Methods for Linear Elasticity

Naturally, the study of the interaction of a fluid and a structure begins with the study of each component separately. In this chapter we focus on the structure. Although the structure in our FSI problem will ultimately be modeled as a time-dependent problem of linear elasticity, which is also referred to as elastodynamic, we begin with a study of the static or steady version of the problem. This is because we seek to use MFEMs and the method of lines [49, 82]. Naturally these are based on existing MFEMs for stationary elasticity problems.

The rest of this chapter will be organized as follows. We begin with a brief derivation of the linear elasticity equations. Then some necessary and useful notation for using finite element methods are introduced. Next the linear elasticity model in the Hellinger-Reissner formulation is used to derive the weak form used. Then, as the method of lines make use of them, some existing MFEMs for the electrostatic problem are described. Particular attention is paid to a pair of elements developed by Arnold and Winter [6, 8] as these elements are used for testing and we provide an improved error analysis for the nonconforming elements. Some numerical results are included to confirm this result. Finally, we describe the extension to an electrodynamics problem and some numerical results are presented.

2.1 Derivation of Linear Elasticity Equations

Elasticity is the mathematical study of how a solid object is stressed and deformed in response to some load, where the solid is modeled as a continuous mass or continua. This subject has been studied in numerous texts such as [13, 34, 66, 80, 84]. Therefore, we describe only some of the basic details here.

In this dissertation, we are considering only isotropic linear elasticity, which is a simplification of the general, nonlinear elasticity. This requires the consideration of the relationship between stress, the distribution of forces, and strain, the response to stress. The linearization assumptions are that the relationship between stress and strain is linear and that only infinitesimal strains are present. This means that we consider only relatively small displacements. Furthermore, the material will return to its original shape when a given load is removed. That is, the material will not yield. These assumptions are valid for engineering materials up to their elastic limit [66]. The isotropic assumption requires that the medium is uniform in all directions. This is generally accepted for the macroscopic behavior of materials because although an individual crystals is not isotropic, there are a large number of crystals randomly orientated in the solid [84].

To obtain the linear elasticity equations, first consider the stress $\boldsymbol{\sigma}$. We note that continuous materials must satisfy a number of basic laws, such as conservation of mass and the principle of momentum. To satisfy conservation of mass, we required that the density of medium does not depend on time. In this case the equation of motion for the linear elastic material is

$$\nabla \cdot \boldsymbol{\sigma} + \boldsymbol{f}_s = \rho_s \boldsymbol{u}_{tt}, \tag{2.1}$$

where $\boldsymbol{f}_s$ is a body force, ρ_s is the density of the solid and $\boldsymbol{u}$ is the displacement vector. This arrived at using Newton's second law, $F = ma$. By the complementary property of shear the stress tensor is symmetric [84].

Next we consider the relationship between the stress, $\boldsymbol{\sigma}$ and the strain $\epsilon(\boldsymbol{u})$. For isotropic materials, normal stresses can only cause normal strains and, similarly, shear stresses can

only cause shear engineering strains. This is due to the fact that for isotropic materials properties are not dependent on directions. Therefore,rotation will not change the stress-strain relationship. A detailed description of this can be found, for example, in [84]. In this case, we consider a linear isotropic material which is governed by Hooke's law. This is written as

$$\boldsymbol{\sigma} = C\epsilon(\boldsymbol{u}), \tag{2.2}$$

where C is the forth order elasticity tensor of constant values. Alternatively, for an isotropic material this generalized Hooke's law can be written as

$$\boldsymbol{\sigma} = 2\mu_s \boldsymbol{\epsilon}(\boldsymbol{u}) + \lambda tr(\boldsymbol{\epsilon}(\boldsymbol{u}))\,\mathbf{I}, \tag{2.3}$$

where μ_s and λ are the Lam*é* parameters of the material and I is the identity matrix. The trace is defined for a tensor $\boldsymbol{\tau} = \begin{bmatrix} \boldsymbol{\tau}_{11} & \boldsymbol{\tau}_{12} \\ \boldsymbol{\tau}_{21} & \boldsymbol{\tau}_{22} \end{bmatrix}$ as

$$tr(\boldsymbol{\tau}) = \boldsymbol{\tau}_{11} + \boldsymbol{\tau}_{22}.$$

Finally the relationship between strain and displacement is given by

$$\boldsymbol{\epsilon}(\boldsymbol{u}) = \frac{1}{2}\left[\nabla \boldsymbol{u} + (\nabla \boldsymbol{u})^T\right] \tag{2.4}$$

for small deformations. Here the normal strains, ϵ_{ii} for $i = 1, 2$, are a measure of the change in length of a line segment to its original length. The shear strains, ϵ_{ij} for $i \neq j$, are a measure or the change in angle between lines originally in the x and y direction as the media is deformed. For a detail description of this relationship see, for example, Section 3.4 of [84].

Often the system of (2.1), (2.3) and (2.4) are expressed together in the displacement formulation, where displacement is the only unknown variable. This is done by substituting (2.3) and (2.4) into (2.1) to find

$$\rho_s \boldsymbol{u}_{tt} - 2\mu_s \nabla \cdot \boldsymbol{\epsilon}(\boldsymbol{u}) - \lambda \nabla \cdot (\nabla \cdot \boldsymbol{u})\,\mathbf{I} = \boldsymbol{f}_s. \tag{2.5}$$

However in this dissertation, we would like stress to be a primary variable in the system of equations. To obtain this formulation, (2.2) is re-written as

$$\mathcal{A}\boldsymbol{\sigma} = \epsilon(\boldsymbol{u}),$$

where

$$\mathcal{A}\boldsymbol{\tau} := \frac{1}{2\mu}\left(\boldsymbol{\tau} - \frac{\lambda}{2(\lambda+\mu_s)} tr(\boldsymbol{\tau})\mathbf{I}\right).$$

Now (2.5) can be written in mixed form as

$$\rho_s \boldsymbol{u}_{tt} - \nabla \cdot \boldsymbol{\sigma} = \boldsymbol{f}_s, \tag{2.6a}$$

$$\mathcal{A}\boldsymbol{\sigma} - \epsilon(\boldsymbol{u}) = 0. \tag{2.6b}$$

2.2 Notations

To obtain a weak formulation for this problem and use an MFEM, some additional notations will be necessary. We will be considering the elasticity problem on a domain $\Omega \subset \mathcal{R}^2$. The boundary $\partial\Omega$ of Ω may be partitioned into $\{\Gamma_D, \Gamma_N\}$ such that $\partial\Omega = \Gamma_D \cup \Gamma_N$ and $\Gamma_D \cap \Gamma_N = \emptyset$.

Here we will define some function spaces and their associated norms that will be used to define a mixed variational formulation. We will make use of the Sobolev spaces, $H^m(D)$, with the associates semi-norm, $|\cdot|_{m,D}$, and norm, $\|\cdot\|_{m,D}$. In the case where $D = \Omega$, the subscript D will be dropped. This space requires a function and all of its partial derivatives of degree m or lower to be square integrable. That is, for $m \geq 1$

$$H^m(D) = \{v \in H^{m-1}(D) : \frac{\partial v}{\partial x}, \frac{\partial v}{\partial y} \in H^{m-1}(D)\}$$

with

$$H^1(D) = \{v \in L^2(D) : \frac{\partial v}{\partial x}, \frac{\partial v}{\partial y} \in L^2(D)\}.$$

In the case where $m = 0$, $H^0(D)$ is exactly $L^2(D)$. In the special case of $m = 0$, the inner product and norm will be denoted by $(\cdot,\cdot)_D$ and $\|\cdot\|_D$ respectively. More specifically, for

any $f, g \in L^2(D)$

$$(f, g)_D = \int_D fg\, dx.$$

For simplicity, when $D = \Omega$, the subscript will be omitted. We will also use the notation

$$< f, g >_d = \int_d fg\, ds,$$

when d is a line or boundary. In the interest of defining a weak formulation, the following Hilbert spaces will be needed. Let

$$\boldsymbol{H}(\mathrm{div}; \Omega) = \{\boldsymbol{\tau} \in (L^2(\Omega))^{2\times 2} : \nabla \cdot \boldsymbol{\tau} \in (L^2(\Omega))^2\}$$

with the associated norm $\|\boldsymbol{\tau}\|_{\boldsymbol{H}(\mathrm{div})} = (\|\boldsymbol{\tau}\|_0^2 + \|\nabla \cdot \boldsymbol{\tau}\|_0^2)^{\frac{1}{2}}$. This is the space of square integrable tensors with square integrable divergences. Next, let the space $\mathbb{S} = \mathbb{R}^{2x2}$ be the space of symmetric tensors. Then

$$\boldsymbol{H}(\mathrm{div}; \Omega; \mathbb{S}) = \{\boldsymbol{\tau} \in \boldsymbol{H}(\mathrm{div}; \Omega) : \boldsymbol{\tau}_{ij} = \boldsymbol{\tau}_{ji}, i \leq i, j \leq 2\}.$$

Let $\boldsymbol{n}$ be an outward facing normal vector to Ω, then

$$\boldsymbol{H}_{0,\Gamma_N}(\mathrm{div}; \Omega; \mathbb{S}) = \{\boldsymbol{\tau} \in \boldsymbol{H}(\mathrm{div}; \Omega; \mathbb{S}) : \boldsymbol{\tau}\boldsymbol{n}|_{\Gamma_N} = 0\}.$$

and

$$\boldsymbol{H}_{\Gamma_N}(\mathrm{div}; \Omega; \mathbb{S}) = \{\boldsymbol{\tau} \in \boldsymbol{H}(\mathrm{div}; \Omega; \mathbb{S}) : \boldsymbol{\tau}\boldsymbol{n}|_{\Gamma_N} = \widetilde{\boldsymbol{\sigma}}_0\}.$$

Additionally, for a normed space P let $\mathcal{C}^k(0, T; P)$ denote the space of k time continuously differentiable maps from $[0, T]$ into P.

2.3 Elastostatics

As stated above, the elastodynamic model will be based on the elastostatic model. Therefore, we discuss the static case first.

2.3.1 Weak Formulation of the Elastostatic Model

In the case where $\boldsymbol{u}_{tt} = 0$ the static form (2.6) is written as

$$-\nabla \cdot \boldsymbol{\sigma} = \boldsymbol{f}_s, \tag{2.7a}$$

$$\mathcal{A}\boldsymbol{\sigma} - \epsilon(\boldsymbol{u}) = 0. \tag{2.7b}$$

A new norm is defined as

$$\|\boldsymbol{\tau}\|^2_{\mathcal{A},\Omega} = \int_\Omega \mathcal{A}\boldsymbol{\tau} : \boldsymbol{\tau} dx.$$

Note that this norm $\|\cdot\|^2_{\mathcal{A},\Omega}$ is equivalent to the L^2-norm [6, 100]

$$C_1\|\boldsymbol{\tau}\|_0^2 \leq \|\boldsymbol{\tau}\|^2_{\mathcal{A},\Omega} \leq C_2\|\boldsymbol{\tau}\|_0^2. \tag{2.8}$$

To complete the system(2.7), the required boundary conditions are

$$\boldsymbol{u} = \boldsymbol{u}_D \quad \text{on } \Gamma_D,$$

$$\boldsymbol{\sigma}\boldsymbol{n} = \boldsymbol{\sigma}_N \quad \text{on } \Gamma_N,$$

where $\boldsymbol{n}$ is the outward unit normal vector.

Let

$$\boldsymbol{\Sigma} = \boldsymbol{H}(\text{div}; \Omega; \mathbb{S}) \quad \text{and} \quad \mathcal{V} = (L^2(\Omega))^2.$$

We also make use the following formula for integration by parts for a symmetric function $\boldsymbol{\tau} \in \boldsymbol{\Sigma}$:

$$(\epsilon(\boldsymbol{u}), \boldsymbol{\tau}) = -(\boldsymbol{u}, \nabla \cdot \boldsymbol{\tau}) + < \boldsymbol{u}, \boldsymbol{\tau} \cdot \boldsymbol{n} >_\Gamma$$

Then the weak form of (2.7) is to find $(\boldsymbol{\sigma}, \boldsymbol{u}) \in (\boldsymbol{\Sigma}, \mathcal{V})$ in

$$-(\nabla \cdot \boldsymbol{\sigma}, \boldsymbol{\nu}) = (\boldsymbol{f}_s, \boldsymbol{\nu}), \qquad \forall \boldsymbol{\nu} \in \mathcal{V}, \tag{2.9a}$$

$$(\mathcal{A}\boldsymbol{\sigma}, \boldsymbol{\tau}) + (\boldsymbol{u}, \nabla \cdot \boldsymbol{\tau}) - < \boldsymbol{u}, \boldsymbol{\tau} \cdot \boldsymbol{n} >_\Gamma = 0, \qquad \forall \boldsymbol{\tau} \in \boldsymbol{\Sigma}. \tag{2.9b}$$

To discretize this weak formulation, we will employ some finite dimensional spaces $\boldsymbol{\Sigma}_h$ and $\mathcal{V}_h$ which are approximations to $\boldsymbol{\Sigma}$ and $\mathcal{V}$ respectively. The pair $\boldsymbol{\Sigma}_h$ and $\mathcal{V}_h$ may not be chosen arbitrarily. Thus, we approximate $(\boldsymbol{\sigma}, \boldsymbol{u}) \in (\boldsymbol{\Sigma}, \mathcal{V})$ with some $(\boldsymbol{\sigma}_h, \boldsymbol{u}_h) \in (\boldsymbol{\Sigma}_h, \mathcal{V}_h)$. Let $\mathcal{T}_h$ be a family of triangulations of Ω into elements T_i, $i = 1, 2, ..., I$ of size $\mathcal{O}(h)$. As the size of the elements, h is reduced these approximations will converge to the true solution with some order which depends on the element spaces chosen. Below we discuss some known mixed finite element space pairs for this formulation.

2.3.2 Overview of Existing Mixed Finite Element Methods for Linear Elasticity

Often, the linear elasticity equation are expressed in terms of displacement only as in (2.5). In the displacement formulation, an approximation to displacement is found, using traditional finite element methods for elliptic equations. Then a numerical approximation for stress can be found by post processing. However, an alternative method is to consider MFEMs in which multiple variables are approximated simultaneously. The basics of these methods are discussed in many books, see for example [71]. In these methods, the governing equations are expressed using several primary variables. Here we consider cases where the displacement vector and the stress tensor become the primary unknowns. This leads to the HellingerReissner [53] variational principle. In exchange for an increase in the number of unknowns and equations in the linear system, these methods offer additional benefits such as delivering numerical solutions for both displacement and stress simultaneously without the need for post processing. Additionally, in the case of elasticity, using a mixed method is a possible remedy for locking, which can cause spurious oscillations when nearly incompressible materials are considered [19].

Solving a the resulting system requires a pair of finite element spaces which satisfy certain stability conditions for mixed methods [19]. Although there are several known stable spaces for scalar second order elliptic problems, where the unknowns are a scalar and a

vector, the extension of these spaces to the vector and tensor pair has been difficult, see for example [19, 45, 71] and the references within. Specifically, the need for both symmetry and continuity conditions in the stress tensor field has presented a significant difficultly in developing stable mixed finite element pairs.

Researchers have attempted to circumvent this problem in several ways. Some have attempted to use the equilibrium method in which composite elements are used [4, 101, 62]. In these models an element is subdivided. In [62], a triangular element contains three subtriangles which are obtained by connecting an interior point to the vertices. This type of construction can make implementation difficult. Another possible method is to only weakly enforce symmetry, see for example [1, 3, 33, 48, 85] and the references within. However these methods modify the Hellinger-Reissner functional so that symmetry of the stress tensor can be only weakly enforced or neglected. Schöberl and Sinwel [83] constructed an element between the concepts of conformity and weak symmetry by proposing elements in which the tangential components for the displacement and the normal-normal component of the stress are continuous. In this paper we focus only on conforming methods, in which the required conditions are satisfied, and nonconforming methods, in which the conformity requirement is relaxed.

Despite the difficulty associated with the symmetry and continuity of the stress tensor, some conforming spaces have been discovered for the HellingerReissner variational principle. In [6] Arnold and Winther construct a family of stable conforming mixed finite element spaces on triangular meshes using polynomial shape functions. However, the lowest order element in this family requires 24 local degrees of freedom for the stress variable and 6 local degrees of freedom for the displacement. These elements have been used in this paper and will be discussed in more detail below. The authors have also provided a slight simplification for the lowest order element requiring 21 and 3 local degrees of freedom for stress and displacement, respectively.

Other conforming finite element space have been constructed on rectangular grids. In [2], Arnold and Awanou extend the above mentioned family of mixed finite elements to

rectangular meshes. The lowest order element in this family requires 45 and 12 local degrees of freedom for stress and displacement respectively. Another conforming family was constructed by Chen and Wang [32]. The lowest order element in this family requires 17 local degrees for freedom for stress and 4 local degrees for freedom for displacement.

In [7], it is noted that when using polynomial shape functions, conforming methods must include vertex degrees of freedom for stress and thus imply continuity of stress at the vertices. This continuity at the vertices is not required by the weak formulation, and may not be desirable. Therefore, Arnold and Winther [8] have developed a nonconforming MFEM analogous to the aforementioned lowest order conforming element. For these elements, the vertex degrees of freedom are removed and the required continuity of the normal component of stress is not imposed strongly. However, it is shown [8], that the weak continuity that is imposed is sufficient to form a convergent MFEM. This element requires 15 and 6 degrees of freedom for stress and displacement respectively. The authors obtain a convergence rate of $O(h)$ for both displacement and stress. They are also able to obtain a simplified element, as in the conforming case. Another nonconforming element on triangular grids is proposed by Cai and Ye [25] in which an additional jump term is added to the constitutive equation to weakly enforce continuity. This makes use of a previously developed stable and economic, but not convergent, element. Additionally in [47] Guzman and Gopalakrishnan construct a family of nonconforming elements which has the simplified element of [8] as its lowest order element.

Nonconforming spaces on rectangular meshes have also been designed. In [98], Yi develops a nonconforming element using the same unisolvent set of degrees of freedom as used by the nonconforming Arnold-Winther element, however the author obtains second order convergence rate in the L^2 norm for displacement. This element requires 19 and 6 local degrees of freedom for stress and displacement respectively. Later Yi [99] and Hu and Shi [58] independently construct another element which, in two dimensions, is a subspace of the previous element locally, but has different global construction and requires slightly fewer local degrees of freedom. In [58], Hu and Shi propose an additional element and a

rotated element has been constructed by Awanou [10].

Numerical results obtained using some of these mixed finite element methods are compared in [26]. Specifically, the authors compare some of the MFEMs mentioned above to higher order displacement only FEMs and to other more commonly used method such as the weakly symmetric PEERS [3].

In this dissertation, numerical results will be presented in several sections. To obtain these results, we have used one conforming and one nonconforming MFEM. Specifically, these are the elements developed by Arnold and Winther in [6] and [8]. Details on implementing these elements have been discussed in [28] and [26] respectively. These elements will be discussed in more detail in the following sections.

2.3.3 Arnold-Winther Conforming Mixed Finite Element Spaces for Elasticity

This section describes the conforming Arnold-Winther elements detailed in [6]. For the remainder of this dissertation we will refer to this element as the conforming element as it will be the only conforming element used in our numerical experimentation. Since these elements were developed as mixed finite elements for elasticity, we will describe them in that context in this section. However, these elements will also be used with the Stokes equations for fluid flow later.

These elements were developed for the static linear elasticity model (2.7) with weak formulation (2.9) however, the boundary is considered to be clamped:

$$\boldsymbol{u} = 0 \quad \text{on } \delta\Omega.$$

The MFEM then requires the construction of a pair of finite element spaces $\boldsymbol{\Sigma}_h$ and $\mathcal{V}_h$. The method will find approximations to the stress and displacement, $\boldsymbol{\sigma}_h$ and $\boldsymbol{u}_h$, in these spaces. Furthermore, these spaces must satisfy certain compatibility conditions [18, 19].

We will describe the lowest order element for this family. Let $\mathcal{T}_h$ be a family of triangulations of Ω into elements T_i, $i = 1, 2, ..., I$ of size $\mathcal{O}(h)$. Now, the finite element spaces

are formed by first considering a single triangle T. On T define

$$\begin{aligned}\boldsymbol{\Sigma}_T &= \{\boldsymbol{\tau} \in \mathcal{P}_3(T;\mathbb{S}) \,|\, \nabla\cdot\boldsymbol{\tau} \in \mathcal{P}_1(T;\mathbb{R}^2)\}\\ \mathcal{V}_T &= \mathcal{P}_1(T;\mathbb{R}^2).\end{aligned}$$

The degrees of freedom for $\boldsymbol{\sigma}_T$ on a triangle are then:

- the three values of the components of $\boldsymbol{\tau}(x)$ on the vertices of T(9 total).
- the values of moments of degree 0 and 1 of the normal components $\boldsymbol{\tau n}$ along each edge e of T(12 total).
- the three values of the components of the moment of 0 degree of $\boldsymbol{\tau}$ on T(3 total).

There are 6 degrees of freedom for $\mathcal{V}_T$ for each triangle. The vertex and edge degrees of freedom define $\boldsymbol{\tau n}$ on an edge. So this forms a conforming approximation to $\boldsymbol{H}(\mathrm{div};\Omega;\mathbb{S})$.

For some appropriate triangulation $\mathcal{T}_h$ of Ω, the associated finite element space $\mathcal{V}_h$ becomes the space of all piecewise linear vector fields with respect to this triangulation. Note that this space does not require any inter-element continuity conditions. The space $\boldsymbol{\Sigma}_h$ is the space of all tensor fields belonging piecewise to $\boldsymbol{\sigma}_T$ with the continuity conditions that all three components are continuous at any mesh vertex and the normal components are continuous across mesh edges.

Using these global spaces, the MFEM proposed to discretize (2.7) is to find $(\boldsymbol{\sigma}_h, \boldsymbol{u}_h) \in (\boldsymbol{\Sigma}_h, \mathcal{V}_h)$ such that

$$-(\nabla\cdot\boldsymbol{\sigma}_h, \boldsymbol{\nu}) = (\boldsymbol{f}_s, \boldsymbol{\nu}), \quad \boldsymbol{\nu} \in \mathcal{V}_h, \tag{2.10a}$$

$$(\mathcal{A}\boldsymbol{\sigma}_h, \boldsymbol{\tau}) + (\boldsymbol{u}_h, \nabla\cdot\boldsymbol{\tau}) = 0, \qquad \boldsymbol{\tau} \in \boldsymbol{\Sigma}_h. \tag{2.10b}$$

Furthermore, the authors show second and third order convergence rates

$$\begin{aligned}\|\boldsymbol{\sigma} - \boldsymbol{\sigma}_h\|_0 &\le Ch^m\|\boldsymbol{\sigma}\|_m, && 1 \le m \le 3,\\ \|\nabla\cdot\boldsymbol{\sigma} - \nabla\cdot\boldsymbol{\sigma}_h\|_0 &\le Ch^m\|\nabla\cdot\boldsymbol{\sigma}\|_m, && 0 \le m \le 2,\\ \|\boldsymbol{u} - \boldsymbol{u}_h\|_0 &\le Ch^m\|\boldsymbol{u}\|_{m+1}, && 1 \le m \le 2.\end{aligned}$$

However, it is also noted that the vertex degrees of freedom, which lead to continuity at the vertices, are unavoidable for a conforming method with polynomial shape functions [7]. This continuity is not required by the weak formulation and may lead to undesirable results and complications in implementation. Despite these complications, a detailed description on implementation can be found in [28] and the open source Finite Element Framework code [24] ($\mathrm{F_FW}$) written for MATLAB provides a working implementation for the elastostatic problem.

2.3.4 Arnold-Winther Nonconforming Mixed Finite Element Spaces for Elasticity

Due to the undesirable continuity of $\boldsymbol{\sigma}$ of the conforming element we also consider the nonconforming Arnold-Winther [8] mixed finite element space. For the remainder of this dissertation, we will refer to this as the nonconforming element as it will be the only nonconforming element used in our numerical experimentation. For a family of shape regular triangulations $\mathcal{T}_h$ of the domain Ω, on a single triangle T, define

$$\begin{aligned}\boldsymbol{\Sigma}_T &= \{\boldsymbol{\tau} \in \mathcal{P}_2(T, \mathbb{S}) \,|\, \boldsymbol{n} \cdot \boldsymbol{\tau}\boldsymbol{n} \in \mathcal{P}_1(e), \text{ for each edge } e \text{ of T}\},\\ \mathcal{V}_T &= \mathcal{P}_1(T, \mathbb{R}^2).\end{aligned}$$

For this element the degrees of freedom are similar to the conforming case without those at the vertices. Specifically, for Σ_T the degrees of freedom are then:

- the values of moments of degree 0 and 1 of the normal components $\boldsymbol{\tau}\boldsymbol{n}$ along each edge e of T(12 total).
- the three values of the components of the moment of 0 degree of $\boldsymbol{\tau}$ on T(3 total).

There are again 6 degrees of freedom for $\mathcal{V}_T$ for each triangle. Then $\mathcal{V}_h$ is the space of all peicewise linear vector fields with respect to $\mathcal{T}_h$ and $\boldsymbol{\Sigma}_h$ is the space of all tensor fields

which belong piecewise to $\boldsymbol{\sigma}_T$, and are also subject to two continuity conditions. These conditions are that the two lowest order moments of the normal components are continuous across mesh edges. Note that this continuity requirement is not strong enough to ensure $\boldsymbol{\Sigma}_h \subset \boldsymbol{H}(\mathrm{div}; \Omega; \mathbb{S})$.

Using these nonconforming global spaces, the MFEM proposed to discretize (2.7) is to find $(\boldsymbol{\sigma}_h, \boldsymbol{u}_h) \in (\boldsymbol{\Sigma}_h, \mathcal{V}_h)$

$$-\left(\nabla_h \cdot \boldsymbol{\sigma}_h, \boldsymbol{\nu}\right) = \left(\boldsymbol{f}_s, \boldsymbol{\nu}\right), \qquad \boldsymbol{\nu} \in \mathcal{V}_h, \tag{2.11a}$$

$$\left(\mathcal{A}\boldsymbol{\sigma}_h, \boldsymbol{\tau}\right) + \left(\boldsymbol{u}_h, \nabla_h \cdot \boldsymbol{\tau}\right) = 0, \qquad \boldsymbol{\tau} \in \boldsymbol{\Sigma}_h. \tag{2.11b}$$

where $\nabla_h \cdot$ is the divergence operator applied element-wise. The authors have shown that this results in a convergent method with the following rates

$$\begin{aligned} \|\boldsymbol{\sigma} - \boldsymbol{\sigma}_h\|_0 &\leq Ch\|\boldsymbol{u}\|_2, \\ \|\nabla \cdot \boldsymbol{\sigma} - \nabla \cdot \boldsymbol{\sigma}_h\|_0 &\leq Ch^m \|\nabla \cdot \boldsymbol{\sigma}\|_m, \qquad 0 \leq m \leq 2, \\ \|\boldsymbol{u} - \boldsymbol{u}_h\|_0 &\leq Ch\|\boldsymbol{u}\|_2. \end{aligned}$$

We see a lower convergence rate than when considering the conforming method. This is due to a so called consistency error which occurs since $\boldsymbol{\tau}\boldsymbol{n}$ is no longer continuous across interelement edges. Implementation of this elements is discussed in [26], where it is shown that this is a small modification from the implementation of the lowest order conforming element discussed above.

In the remainder of this sections, we will show an improvement in the error bound for $\boldsymbol{\sigma}$. For this analysis, we will make use of the projection operators defined and used for this space. First, $\mathcal{P}_h : (L^2(\Omega))^2 \to \mathcal{V}_h$ is the orthogonal projection. Then, $\Pi_h : \boldsymbol{H}^1(\Omega, \mathbb{S}) \to \boldsymbol{\Sigma}_h$ is a corresponding interpolation for tensors with the additional property that $\nabla_h \cdot \Pi_h \boldsymbol{\tau} = \mathcal{P}_h \nabla \cdot \boldsymbol{\tau}$. This additional property gives $\nabla_h \cdot \boldsymbol{\Sigma}_h = \mathcal{V}_h$.

Since $\mathcal{P}_h$ is the orthogonal projection

$$\left(\boldsymbol{u} - \mathcal{P}_h \boldsymbol{u}, \boldsymbol{\nu}\right) = 0, \quad \boldsymbol{\nu} \in \mathcal{V}_h. \tag{2.12}$$

But since $\nabla_h \cdot \boldsymbol{\tau} \in \mathcal{V}_h$ for $\boldsymbol{\tau} \in \boldsymbol{\Sigma}_h$

$$(\nabla_h \cdot \boldsymbol{\tau}, \boldsymbol{u} - \mathcal{P}_h \boldsymbol{u}) = 0, \quad \boldsymbol{\tau} \in \boldsymbol{\Sigma}_h. \tag{2.13}$$

We also have

$$(\nabla_h \cdot \boldsymbol{\tau} - \nabla_h \cdot \Pi_h \boldsymbol{\tau}, \boldsymbol{\nu}) = 0, \quad \boldsymbol{\nu} \in \mathcal{V}_h \tag{2.14}$$

since $\nabla_h \cdot \Pi_h \boldsymbol{\tau} = \mathcal{P}_h \nabla \cdot \boldsymbol{\tau}$. For these mixed finite element spaces [8] the following approximation properties hold:

$$\|\Pi_h \boldsymbol{\tau} - \boldsymbol{\tau}\|_0 \leq C h^m \|\boldsymbol{\tau}\|_m, \qquad 1 \leq m \leq 2, \tag{2.15a}$$

$$\|\mathcal{P}_h \boldsymbol{\nu} - \boldsymbol{\nu}\|_0 \leq C h^m \|\boldsymbol{\nu}\|_m, \qquad 0 \leq m \leq 2. \tag{2.15b}$$

One last point about this nonconforming MFEM will be used repeatedly in the following analysis. In order to use the element-wise divergence operator in the weak form consider (2.7b) on an element, multiply it by $\boldsymbol{\tau} \in \boldsymbol{\Sigma}_h$, integrate and take sum over elements. This gives

$$(\mathcal{A}\boldsymbol{\sigma}, \boldsymbol{\tau}) + (\boldsymbol{u}, \nabla_h \cdot \boldsymbol{\tau}) = \sum_{j=1}^{J} \int_{\partial T_j} \boldsymbol{\tau}\boldsymbol{n} \cdot \boldsymbol{u}\, ds, \quad \forall \boldsymbol{\tau} \in \boldsymbol{\Sigma}_h \tag{2.16}$$

where ∂T_j denotes the edges of a triangle T_j in a triangulation $\mathcal{T}_h$. The terms on the right hand side are referred to as the consistency error. By recalling the boundary condition $\boldsymbol{u} = 0$ on the external edge, (2.16) can be re-written by considering the interior edges as

$$\sum_{j=1}^{J} \int_{\partial T_j} \boldsymbol{\tau}\boldsymbol{n} \cdot \boldsymbol{u} ds = \sum_{e \in \mathcal{E}_h} \int_e [\boldsymbol{\tau}\boldsymbol{n}] \cdot \boldsymbol{u}\, ds, \quad \forall\, \boldsymbol{\tau} \in \boldsymbol{\Sigma}_h \tag{2.17}$$

where e is an edge in $\mathcal{E}_h$ the set of all interior edges for a triangulation $\mathcal{T}_h$. The notation $[\cdot]$ denotes the jump or change in a quantity across an edge and $\boldsymbol{n}$ is a normal vector to an edge e with some globally defined direction. Note that in a conforming case, $\boldsymbol{\Sigma}_h \subset \boldsymbol{H}(\mathrm{div}; \Omega; \mathbb{S})$ and, therefore, (2.17) is 0 by construction since $[\boldsymbol{\tau}\boldsymbol{n}] = 0$ for each interior edge. In the case of the nonconforming element the degrees of freedom used are sufficient to ensure $\boldsymbol{n} \cdot \boldsymbol{\tau}\boldsymbol{n}$

and the first two moments of $\boldsymbol{t} \cdot \boldsymbol{\tau n}$ where $\boldsymbol{t}$ is a globally defined tangential to the edge, are continuous across an interior edge[8]. Therefore,the right hand side of (2.16) can be simplified to

$$\mathbb{E}_h(\boldsymbol{u}, \boldsymbol{\tau}) = \sum_{e \in \mathcal{E}_h} \int_e [\boldsymbol{t} \cdot \boldsymbol{\tau n}] \boldsymbol{u} \cdot \boldsymbol{t}\, ds. \tag{2.18}$$

In [8], this so called consistency error (2.18) is bounded by

$$\mathbb{E}_h(\boldsymbol{u}, \boldsymbol{\tau}) \leq Ch \|\boldsymbol{\tau}\|_0 \|\boldsymbol{u}\|_2. \tag{2.19}$$

We note here that this proof uses the fact that the first two moments of $\boldsymbol{t} \cdot \boldsymbol{\tau n}$ are determined by the degrees of freedom and the projection properties of $\mathcal{P}_h$. It is valid for any $\boldsymbol{\tau} \in \boldsymbol{\Sigma}_h$ and $\boldsymbol{u} \in (H^2(\Omega))^2$.

However, during numerical experiments, a second order convergence rate is observed for the displacement error. This rate is better than the rate proved in Theorem 4.1 of [6]. By following the work of [99], in which rectangular elements with the same degrees of freedom are considered, we show an improvement in the proved convergence rate with certain conditions on the boundary $\partial\Omega$. Let $\boldsymbol{f} \in (L^2(\Omega))^2$ then there is a unique solution, $(\boldsymbol{u}, \boldsymbol{\sigma})$ to (2.7) satisfying [5]

$$\|\boldsymbol{u}\|_1 + \|\boldsymbol{\sigma}\|_0 \leq C \|\boldsymbol{f}\|_0.$$

When certain conditions are imposed on the boundary $\partial\Omega$, then $\boldsymbol{u} \in (H^2(\Omega))^2$ and

$$\|\boldsymbol{u}\|_2 + \|\boldsymbol{\sigma}\|_1 \leq C \|\boldsymbol{f}\|_0. \tag{2.20}$$

The validity of (2.20) depends on the location of the point where the boundary conditions change and also on the vertex angles of $\partial\Omega$ [65, 96]. An example of such a case is when $\partial\Omega$ is smooth and $\overline{\Gamma_D} \bigcap \overline{\Gamma_N} = \emptyset$ [91].

First we show an intermediate lemma. Note that this corresponds to Lemma 3.5 in [99]

Lemma 2.3.1. *For all $\boldsymbol{\tau} \in \boldsymbol{\Sigma}_h$ and all $\boldsymbol{u} \in (H^2(\Omega))^2$ with $\boldsymbol{u} = 0$ on Γ_D*

$$|\, \mathbb{E}_h(\boldsymbol{\tau}, \boldsymbol{u}) \,| \leq Ch^{k+m-1} \|\boldsymbol{\tau}\|_k \|\boldsymbol{u}\|_m, \quad 1 \leq k, m \leq 2. \tag{2.21}$$

Proof. Recall that

$$\mathbb{E}_h(\boldsymbol{u},\boldsymbol{\tau}) = \sum_{e\in\mathcal{E}_h}\int_e [\boldsymbol{t}\cdot\boldsymbol{\tau}\boldsymbol{n}]\boldsymbol{u}\cdot\boldsymbol{t}\,ds.$$

Let $\mathcal{R}: H^2 \to P_h$ be the L^2-projection, where P_h is the set of all piecewise linear functions on $\mathcal{E}_h$. Using the standard polynomial approximation and the fact the $\mathcal{R}$ reproduces linear functions on edges, we have

$$\|\omega - \mathcal{R}\omega\|_{0,\partial T_j} \le Ch^{m-1/2}\|\omega\|_{m,T_j}, \quad m = 1,2,\ \forall\omega\in H^2(\Omega_j),\ \forall T_j. \tag{2.22}$$

Now because the moment of degree 1 of $\boldsymbol{\tau}\boldsymbol{n}$ on each edge is a degree of freedom and $\mathcal{R}(\boldsymbol{u}\cdot\boldsymbol{t})$ is linear on each edge

$$\mathbb{E}_h(\boldsymbol{u},\boldsymbol{\tau}) = \sum_{e\in\mathcal{E}_h}\int_e [\boldsymbol{t}\cdot\boldsymbol{\tau}\boldsymbol{n}]\left(\boldsymbol{u}\cdot\boldsymbol{t} - \mathcal{R}(\boldsymbol{u}\cdot\boldsymbol{t})\right)ds.$$

Since the L^2-projection is an orthogonal projection and by using the Cauchy-Schwarz Inequality we find

$$\begin{aligned}\mathbb{E}_h(\boldsymbol{u},\boldsymbol{\tau}) &= \sum_{e\in\mathcal{E}_h}\int_e \left([\boldsymbol{t}\cdot\boldsymbol{\tau}\boldsymbol{n}] - \mathcal{R}([\boldsymbol{t}\cdot\boldsymbol{\tau}\boldsymbol{n}])\right)\left(\boldsymbol{u}\cdot\boldsymbol{t} - \mathcal{R}(\boldsymbol{u}\cdot\boldsymbol{t})\right)ds\\ &\le \sum_{e\in\mathcal{E}_h}\|[\boldsymbol{t}\cdot\boldsymbol{\tau}\boldsymbol{n}] - \mathcal{R}([\boldsymbol{t}\cdot\boldsymbol{\tau}\boldsymbol{n}])\|_{0,e}\|\boldsymbol{u}\cdot\boldsymbol{t} - \mathcal{R}(\boldsymbol{u}\cdot\boldsymbol{t})\|_{0,e}.\end{aligned}$$

The result (2.21) follows by applying (2.22). □

The next proof will make use of the following trace theorem as stated in theorem 1.6.6 of Brenner [17] which we state here for completeness.

Theorem 2.3.2 (Trace Theorem)**.** *For a domain Ω with a Lipshitz boundary, there is a constant C such that*

$$\|v\|_{L^2(\partial\Omega)} \le C\|v\|^{1/2}_{L^2(\Omega)}\|v\|^{1/2}_{W^1_2(\Omega)}, \quad \forall v\in H^m. \tag{2.23}$$

We make the following inverse assumption on function in the discrete spaces formed for MFEMs. Let W_h be some discrete space. It states that there exists constant C_0 independent of h such that

$$\|\nabla\phi\|_{L^2(\Omega)} \le C_0 h^{-1}\|\phi\|_{L^2(\Omega)}. \tag{2.24}$$

for $\phi \in W_h$. Therefore,using Theorem 2.3.2 and (2.24), for the discrete parts, we find

$$\|\phi\|_{H^m(\partial\Omega)} \leq Ch^{-1/2}\|\phi\|_{L^2(\Omega)}. \tag{2.25}$$

In the error analysis section of this work we will use the following notation convention. The variable χ will denote a discrete error. That is the difference between an approximation and the projection of the weak form answer into the test space. The variable η will be used to denote the error between a continuous function and its projection into a particular test space.

Theorem 2.3.3. *Let* $(\boldsymbol{\sigma}, \boldsymbol{u}) \in (\boldsymbol{\Sigma}, \mathcal{V})$ *and* $(\boldsymbol{\sigma}_h, \boldsymbol{u}_h) \in (\boldsymbol{\Sigma}_h, \mathcal{V}_h)$ *be the solution of* (2.7) *and* (2.11) *respectively. Then,*

$$\|\boldsymbol{u} - \boldsymbol{u}_h\|_0 \leq Ch^2 \left(\|\boldsymbol{u}\|_2 + \|\boldsymbol{\sigma}\|_1\right). \tag{2.26}$$

Proof. The following properties are proved in [8] and we state them without proof.

$$\nabla_h \cdot \boldsymbol{\sigma}_h = \mathcal{P}_h \nabla \cdot \boldsymbol{\sigma} = \nabla_h \cdot \Pi_h \boldsymbol{\sigma}. \tag{2.27}$$

$$\|\Pi_h \boldsymbol{\sigma}\|_0 \leq C\|\boldsymbol{\sigma}\|_1. \tag{2.28}$$

For this nonconforming method, consider the difference between (2.16) and (2.11b) to find

$$\left(\mathcal{A}\left(\boldsymbol{\sigma} - \boldsymbol{\sigma}_h\right), \boldsymbol{\tau}\right) + \left(\boldsymbol{u} - \boldsymbol{u}_h, \nabla \cdot \boldsymbol{\tau}\right) = \mathbb{E}_h\left(\boldsymbol{u}, \boldsymbol{\tau}\right). \tag{2.29}$$

Using the test function $\boldsymbol{\tau} = \Pi_h \boldsymbol{\sigma} - \boldsymbol{\sigma}_h$, (2.27) and (2.21) in (2.29) we find

$$\begin{aligned}\left(\mathcal{A}\left(\boldsymbol{\sigma} - \boldsymbol{\sigma}_h\right), \Pi_h \boldsymbol{\sigma} - \boldsymbol{\sigma}_h\right) &= \mathbb{E}_h\left(\boldsymbol{u}, \Pi_h \boldsymbol{\sigma} - \boldsymbol{\sigma}_h\right) \\ &\leq Ch\|\Pi_h \boldsymbol{\sigma} - \boldsymbol{\sigma}_h\|_0 \|\boldsymbol{u}\|_2. \end{aligned} \tag{2.30}$$

Now we consider the term $\|\Pi_h \boldsymbol{\sigma} - \boldsymbol{\sigma}_h\|_{\mathcal{A}}^2$. By adding and subtracting $\mathcal{A}\boldsymbol{\sigma}$, then using (2.30) we find

$$\begin{aligned}\|\Pi_h \boldsymbol{\sigma} - \boldsymbol{\sigma}_h\|_{\mathcal{A}}^2 &= \left(\mathcal{A}\left(\boldsymbol{\sigma} - \boldsymbol{\sigma}_h\right), \Pi_h \boldsymbol{\sigma} - \boldsymbol{\sigma}_h\right) + \left(\mathcal{A}\left(\Pi_h \boldsymbol{\sigma} - \boldsymbol{\sigma}\right), \Pi_h \boldsymbol{\sigma} - \boldsymbol{\sigma}_h\right) \\ &\leq Ch\|\Pi_h \boldsymbol{\sigma} - \boldsymbol{\sigma}_h\|_0 \|\boldsymbol{u}\|_2 + Ch\|\Pi_h \boldsymbol{\sigma} - \boldsymbol{\sigma}_h\|_0 \|\boldsymbol{\sigma}\|_1.\end{aligned}$$

Since the $\|\cdot\|_{\mathcal{A}}$ is equivalent to the $\|\cdot\|_0$ norm by (2.8),

$$\|\Pi_h\boldsymbol{\sigma} - \boldsymbol{\sigma}_h\|_0 \leq Ch\left(\|\boldsymbol{u}\|_2 + \|\boldsymbol{\sigma}\|_1\right). \tag{2.31}$$

Let $\boldsymbol{\sigma}^* \in \boldsymbol{H}^1(\Omega;\mathbb{S})$ such that $\nabla\cdot\boldsymbol{\sigma}^* = \mathcal{P}_h\boldsymbol{u} - \boldsymbol{u}_h$ with $\|\boldsymbol{u}^*\|_2 + \|\boldsymbol{\sigma}^*\|_1 \leq C\|\mathcal{P}_h\boldsymbol{u} - \boldsymbol{u}_h\|_0$. This is possible by taking $\boldsymbol{f} = \mathcal{P}_h\boldsymbol{u} - \boldsymbol{u}_h$ in (2.7) and (2.20). Additionally, by recalling (2.16) and (2.18)

$$(\mathcal{A}\boldsymbol{\sigma}^*, \boldsymbol{\tau}) + (\boldsymbol{u}^*, \nabla_h\cdot\boldsymbol{\tau}) = \mathbb{E}_h\left(\boldsymbol{u}^*, \boldsymbol{\tau}\right), \quad \forall\boldsymbol{\tau}\in\boldsymbol{\Sigma}_h. \tag{2.32}$$

By noting that $\nabla\cdot\boldsymbol{\sigma}^* \in \mathcal{V}_h$ and using (2.27)

$$\nabla_h\cdot\Pi_h\boldsymbol{\sigma}^* = \mathcal{P}_h\boldsymbol{u} - \boldsymbol{u}_h. \tag{2.33}$$

Additionally, by this definition of $\boldsymbol{\sigma}^*$ and (2.28)

$$\|\Pi_h\boldsymbol{\sigma}^*\|_0 \leq C\|\mathcal{P}_h\boldsymbol{u} - \boldsymbol{u}_h\|_0. \tag{2.34}$$

Now using (2.33)

$$\|\mathcal{P}_h\boldsymbol{u} - \boldsymbol{u}_h\|_0^2 = (\nabla_h\cdot\Pi_h\boldsymbol{\sigma}^*, \mathcal{P}_h\boldsymbol{u} - \boldsymbol{u}_h).$$

Using (2.13) and the test function $\boldsymbol{\tau} = \Pi_h\boldsymbol{\sigma}^*$ in (2.29) gives

$$(\mathcal{A}\left(\boldsymbol{\sigma} - \boldsymbol{\sigma}_h\right), \Pi_h\boldsymbol{\sigma}^*) + (\mathcal{P}_h\boldsymbol{u} - \boldsymbol{u}_h, \nabla\cdot\Pi_h\boldsymbol{\sigma}^*) = \mathbb{E}_h\left(\boldsymbol{u}, \Pi_h\boldsymbol{\sigma}^*\right)$$

and therefore

$$\|\mathcal{P}_h\boldsymbol{u} - \boldsymbol{u}_h\|_0^2 \leq \mid \mathbb{E}_h\left(\boldsymbol{u}, \Pi_h\boldsymbol{\sigma}^*\right) \mid + \mid \left(\mathcal{A}\left(\boldsymbol{\sigma} - \boldsymbol{\sigma}_h\right), \Pi_h\boldsymbol{\sigma}^*\right) \mid . \tag{2.35}$$

It remains to bound the term $\mid \left(\mathcal{A}\left(\boldsymbol{\sigma} - \boldsymbol{\sigma}_h\right), \Pi_h\boldsymbol{\sigma}^*\right) \mid$. We add and subtract $(\mathcal{A}\Pi_h\boldsymbol{\sigma}, \Pi_h\boldsymbol{\sigma}^*)$, $(\mathcal{A}\Pi_h\boldsymbol{\sigma}, \boldsymbol{\sigma}^*)$ and $(\mathcal{A}\boldsymbol{\sigma}, \boldsymbol{\sigma}^*)$ to find

$$\mid \left(\mathcal{A}\left(\boldsymbol{\sigma} - \boldsymbol{\sigma}_h\right), \Pi_h\boldsymbol{\sigma}^*\right) \mid \leq I + II + III$$

with

$$\begin{aligned} I =& \mid (\mathcal{A}(\boldsymbol{\sigma} - \Pi_h\boldsymbol{\sigma}), \Pi_h\boldsymbol{\sigma}^*) \mid, \\ II =& \mid (\mathcal{A}(\Pi_h\boldsymbol{\sigma} - \boldsymbol{\sigma}_h), \Pi_h\boldsymbol{\sigma}^* - \boldsymbol{\sigma}^*) \mid, \\ III =& \mid (\mathcal{A}(\Pi_h\boldsymbol{\sigma} - \boldsymbol{\sigma}_h), \boldsymbol{\sigma}^*) \mid . \end{aligned}$$

Now I is bounded using the Cauchy-Schwarz Inequality, (2.8), (2.15a) and (2.34) as

$$\begin{aligned} I &\leq C\|\boldsymbol{\sigma} - \Pi_h\boldsymbol{\sigma}\|_0\|\Pi_h\boldsymbol{\sigma}^*\|_0 \\ &\leq Ch^r\|\boldsymbol{\sigma}\|_r\|\Pi_h\boldsymbol{\sigma}^*\|_0 \\ &\leq Ch^r\|\boldsymbol{\sigma}\|_r\|\mathcal{P}_h\boldsymbol{u} - \boldsymbol{u}_h\|_0. \end{aligned}$$

Similarly,

$$II \leq Ch^{m-1}\|\boldsymbol{\sigma}^*\|_{m-1}\|\Pi_h\boldsymbol{\sigma} - \boldsymbol{\sigma}_h\|_0,$$

where $m = 2$ for $\boldsymbol{\sigma}^* \in \boldsymbol{H}^1(\Omega; \mathbb{S})$. Finally by noting the symmetry of $(\mathcal{A}\cdot, \cdot)$, (2.14), and (2.32) we find

$$III \leq \mid \mathbb{E}_h(\boldsymbol{u}^*, \Pi_h\boldsymbol{\sigma} - \boldsymbol{\sigma}_h) \mid + \mid (\boldsymbol{u}^* - \mathcal{P}_h\boldsymbol{u}^*, \nabla_h \cdot (\Pi_h\boldsymbol{\sigma} - \boldsymbol{\sigma}_h)) \mid .$$

Then this is bounded using (2.21), the Cauchy-Schwarz Inequality, the Trace Theorem, (2.8), (2.15b) and (2.15a) as

$$\begin{aligned} III &\leq Ch^{m-1}\|\Pi_h\boldsymbol{\sigma} - \boldsymbol{\sigma}_h\|_0\|\boldsymbol{u}^*\|_m + \|\boldsymbol{u}^* - \mathcal{P}_h\boldsymbol{u}^*\|_0\|\nabla_h \cdot (\Pi_h\boldsymbol{\sigma} - \boldsymbol{\sigma}_h)\|_0 \\ &\leq Ch^{m-1}\|\Pi_h\boldsymbol{\sigma} - \boldsymbol{\sigma}_h\|_0\|\boldsymbol{u}^*\|_m + Ch^{m-1}\|\boldsymbol{u}^*\|_m\|\Pi_h\boldsymbol{\sigma} - \boldsymbol{\sigma}_h\|_0. \end{aligned}$$

Therefore,using (2.31)

$$\begin{aligned} II + III &\leq Ch^{m-1}\left(\|\boldsymbol{\sigma}^*\|_{m-1} + \|\boldsymbol{u}^*\|_m\right)\|\Pi_h\boldsymbol{\sigma} - \boldsymbol{\sigma}_h\|_0 \\ &\leq Ch^2\left(\|\boldsymbol{\sigma}^*\|_1 + \|\boldsymbol{u}^*\|_2\right)\left(\|\boldsymbol{\sigma}\|_1 + \|\boldsymbol{u}\|_2\right) \\ &\leq Ch^2\left(\|\boldsymbol{\sigma}\|_1 + \|\boldsymbol{u}\|_2\right)\|\mathcal{P}_h\boldsymbol{u} - \boldsymbol{u}_h\|_0 \end{aligned}$$

The result (2.26) follows by noting the sum of $I + II + III$ on the right hand side of (2.35) □

2.3.5 Computational Results

We use as a starting point the implementation of the lowest order Arnold-Winther conforming MFEM for static linear elasticity provided in $\mathrm{F_FW}$ [24]. Studies in this paper are performed using the resources at the Texas Advanced Computing Center (TACC) [86].

Elastostatic Example 1

We make use of the academic example used in [26] which we will refer to as Elastostatic Example 1. Let $\Omega = (0,1) \times (0,1)$ with homogeneous Dirichlet boundary conditions. Let the analytic solution for displacement be

$$\boldsymbol{u} = \begin{bmatrix} \pi \cos(\pi y) \sin^2(\pi x) \sin(\pi y) \\ -\pi \cos(\pi x) \sin(\pi x) \sin^2(\pi y) \end{bmatrix}.$$

The other variables $\boldsymbol{\sigma}$ and $\boldsymbol{f}_s$ are calculated from this result. In the static case

$$\boldsymbol{f}_s = \begin{bmatrix} -2\mu\pi^3 \cos(\pi y) \sin(\pi y)(2\cos(2\pi x) - 1) \\ 2\mu\pi^3 \cos(\pi x) \sin(\pi x)(2\cos(2\pi y) - 1) \end{bmatrix}.$$

Table 2.1 shows convergence study results for this example problem with $E = 10^5$ and $\nu = 0.3$. Here E is Young's Modulus and ν is Poisson's ratio. These constants are related to the Lam*é* constants by the following formulas:

$$E = \frac{\mu_s(3\lambda + \mu_s)}{\lambda + \mu_s}.$$
$$\nu = \frac{\lambda}{2(\lambda + \mu_s)}.$$

We observe the expected second order convergence for displacement and third order convergence for stress. These results are also shown graphically in Figure 2.1.

Also for comparison, we show an example figure for displacement and stress. In Figure 2.2 we see a graph of the approximate solution using the conforming element on the left. This can be compared to the graph of the analytic solution shown on the bottom. Similarly,

Figure 2.3 shows a representative graph for stress and a comparison to the analytic solution. Specifically, using the notation

$$\boldsymbol{\sigma} = \begin{bmatrix} \boldsymbol{\sigma}_{11} & \boldsymbol{\sigma}_{12} \\ \boldsymbol{\sigma}_{21} & \boldsymbol{\sigma}_{22} \end{bmatrix}, \tag{2.36}$$

we show the graph of $\boldsymbol{\sigma}_{11}$.

Next, using the description in [26], the $\mathrm{F_FW}$ code is modified to make use of the non-conforming MFEM. The authors note that this non-conforming element is closely related to the conforming element and thus there is a minor modification needed to implement the nonconforming case. To confirm the convergence rates, Table 2.2 shows the results of a convergence study for the elastostatic example 1. In this table a linear rate of convergence is shown for stress and a quadratic rate of convergence for displacement. These results are also shown graphically in Figure 2.4. We also note that the computational results discussed in [26] are concerned with the stress variables. The authors of this paper do not discuss error result for displacement so we cannot make a comparison.

Figures 2.2 and 2.3 show representative figures. In Figure 2.2 the graph on the right shows results for the nonconforming element. We see that these results are nearly indistinguishable from the results using the conforming element. In Figure 2.3 the graph on the right hand side shows results for $\boldsymbol{\sigma}_{11}$ using the nonconforming elements. We clearly see that the non-conforming element does not force continuity of stress across elements. This is also seen in the convergence rate shown in Table 2.2.

For comparison, we attempt the same example problem on a different grid. Figure 2.5 shows the initial grids for these trials. On the left we see that Grid A contains all right triangles. This pattern will continues as the grid is refined and may result in better convergence rates. Therefore,a convergence study is done using grid B. Table 2.3 and Figure 2.6 show the results of this convergence study. Again we see second order convergence for the displacement variable.

Table 2.1: Convergence study results for Elastostatic Example 1 with the conforming element

h	$\|\boldsymbol{u} - \boldsymbol{u}_h\|$	Order	$\|\boldsymbol{\sigma} - \boldsymbol{\sigma}_h\|$	Order
$\frac{1}{2}$	3.613E-01	—	6.870E+04	—
$\frac{1}{4}$	9.859E-02	1.87	1.213E+04	2.50
$\frac{1}{8}$	2.573E-02	1.94	1.624E+03	2.90
$\frac{1}{16}$	6.513E-03	1.98	2.074E+02	2.97
$\frac{1}{32}$	1.634E-03	2.00	2.613E+01	2.99
$\frac{1}{64}$	4.087E-04	2.00	3.276E+00	3.00

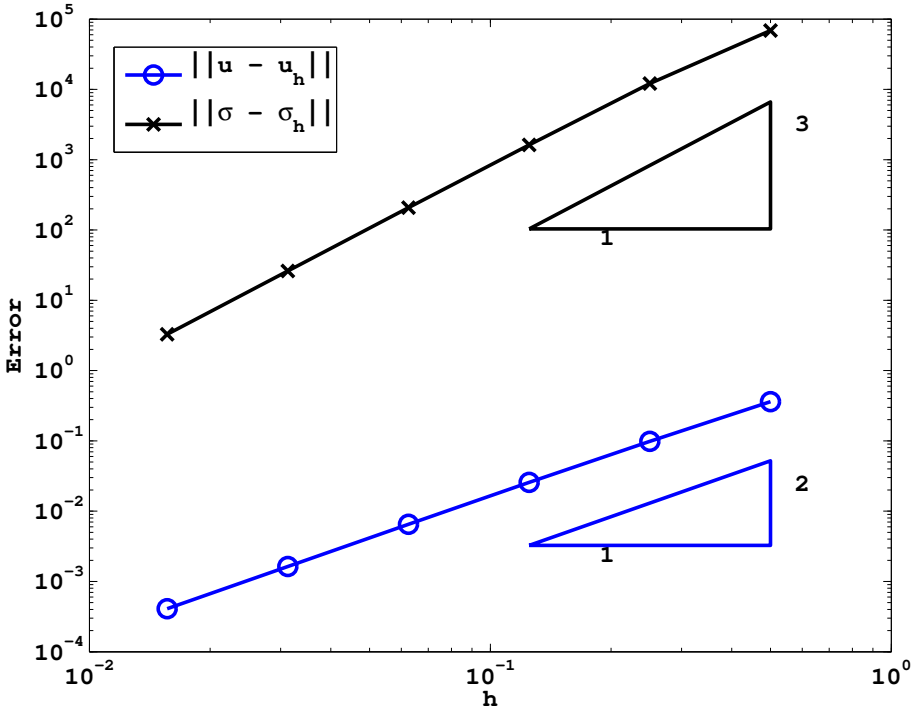

Figure 2.1: Graphical representation of the convergence study results for Elastostatic Example 1 with the conforming element

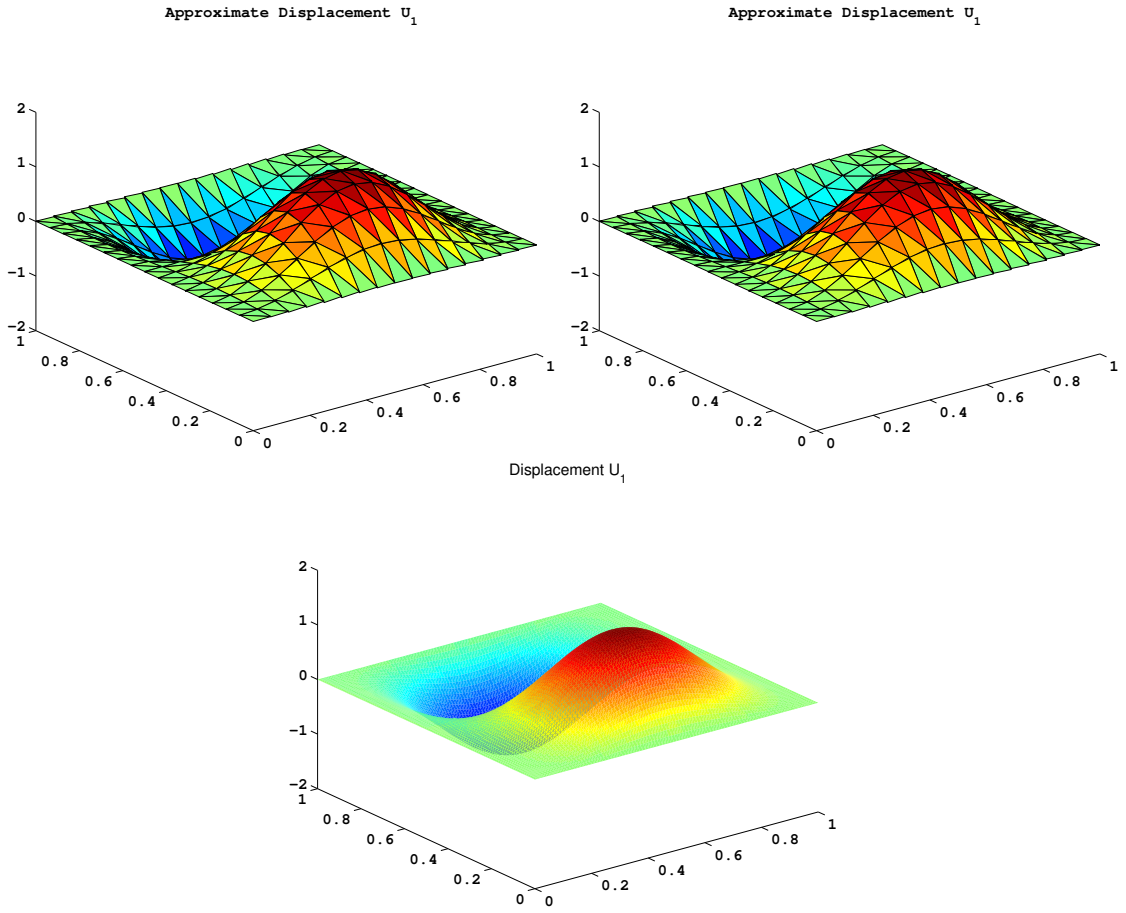

Figure 2.2: Solution graphs for the first component of displacement $\boldsymbol{u}_1$ for elastostatic example 1 with $h = \frac{1}{16}$: using the conforming element (left), using the nonconforming element (right), and the exact analytic solution (bottom).

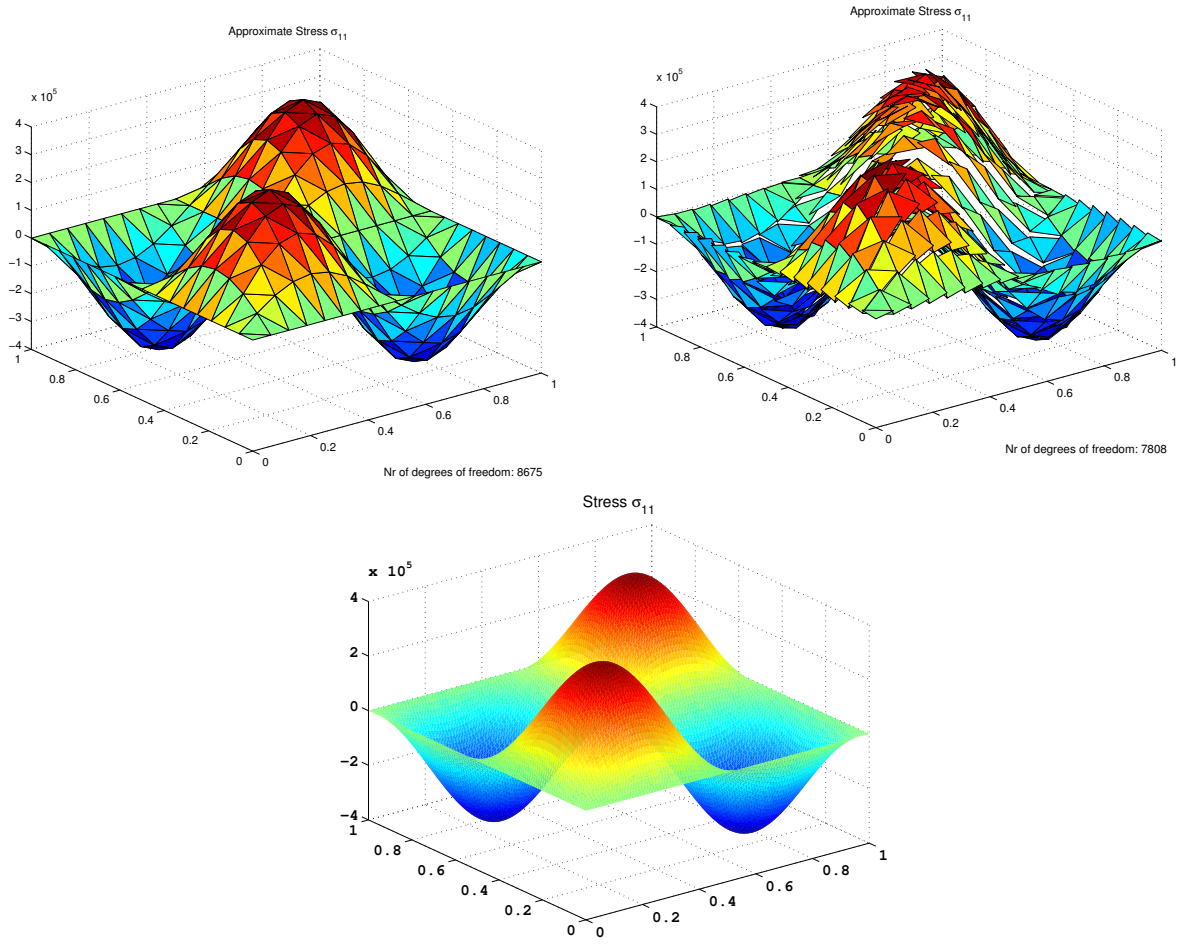

Figure 2.3: Solution graphs for the first component of stress, $\boldsymbol{\sigma}_{11}$ for elastostatic example 1, with $h = \frac{1}{16}$: using the conforming element (left), using the nonconforming element (right), and the exact analytic solution (bottom).

Table 2.2: Convergence study for Elastostatic Example 1 with the nonconforming element

h	$\|\boldsymbol{u}-\boldsymbol{u}_h\|$	Order	$\|\boldsymbol{\sigma}-\boldsymbol{\sigma}_h\|$	Order
$\frac{1}{2}$	3.764E-01	—	1.158E+05	—
$\frac{1}{4}$	1.013E-01	1.89	4.641E+04	1.32
$\frac{1}{8}$	2.637E-02	1.94	2.194E+04	1.08
$\frac{1}{16}$	6.657E-03	1.99	1.105E+04	0.99
$\frac{1}{32}$	1.668E-03	2.00	5.558E+03	0.99
$\frac{1}{64}$	4.172E-04	2.00	2.784E+03	1.00

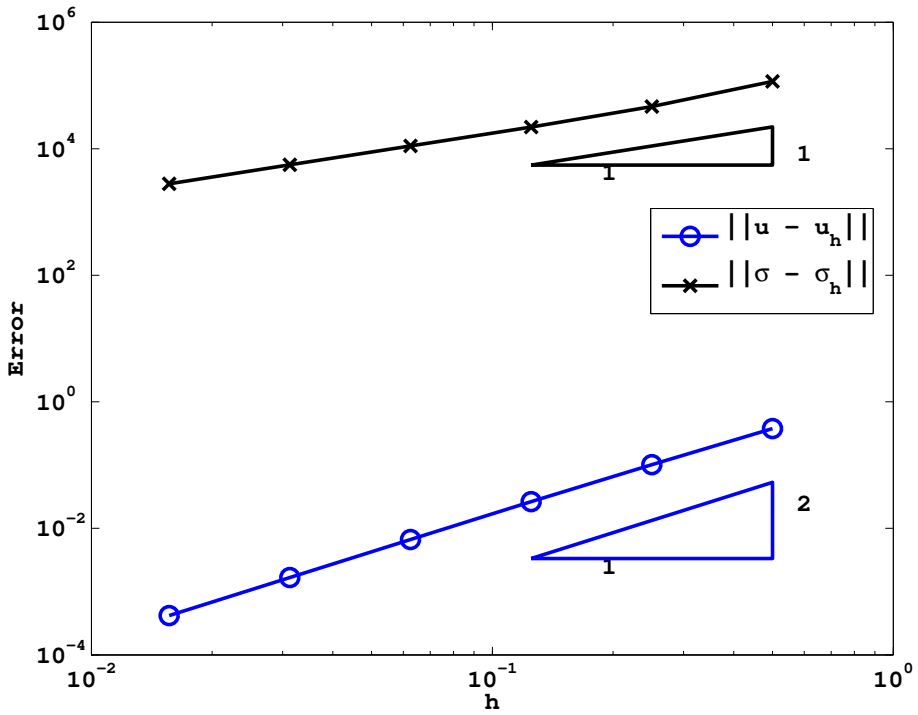

Figure 2.4: Graphical representation of the convergence study results for Elastostatic Example 1 with the nonconforming element

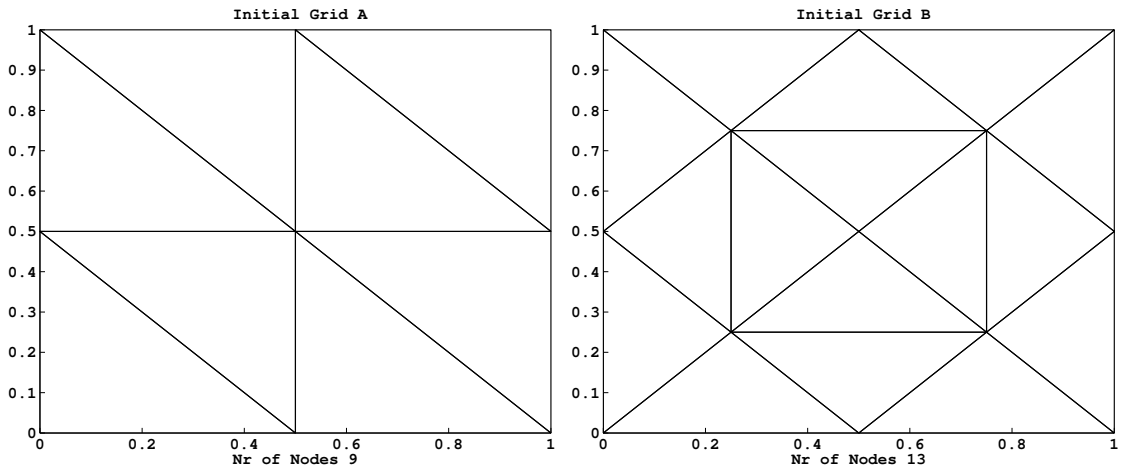

Figure 2.5: Initial grids used to test Example 1.

2.4 Mixed Finite Element Methods for Elastodynamics

2.4.1 Semidiscrete Model

We now move to the dynamic case in which $u_{tt} \neq 0$ in (2.6). Now to complete the system (2.6) in this case, both boundary and initial conditions are required. As before the required boundary conditions are

$$\begin{aligned} \boldsymbol{u} &= \boldsymbol{u}_D \quad \text{on}\, \Gamma_D, \\ \boldsymbol{\sigma n} &= \boldsymbol{\sigma}_N \quad \text{on}\, \Gamma_N, \end{aligned}$$

where $\boldsymbol{n}$ is the outward unit normal vector. Now the required initial conditions are

$$\begin{aligned} \boldsymbol{u}(\cdot, 0) &= \boldsymbol{u}_0 \quad \text{in}\, \Omega, \\ \boldsymbol{u}_t(\cdot, 0) &= \boldsymbol{s}_0 \quad \text{in}\, \Omega. \end{aligned}$$

Table 2.3: Convergence study for Elastostatic Example 1 with the nonconforming element on grid B

h	$\|\boldsymbol{u} - \boldsymbol{u}_h\|$	Order	$\|\boldsymbol{\sigma} - \boldsymbol{\sigma}_h\|$	Order
$\frac{1}{2}$	1.927E-01	—	9.918E+04	—
$\frac{1}{4}$	4.223E-02	2.19	4.399E+04	1.17
$\frac{1}{8}$	1.086E-02	1.96	2.194E+04	1.00
$\frac{1}{16}$	2.728E-03	1.99	1.096E+04	1.00
$\frac{1}{32}$	6.827E-04	2.00	5.485E+03	1.00
$\frac{1}{64}$	1.707E-04	2.00	2.744E+03	1.00

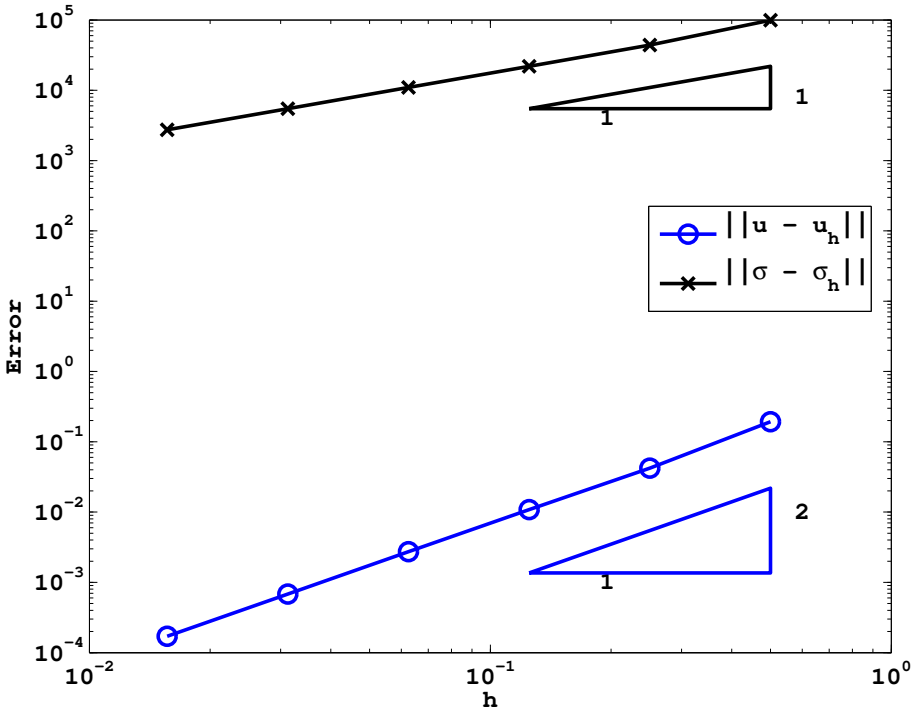

Figure 2.6: Graphical representation of the convergence study results for Elastostatic Example 1 with the nonconforming element on grid B

Then the weak form of (2.7) to find $(\boldsymbol{\sigma}, \boldsymbol{u}) \in (\mathcal{C}^0(0,T;\boldsymbol{\Sigma}), \mathcal{C}^2(0,T;\mathcal{V}))$ such that

$$\rho_s \left(\boldsymbol{u}_{tt}, \boldsymbol{\nu}\right) - \left(\nabla \cdot \boldsymbol{\sigma}, \boldsymbol{\nu}\right) = \left(\boldsymbol{f}_s, \boldsymbol{\nu}\right), \qquad \boldsymbol{\nu} \in \mathcal{V}, \tag{2.37a}$$

$$\left(\mathcal{A}\boldsymbol{\sigma}, \boldsymbol{\tau}\right) + \left(\boldsymbol{u}, \nabla \cdot \boldsymbol{\tau}\right) - < \boldsymbol{u}, \boldsymbol{\tau}\boldsymbol{n} >_\Gamma = 0, \qquad \boldsymbol{\tau} \in \boldsymbol{\Sigma}. \tag{2.37b}$$

However, we consider $\boldsymbol{\sigma} \in \mathcal{C}^1(0,T;\boldsymbol{\Sigma})$ as is done in[35]. The weak form is obtained by considering the boundary and initial conditions and by differentiating (2.6b) with respect to time. In [35], this is done in consideration of absorbing boundary conditions and to complete a priori analysis. In this dissertation, there will be an additional benefit to considering this form when the FSI problem is considered. Specifically, in chapter 4 differentiating this equations guides our choice for enforcing the interface conditions. The system of equations we consider is

$$\rho_s \boldsymbol{u}_{tt} - \nabla \cdot \boldsymbol{\sigma} = \boldsymbol{f}_s, \tag{2.38a}$$

$$\mathcal{A}\boldsymbol{\sigma}_t - (\epsilon(\boldsymbol{u}))_t = 0. \tag{2.38b}$$

The weak form of (2.38) seeks to find $(\boldsymbol{\sigma}, \boldsymbol{u}) \in (\mathcal{C}^1(0,T;\boldsymbol{\Sigma}), \mathcal{C}^2(0,T;\mathcal{V}))$ such that

$$\left(\boldsymbol{u}(0), \boldsymbol{\nu}\right) = \left(\boldsymbol{u}_0, \boldsymbol{\nu}\right), \qquad \boldsymbol{\nu} \in \mathcal{V}, \tag{2.39a}$$

$$\left(\mathcal{A}\boldsymbol{\sigma}(0), \boldsymbol{\tau}\right) + \left(\boldsymbol{u}_0, \nabla \cdot \boldsymbol{\tau}\right) =< \boldsymbol{u}_0, \boldsymbol{\tau}\boldsymbol{n} >_\Gamma, \qquad \boldsymbol{\tau} \in \boldsymbol{\Sigma}, \tag{2.39b}$$

$$\left(\boldsymbol{u}_t(0), \boldsymbol{\nu}\right) = \left(\boldsymbol{s}_0, \boldsymbol{\nu}\right), \qquad \boldsymbol{\nu} \in \mathcal{V}, \tag{2.39c}$$

$$\rho_s \left(\boldsymbol{u}_{tt}, \boldsymbol{\nu}\right) - \left(\nabla \cdot \boldsymbol{\sigma}, \boldsymbol{\nu}\right) = \left(\boldsymbol{f}_s, \boldsymbol{\nu}\right), \qquad \boldsymbol{\nu} \in \mathcal{V}, \quad t > 0, \tag{2.39d}$$

$$\left(\mathcal{A}\boldsymbol{\sigma}_t, \boldsymbol{\tau}\right) + \left(\boldsymbol{u}_t, \nabla \cdot \boldsymbol{\tau}\right) - < \boldsymbol{u}_t, \boldsymbol{\tau} \cdot \boldsymbol{n} >_\Gamma = 0, \qquad \boldsymbol{\tau} \in \boldsymbol{\Sigma}, \quad t > 0. \tag{2.39e}$$

To develop a fully discrete model for the elastodynamic problem, discrete time derivatives must also be considered. Therefore,we introduce some notations.

2.4.2 Notations

We will make use of two and three level θ schemes using the following definitions. First let $\Delta t = T_f/N$, where $N > 0$ is a positive integer and T_f is the final time for a particular

simulation. We denote $t^n = n\Delta t$ for a positive integer n. Now, for any function of time ϕ we denote

$$\phi(t^n) = \phi^n, \quad 0 \leq n \leq N.$$

The three level weighted average is defined as

$$\phi^{n,\theta,3} = \theta\phi^{n+1} + (1-2\theta)\phi^n + \theta\phi^{n-1}$$

and the two level weighted average is defined as

$$\phi^{n,s,2} = s\phi^{n+1} + (1-s)\phi^n.$$

We will most commonly be considering the cases $\theta = \frac{1}{4}$ and $s = \frac{1}{2}$ as these are the case we expect to result in better convergence than other values of s and θ. In these cases we will use the following simplified notation

$$\widetilde{\phi^n} = \frac{1}{4}\left(\phi^{n+1} + 2\phi^n + \phi^{n-1}\right), \quad n \geq 1, \tag{2.40}$$

$$\overline{\phi^{n+1/2}} = \frac{1}{2}\left(\phi^{n+1} + \phi^n\right), \qquad n \geq 0. \tag{2.41}$$

Here the tilde and bar are used to distinguish between the three and two level weighted averages. The superscript in each of these notations denotes the central, which also indicates the time at which the value is approximated. That is, for example, $\overline{\phi^{n+1/2}}$ is an approximation to $\phi^{n+1/2} = \phi((n+\frac{1}{2})\Delta t)$. Also in this case we note

$$\widetilde{\phi^n} = \frac{\overline{\phi^{n+1/2}}}{2} + \frac{\overline{\phi^{n-1/2}}}{2}. \tag{2.42}$$

Next we will make use of the following notations with regards to time derivatives.

$$\partial_t\phi^{n+1/2} = \frac{\phi^{n+1} - \phi^n}{\Delta t}, \qquad n \geq 0, \tag{2.43}$$

$$\partial_t^c\phi^n = \frac{\partial_t\phi^{n+1/2} + \partial_t\phi^{n-1/2}}{2} = \frac{\phi^{n+1} - \phi^{n-1}}{2\Delta t}, \qquad n \geq 1, \tag{2.44}$$

$$\partial_t^2\phi^n = \frac{\phi^{n+1} - 2\phi^n + \phi^{n-1}}{\Delta t^2} = \frac{\partial_t\phi^{n+1/2} - \partial_t\phi^{n-1/2}}{\Delta t}, \quad n \geq 1. \tag{2.45}$$

Again we note that the superscript value is the central value to the derivative and indicates the time at which the derivative is approximated. For example, $\partial_t^2\phi^n$ is an approximation to ϕ_{tt}^n. Furthermore, it is clear that the approximation $\partial_t^2\phi^n$ uses information at three distinct time steps, $n-1, n$ and $n+1$. However, for a given system of equations, it will be necessary to have unknowns in only one time step. Specifically, when dealing with equations that contain an approximation of the form $\partial_t^2\phi^n$ we will need to already know the values of ϕ^n and ϕ^{n-1}. The unknown value is ϕ^{n+1}. That is, we will commonly use approximations of model equations at time step n to find approximations to the primary variables at the next time step $n+1$. This is explained in the context of the elastodynamics equations below. Similar notations are used when dealing with second order equations in [38, 35, 61, 64].

Also, we will not be considering negative time steps. So at time step $n = 0$ we revert to using the two level schemes. That is,

$$\partial_t^c\phi^0 = \partial_t\phi^{1/2}, \tag{2.46a}$$

$$\widetilde{\phi^0} = \overline{\phi^0}. \tag{2.46b}$$

Additionally, we will define some norms involving time. For a normed space $\mathcal{P}$ with a norm $\|\cdot\|_{\mathcal{P}}$ let $\phi \in \mathcal{C}^k(0,T;\mathcal{P})$. Then define the associated norms for $1 \le p < \infty$ as

$$\|\phi\|_{L^p(0,T;\mathcal{P})} = \left(\int_0^T \|\phi(t)\|_{\mathcal{P}}^p dt\right)^{1/p}.$$

We will also make use of L^∞-norms for the time discrete functions

$$\|\phi\|_{L^\infty_{\Delta t}(0,T;P)} = \max_{0\le n\le N} \|\phi^n\|_P, \tag{2.47a}$$

$$\|\phi\|_{\overline{L^\infty_{\Delta t}}(0,T;P)} = \max_{0\le n\le N-1} \|\overline{\phi^{n+1/2}}\|_P, \tag{2.47b}$$

$$\|\phi\|_{\widetilde{L^\infty_{\Delta t}}(0,T;P)} = \max_{1\le n\le N-1} \|\widetilde{\phi^n}\|_P. \tag{2.47c}$$

The maximum is to be taken over the values of n for which ϕ is used. For example, if ϕ^n is defined for $0 \le n \le N$ then $\widetilde{\phi^n}$ is defined for $1 \le n \le N-1$. When the L^∞-norm is taken over the entire time domain, the range $[0,T]$ will be omitted in the notations subscript.

2.4.3 Fully Discrete Model

To fully discretize the elastodyanmic model, we will discretize the time derivatives. Consider some finite dimensional spaces $\boldsymbol{\Sigma}_h$ and $\mathcal{V}_h$ which are approximation to $\boldsymbol{\Sigma}$ and $\mathcal{V}$ respectively. These may be conforming or nonconforming spaces. Therefore,we express the following models using the element-wise divergence operator, $\nabla_h \cdot$, with the understanding that in the case of a conforming space, this is the same as the standard divergence $\nabla \cdot$. For a given n we assume that all pairs $(\boldsymbol{u}_h^i, \boldsymbol{\sigma}_h^i)$ for $i \leq n$ are known. Therefore,the unknown pair in the system for a given n is $(\boldsymbol{u}_h^{n+1}, \boldsymbol{\sigma}_h^{n+1})$. We are always seeking an approximation at the next time step. The mixed finite element approximation we consider seeks to find $(\boldsymbol{u}_h^{n+1}, \boldsymbol{\sigma}_h^{n+1}) \in (\mathcal{V}_h, \boldsymbol{\Sigma}_h), 1 \leq n \leq N-1$ such that

$$\rho_s \left(\partial_t^2 \boldsymbol{u}_h^n, \boldsymbol{\nu}\right) - \left(\nabla_h \cdot \widetilde{\boldsymbol{\sigma}_h^n}, \boldsymbol{\nu}\right) = \left(\widetilde{\boldsymbol{f}_s^n}, \boldsymbol{\nu}\right), \quad \boldsymbol{\nu} \in \mathcal{V}_h,\, n \geq 1, \tag{2.48a}$$

$$(\mathcal{A}\partial_t^c \boldsymbol{\sigma}_h^n, \boldsymbol{\tau}) + (\partial_t^c \boldsymbol{u}_h^n, \nabla_h \cdot \boldsymbol{\tau}) = 0, \qquad \boldsymbol{\tau} \in \boldsymbol{\Sigma}_h,\, n \geq 1. \tag{2.48b}$$

This model must also include initial conditions. Consider the time step with $n = 1$, which is the first time step for which (2.48) is defined. At this step, we seek to find the $(\boldsymbol{u}_h^2, \boldsymbol{\sigma}_h^2)$ while $\boldsymbol{u}_h^0, \boldsymbol{\sigma}_h^0, \boldsymbol{u}_h^1$, and $\boldsymbol{\sigma}_h^1$ are assumed to be known. The values $\boldsymbol{u}_h^0$ and $\boldsymbol{\sigma}_h^0$ are found directly from the given initial condition as

$$\left(\boldsymbol{u}_h^0, \boldsymbol{\nu}\right) = \left(\boldsymbol{u}_0, \boldsymbol{\nu}\right), \qquad \boldsymbol{\nu} \in \mathcal{V}_h, \tag{2.49a}$$

$$\left(\mathcal{A}\boldsymbol{\sigma}_h^0, \boldsymbol{\tau}\right) + \left(\boldsymbol{u}_h^0, \nabla_h \cdot \boldsymbol{\tau}\right) = < \boldsymbol{u}_0, \boldsymbol{\tau}\boldsymbol{n} >_\Gamma, \quad \boldsymbol{\tau} \in \boldsymbol{\Sigma}_h. \tag{2.49b}$$

However to find the values $\boldsymbol{u}_h^1$ and $\boldsymbol{\sigma}_h^1$ we temporarily allow the fictitious quantity $\partial_t \boldsymbol{u}_h^{-1/2}$ following the work of [35]. Then

$$\begin{aligned}
\partial_t^2 \boldsymbol{u}_h{}^0 &= \frac{\partial_t \boldsymbol{u}_h{}^{1/2} - \partial_t \boldsymbol{u}_h{}^{-1/2}}{\Delta t} \\
&= \frac{2\partial_t \boldsymbol{u}_h{}^{1/2} - (\partial_t \boldsymbol{u}_h{}^{1/2} + \partial_t \boldsymbol{u}_h{}^{-1/2})}{\Delta t} \\
&= \frac{2\partial_t \boldsymbol{u}_h{}^{1/2}}{\Delta t} - \frac{2\partial_t \boldsymbol{u}_h{}^0}{\Delta t}.
\end{aligned}$$

Now using the initial condition, we let $\partial_t \boldsymbol{u}_h{}^0 = \boldsymbol{s}_0$. Additionally, we are unable to use the three level θ scheme at this first time step and simply use a two level average. The system at $n = 0$ is to find $(\boldsymbol{\sigma}_h^1, \boldsymbol{u}_h^1) \in (\boldsymbol{\Sigma}_h, \mathcal{V}_h)$ such that

$$\frac{2\rho_s}{\Delta t}\left(\partial_t \boldsymbol{u}_h^{1/2}, \boldsymbol{\nu}\right) - \left(\nabla_h \cdot \overline{\boldsymbol{\sigma}_h^{1/2}}, \boldsymbol{\nu}\right) = \left(\overline{\boldsymbol{f}_s^{1/2}} + \frac{2\rho_s}{\Delta t}\boldsymbol{s}_0, \boldsymbol{\nu}\right), \quad \boldsymbol{\nu} \in \mathcal{V}_h, \tag{2.50a}$$

$$\left(\mathcal{A}\partial_t \boldsymbol{\sigma}_h^{1/2}, \boldsymbol{\tau}\right) + \left(\partial_t \boldsymbol{u}_h^{1/2}, \nabla_h \cdot \boldsymbol{\tau}\right) = 0, \qquad \boldsymbol{\tau} \in \boldsymbol{\Sigma}_h. \tag{2.50b}$$

A priori error estimates for this problem rely heavily on the work of Cowsar, Dupont and Wheeler [35]. In this paper, the authors study a second order hyperbolic equation with first order absorbing boundary conditions stated as

$$\begin{aligned} u_{tt} - \nabla \cdot \boldsymbol{z} &= f && \text{in } \Omega \times (0,T) \\ A^{-1}\boldsymbol{z} + \nabla u &= f && \text{in } \Omega \times (0,T) \\ u_t + \alpha(A\nabla u) \cdot \boldsymbol{n} &= g && \text{on } \partial\Omega \times (0,T) \end{aligned}$$

where A is a symmetric uniformly bounded matrix. In the authors' case, u is a scalar quantity and $\boldsymbol{z}$ is a vector quantity so the authors' analysis considers a Raviart-Thomas-Nedelec [78] (RTN) pair which is used to find a vector and scalar pair. However, their analysis should be extendable to the elastodynamics problem by noting, as the authors have, that when $\alpha = 0$ this is just a non-standard formulation of a Dirichlet problem, and the assumptions made on the projections for the RTN space hold for the conforming and nonconforming spaces. Specifically, for the nonconforming element, these assumptions are those stated in Section 2.3.3 in equations (2.13), (2.14) and (2.15). When using a non-conforming method, we expect the consistency error to have an effect similar to the effect seen in the static case. In Theorems 6.1 and 6.2 [35], a priori error estimates show that when the solution is sufficiently regular, the error for both the scalar quantity u and the vector quantity $\boldsymbol{z}$ can be expected to be second order in time and limit spatially by the mixed finite element. In this analysis, the approximation properties for both the scalar and vector spaces effect the final error estimate. More details will be provided in error analysis

for the FSI problem, however, here we merely state the expected results for applying this analysis to the elastodynamic problem.

By applying this analysis, we expect that the convergence will have the same rates spatially as the MFEM chosen for the static case and second order convergence in time. For example, for the conforming element we expect

$$\|\boldsymbol{\sigma} - \boldsymbol{\sigma}_h\|_{L^\infty_{\Delta t}(\Omega)} \leq C(\Delta t^2 + h^2),$$
$$\|\boldsymbol{u} - \boldsymbol{u}_h\|_{L^\infty_{\Delta t}(\Omega)} \leq C(\Delta t^2 + h^2).$$

For example, for the nonconforming element we expect

$$\|\boldsymbol{\sigma} - \boldsymbol{\sigma}_h\|_{L^\infty_{\Delta t}(\Omega)} \leq C(\Delta t^2 + h),$$
$$\|\boldsymbol{u} - \boldsymbol{u}_h\|_{L^\infty_{\Delta t}(\Omega)} \leq C(\Delta t^2 + h).$$

2.4.4 Computational Results

In this section, we include some computational results to verify the application of the analysis in [35] to the elastodynamics problem. For verification testing, we make use of two test problems and two MFEMs as in the previous sections.

Elastodynamic Example 1

Let $\Omega = (0,1) \times (0,1)$. Then

$$\boldsymbol{u} = \begin{bmatrix} e^t \sin(x)\sin(y) \\ e^t \cos(x)\cos(y) \end{bmatrix}.$$

The other variables $\boldsymbol{\sigma}$ and $\boldsymbol{f}_s$ are calculated from this result.

$$\boldsymbol{f}_s \begin{bmatrix} e^t(\rho_s - 2\mu)\sin(x)\sin(y) \\ e^t(\rho_s - 2\mu)\cos(x)\cos(y) \end{bmatrix}.$$

Additionally, boundary conditions are found using the analytic solutions. We consider mixed boundary conditions where the top and bottom edges have Dirichlet conditions and the left and right edges have Neumann conditions. For this trial $\lambda = 1.43 \times 10^5$ and $\mu = 3.57 \times 10^5$. Table 2.4 shows a convergence study for this example using the conforming element. In the early stages we see the third order convergence in the sigma error. However as the refinement continues, this rate begins to drop off. This is expected as the method is only expected to be second order in time and both h and Δt are being cut in half with each refinement. The expected second order convergence is observed for the displacement variable. This is also shown graphically in Figure 2.7

We again show some example graphs for this problem. In Figure 2.8 an example for the approximate solution at the final time of $T_f = 1$. In Figure 2.9 the approximation for $\boldsymbol{\sigma}_{h11}$ at the same time is shown.

Next we compare these to the non-conforming results. In Table 2.5 the results of a convergence study using the nonconforming element are shown. For this trial both h and Δt have been cut in half for each refinement. In this case, we again see second order convergence rate for the displacement error. This is similar to the elastostatic case, although this rate is better than the expected first order rate from the analysis. However for the stress error we see first order convergence as expected. These results are also shown graphically in Figure 2.10.

In Figure 2.8 the graph on the right is an example for the approximate solution for the first component of displacement, using the nonconforming element, at the final time of $T_f = 1$. In Figure 2.9 the approximation for $\boldsymbol{\sigma}_{h11}$ at the same time is shown. The non-conforming nature of this approximation is not as visible in this case as it was in example 1. However the lack of continuity can bee seen most clearly in the upper left corner, closest to the point $(1, 1)$.

Table 2.4: Convergence study for Elastodynamic Example 1 with the conforming element

h	Δt	$\|\boldsymbol{u}-\boldsymbol{u}_h\|_{L^\infty_{\Delta t}(\Omega)}$	Order	$\|\boldsymbol{\sigma}-\boldsymbol{\sigma}_h\|_{L^\infty_{\Delta t}(\Omega)}$	Order
$\frac{1}{2}$	1.000E-01	3.951E-02	—	2.993E+02	—
$\frac{1}{4}$	5.000E-02	9.843E-03	2.01	3.765E+01	2.99
$\frac{1}{8}$	2.500E-02	2.459E-03	2.00	4.712E+00	3.00
$\frac{1}{16}$	1.250E-02	6.146E-04	2.00	5.757E-01	3.03
$\frac{1}{32}$	6.250E-03	1.536E-04	2.00	6.936E-02	3.05
$\frac{1}{64}$	3.125E-03	3.841E-05	2.00	9.334E-03	2.89

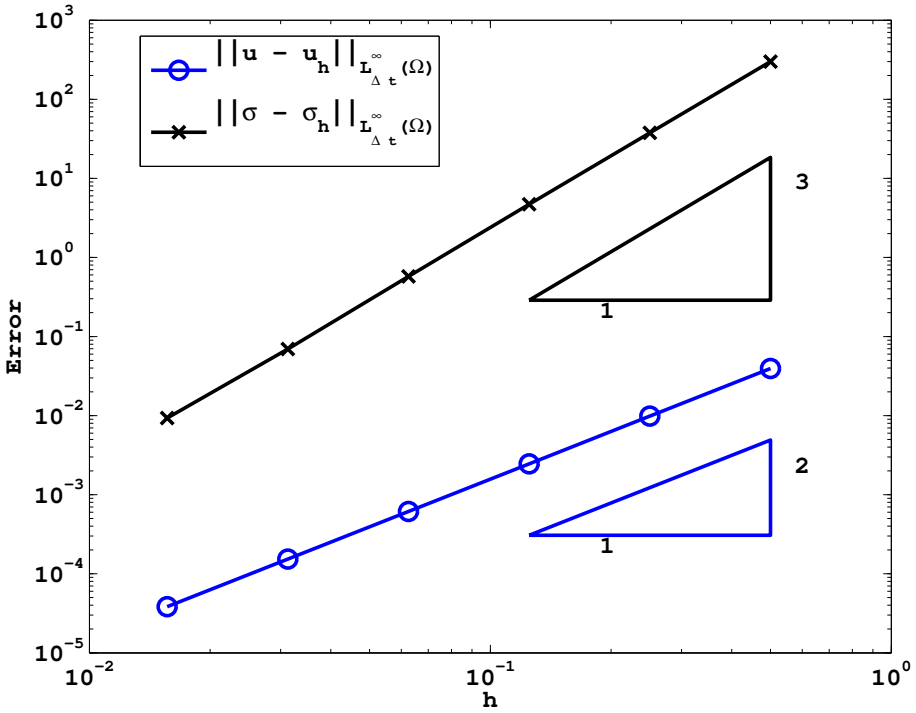

Figure 2.7: Graphical representation of the convergence study results for Elastodynamic Example 1 with the conforming element

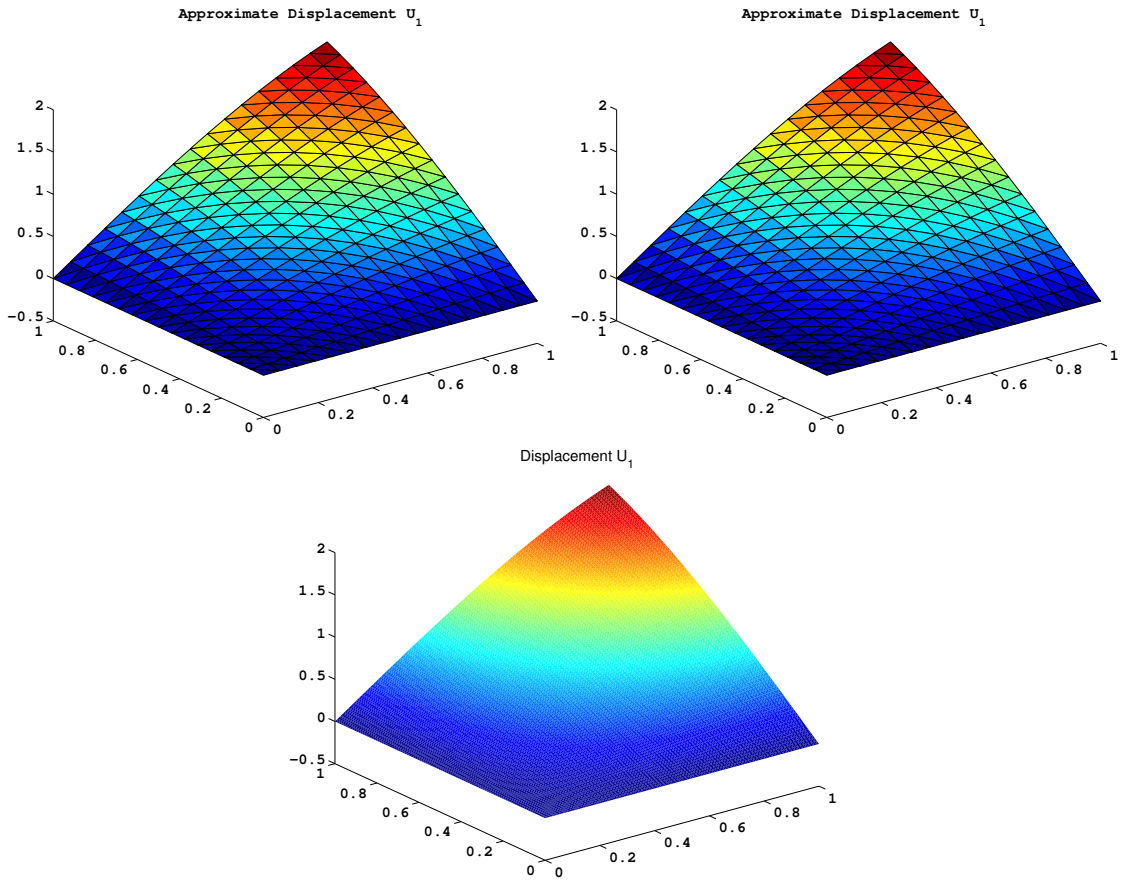

Figure 2.8: Solution graphs for the first component of displacement, $\boldsymbol{u}_1$ for the elastodynamic example 1 at $T_f = 1$ with $h = \frac{1}{16}$ and $\Delta t = 1.25 \times 10^{-2}$: using the conforming element (left), using the nonconforming element (right), and the exact analytic solution (bottom).

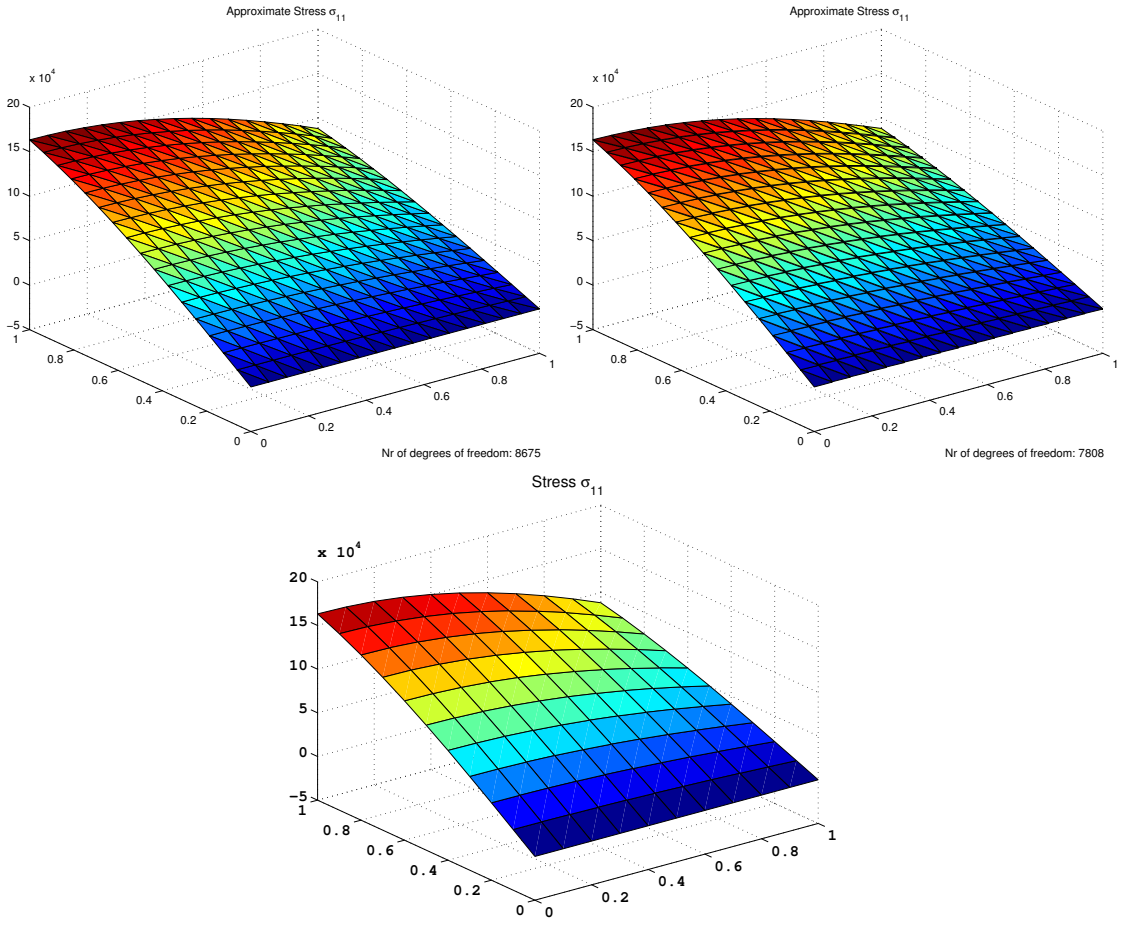

Figure 2.9: Solution graphs for the first component of stress, $\boldsymbol{\sigma}_{11}$ for the elastodynamic example 1 at $T_f = 1$ with $h = \frac{1}{16}$ and $\Delta t = 1.25 \times 10^{-2}$: using the conforming element (left), using the nonconforming element (right), and the exact analytic solution (bottom).

Table 2.5: Convergence study for the Elastodynamic Example 1 with the nonconforming element

h	Δt	$\|\boldsymbol{u}-\boldsymbol{u}_h\|_{L^\infty_{\Delta t}(\Omega)}$	Order	$\|\boldsymbol{\sigma}-\boldsymbol{\sigma}_h\|_{L^\infty_{\Delta t}(\Omega)}$	Order
$\frac{1}{2}$	1.000E-01	3.964E-02	—	5.010E+03	—
$\frac{1}{4}$	5.000E-02	9.876E-03	2.00	2.617E+03	0.94
$\frac{1}{8}$	2.500E-02	2.467E-03	2.00	1.342E+03	0.96
$\frac{1}{16}$	1.250E-02	6.170E-04	2.00	6.674E+02	1.01
$\frac{1}{32}$	6.250E-03	1.545E-04	2.00	3.230E+02	1.05

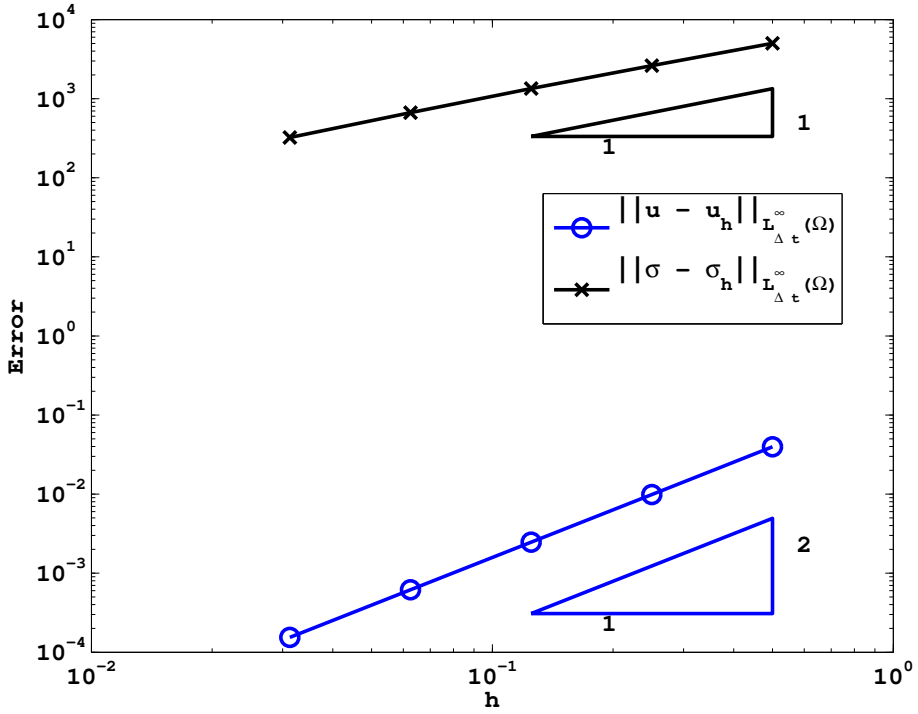

Figure 2.10: Graphical representation of the convergence study results for Elastodynamic Example 1 with the nonconforming element

Elastodynamic Example 2

We consider the analytic solution used in [69]. For the solid problem only this is

$$\boldsymbol{u} = \begin{bmatrix} \sin(x+t)\sin(y+t) \\ \cos(x+t)\cos(y+t) \end{bmatrix}.$$

The other variables $\boldsymbol{\sigma}$ and $\boldsymbol{f}_s$ be calculated from this result.

We again consider mixed boundary conditions where the top and bottom edges have Dirichlet conditions and the left and right edges have Neumann conditions. For this trial $\lambda = 114$ and $\mu = 455$. Table 2.6 shows a convergence study for this example using the conforming element. Again we reduce both h and Δt by factor of 2 for each refinement. Despite seeing a third order convergence in the sigma error early on we see dropping toward the expected second order convergence for both variables as the study progresses. Figure 2.11 shows this graphically.

We again show some example graphs for this problem. In Figure 2.12 the graph on the right is an example of the approximate solution for the first component of displacement at the final time of $T_f = 1$. In Figure 2.13 the approximation for $\boldsymbol{\sigma}_{h22}$ at the same time is shown.

Next we compare these to the non-conforming results. In Table 2.14 and Figure 2.15 the results of convergence study using the nonconforming element are shown. We again see second order convergence in the displacement error while seeing a first order rate of convergence for the stress variable.

In Figure 2.12 the graph on the left is an example for the approximate solution for the first component of displacement, using the nonconforming element, at the final time of $T_f = 1$. In Figure 2.13 the approximation for $\boldsymbol{\sigma}_{h22}$ at the same time is shown.

Table 2.6: Convergence study for Elastodynamic Example 2 with the conforming element

h	Δt	$\|\boldsymbol{u}-\boldsymbol{u}_h\|_{L^\infty_{\Delta t}(\Omega)}$	Order	$\|\boldsymbol{\sigma}-\boldsymbol{\sigma}_h\|_{L^\infty_{\Delta t}(\Omega)}$	Order
$\frac{1}{2}$	1.000E-01	1.496E-02	—	1.824E+00	—
$\frac{1}{4}$	5.000E-02	3.729E-03	2.00	2.135E-01	3.09
$\frac{1}{8}$	2.500E-02	9.315E-04	2.00	2.648E-02	3.01
$\frac{1}{16}$	1.250E-02	2.328E-04	2.00	3.481E-03	2.93
$\frac{1}{32}$	6.250E-03	5.821E-05	2.00	5.714E-04	2.61

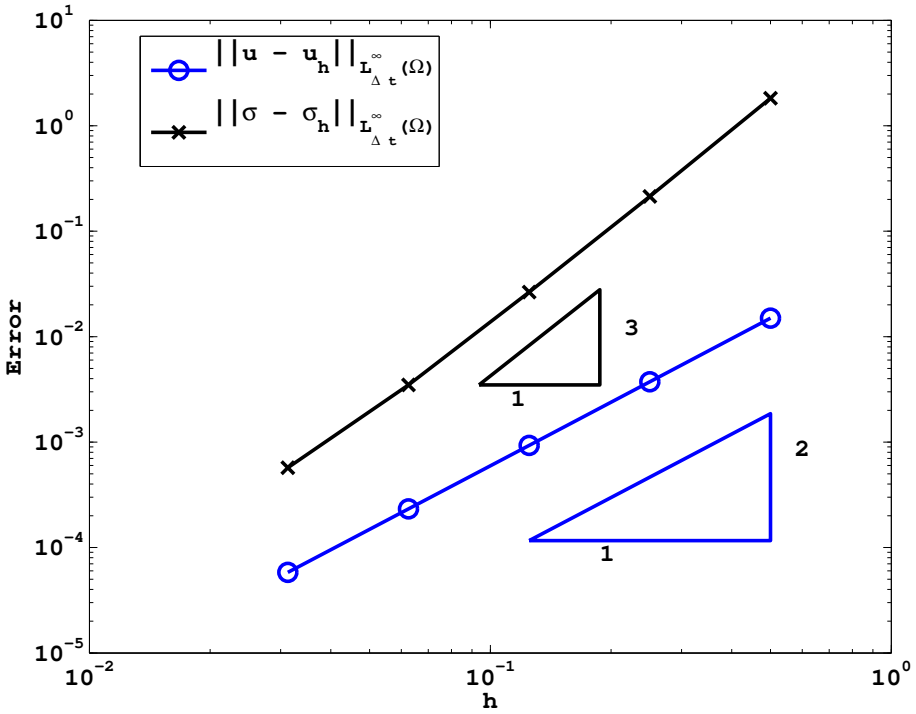

Figure 2.11: Graphical representation of the convergence study results for Elastodynamic Example 2 with the conforming element

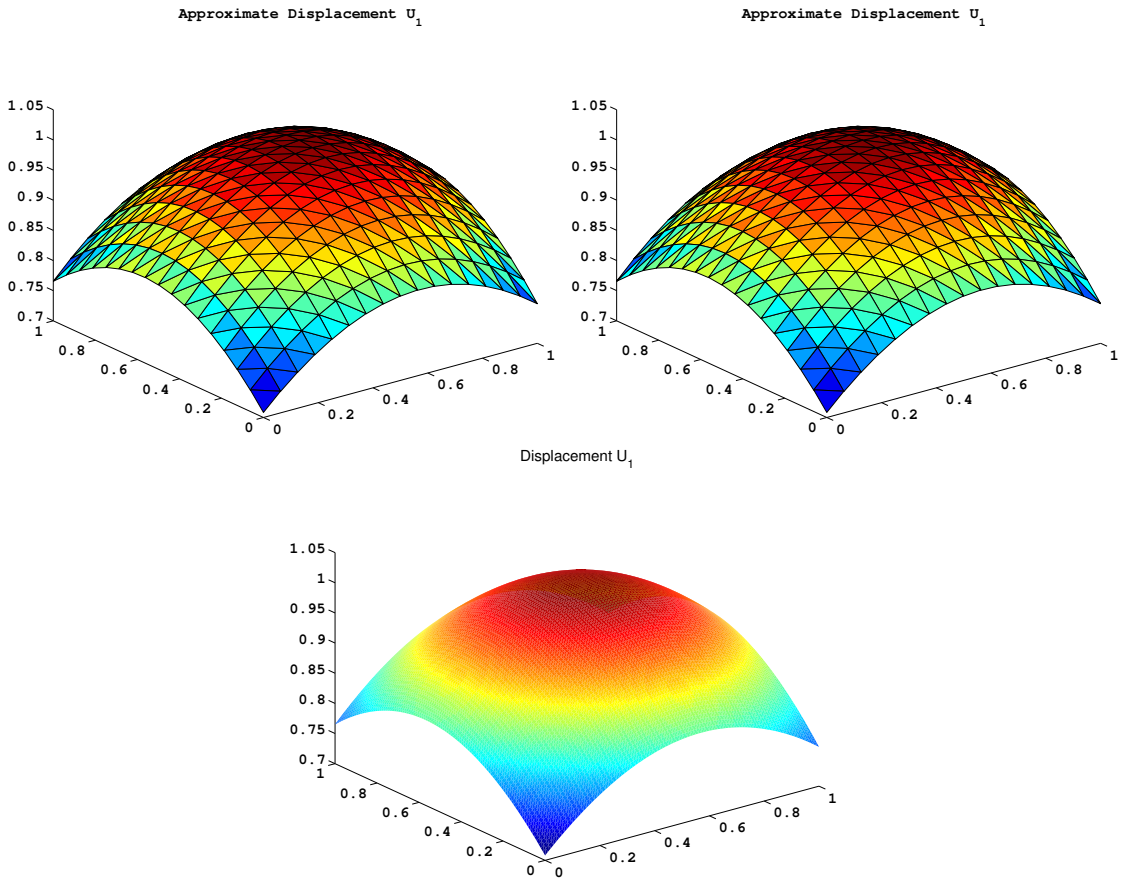

Figure 2.12: Solution graphs for the first component of displacement, $\boldsymbol{u}_1$ for the elasto-dynamic example 2 at $T_f = 1$ with $h = \frac{1}{16}$ and $\Delta t = 1.25 \times 10^{-2}$: using the conforming element (left), using the nonconforming element (right), and the exact analytic solution (bottom).

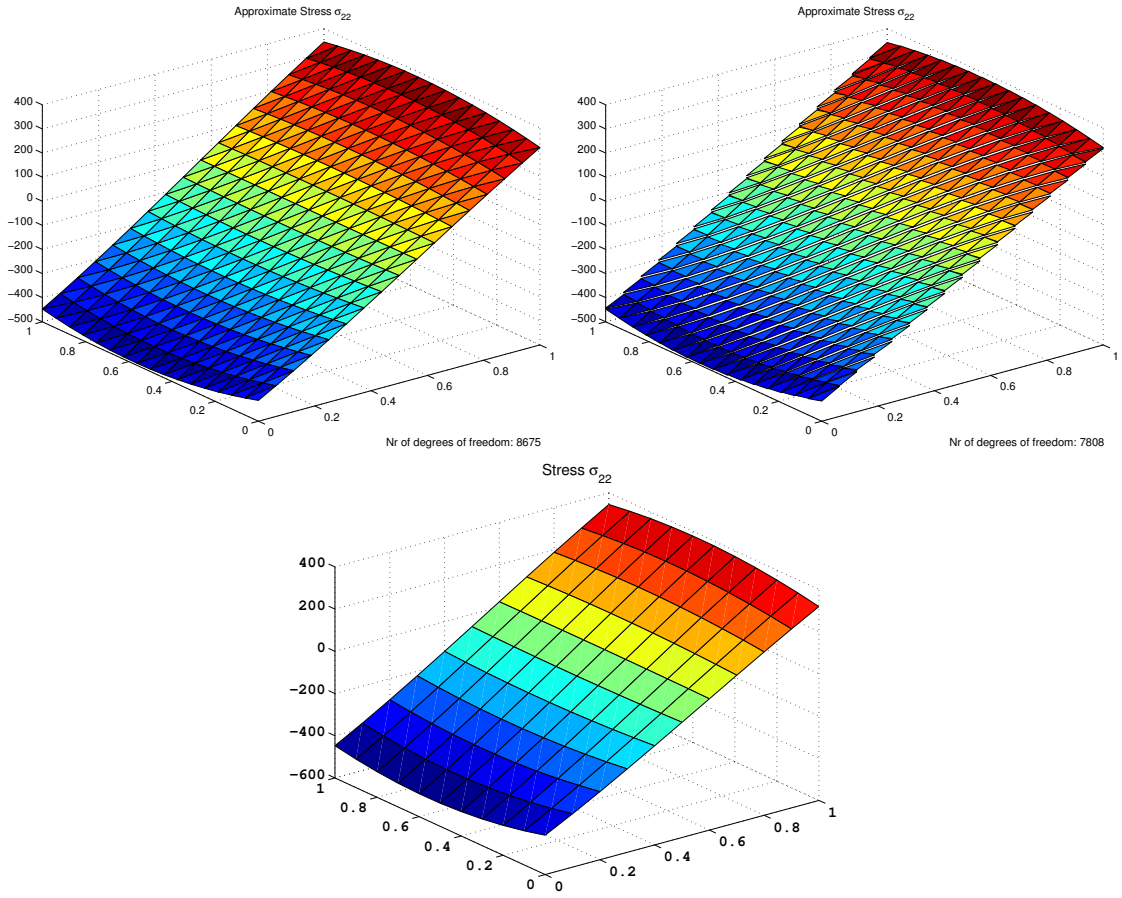

Figure 2.13: Solution graphs for the last component of stress, $\boldsymbol{\sigma}_{22}$ for the elastodynamic example 2 at $T_f = 1$ with $h = \frac{1}{16}$ and $\Delta t = 1.25 \times 10^{-2}$: using the conforming element (left), using the nonconforming element (right), and the exact analytic solution (bottom).

Figure 2.14: Convergence study for Elastodynamic Example 2 with the nonconforming element

h	Δt	$\|\boldsymbol{u}-\boldsymbol{u}_h\|_{L^\infty_{\Delta t}(\Omega)}$	Order	$\|\boldsymbol{\sigma}-\boldsymbol{\sigma}_h\|_{L^\infty_{\Delta t}(\Omega)}$	Order
$\frac{1}{2}$	1.000E-01	1.514E-02	—	2.751E+01	—
$\frac{1}{4}$	5.000E-02	3.793E-03	2.00	1.344E+01	1.03
$\frac{1}{8}$	2.500E-02	9.462E-04	2.00	6.698E+00	1.01
$\frac{1}{16}$	1.250E-02	2.367E-04	2.00	3.352E+00	1.00
$\frac{1}{32}$	6.250E-03	5.919E-05	2.00	1.678E+00	1.00

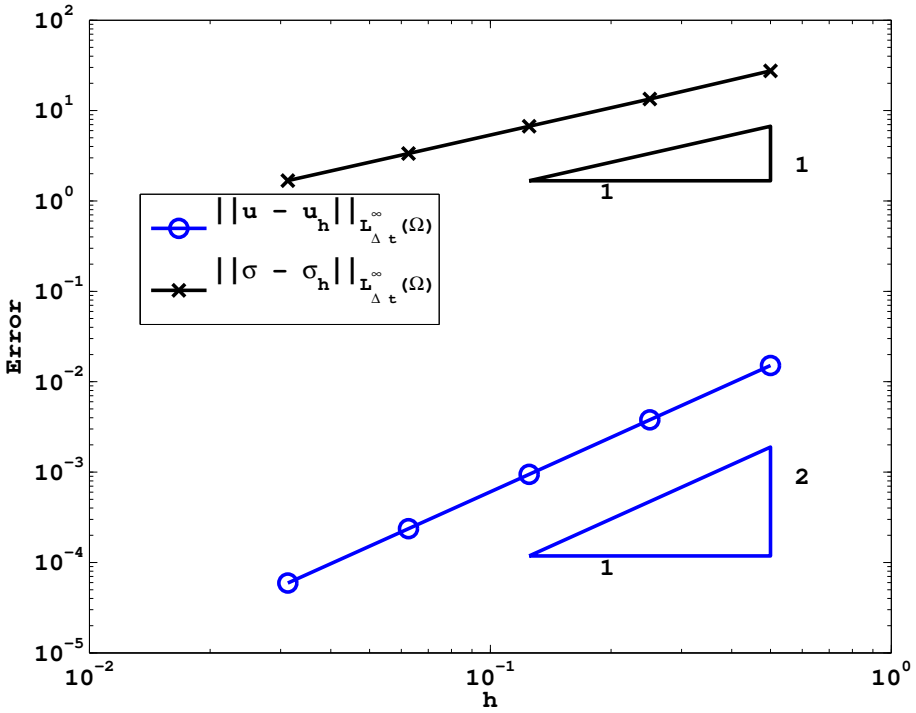

Figure 2.15: Graphical representation of the convergence study results for Elastodynamic Example 2 with the nonconforming element

Chapter 3

Mixed Finite Element Methods for Stokes Flow

In this chapter, we will focus on the fluid flow section of our FSI problem. In dissertation, we limit our study to the case of a slow flow of a slightly compressible fluid where the nonstationary or unsteady Stokes equations describe the flow.

Traditionally, the MFEM for the Stokes equation would use velocity and pressure as the primary variables. In this case the unknown pair is a vector and a scalar. A number of stable mixed finite element spaces for such problems have been found, see for example [71]. Many other works have been devoted to the study of the Stokes and Navier-Stokes equations in the context of finite element methods. For example, the work of Huang et al. [59] studies the use of a stabilized finite element in space and the Crank-Nicholson scheme in time to the nonstationary Stokes problem. In this case fluid velocity and pressure are considered primary variables. Furthermore, in [93] the general problem of parabolic equations using a similar method of finite elements in space and a Crank-Nicholson approach in time is studied.

However, we know ahead of time that we wish to consider a formulation in which the primary variables are fluid velocity and stress to match the variables in the elastodynamics equation. The stationary version of this formulation has been studied by Carstensen et al. [27] where the Arnold-Winther finite element is used for spatial discretization. Furthermore, this is a limiting case of the linear elasticity problem. Therefore MFEMs designed for the elasticity equations can be used for Stokes equations too. Specifically, we should be able to use the nonconforming element in this formulation of Stokes equations as well. We will

build on this work by studying the nonstationary Stokes equations discretized spatially using the Arnold-Winther element. However the nonstationary Stokes equation has only a first derivative with respect to time unlike the elastodynamics problem which contains a second derivative with respect to time. Since the discretization for the elasticity problem discussed in the previous section is expected to be second order in time, the Crank-Nicholson scheme is used for the time discretization of this problem to match.

3.1 Model Equations for Nonstationary Stokes Flow

3.1.1 Derivation of Model Equations

As we already know that we would like our model equations to be expressed in terms of velocity and stress, we will think of the Stokes equations as a limit of case of linear elasticity as $\lambda \to \infty$ [40, 27]. Recall the compliance tensor 2.1 used to express Hooke's law. In the limit of $\lambda \to \infty$ we find the deviatoric operator

$$\mathcal{A}_\infty \boldsymbol{\tau} := \frac{1}{2\mu_f}\left(\boldsymbol{\tau} - \frac{1}{2}\mathrm{tr}(\boldsymbol{\tau})\mathbf{I}\right), \tag{3.1}$$

where μ_f is the viscosity. There must also be a slightly different definition for fluid stress than solid stress. Fluid stress is defined as

$$\boldsymbol{\sigma} = 2\mu_f \boldsymbol{\epsilon}(\boldsymbol{v}) - p\mathbf{I}, \tag{3.2}$$

where $\boldsymbol{v}$ is fluid velocity and p is the fluid pressure. This stress is made up of the static and dynamic parts. For a fluid at rest, Pascal's Law,see for example [75], shows

$$\boldsymbol{\sigma}_r = -p\mathbf{I}.$$

For the fluid in motion first consider the following property. Consider an infinitesimal volume of fluid, This flow is subject to the conservation of mass. However since we consider an incompressible flow, the density is constant. That is ρ_f is constant. Therefore, the

volume must also be constant. This is written as

$$\nabla \cdot \boldsymbol{v} = 0. \tag{3.3}$$

Note also that

$$\nabla \cdot \boldsymbol{v} = \mathrm{tr}(\epsilon(\boldsymbol{v})).$$

Therefore by considering Hooke's law (2.3) applied now to the fluid, the dynamic part of the fluid stress is

$$\boldsymbol{\sigma}_d = 2\mu_f \boldsymbol{\epsilon}(\boldsymbol{v}).$$

Adding these static and dynamic parts yields the definition (3.2). By recalling the system (2.6) the stress-velocity formulation for the nonstationary Stokes equation as a limiting case of linear elasticity is

$$\rho_f \frac{\partial}{\partial t}\boldsymbol{v} - \nabla \cdot \boldsymbol{\sigma} = \boldsymbol{f}_f, \tag{3.4a}$$

$$\mathcal{A}_\infty \boldsymbol{\sigma} - \epsilon(\boldsymbol{v}) = 0. \tag{3.4b}$$

Equation (3.3) can be obtained from this formulation by applying the trace operator to (3.4b). We note that nonstationary Stokes equations are traditionally expressed as

$$\rho_f \boldsymbol{v}_t - 2\mu_f \nabla \cdot \boldsymbol{\epsilon}(\boldsymbol{v}) + \nabla p = \boldsymbol{f}_f, \tag{3.5a}$$

$$\nabla \cdot \boldsymbol{v} = 0. \tag{3.5b}$$

More information about these equations can be found for example in [71, 54] and more information about the derivation of these equations can be found in introductory fluid dynamics texts, for example [15]. This system is arrived at by using the definition (3.2) in (3.4a) and using (3.3) directly. To complete either system we need boundary and initial conditions. The boundary conditions are

$$\boldsymbol{v} = \boldsymbol{v}_d \quad \text{on } \Gamma_D,$$

$$\boldsymbol{\sigma}\boldsymbol{n} = \sigma_N \quad \text{on } \Gamma_N.$$

Note that if $\Gamma_N = \emptyset$, then the pressure in this case is unique only up to an additive constant. When using (3.5), the value of pressure often is fixed by enforcing a compatibility condition

$$\int_\Omega p dx = 0. \tag{3.6}$$

However as we will be using the system (3.4) we note that by taking the trace of $\boldsymbol{\sigma}$, we find

$$\mathrm{tr}\boldsymbol{\sigma} = -2p.$$

Therefore, the compatibility condition for (3.4) is

$$\int_\Omega \mathrm{tr}\boldsymbol{\sigma} dx = 0.$$

Finally, the required initial condition is

$$\boldsymbol{v}(0) = \boldsymbol{v}_0 \quad \text{in}\,\Omega. \tag{3.7}$$

3.1.2 Semidiscrete Model

Here we will express the semidiscrete form of our model governed by the system (3.4). However, we first note that the new definition (3.1) leads to a new norm defined as

$$\|\boldsymbol{\tau}\|^2_{\mathcal{A}_\infty,\Omega} = \int_\Omega \mathcal{A}_\infty \boldsymbol{\tau} : \boldsymbol{\tau} dx.$$

This norm $\|\cdot\|^2_{\mathcal{A}_\infty,\Omega}$ is equivalent to the L^2-norm

$$C_1\|\boldsymbol{\tau}\|_0^2 \leq \|\boldsymbol{\tau}\|^2_{\mathcal{A}_\infty,\Omega} \leq C_2\|\boldsymbol{\tau}\|_0^2. \tag{3.8}$$

Now recall that

$$\boldsymbol{\Sigma} = \boldsymbol{H}(\mathrm{div};\Omega;\mathbb{S}) \quad \text{and} \quad \mathcal{V} = (L^2(\Omega))^2.$$

Then the weak formulation seeks to find $(\boldsymbol{\sigma}, \boldsymbol{v}) \in (\mathcal{C}(0,T;\boldsymbol{\Sigma}), \mathcal{C}^1(0,T;\mathcal{V}))$ such that

$$(\boldsymbol{v}(0), \boldsymbol{\nu}) = (\boldsymbol{v}_0, \boldsymbol{\nu}), \qquad \boldsymbol{\nu} \in \mathcal{V}, \tag{3.9a}$$

$$\rho_f (\boldsymbol{v}_t, \boldsymbol{\nu}) - (\nabla \cdot \boldsymbol{\sigma}, \boldsymbol{\nu}) = (\boldsymbol{f}_f, \boldsymbol{\nu}), \qquad \boldsymbol{\nu} \in \mathcal{V}, \quad t > 0, \tag{3.9b}$$

$$(\mathcal{A}_\infty \boldsymbol{\sigma}, \boldsymbol{\tau}) + (\boldsymbol{v}, \nabla \cdot \boldsymbol{\tau}) - < \boldsymbol{v}, \boldsymbol{\tau}\boldsymbol{n} >_\Gamma = 0, \quad \boldsymbol{\tau} \in \boldsymbol{\Sigma}, \quad t > 0. \tag{3.9c}$$

Consider some finite dimensional spaces $\boldsymbol{\Sigma}_h$ and $\mathcal{V}_h$ which are approximations to $\boldsymbol{\Sigma}$ and $\mathcal{V}$ respectively. These may be conforming or nonconforming spaces. Therefore we express the following models using the element-wise divergence operator, $\nabla_h \cdot$, with the understanding that in the case of a conforming space, this is the same as the standard divergence $\nabla \cdot$. The semidiscrete model seeks to find $(\boldsymbol{\sigma}_h, \boldsymbol{v}_h) \in (\mathcal{C}(0,T;\boldsymbol{\Sigma}_h), \mathcal{C}^1(0,T;\mathcal{V}_h))$ such that

$$(\boldsymbol{v}_h(0), \boldsymbol{\nu}) = (\boldsymbol{v}_0, \boldsymbol{\nu}), \qquad \boldsymbol{\nu} \in \mathcal{V}_h, \tag{3.10a}$$

$$\rho_f\left((\boldsymbol{v}_h)_t, \boldsymbol{\nu}\right) - (\nabla \cdot \boldsymbol{\sigma}_h, \boldsymbol{\nu}) = (\boldsymbol{f}_f, \boldsymbol{\nu}), \qquad \boldsymbol{\nu} \in \mathcal{V}_h, \quad t > 0, \tag{3.10b}$$

$$(\mathcal{A}_\infty \boldsymbol{\sigma}_h, \boldsymbol{\tau}) + (\boldsymbol{v}_h, \nabla \cdot \boldsymbol{\tau}) - < \boldsymbol{v}_h, \boldsymbol{\tau}\boldsymbol{n} >_\Gamma = 0, \quad \boldsymbol{\tau} \in \boldsymbol{\Sigma}_h, \quad t > 0. \tag{3.10c}$$

3.2 Fully Discrete Model

We wish to consider a second order time discretization for this problem. Therefore we consider a Crank-Nicholson discretization. This type of scheme has been used in the velocity-pressure formulation in [55, 51, 52, 63, 89]. As in the the previous chapter, in this notation, for a given n we assume that all pairs $(\boldsymbol{\sigma}_h^i, \boldsymbol{u}_h^i)$ where $i \leq n$ are known. Therefore, the unknown pair in the above system for a given n is $(\boldsymbol{\sigma}_h^{n+1}, \boldsymbol{u}_h^{n+1})$. The fully discrete method is to find $(\boldsymbol{\sigma}_h^{n+1}, \boldsymbol{v}_h^{n+1}) \in (\boldsymbol{\Sigma}_h, \mathcal{V}_h), 0 \leq n \leq N-1$ such that

$$\rho_f\left(\partial_t v^{n+1/2}, \boldsymbol{\nu}\right) - \left(\nabla_h \cdot \overline{\boldsymbol{\sigma}_h^{n+1/2}}, \boldsymbol{\nu}\right) = \left(\overline{\boldsymbol{f}_f^{n+1/2}}, \boldsymbol{\nu}\right), \qquad \boldsymbol{\nu} \in \mathcal{V}_h, \quad n \geq 0, \tag{3.11a}$$

$$\left(\mathcal{A}_\infty \overline{\boldsymbol{\sigma}_h^{n+1/2}}, \boldsymbol{\tau}\right) + \left(\overline{\boldsymbol{\sigma}_h^{n+1/2}}, \nabla_h \cdot \boldsymbol{\tau}\right) - < \overline{\boldsymbol{v}_h^{n+1/2}}, \boldsymbol{\tau}\boldsymbol{n} >_\Gamma = 0, \quad \boldsymbol{\tau} \in \boldsymbol{\Sigma}_h, \quad n \geq 0. \tag{3.11b}$$

3.2.1 Initial Conditions

Let $n = 0$ in (3.11a) be used to find $\boldsymbol{v}_h^1$ and, $\boldsymbol{\sigma}_h^1$. In order to use this both $\boldsymbol{v}_h^0$ and $\boldsymbol{\sigma}_h^0$ are assumed to be known from given initial condition. The former can be found using

$$\left(\boldsymbol{v}_h^0, \boldsymbol{\nu}\right) = (\boldsymbol{v}_0, \boldsymbol{\nu}), \quad \boldsymbol{\nu} \in \mathcal{V}_h. \tag{3.12}$$

However, we cannot find $\boldsymbol{\sigma}_h^0$ using

$$\left(\mathcal{A}_\infty \boldsymbol{\sigma}_h^0, \boldsymbol{\tau}\right) + \left(\boldsymbol{v}_h^0, \nabla_h \cdot \boldsymbol{\tau}\right) - < \boldsymbol{v}_h^0, \boldsymbol{\tau}\boldsymbol{n} >_\Gamma = 0, \quad \boldsymbol{\tau} \in \boldsymbol{\Sigma}_h.$$

as this results in a nonsingular matrix. Instead, at t=0, consider

$$-\nabla \cdot \boldsymbol{\sigma} = \boldsymbol{f}_f - \rho_f \boldsymbol{v}_t = \boldsymbol{g}, \tag{3.13a}$$

$$\mathcal{A}_\infty \boldsymbol{\sigma} - \epsilon(\boldsymbol{v}) = 0. \tag{3.13b}$$

As the application of the conforming Arnold Winther MFEM to this problem has already been studied in [27], the convergence rate of (3.13) would be known assuming that $\boldsymbol{g}$ is found with enough accuracy. Therefore, consider (3.5a) at t=0

$$-2\mu_f \nabla \cdot \boldsymbol{\epsilon}(\boldsymbol{v}^0) + \nabla p^0 = \boldsymbol{f}_f - \rho_f \boldsymbol{v}_t = \boldsymbol{g}. \tag{3.14}$$

Since $\boldsymbol{v}^0$ is given as the initial condition, we can approximate $\boldsymbol{g}$ if we can approximate p^0.

Therefore we consider the work of Heywood [54] which notes that, for the system 3.5, pressure at $t = 0$ may be found using an overdetermined Neumann system, if the boundary is clamped, i.e. $\boldsymbol{v}_d = 0$ and $\Gamma_N = \emptyset$. This statement is arrived at by applying the divergence operator to the momentum equation. Specifically, consider the divergence applied to (3.5a) at $t = 0$ which gives

$$\triangle p^0 = \nabla \cdot \boldsymbol{f}_f^0 \qquad \text{in } \Omega, \tag{3.15a}$$

$$\nabla p^0 \cdot \boldsymbol{n} = 2\mu_f \nabla \cdot \boldsymbol{\epsilon}(\boldsymbol{v}_d^0) \cdot \boldsymbol{n} + \boldsymbol{f}_f^0 \cdot \boldsymbol{n} \quad \text{on } \partial\Omega. \tag{3.15b}$$

For these boundary conditions, a compatibility condition as seen in (3.6) is used. For more information see [81]. Finding an approximate solution for the Poisson equation (3.15) requires another finite element or finite difference method. This method must be accurate enough to ensure the convergence rate of stress. For purposes of this dissertation, we will use the methods available in $\mathrm{F_FW}$ [24] as a black box to find a finite element approximation p_h^0 to the solution of (3.15), p^0. Therefore we expect a bound of the form

$$\|p^0 - p_h^0\| \leq Ch^r \|p^0\|_r, \tag{3.16}$$

where the value of r is determined by the chosen finite element space. Note that this will require certain regularity of the solution p^0. For certain cases, such as pure Neumann boundary conditions and a smooth $\partial\Omega$

$$\|p^0\|_2 \leq C\|f\|,$$

where f is the right hand side function of (3.15a), see for example [46] for the case of homogeneous boundary conditions. This may sufficient when using a nonconforming element for approximating (3.11). However, when dealing with a conforming element the following extension may be used [45, 29]

$$\|p^0\|_{m+2} \leq C\|f\|_m + \|\boldsymbol{v}_d\|_{m+2-1/2,\partial\Omega},$$

for certain boundary classifications.

Once p_h^0 is found with sufficient accuracy we approximate $\boldsymbol{g}$ with

$$\boldsymbol{g}_h = -2\mu_f \nabla \cdot \boldsymbol{\epsilon}(\boldsymbol{v}^0) + \nabla p_h^0 \tag{3.17}$$

Finally, $\boldsymbol{\sigma}_h^0$ is found by seeking $(\widehat{\boldsymbol{v}_h}^0, \boldsymbol{\sigma}_h^0) \in (\mathcal{V}_h, \boldsymbol{\Sigma}_h)$

$$-\left(\nabla_h \cdot \boldsymbol{\sigma}_h^0, \boldsymbol{\nu}\right) = \left(\boldsymbol{g}_h, \boldsymbol{\nu}\right), \qquad \boldsymbol{\nu} \in \mathcal{V}_h, \tag{3.18a}$$

$$\left(\mathcal{A}_\infty \boldsymbol{\sigma}_h^0, \boldsymbol{\tau}\right) + \left(\widehat{\boldsymbol{v}_h}^0, \nabla_h \cdot \boldsymbol{\tau}\right) =< \boldsymbol{v}_h^0, \boldsymbol{\tau}\boldsymbol{n} >_\Gamma, \quad \boldsymbol{\tau} \in \boldsymbol{\Sigma}_h. \tag{3.18b}$$

Note that $\widehat{\boldsymbol{v}_h}^0$ is also an approximation to $\boldsymbol{v}_0$. However we use the projection approximation from (3.12) as our approximation to $\boldsymbol{v}_0$.

Lemma 3.2.1. *Let $\boldsymbol{g}$ be defined by* (3.14) *and $\boldsymbol{g}_h$ be as defined in* (3.17). *Then*

$$\|\boldsymbol{g} - \boldsymbol{g}_h\| \leq Ch^{r-1}\|p^0\|_r. \tag{3.19}$$

Proof. Consider the difference between (3.14) and (3.17)

$$\boldsymbol{g} - \boldsymbol{g}_h = \nabla\left(p^0 - p_h^0\right).$$

The desired result is obtained using the bound (3.16) and noting the effect of the gradient.

□

Theorem 3.2.2. *For some $\boldsymbol{g}_h$, the solutions to* (3.13) *and* (3.18) *converge at the same rate.*

Proof. If the finite element method used to find p_h^0 is accurate enough to ensure that (3.19) is converging at a faster rate than solutions to (3.13), then the solution to (3.18) converges at the same rate. □

We will choose a finite element space for (3.18) such that $r-1$ is larger than the expected convergence rate from the mixed finite element space used for (3.11). For example, when using the conforming element we chose the P^3 element when finding p_h^0 so $r = 4$.

For completeness, we state the fully discrete model. Find $(\boldsymbol{\sigma}_h^{n+1}, \boldsymbol{v}_h^{n+1}) \in (\boldsymbol{\Sigma}_h, \mathcal{V}_h), 0 \leq n \leq N-1$ such that

$$\left(\boldsymbol{v}^0, \boldsymbol{\nu}\right) = \left(\boldsymbol{v}_0, \boldsymbol{\nu}\right), \qquad \boldsymbol{\nu} \in \mathcal{V}_h, \tag{3.20a}$$

$$-\left(\nabla_h \cdot \boldsymbol{\sigma}_h^0, \boldsymbol{\nu}\right) = \left(\boldsymbol{g}_h, \boldsymbol{\nu}\right), \qquad \boldsymbol{\nu} \in \mathcal{V}_h, \tag{3.20b}$$

$$\left(\mathcal{A}_\infty \boldsymbol{\sigma}_h^0, \boldsymbol{\tau}\right) + \left(\widehat{\boldsymbol{v}_h}^0, \nabla_h \cdot \boldsymbol{\tau}\right) =< \boldsymbol{v}_h^0, \boldsymbol{\tau}\boldsymbol{n} >_\Gamma, \qquad \boldsymbol{\tau} \in \boldsymbol{\Sigma}_h, \tag{3.20c}$$

$$\rho_f \left(\partial_t v^{n+1/2}, \boldsymbol{\nu}\right) - \left(\nabla_h \cdot \overline{\boldsymbol{\sigma}_h^{n+1/2}}, \boldsymbol{\nu}\right) = \left(\overline{\boldsymbol{f}_f^{n+1/2}}, \boldsymbol{\nu}\right), \qquad \boldsymbol{\nu} \in \mathcal{V}_h, \quad n \geq 0, \tag{3.20d}$$

$$\left(\mathcal{A}_\infty \overline{\boldsymbol{\sigma}_h^{n+1/2}}, \boldsymbol{\tau}\right) + \left(\overline{\boldsymbol{v}_h^{n+1/2}}, \nabla_h \cdot \boldsymbol{\tau}\right) - < \overline{\boldsymbol{v}_h^{n+1/2}}, \boldsymbol{\tau}\boldsymbol{n} >_\Gamma = 0, \quad \boldsymbol{\tau} \in \boldsymbol{\Sigma}_h, \quad n \geq 0. \tag{3.20e}$$

3.2.2 Numerical results

Here we perform some computations using the numerical model expressed in (3.20) to confirm expected convergence results. Again we use two test problems.

Fluid Example 1

First we consider the following example referred to as Fluid example 1. Let $\Omega = (0,1) \times (0,1)$. Let the analytic solution for velocity be

$$\boldsymbol{v} = \begin{bmatrix} e^t \sin(x)\sin(y) \\ e^t \cos(x)\cos(y) \end{bmatrix}.$$

The other variables $\boldsymbol{\sigma}$ and $\boldsymbol{f}_f$ are calculated from this result.

$$\boldsymbol{f}_f = \begin{bmatrix} e^t(\rho_f - 2\mu_f)\sin(x)\sin(y) \\ e^t(\rho_f - 2\mu_f)\cos(x)\cos(y) \end{bmatrix}.$$

As in the previous section, we use mixed boundary conditions and $\mu_f = 8.9x10^{-4}$. Table 3.1 shows a convergence study for this example using the conforming element. Both variables appear to have a second order convergence rate. This is expected as the method is second order in time. Table 3.2 shows the results of a convergence study using the nonconforming element. In this case, the rate of convergence for the stress variable is less than when using the conforming element, as is expected.

Figures 3.2 and 3.3 show example graphs for the displacement and stress for comparisons to the analytic solutions. In both figures we see the results from using the conforming element, on the left, the results using the nonconforming element, on the right, and the graphs of the analytic solution, at the bottom, are quite similar.

Fluid Example 2

Secondly, we consider the test problem from [69]. This will be referred to as Fluid Example 2. Let the analytic solution for velocity be

$$\boldsymbol{v} = \begin{bmatrix} \cos(x+t)\sin(y+t) + \sin(x+t)\cos(y+t) \\ -\sin(x+t)\cos(y+t) - \cos(x+t)\sin(y+t) \end{bmatrix}.$$

The other variables $\boldsymbol{\sigma}$ and $\boldsymbol{f}_f$ are calculated from this result.

We again preform convergence studies where h and Δt are reduced by a factor of two in each refinement. The results of such a study using the conforming element are shown in Table 3.3 and Figure 3.5. The expected second order convergence rate is seen from both variables. The results in Table 3.4 and Figure 3.8 are obtain using the same example and the nonconforming element. The observed rate of convergence for the stress variable is one in this case, as expected when using the nonconforming element.

Table 3.1: Convergence study for Fluid Example 1 with the conforming element

h	Δt	$\|\boldsymbol{v} - \boldsymbol{v}_h\|_{L^\infty_{\Delta t}(\Omega)}$	Order	$\|\boldsymbol{\sigma} - \boldsymbol{\sigma}_h\|_{L^\infty_{\Delta t}(\Omega)}$	Order
$\frac{1}{2}$	1.000E-01	3.952E-02	—	3.931E-04	—
$\frac{1}{4}$	5.000E-02	9.845E-03	2.01	1.046E-04	1.91
$\frac{1}{8}$	2.500E-02	2.459E-03	2.00	2.705E-05	1.95
$\frac{1}{16}$	1.250E-02	6.147E-04	2.00	6.864E-06	1.98
$\frac{1}{32}$	6.250E-03	1.537E-04	2.00	1.726E-06	1.99
$\frac{1}{64}$	3.125E-03	3.842E-05	2.00	4.326E-07	2.00

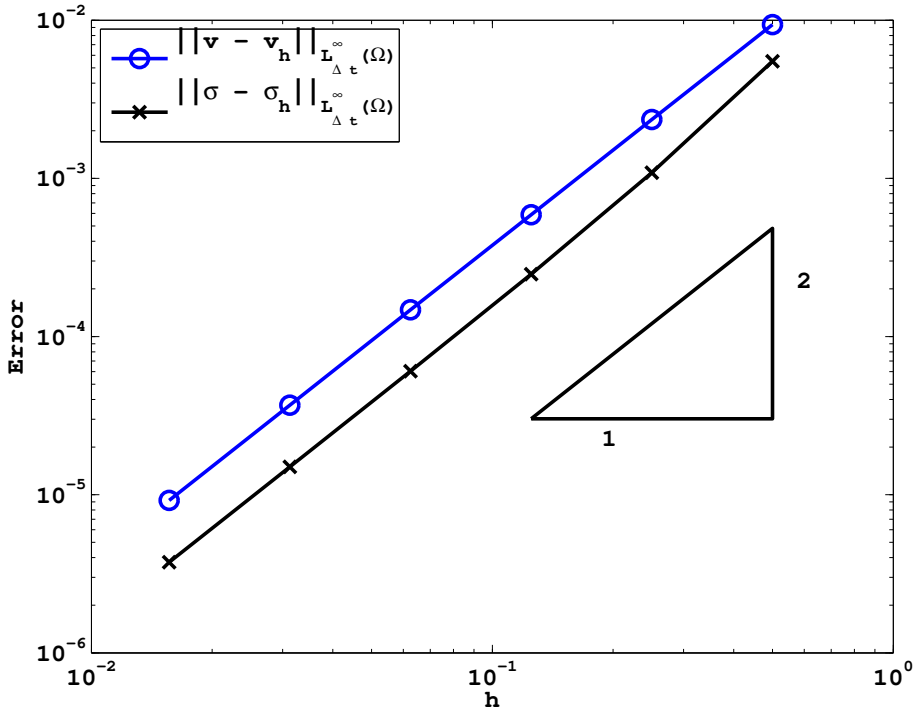

Figure 3.1: Graphical representation of the convergence study results for Fluid Example 1 with the conforming element

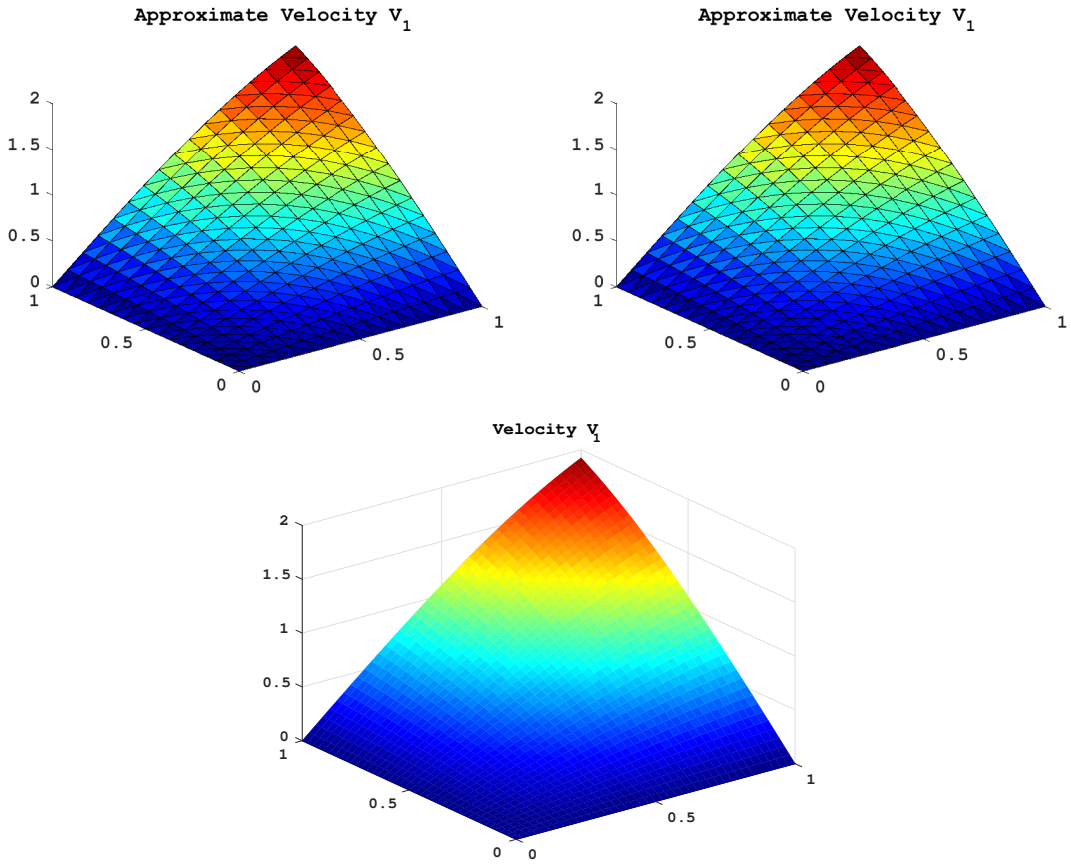

Figure 3.2: Solution graphs for the first component of velocity, $\boldsymbol{v}_1$ for fluid example 1 at $T_f = 1$ with $h = \frac{1}{16}$ and $\Delta t = 1.25 \times 10^{-2}$: using the conforming element (left), using the nonconforming element (right), and the exact analytic solution (bottom).

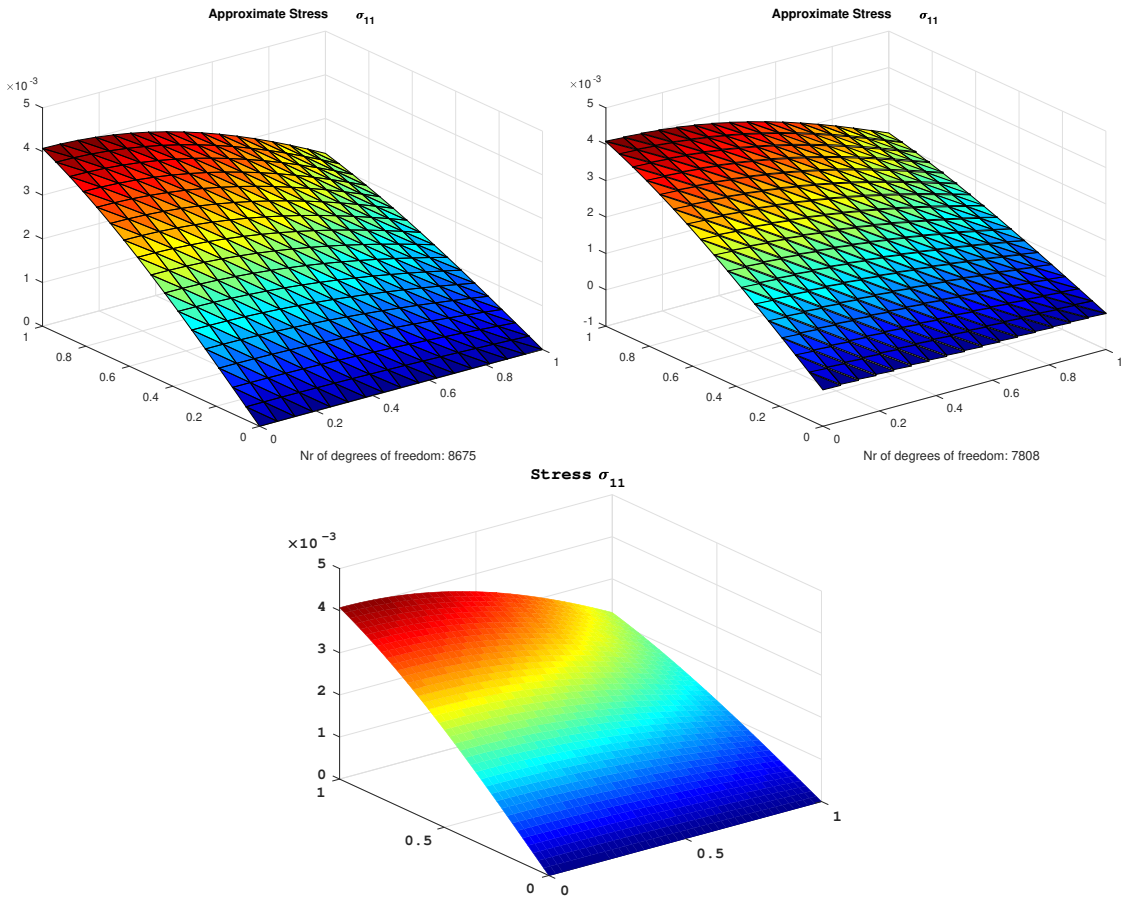

Figure 3.3: Solution graphs for the first component of stress, $\boldsymbol{\sigma}_{11}$ for fluid example 1 at $T_f = 1$ with $h = \frac{1}{16}$ and $\Delta t = 1.25 \times 10^{-2}$: using the conforming element (left), using the nonconforming element (right), and the exact analytic solution (bottom).

Table 3.2: Convergence study for the Fluid Example 1 with the nonconforming element

h	Δt	$\|\boldsymbol{v} - \boldsymbol{v}_h\|_{L^\infty_{\Delta t}(\Omega)}$	Order	$\|\boldsymbol{\sigma} - \boldsymbol{\sigma}_h\|_{L^\infty_{\Delta t}(\Omega)}$	Order
$\frac{1}{2}$	1.000E-01	3.960E-02	—	3.198E-04	—
$\frac{1}{4}$	5.000E-02	9.870E-03	2.00	1.141E-04	1.49
$\frac{1}{8}$	2.500E-02	2.468E-03	2.00	4.228E-05	1.43
$\frac{1}{16}$	1.250E-02	6.172E-04	2.00	1.863E-05	1.18
$\frac{1}{32}$	6.250E-03	1.543E-04	2.00	8.998E-06	1.05
$\frac{1}{64}$	3.125E-03	3.857E-05	2.00	4.467E-06	1.01

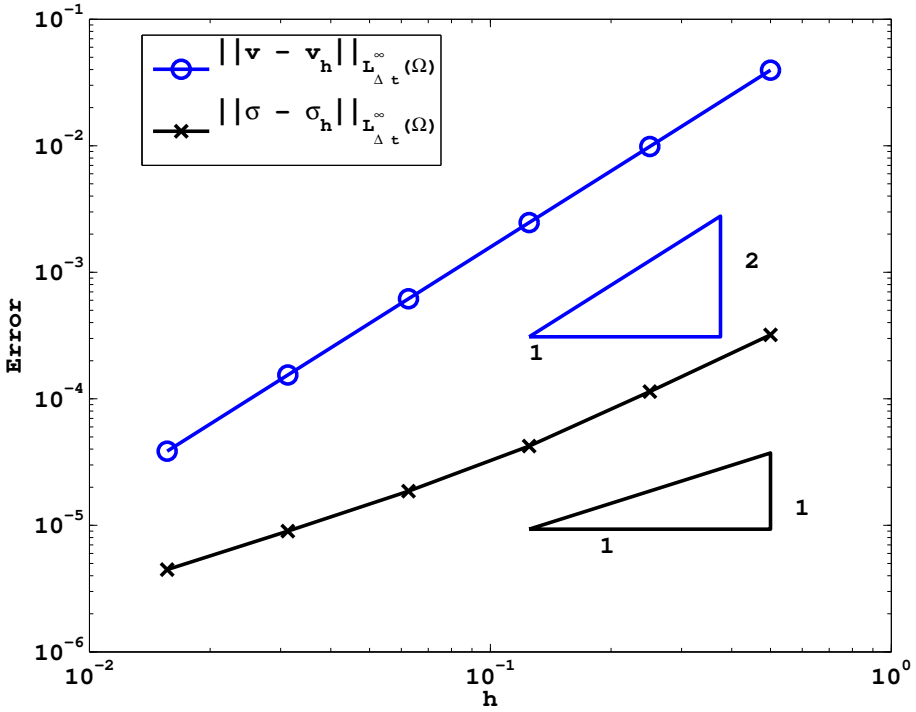

Figure 3.4: Graphical representation of the convergence study results for Fluid Example 1 with the nonconforming element

Table 3.3: Convergence study for Fluid Example 2 with the conforming element

h	Δt	$\|\boldsymbol{v} - \boldsymbol{v}_h\|_{L^\infty_{\Delta t}(\Omega)}$	Order	$\|\boldsymbol{\sigma} - \boldsymbol{\sigma}_h\|_{L^\infty_{\Delta t}(\Omega)}$	Order
$\frac{1}{2}$	1.000E-01	9.374E-03	—	5.501E-03	—
$\frac{1}{4}$	5.000E-02	2.354E-03	1.99	1.086E-03	2.34
$\frac{1}{8}$	2.500E-02	5.892E-04	2.00	2.477E-04	2.13
$\frac{1}{16}$	1.250E-02	1.474E-04	2.00	6.032E-05	2.04
$\frac{1}{32}$	6.250E-03	3.685E-05	2.00	1.499E-05	2.01
$\frac{1}{64}$	3.125E-03	9.212E-06	2.00	3.743E-06	2.00

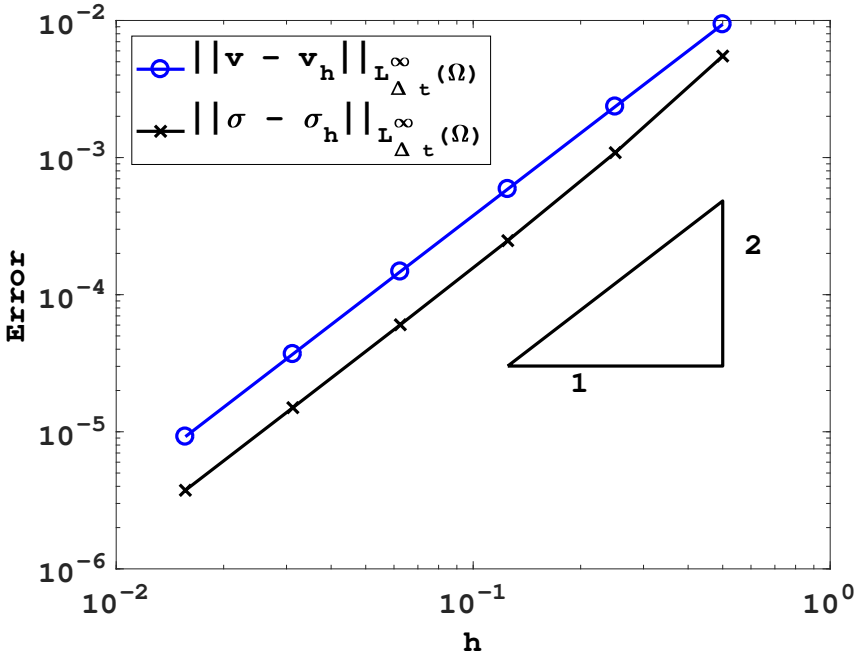

Figure 3.5: Graphical representation of the convergence study results for Fluid Example 1 with the conforming element

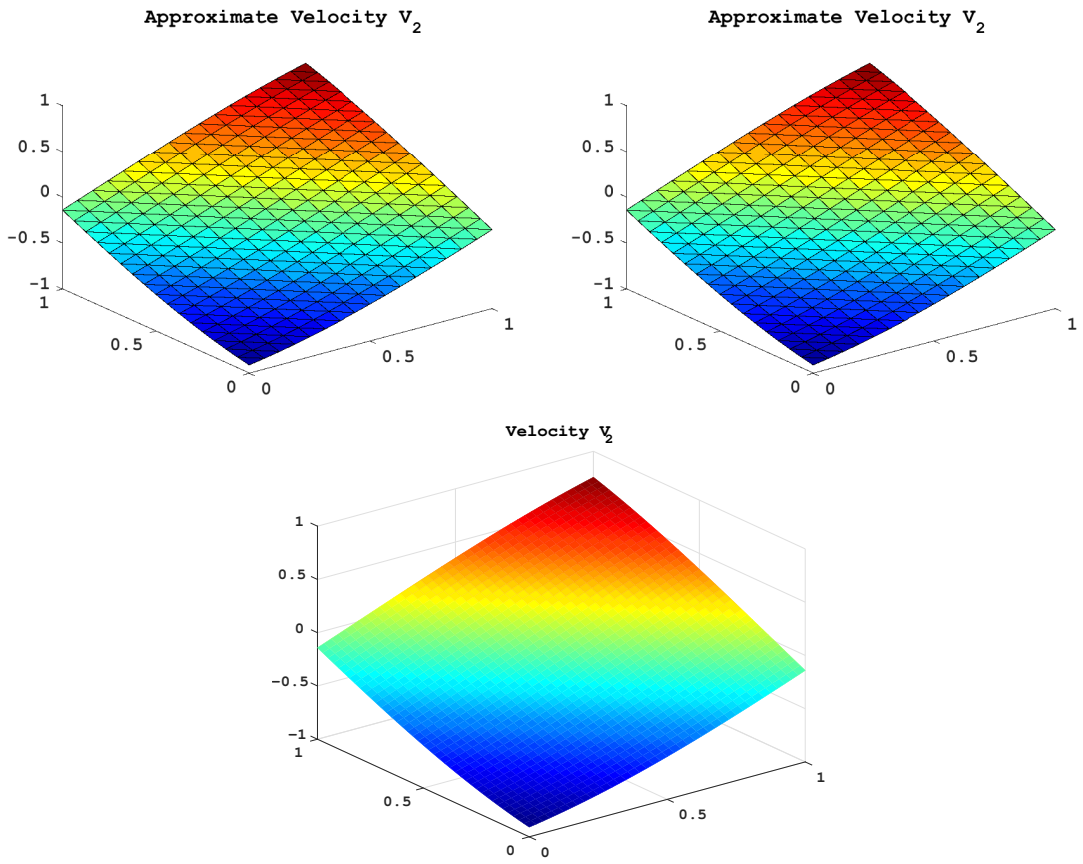

Figure 3.6: Solution graphs for the second component of velocity, $\boldsymbol{v}_2$ for example 2 at $T_f = 1$ with $h = \frac{1}{16}$ and $\Delta t = 1.25 \times 10^{-2}$: using the conforming element (left), using the nonconforming element (right), and the exact analytic solution (bottom).

Figures 3.6 and 3.7 show example graphs for the displacement and stress for comparisons with the analytic solutions. In both figures we see that the results from using both elements are quite similar to the analytic solution.

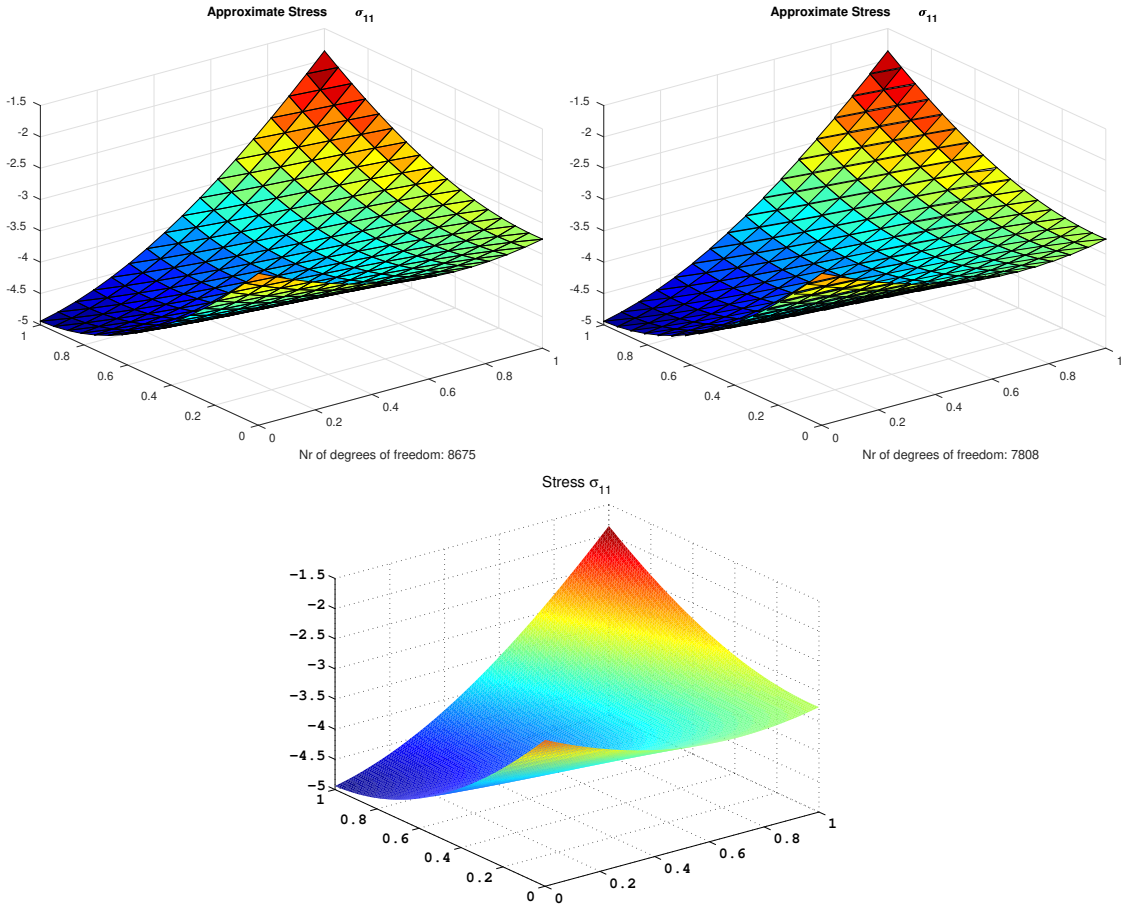

Figure 3.7: Solution graphs for the first component of stress, $\boldsymbol{\sigma}_{11}$ for example 2 at $T_f = 1$ with $h = \frac{1}{16}$ and $\Delta t = 1.25 \times 10^{-2}$: using the conforming element (left), using the nonconforming element (right), and the exact analytic solution (bottom).

Table 3.4: Convergence study for Fluid Example 2 with the nonconforming element

h	Δt	$\|\boldsymbol{v} - \boldsymbol{v}_h\|_{L^\infty_{\Delta t}(\Omega)}$	Order	$\|\boldsymbol{\sigma} - \boldsymbol{\sigma}_h\|_{L^\infty_{\Delta t}(\Omega)}$	Order
$\frac{1}{2}$	1.000E-01	9.858E-03	—	7.450E-02	—
$\frac{1}{4}$	5.000E-02	2.469E-03	2.00	3.744E-02	0.99
$\frac{1}{8}$	2.500E-02	6.169E-04	2.00	1.815E-02	1.04
$\frac{1}{16}$	1.250E-02	1.539E-04	2.00	8.901E-03	1.03
$\frac{1}{32}$	6.250E-03	3.841E-05	2.00	4.401E-03	1.02
$\frac{1}{64}$	3.125E-03	9.591E-06	2.00	2.188E-03	1.01

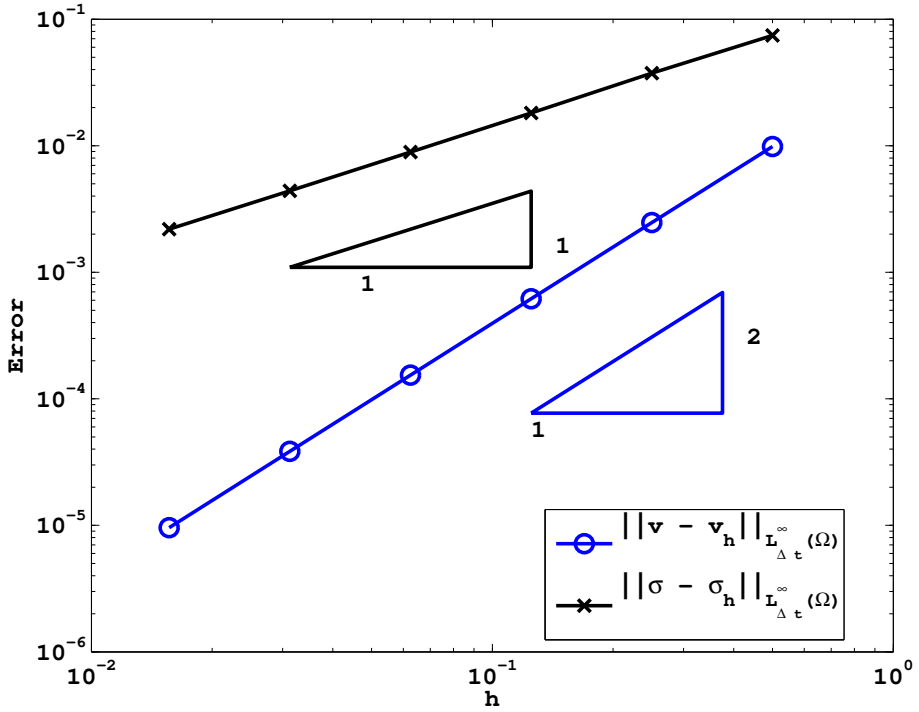

Figure 3.8: Graphical representation of the convergence study results for Fluid Example 2 with the nonconforming element

Chapter 4

Mixed Finite Element Methods for Fluid Structure Interactions

In this chapter, the models in the previous chapters will be combined to study the interaction between a fluid and solid. This interaction problem will also require some interface equations that describe the interaction between the different materials. Specifically, we consider interface conditions which enforce continuity of the velocity and stress force.

4.1 Preliminaries and Notations

Let Ω be a bounded domain in $\mathbb{R}^2$ with boundary $\partial\Omega$ and an outward normal $\boldsymbol{n}$. This domain may be divided into a solid region, Ω_s and a fluid region Ω_f such that $\Omega = \Omega_s \bigcup \Omega_f$. Let $\partial\Omega_s$ denote the boundary of the solid region with the outward normal vector $\boldsymbol{n}_s$ and similarly $\partial\Omega_f$ denotes the boundary of the fluid region with the outward normal vector $\boldsymbol{n}_f$. With this division, there is a portion of the boundary that is shared by the solid and fluid domains. This is referred to as the interface and is denoted $\Gamma = \partial\Omega_s \bigcap \partial\Omega_f$. Along this interface certain conditions apply. The boundary of Ω is divided as $\partial\Omega = \partial\Omega_s \bigcup \partial\Omega_f \setminus \Gamma$. Note that for simplicity, we have considered only a single interface. However these arguments can be extended to include multiple interfaces and domains. Figure 4.1 shows a simple domain.

Furthermore, the domain will be divided into a finite number of elements. Let $\mathcal{T}_h$ be a family of triangulations of Ω into elements T_i, $i = 1, 2, ..., I$ of size $\mathcal{O}(h)$. The notations T_{sj} , $j = 1, 2, ..., J$ and T_{fk}, $k = 1, 2, ..., K$ with $J + K = I$ are used to specify whether an element lies in the solid or fluid region, respectively. For this study, no element may

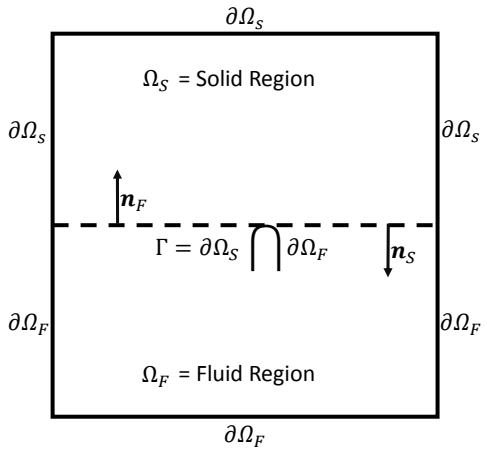

Figure 4.1: Model domain.

be in both the fluid and solid subdomains. That is, the interface Γ falls between elements. Denote by ${\Gamma^s}_{j,k} = {\Gamma^s}_{k,j} = \partial T_{sj} \bigcup \partial T_{sk}$ the edges shared by elements j and k in the solid domain. These are referred to as interior edges of the solid domain and the set of all interior edges of the solid domain is denoted by $\mathcal{E}_{sh} = \bigcup_{j,k} {\Gamma^s}_{j,k}$. Similarly in the fluid domain we have interior edges ${\Gamma^f}_{j,k} = {\Gamma^f}_{k,j} = \partial T_{f_j} \bigcup \partial T_{f_k}$ and the set of interior edges in the fluid domain is $\mathcal{E}_{fh} = \bigcup_{j,k} {\Gamma^f}_{j,k}$. The outward normal vector to the boundary of an element T_{sj} is denoted $\boldsymbol{n}_{s,j}$. Notice that for adjacent elements T_{sj} and T_{sk} on the shared edge ${\Gamma^s}_{j,k}$ the outward normal vectors have opposite direction, $\boldsymbol{n}_{s,j} = -\boldsymbol{n}_{s,k}$. A similar notation is used for the fluid elements. Therefore the notation $\boldsymbol{n}$ is used to denote the normal to an edge in a globally defined direction.

We will be presenting a unified finite element model and error analysis in this the following sections. The intentions is to provide an analysis for both conforming and non-conforming analysis. To this end, we will use the element wise divergence $\nabla_h \cdot$ in our presentation. This is used with the understanding that in the conforming case, this is the same as standard divergence $\nabla \cdot$. Additionally, we will present our analysis with consistency error terms which arise when nonconforming methods are used. This is done with the

understanding that when a conforming mixed finite element space is used, this consistency error is zero.

4.2 Fluid Structure Interaction

In the subdomain Ω_s we consider an elastic solid governed by the Hellinger-Reissner form of the elasticity equations as stated in (2.6). In the subdomain Ω_f we consider the slow flow governed by the equations as stated in (3.4). For completeness, the equations are

$$\rho_s \boldsymbol{u}_{tt} - \nabla \cdot \boldsymbol{\sigma}_s = \boldsymbol{f}_s \quad \text{in } \Omega_s, \tag{4.1a}$$

$$\mathcal{A}\boldsymbol{\sigma}_s - \epsilon(\boldsymbol{u}) = 0 \quad \text{in } \Omega_s, \tag{4.1b}$$

$$\rho_f \boldsymbol{v}_t - \nabla \cdot \boldsymbol{\sigma}_f = \boldsymbol{f}_f \quad \text{in } \Omega_f, \tag{4.1c}$$

$$\mathcal{A}_\infty \boldsymbol{\sigma}_f - \epsilon(\boldsymbol{v}) = 0 \quad \text{in } \Omega_f. \tag{4.1d}$$

Recall from section 2.4.1 that we have differentiated the solid equation (4.1b) with respect to time. Therefore, we consider the case where (4.1b) may replaced with

$$\mathcal{A}(\boldsymbol{\sigma}_s)_t - \epsilon(\boldsymbol{u}_t) = 0 \qquad \text{in } \Omega_s. \tag{4.2}$$

On the exterior boundary $\partial\Omega_s \bigcup \partial\Omega_f \setminus \Gamma$ the boundary conditions are chosen as clamped or no-slip

$$\boldsymbol{u} = \boldsymbol{0} \quad \text{on } \partial\Omega_s \setminus \Gamma,$$

$$\boldsymbol{v} = \boldsymbol{0} \quad \text{on } \partial\Omega_f \setminus \Gamma,$$

and the initial conditions are

$$\boldsymbol{u}(\cdot, 0) = \boldsymbol{u}_0 \quad \text{in } \Omega_s,$$

$$\boldsymbol{u}_t(\cdot, 0) = \boldsymbol{s}_0 \quad \text{in } \Omega_s,$$

$$\boldsymbol{v}(\cdot, 0) = \boldsymbol{v}_0 \quad \text{in } \Omega_f.$$

Along the interface Γ additional interface conditions must be imposed. These conditions are obtained by enforcing continuity of velocity and normal component of stress along this

interface

$$\boldsymbol{u}_t = \boldsymbol{v} \qquad \text{on } \Gamma, \tag{4.3a}$$

$$\boldsymbol{\sigma}_s \boldsymbol{n}_s = -\boldsymbol{\sigma}_f \boldsymbol{n}_f \quad \text{on } \Gamma. \tag{4.3b}$$

In the interest of stating a variational formulation we introduce the notation

$$\boldsymbol{\sigma} = \begin{cases} \boldsymbol{\sigma}_s & \text{in } \Omega_s, \\ \boldsymbol{\sigma}_f & \text{in } \Omega_f, \end{cases}$$

$$\boldsymbol{\omega} = \begin{cases} \boldsymbol{u} & \text{in } \Omega_s, \\ \boldsymbol{v} & \text{in } \Omega_f, \end{cases}$$

$$\boldsymbol{f} = \begin{cases} \boldsymbol{f}_s & \text{in } \Omega_s, \\ \boldsymbol{f}_f & \text{in } \Omega_f \end{cases}$$

and the solution spaces

$$\boldsymbol{\Sigma} = \boldsymbol{H}(\mathrm{div}; \Omega; \mathbb{S}),$$
$$\mathcal{V} = (L^2(\Omega))^2.$$

Then, the weak form of (4.1) seeks to find $(\boldsymbol{\sigma}, \boldsymbol{\omega}) \in (\mathcal{C}^1(0, T; \boldsymbol{\Sigma}), \mathcal{C}^2(0, T; \mathcal{V}))$ such that

$$(\boldsymbol{u}(0),\boldsymbol{\nu})_{\Omega_s}+(\boldsymbol{v}(0),\boldsymbol{\nu})_{\Omega_f}=(\boldsymbol{u}_0,\boldsymbol{\nu})_{\Omega_s}+(\boldsymbol{v}_0,\boldsymbol{\nu})_{\Omega_f}\,, \qquad \boldsymbol{\nu}\in\mathcal{V}, \tag{4.4a}$$

$$\begin{aligned}&(\mathcal{A}\boldsymbol{\sigma}_s(0),\boldsymbol{\tau})_{\Omega_s}+(\mathcal{A}_\infty\boldsymbol{\sigma}_f(0),\boldsymbol{\tau})_{\Omega_f}+(\boldsymbol{u}_0,\nabla\cdot\boldsymbol{\tau})_{\Omega_s}+(\boldsymbol{v}_0,\nabla\cdot\boldsymbol{\tau})_{\Omega_f}\\ &\qquad =<\boldsymbol{u}_0,\boldsymbol{\tau}\boldsymbol{n}_s>_\Gamma+<\boldsymbol{v}_0,\boldsymbol{\tau}\boldsymbol{n}_f>_\Gamma, \qquad \boldsymbol{\tau}\in\boldsymbol{\Sigma},\end{aligned} \tag{4.4b}$$

$$(\boldsymbol{u}_t(0),\boldsymbol{\nu})_{\Omega_s}=(\boldsymbol{s}_0,\boldsymbol{\nu})_{\Omega_s}\,, \qquad \boldsymbol{\nu}\in\mathcal{V}, \tag{4.4c}$$

$$\begin{aligned}&\rho_s\,(\boldsymbol{u}_{tt}(t),\boldsymbol{\nu})_{\Omega_s}+\rho_f\,(\boldsymbol{v}_t(t),\boldsymbol{\nu})_{\Omega_f}-(\nabla\cdot\boldsymbol{\sigma}_s(t),\boldsymbol{\nu})_{\Omega_s}-(\nabla\cdot\boldsymbol{\sigma}_f(t),\boldsymbol{\nu})_{\Omega_f}\\ &\qquad =(\boldsymbol{f}_s(t),\boldsymbol{\nu})_{\Omega_s}+(\boldsymbol{f}_f(t),\boldsymbol{\nu})_{\Omega_f}\,, \qquad \boldsymbol{\nu}\in\mathcal{V},\quad t>0,\end{aligned} \tag{4.4d}$$

$$\begin{aligned}&(\mathcal{A}(\boldsymbol{\sigma}_s)_t(t),\boldsymbol{\tau})_{\Omega_s}+(\mathcal{A}_\infty\boldsymbol{\sigma}_f(t),\boldsymbol{\tau})_{\Omega_f}+(\boldsymbol{u}_t(t),\nabla\cdot\boldsymbol{\tau})_{\Omega_s}+(\boldsymbol{v}(t),\nabla\cdot\boldsymbol{\tau})_{\Omega_f}\\ &\qquad =<\boldsymbol{u}_t(t),\boldsymbol{\tau}\boldsymbol{n}_s>_\Gamma+<\boldsymbol{v}(t),\boldsymbol{\tau}\boldsymbol{n}_f>_\Gamma, \qquad \boldsymbol{\tau}\in\boldsymbol{\Sigma},\quad t>0.\end{aligned} \tag{4.4e}$$

Recall from section 2.4.1 that we have differentiated the solid equation 4.1*b* with respect to time. This has the following additional benefit. Consider the terms occurring on the interface in (4.4e)

$$I=<\boldsymbol{u}_t(t),\boldsymbol{\tau}\boldsymbol{n}_s>_\Gamma+<\boldsymbol{v}(t),\boldsymbol{\tau}\boldsymbol{n}_f>_\Gamma\,.$$

On the interface, $\boldsymbol{v}=\boldsymbol{u}_t$. Therefore

$$I=<\boldsymbol{u}_t(t),\boldsymbol{\tau}\boldsymbol{n}_s+\boldsymbol{\tau}\boldsymbol{n}_f>_\Gamma\,.$$

Recall that $\boldsymbol{n}_s$ and $\boldsymbol{n}_f$ are outward normals to the interface and therefore have opposite sign. So if we consider a normal to the interface in a global direction $\boldsymbol{n}=\boldsymbol{n}_s=-\boldsymbol{n}_f$ then the interface term can be expressed as

$$I=<\boldsymbol{u}_t(t),[\boldsymbol{\tau}\boldsymbol{n}]>_\Gamma\,.$$

However for $\boldsymbol{\tau}\in\boldsymbol{\Sigma}$, $I=0$.

4.2.1 Fully Discrete Implicit in Time Method

We begin by expressing our proposed fully discrete model for a time step where $n \geq 1$. Then we will describe the needed initial conditions. As above, we will use

$$\boldsymbol{\sigma}_h = \begin{cases} \boldsymbol{\sigma}_{s_h} & \text{in } \Omega_s, \\ \boldsymbol{\sigma}_{f_h} & \text{in } \Omega_f, \end{cases}$$

and

$$\boldsymbol{\omega}_h = \begin{cases} \boldsymbol{u}_h & \text{in } \Omega_s, \\ \boldsymbol{v}_h & \text{in } \Omega_f. \end{cases}$$

Also let $\mathcal{V}_h$ and $\boldsymbol{\Sigma}_h$ be appropriate mixed finite element spaces for the Hellinger-Reissner formulation. We assume that these spaces have the following properties like the Arnold-Winther spaces discussed in Chapter 2. First, $\mathcal{P}_h : (L^2(\Omega))^2 \to \mathcal{V}_h$ is the orthogonal projection. Then, $\Pi_h : \boldsymbol{H}^1(\Omega, \mathbb{S}) \to \boldsymbol{\Sigma}_h$ is a corresponding interpolation for tensors with the additional property that

$$\nabla_h \cdot \Pi_h \boldsymbol{\tau} = \mathcal{P}_h \nabla \cdot \boldsymbol{\tau} \quad \boldsymbol{\tau} \in \boldsymbol{H}^1(\Omega, \mathbb{S}). \tag{4.5}$$

This additional property gives $\nabla_h \cdot \boldsymbol{\Sigma}_h = \mathcal{V}_h$.

Since $\mathcal{P}_h$ is the orthogonal projection, for $\boldsymbol{u} \in (L^2(\Omega))^2$

$$(\boldsymbol{u} - \mathcal{P}_h \boldsymbol{u}, \boldsymbol{\nu}) = 0, \quad \boldsymbol{\nu} \in \mathcal{V}_h. \tag{4.6}$$

But since $\nabla_h \cdot \boldsymbol{\tau} \in \mathcal{V}_h$ for $\boldsymbol{\tau} \in \boldsymbol{\Sigma}_h$

$$(\nabla_h \cdot \boldsymbol{\tau}, \boldsymbol{u} - \mathcal{P}_h \boldsymbol{u}) = 0, \quad \boldsymbol{\tau} \in \boldsymbol{\Sigma}_h. \tag{4.7}$$

We also have

$$(\nabla_h \cdot \boldsymbol{\tau} - \nabla_h \cdot \Pi_h \boldsymbol{\tau}, \boldsymbol{\nu}) = 0 \quad \boldsymbol{\nu} \in \mathcal{V}_h \tag{4.8}$$

as a consequence of (4.5). Additionally, the following approximation properties hold:

$$\|\Pi_h \boldsymbol{\tau} - \boldsymbol{\tau}\|_0 \leq C h^{m_1} \|\boldsymbol{\tau}\|_{m_1}, \tag{4.9a}$$

$$\|\mathcal{P}_h \boldsymbol{\nu} - \boldsymbol{\nu}\|_0 \leq C h^{m_2} \|\boldsymbol{\nu}\|_{m_2}, \tag{4.9b}$$

where m_1 and m_2 are determined by the mixed finite element spaces chosen. Recall that in this notation, for a given n we assume that all pairs $(\boldsymbol{\sigma}_h^i, \boldsymbol{\omega}_h^i)$ for $i \leq n$ are known. Therefore, the unknown pair in the above system for a given n is $(\boldsymbol{\sigma}_h^{n+1}, \boldsymbol{\omega}_h^{n+1})$. We seek to find $(\boldsymbol{\sigma}_h^{n+1}, \boldsymbol{\omega}_h^{n+1}) \in (\boldsymbol{\Sigma}_h, \mathcal{V}_h), 1 \leq n \leq N-1$ such that

$$\begin{aligned}
&\rho_s \left(\partial_t^2 \boldsymbol{u}_h{}^n, \boldsymbol{\nu}\right)_{\Omega_s} + \rho_f \left(\partial_t^c \boldsymbol{v}_h^n, \boldsymbol{\nu}\right)_{\Omega_f} - \left(\nabla_h \cdot \widetilde{\boldsymbol{\sigma}_{s_h}^n}, \boldsymbol{\nu}\right)_{\Omega_s} - \left(\nabla_h \cdot \widetilde{\boldsymbol{\sigma}_{f_h}^n}, \boldsymbol{\nu}\right)_{\Omega_f} \\
&\qquad = \left(\widetilde{\boldsymbol{f}_s^n}, \boldsymbol{\nu}\right)_{\Omega_s} + \left(\widetilde{\boldsymbol{f}_f^n}, \boldsymbol{\nu}\right)_{\Omega_f}, \qquad \boldsymbol{\nu} \in \mathcal{V}_h,\ n \geq 1,
\end{aligned} \tag{4.10a}$$

$$\left(\mathcal{A} \partial_t^c \boldsymbol{\sigma}_{s_h}^n, \boldsymbol{\tau}\right)_{\Omega_s} + \left(\mathcal{A}_\infty \widetilde{\boldsymbol{\sigma}_{f_h}^n}, \boldsymbol{\tau}\right)_{\Omega_f} + \left(\partial_t^c \boldsymbol{u}_h^n, \nabla_h \cdot \boldsymbol{\tau}\right)_{\Omega_s} + \left(\widetilde{\boldsymbol{v}_h^n}, \nabla_h \cdot \boldsymbol{\tau}\right)_{\Omega_f} = 0, \quad \boldsymbol{\tau} \in \boldsymbol{\Sigma}_h,\ n \geq 1. \tag{4.10b}$$

Again, modifications are required to use the initial conditions. First, to find $(\boldsymbol{\sigma}_h^0, \boldsymbol{\omega}_h^0) \in (\boldsymbol{\Sigma}_h, \mathcal{V}_h)$ we recall the initial systems used for the elastodyanmics equations (2.49) and the initial system used for the nonstationary Stokes equations (3.18) separately. Specifically, we seek to find $(\boldsymbol{\sigma}_h^0, \boldsymbol{\omega}_h^0) \in (\boldsymbol{\Sigma}_h, \mathcal{V}_h)$ such that

$$\left(\boldsymbol{u}_h^0, \boldsymbol{\nu}\right)_{\Omega_s} + \left(\boldsymbol{v}_h^0, \boldsymbol{\nu}\right)_{\Omega_f} = \left(\boldsymbol{u}_0, \boldsymbol{\nu}\right)_{\Omega_s} + \left(\boldsymbol{v}_0, \boldsymbol{\nu}\right)_{\Omega_f}, \qquad \boldsymbol{\nu} \in \mathcal{V}_h, \tag{4.11a}$$

$$-\left(\nabla_h \cdot \boldsymbol{\sigma}_h^0, \boldsymbol{\psi}\right) = \left(\boldsymbol{g}_h, \boldsymbol{\psi}\right), \qquad \boldsymbol{\psi} \in \mathcal{V}_h, \tag{4.11b}$$

$$\begin{aligned}
&\left(\mathcal{A} \boldsymbol{\sigma}_{s_h}^0, \boldsymbol{\tau}\right)_{\Omega_s} + \left(\mathcal{A}_\infty \boldsymbol{\sigma}_h^0, \boldsymbol{\tau}\right) + \left(\boldsymbol{u}_h^0, \nabla_h \cdot \boldsymbol{\tau}\right)_{\Omega_s} + \left(\widehat{\boldsymbol{v}_h}^0, \nabla_h \cdot \boldsymbol{\tau}\right) \\
&\qquad = < \boldsymbol{u}_0, \boldsymbol{\tau} \boldsymbol{n}_s >_\Gamma + < v_0, \boldsymbol{\tau} \boldsymbol{n} >_\Gamma, \qquad \boldsymbol{\tau} \in \boldsymbol{\Sigma}_h.
\end{aligned} \tag{4.11c}$$

Here, $\boldsymbol{g}_h$ and $\widehat{\boldsymbol{v}_h}^0$ are needed to obtain an approximation to $\boldsymbol{\sigma}_h^0$ as described in Section 3.2.1. Specifically, $\boldsymbol{g}_h$ is described in (3.17) and is an approximation to the forcing function for the stationary Stokes equation and $\widehat{\boldsymbol{v}_h}^0$ is part of the solution to the stationary Stokes

system described in (3.18). Note that $\widehat{\boldsymbol{v}_h}^0$ is also an approximation to $\boldsymbol{v}_0$, but we use the projection of $\boldsymbol{v}_0$ as $\boldsymbol{v}_h^0$.

Once $\boldsymbol{\omega}_h^0$ and $\boldsymbol{\sigma}_h^0$ are found we seek to find $(\boldsymbol{\sigma}_h^1, \boldsymbol{\omega}_h^1) \in (\boldsymbol{\Sigma}_h, \mathcal{V}_h)$ such that

$$\begin{aligned}\frac{2\rho_s}{\Delta t}\left(\partial_t \boldsymbol{u}_h^{1/2}, \boldsymbol{\nu}\right)_{\Omega_s} - \left(\nabla_h \cdot \overline{\boldsymbol{\sigma}_{s_h}^{1/2}}, \boldsymbol{\nu}\right)_{\Omega_s} + \rho_f \left(\partial_t \boldsymbol{v}_h^{1/2}, \boldsymbol{\nu}\right)_{\Omega_f} - \left(\nabla_h \cdot \overline{\boldsymbol{\sigma}_{f_h}^{1/2}}, \boldsymbol{\nu}\right)_{\Omega_f} \\ = \left(\overline{\boldsymbol{f}_s^{1/2}} + \frac{2\rho_s}{\Delta t} g_0, \boldsymbol{\nu}\right)_{\Omega_s} + \left(\overline{\boldsymbol{f}_f^{1/2}}, \boldsymbol{\nu}\right)_{\Omega_f}, \qquad \boldsymbol{\nu} \in \mathcal{V}_h,\end{aligned} \tag{4.12a}$$

$$\left(\mathcal{A}\partial_t \boldsymbol{\sigma}_{s_h}^{1/2}, \boldsymbol{\tau}\right)_{\Omega_s} + \left(\mathcal{A}_\infty \overline{\boldsymbol{\sigma}_{f_h}^{1/2}}, \boldsymbol{\tau}\right)_{\Omega_f} + \left(\partial_t \boldsymbol{u}_h^{1/2}, \nabla_h \cdot \boldsymbol{\tau}\right)_{\Omega_s} + \left(\overline{\boldsymbol{v}_h^{1/2}}, \nabla_h \cdot \boldsymbol{\tau}\right)_{\Omega_f} = 0, \quad \boldsymbol{\tau} \in \boldsymbol{\Sigma}_h. \tag{4.12b}$$

4.3 Unified Error Analysis

The following sections will be concerned with the error analysis for the model described by (4.11), (4.12) and (4.10). We will make use of the following notation for auxiliary errors

$$\begin{aligned}\chi_{\boldsymbol{u}}^n &= {\boldsymbol{u}_h}^n - \mathcal{P}_h \boldsymbol{u}^n, \\ \chi_{\boldsymbol{v}}^n &= {\boldsymbol{v}_h}^n - \mathcal{P}_h \boldsymbol{v}^n, \\ \chi_{\boldsymbol{\sigma}_s}^n &= {\boldsymbol{\sigma}_{s_h}}^n - \Pi_h \boldsymbol{\sigma}_s^n, \\ \chi_{\boldsymbol{\sigma}_f}^n &= {\boldsymbol{\sigma}_{f_h}}^n - \Pi_h \boldsymbol{\sigma}_f^n\end{aligned}$$

and the following for projection errors

$$\begin{aligned}\eta_{\boldsymbol{u}}^n &= \boldsymbol{u}^n - \mathcal{P}_h \boldsymbol{u}^n, \\ \eta_{\boldsymbol{v}}^n &= \boldsymbol{v}^n - \mathcal{P}_h \boldsymbol{v}^n, \\ \eta_{\boldsymbol{\sigma}_s}^n &= \boldsymbol{\sigma}_s^n - \Pi_h \boldsymbol{\sigma}_s^n, \\ \eta_{\boldsymbol{\sigma}_f}^n &= \boldsymbol{\sigma}_f^n - \Pi_h \boldsymbol{\sigma}_f^n.\end{aligned}$$

We will also use the notation

$$C = C(\cdot)$$

to notate that C constant which depends on a value $\cdot$.

4.3.1 Useful Lemmas and Inequalities

In this section, we state some of the inequalities that will be used repeatedly in our analysis. Many of these are simple consequences of one or more well known theorems.

Theorem 4.3.1. (Young's Inequality) *For non-negative real numbers a, b and ϵ*

$$ab \leq \frac{a^2}{2\epsilon} + \frac{\epsilon b^2}{2}.$$

This form of Young's Inequality is frequently used. We will also make frequent use of the following corollary which is a direct consequence of the Triangle Inequality and Young's Inequality.

Corollary 4.3.2. *For a function of time ϕ*

$$\|\overline{\phi^{n+1/2}}\|^2 \leq \|\phi^{n+1}\|^2 + \|\phi^n\|^2. \tag{4.13}$$

We will also make use of the following inequalities pertaining to the L^∞ -norms.

Lemma 4.3.3. *For a normed space P and suitable $\phi \in C^k(0,T;P)$,*

$$\|\phi\|_{\overline{L^\infty_{\Delta t}}(P)} \leq \|\phi\|_{L^\infty_{\Delta t}(P)}, \tag{4.14a}$$

$$\|\phi\|_{\widetilde{L^\infty_{\Delta t}}(P)} \leq \|\phi\|_{\overline{L^\infty_{\Delta t}}(P)}, \tag{4.14b}$$

$$\|\phi\|_{\widetilde{L^\infty_{\Delta t}}(P)} \leq \|\phi\|_{L^\infty_{\Delta t}(P)}, \tag{4.14c}$$

$$\|\partial_t^c \phi\|_{L^\infty_{\Delta t}(P)} \leq \|\partial_t \phi\|_{\overline{L^\infty_{\Delta t}}(P)}. \tag{4.14d}$$

Proof. These inequalities are shown by recalling the definitions (2.47) and using the Triangle Inequality. First consider (4.14a)

$$\begin{aligned}
\|\phi\|_{\overline{L^\infty_{\Delta t}}(P)} &= \max_{0\leq n\leq N-1} \frac{1}{2}\|\phi^n + \phi^{n+1}\|_P \\
&\leq \frac{1}{2}\max_{0\leq n\leq N-1}\|\phi^n\|_P + \frac{1}{2}\max_{0\leq n\leq N-1}\|\phi^{n+1}\|_P \\
&\leq \|\phi\|_{L^\infty_{\Delta t}(P)}.
\end{aligned}$$

The inequalities (4.14b) (4.14d), are shown by recalling (2.42) or (2.44) respectively and using a similar argument. Now (4.14c) is obtained by combining (4.14a) and (4.14b).

□

Lemma 4.3.4. *For a function $\phi(t)$ which is sufficiently differentiable in time,*

$$\|\overline{\phi^{n+1/2}} - \phi^{n+1/2}\|^2 \leq C\Delta t^3 \int_{t^n}^{t^{n+1}} \|\phi_{tt}(s)\|^2 \, ds, \tag{4.15a}$$

$$\|\partial_t \phi^{n+1/2} - \phi_t^{n+1/2}\|^2 \leq C\Delta t^3 \int_{t^n}^{t^{n+1}} \|\phi_{ttt}(s)\|^2 \, ds, \tag{4.15b}$$

$$\|\widetilde{\phi^n} - \phi^n\|^2 \leq C\Delta t^3 \int_{t^{n-1}}^{t^{n+1}} \|\phi_{tt}(s)\|^2 \, ds, \tag{4.15c}$$

$$\|\partial_t^2 \phi^n - \phi_{tt}^n\|^2 \leq \Delta t^3 \int_{t^{n-1}}^{t^{n+1}} \|\phi_{tttt}(s)\|^2 \, ds. \tag{4.15d}$$

Proof. All of these are proved with Taylor series and Hölder's inequality. Since (4.15a) and (4.15b) are stated in [93], here we prove (4.15c). This begins with the following Taylor expansions :

$$\phi^{n+1} = \phi^n + \Delta t \phi_t^n + \int_{t^n}^{t^{n+1}} (t^{n+1} - s)\phi_{tt}(s) \, ds,$$

$$\phi^{n-1} = \phi^n - \Delta t \phi_t^n + \int_{t^n}^{t^{n-1}} (t^{n-1} - s)\phi_{tt}(s) \, ds.$$

Therefore,

$$\begin{aligned}
\widetilde{\phi^n} - \phi^n &= \frac{1}{4}\phi^{n+1} + \frac{1}{2}\phi^n + \frac{1}{4}\phi^{n-1} - \phi^n \\
&= \frac{1}{4} \int_{t^n}^{t^{n+1}} (t^{n+1} - s)\phi_{tt}(s) \, ds + \frac{1}{4} \int_{t^{n-1}}^{t^n} (s - t^{n-1})\phi_{tt}(s) \, ds \\
&\leq \Delta t \int_{t^{n-1}}^{t^{n+1}} \mid \phi_{tt}(s) \mid \, ds.
\end{aligned}$$

Finally,

$$\begin{aligned}\|\widetilde{\phi^n} - \phi^n\|^2 &= \int_\Omega (\widetilde{\phi^n} - \phi^n)^2 dx \\ &\leq \int_\Omega \left(\Delta t \int_{t^{n-1}}^{t^{n+1}} | \, \phi_{tt}(s)\, ds \, | \right)^2 dx.\end{aligned}$$

Now by using Hölder's inequality and changing the order of integration we have

$$\begin{aligned}\|\widetilde{\phi^n} - \phi^n\|^2 &\leq \Delta t^2 \int_\Omega \left(\int_{t^{n-1}}^{t^{n+1}} \phi_{tt}^2(s)\, ds \cdot \int_{t^{n-1}}^{t^{n+1}} (1)^2\, ds \right) dx \\ &\leq \Delta t^3 \int_\Omega \int_{t^{n-1}}^{t^{n+1}} \phi_{tt}^2(s)\, ds dx \\ &= \Delta t^3 \int_{t^n}^{t^{n+1}} \int_\Omega \phi_{tt}^2(s)\, dx ds \\ &= \Delta t^3 \int_{t^n}^{t^{n+1}} \|\phi_{tt}(s)\|^2\, ds.\end{aligned}$$

The other inequalities are shown with a similar series of steps. □

Corollary 4.3.5. *Under the assumptions of Lemma* 4.3.4*,*

$$\|\overline{\phi_t^{n+1/2}} - \partial_t \phi^{n+1/2}\|^2 \leq C\Delta t^3 \int_{t^n}^{t^{n+1}} \|\phi_{ttt}(s)\|^2\, ds, \tag{4.16a}$$

$$\|\widetilde{\phi_t^n} - \partial_t^c \phi^n\|^2 \leq C\Delta t^3 \int_{t^{n-1}}^{t^{n+1}} \|\phi_{ttt}(s)\|^2\, ds, \tag{4.16b}$$

$$\|\partial_t^2 \phi^n - \widetilde{\phi_t^n}\|^2 \leq C\Delta t^3 \int_{t^{n-1}}^{t^{n+1}} \|\phi_{tttt}(s)\|^2\, ds. \tag{4.16c}$$

Proof. By adding and subtracting $\phi_t^{n+1/2}$ to the right and side of (4.16a) then using Lemma (4.3.2), (4.15a) and (4.15b)

$$\begin{aligned}\|\overline{\phi_t^{n+1/2}} - \partial_t \phi^{n+1/2}\|^2 &\leq 2\left(\|\overline{\phi_t^{n+1/2}} - \phi_t^{n+1/2}\|^2 + \|\phi_t^{n+1/2} - \partial_t \phi^{n+1/2}\|^2 \right) \\ &\leq C\Delta t^3 \int_{t^n}^{t^{n+1}} \|\phi_{ttt}(s)\|^2\, ds.\end{aligned}$$

To show (4.16b), we must recall (2.42) and (2.44). Then (4.3.2) and (4.16a) are used as follows:

$$\begin{aligned}
\|\widetilde{\phi_t^n} - \partial_t^c \phi^n\|^2 &= \|\frac{1}{2}\overline{\phi_t^{n+1/2}} + \frac{1}{2}\overline{\phi_t^{n-1/2}} - \frac{1}{2}\partial_t\phi^{n+1/2} - \frac{1}{2}\partial_t\phi^{n-1/2}\|^2 \\
&= \|\frac{1}{2}\overline{\phi_t^{n+1/2}} - \frac{1}{2}\partial_t\phi^{n+1/2} + \frac{1}{2}\overline{\phi^{n-1/2}} - \frac{1}{2}\partial_t\phi^{n-1/2}\|^2 \\
&\leq \|\overline{\phi_t^{n+1/2}} - \partial_t\phi^{n+1/2}\|^2 + \|\overline{\phi_t^{n-1/2}} - \partial_t\phi^{n-1/2}\|^2 \\
&\leq C\Delta t^3 \int_{t^{n-1}}^{t^{n+1}} \|\phi_{ttt}(s)\|^2 \, ds.
\end{aligned}$$

Similarly (4.16c) follows from (4.15d) and (4.15c). □

Finally, we will make frequent use of the following lemma which is merely a combination of Young's Inequality and Hölder's inequality.

Lemma 4.3.6. *Let the final time for a particular simulation by given as $T_F = N\Delta t$ where $N > 0$. Then for non-negative numbers a_i, b, and $\epsilon > 0$,*

$$2\left(\sum_{i=0}^{N-1} a_i\right) b \leq \frac{\epsilon T_F}{\Delta t} \sum_{i=0}^{N-1} a_i^2 + \frac{1}{\epsilon} b^2.$$

Proof. First by Young's Inequality

$$2\sum_{i=0}^{N-1} a_i b \leq \epsilon \left(\sum_{i=0}^{N-1} a_i\right)^2 + \frac{1}{\epsilon} b^2.$$

Next by Hölder's

$$\begin{aligned}
\left(\sum_{i=0}^{N-1} a_i\right)^2 &\leq \sum_{i=0}^{N-1} a_i^2 \sum_{i=0}^{N} 1^2 \\
&= N \sum_{i=0}^{N-1} a_i^2 \\
&= \frac{T_F}{\Delta t}\left(\sum_{i=0}^{N} a_i^2\right).
\end{aligned}$$

Therefore,

$$2\sum_{i=0}^{N-1} a_i b \leq \frac{\epsilon T_f}{\Delta t} \sum_{i=0}^{N-1} a_i^2 + \frac{1}{\epsilon} b^2.$$

□

It is useful to note that ϵT_F is a constant. We also make the following intuitive statement that will be used repeatedly.

Claim 4.3.7. *Let P be a normed space. Then let $q_1(t)$ and $q_2(t)$ be continuous functions with respect to time onto P,i.e $q_1(t), q_2(t) \in C(0,T;P)$. Let $v \in P$ be a test function such that*

$$(q_1(t), v) = (q_2(t), v) \quad \forall t > 0.$$

Then

$$(\overline{q_1^{n+1/2}}, v) = (\overline{q_2^{n+1/2}}, v) \qquad \forall n \geq 0, \tag{4.17a}$$

$$(\widetilde{q_1^n}, v) = (\widetilde{q_2^n}, v) \qquad \forall n \geq 1, \tag{4.17b}$$

$$(\partial_t q_1^{n+1/2}, v) = (\partial_t q_2^{n+1/2}, v) \quad \forall n \geq 0, \tag{4.17c}$$

$$(\partial_t^c q_1^n, v) = (\partial_t^c q_2^n, v) \qquad \forall n \geq 1, \tag{4.17d}$$

$$(\partial_t^2 q_1^n, v) = (\partial_t^2 q_2^n, v) \qquad \forall n \geq 1. \tag{4.17e}$$

These claims are used with q_1 and q_2 representing the right and left hand side of more complex statements. For example, by applying (4.17a) to (4.4d) we have

$$\begin{aligned}\rho_s \left(\overline{u_{tt}^{1/2}}, \boldsymbol{\nu}\right)_{\Omega_s} + \rho_f \left(\overline{v_t^{1/2}}, \boldsymbol{\nu}\right)_{\Omega_f} - \left(\nabla \cdot \overline{\boldsymbol{\sigma}_s^{1/2}}, \boldsymbol{\nu}\right)_{\Omega_s} - \left(\nabla \cdot \overline{\boldsymbol{\sigma}_f^{1/2}}, \boldsymbol{\nu}\right)_{\Omega_f} \\ - \left(\overline{\boldsymbol{f}_s^{1/2}}, \boldsymbol{\nu}\right)_{\Omega_s} - \left(\overline{\boldsymbol{f}_f^{1/2}}, \boldsymbol{\nu}\right)_{\Omega_f} = 0.\end{aligned}$$

We will need to take the difference between these type of statements and the same equations at a particular time. For example, recall that (4.4d) holds at any time t^n so at $t^{1/2}$ have

$$\begin{aligned}\rho_s \left(\boldsymbol{u}_{tt}^{1/2}, \boldsymbol{\nu}\right)_{\Omega_s} + \rho_f \left(v_t^{1/2}, \boldsymbol{\nu}\right)_{\Omega_f} - \left(\nabla \cdot \boldsymbol{\sigma}_s^{1/2}, \boldsymbol{\nu}\right)_{\Omega_s} - \left(\nabla \cdot \boldsymbol{\sigma}_f^{1/2}, \boldsymbol{\nu}\right)_{\Omega_f} \\ - \left(\boldsymbol{f}_s^{1/2}, \boldsymbol{\nu}\right)_{\Omega_s} - \left(\boldsymbol{f}_f^{1/2}, \boldsymbol{\nu}\right)_{\Omega_f} = 0.\end{aligned}$$

Finally, by taking the difference we have

$$\begin{aligned}\rho_s \left(\boldsymbol{u}_{tt}^{1/2} - \overline{u_{tt}^{1/2}}, \boldsymbol{\nu}\right)_{\Omega_s} + \rho_f \left(v_t^{1/2} - \overline{v_t^{1/2}}, \boldsymbol{\nu}\right)_{\Omega_f} - \left(\nabla \cdot \left(\boldsymbol{\sigma}_s^{1/2} - \overline{\boldsymbol{\sigma}_s^{1/2}}\right), \boldsymbol{\nu}\right)_{\Omega_s} \\ - \left(\nabla \cdot \left(\boldsymbol{\sigma}_f^{1/2} - \overline{\boldsymbol{\sigma}_f^{1/2}}\right), \boldsymbol{\nu}\right)_{\Omega_f} - \left(\boldsymbol{f}_s^{1/2} - \overline{\boldsymbol{f}_s^{1/2}}, \boldsymbol{\nu}\right)_{\Omega_s} - \left(\boldsymbol{f}_f^{1/2} - \overline{\boldsymbol{f}_f^{1/2}}, \boldsymbol{\nu}\right)_{\Omega_f} = 0. \quad (4.18)\end{aligned}$$

Equations similar to this are useful in the following proofs. To refer to this type of procedure, we say (4.18) is obtained by taking the difference between (4.4d) at $t^{1/2}$ and (4.17a) applied to (4.4d).

4.3.2 Consistency Error

Also, since the mixed finite element spaces $\mathcal{V}_h$ and $\mathbf{\Sigma}_h$ may be nonconforming, consistency errors will need to be bounded. Specifically, consider the exact solution $\boldsymbol{\sigma} \in H^1(\Omega, \mathbb{S})$ and the sum of (4.2) and (4.1d). Take $\boldsymbol{\tau} \in \mathbf{\Sigma}_h$, multiply, integrate by parts over each element and sum the results over elements to obtain

$$\begin{aligned}(\mathcal{A}(\boldsymbol{\sigma}_s)_t(t), \boldsymbol{\tau})_{\Omega_s} + (\mathcal{A}_\infty \boldsymbol{\sigma}_f(t), \boldsymbol{\tau})_{\Omega_f} + (\boldsymbol{u}_t(t), \nabla_h \cdot \boldsymbol{\tau})_{\Omega_s} + (\boldsymbol{v}(t), \nabla_h \cdot \boldsymbol{\tau})_{\Omega_f} \\ = < \boldsymbol{u}_t(t), \boldsymbol{\tau}\boldsymbol{n}_s >_\Gamma + < \boldsymbol{v}(t), \boldsymbol{\tau}\boldsymbol{n}_f >_\Gamma + \mathbb{E}_h\left(u_t(t), \boldsymbol{\tau}\right)_{\Omega_s} + \mathbb{E}_h\left(v(t), \boldsymbol{\tau}\right)_{\Omega_f}, \end{aligned} \tag{4.19}$$

where the consistency error is defined as

$$\begin{aligned}\mathbb{E}_h\left(\boldsymbol{u}_t(t), \boldsymbol{\tau}\right)_{\Omega_s} &= \sum_{e \in \mathcal{E}_{sh}} \int_e [\boldsymbol{\tau}\boldsymbol{n}] \cdot \boldsymbol{u}_t(t) ds, \\ \mathbb{E}_h\left(\boldsymbol{v}(t), \boldsymbol{\tau}\right)_{\Omega_f} &= \sum_{e \in \mathcal{E}_{fh}} \int_e [\boldsymbol{\tau}\boldsymbol{n}] \cdot \boldsymbol{v}(t) ds,\end{aligned}$$

where $\mathcal{E}_{sh}$ and $\mathcal{E}_{fh}$ are the sets of interior edges in the fluid and solid subdomains respectively. We assume that there is a proven bound on this error of the form

$$\mathbb{E}_h\left(\boldsymbol{u}, \boldsymbol{\tau}\right)_\Omega \leq C h^k \|\boldsymbol{\tau}\|_{0,\Omega} \|\boldsymbol{u}\|_{p,\Omega} \quad 1 \leq p \leq 2, \quad \boldsymbol{u} \in H^2(\Omega, \mathbb{R}^2), \quad \boldsymbol{\tau} \in \mathbf{\Sigma}_h, \tag{4.20}$$

where the values k and p come from the specifics of the element. For example, for the nonconforming Arnold-Winther element, $k = 1$ when $p = 2$ as shown in Lemma 2.3.1. Often in the following analysis error will be bounded by some combination of consistency error and projection error. For the remainder of this paper, we will use notation of the form k to denote the rate of convergence for the consistency error, while m_1 and m_2 will be used for the projection error given by an approximation property.

4.3.3 Error Analysis for the Initial Conditions

This section will be concerned with the error in the approximations of the initial conditions, that is, the error associated with the terms $(\boldsymbol{\sigma}_h^0, \boldsymbol{\omega}_h^0) \in (\boldsymbol{\Sigma}_h, \mathcal{V}_h)$. We begin with an intermediate Lemma.

Lemma 4.3.8. *Let* $(\boldsymbol{\sigma}(t), \boldsymbol{\omega}(t)) \in (\boldsymbol{\Sigma}, \mathcal{V})$ *be the solution to* (4.4) *and* $(\boldsymbol{\sigma}_h^0, \boldsymbol{\omega}_h^0) \in (\boldsymbol{\Sigma}_h, \mathcal{V}_h)$ *be the solution to* (4.11). *Then*

$$\|\chi_{\boldsymbol{u}}^0\|_{\Omega_s} + \|\chi_{\boldsymbol{v}}^0\|_{\Omega_f} = 0, \tag{4.21}$$

$$\|\chi_{\boldsymbol{\sigma}_s}^0\|_{\mathcal{A},\Omega_s}^2 + \|\chi_{\boldsymbol{\sigma}_f}^0\|_{\mathcal{A}_\infty,\Omega_f}^2 \leq C_1 h^{2l}, \tag{4.22}$$

with

$$C_1 = C(\|\boldsymbol{\sigma}_s^0\|_{m_1,\Omega_s}^2, \|\boldsymbol{\sigma}_f^0\|_{m_1,\Omega_f}^2, \|\boldsymbol{u}^0\|_{2,\Omega_s}^2, \|\boldsymbol{v}^0\|_{2,\Omega_f}^2, \|p^0\|_{r-2,\Omega_f}^2, q^0), \tag{4.23}$$

where m_1 *and* m_2 *are convergence rates determined by the mixed finite element spaces chosen as in* (4.9a) *and* (4.9b), r *is determined by the finite element method used to approximate* p^0, *and* q^0 *represents the norm of the initial solution, and* l *is a convergence rate determined by the mixed finite element spaces used.*

Proof. First to show (4.21), consider the equilibrium equations (4.1a) and (4.1c) in the solid and fluid subdomains respectively. From this we find

$$\left(\boldsymbol{u}^0, \boldsymbol{\nu}\right)_{\Omega_s} + \left(\boldsymbol{v}^0, \boldsymbol{\nu}\right)_{\Omega_f} = \left(\boldsymbol{u}_0, \boldsymbol{\nu}\right)_{\Omega_s} + \left(\boldsymbol{v}_0, \boldsymbol{\nu}\right)_{\Omega_f}, \qquad \boldsymbol{\nu} \in \mathcal{V}_h. \tag{4.24}$$

Consider the difference between (4.11a) and (4.24)

$$\left(\boldsymbol{u}_h^0 - \boldsymbol{u}^0, \boldsymbol{\nu}\right)_{\Omega_s} + \left(\boldsymbol{v}_h^0 - \boldsymbol{v}^0, \boldsymbol{\nu}\right)_{\Omega_f} = 0, \qquad \boldsymbol{\nu} \in \mathcal{V}_h.$$

By adding and subtracting the projected value $\mathcal{P}_h \boldsymbol{u}^0$ to the first term and $\Pi_h \boldsymbol{\sigma}_s^0$ to the second term this can be rewritten as

$$\left(\chi_{\boldsymbol{u}}^0 - \eta_{\boldsymbol{u}}^0, \boldsymbol{\nu}\right)_{\Omega_s} + \left(\chi_{\boldsymbol{v}}^0 - \eta_{\boldsymbol{v}}^0, \boldsymbol{\nu}\right)_{\Omega_f} = 0.$$

Using the projection property (4.6), this gives

$$\left(\chi^0_{\boldsymbol{u}}, \boldsymbol{\nu}\right)_{\Omega_s} + \left(\chi^0_{\boldsymbol{v}}, \boldsymbol{\nu}\right)_{\Omega_f} = 0. \tag{4.25}$$

Let

$$\boldsymbol{\nu} = \begin{cases} \chi^0_{\boldsymbol{u}} & \text{in } \Omega_s, \\ \chi^0_{\boldsymbol{v}} & \text{in } \Omega_f, \end{cases}$$

in (4.25) to obtain (4.21).

In order to prove (4.22), we consider the weak formulation at $t = 0$. Recall that $\boldsymbol{\Sigma}_h$ may be nonconforming therefore we begin by summing (4.1b) and (4.1d). Then take $\boldsymbol{\tau} \in \boldsymbol{\Sigma}_h$, multiply, integrate by parts over each element, and sum the results over elements to obtain

$$\begin{aligned} &\left(\mathcal{A}\boldsymbol{\sigma}^0_s, \boldsymbol{\tau}\right)_{\Omega_s} + \left(\mathcal{A}_\infty \boldsymbol{\sigma}^0_f, \boldsymbol{\tau}\right)_{\Omega_f} + \left(\boldsymbol{u}^0, \nabla_h \cdot \boldsymbol{\tau}\right)_{\Omega_s} + \left(\boldsymbol{v}^0, \nabla_h \cdot \boldsymbol{\tau}\right)_{\Omega_f} \\ &\quad = < \boldsymbol{u}^0, \boldsymbol{\tau}\boldsymbol{n}_s >_\Gamma + < \boldsymbol{v}^0, \boldsymbol{\tau}\boldsymbol{n}_f >_\Gamma + \mathbb{E}_h\left(u^0, \boldsymbol{\tau}\right)_{\Omega_s} + \mathbb{E}_h\left(v^0, \boldsymbol{\tau}\right)_{\Omega_f}. \end{aligned} \tag{4.26}$$

Taking the difference between (4.26) and (4.11c) results in

$$\begin{aligned} &\left(\mathcal{A}\left(\boldsymbol{\sigma}^0_{s_h} - \boldsymbol{\sigma}^0_s\right), \boldsymbol{\tau}\right)_{\Omega_s} + \left(\mathcal{A}_\infty\left(\boldsymbol{\sigma}^0_{f_h} - \boldsymbol{\sigma}^0_f\right), \boldsymbol{\tau}\right)_{\Omega_f} + \left(\boldsymbol{u}^0_h - \boldsymbol{u}^0, \nabla_h \cdot \boldsymbol{\tau}\right)_{\Omega_s} + \left(\widehat{\boldsymbol{v}_h}^0 - \boldsymbol{v}^0, \nabla_h \cdot \boldsymbol{\tau}\right)_{\Omega_f} \\ &\quad = -\mathbb{E}_h\left(u^0, \boldsymbol{\tau}\right)_{\Omega_s} - \mathbb{E}_h\left(v^0, \boldsymbol{\tau}\right)_{\Omega_f}. \end{aligned} \tag{4.27}$$

Now we add and subtract appropriate projections to each term of (4.27). For example to $\left(\boldsymbol{\sigma}^0_{s_h} - \boldsymbol{\sigma}^0_s\right)$, we add and subtract $\Pi_h \boldsymbol{\sigma}^0_s$, where as to $\boldsymbol{u}^0_h - \boldsymbol{u}^0$, $\mathcal{P}_h \boldsymbol{u}^0$ is added and subtracted. By recalling the L^2 projection property (4.7) and using (4.25), we have

$$\begin{aligned} &\left(\mathcal{A}\left(\chi^0_{\boldsymbol{\sigma}_s} - \eta^0_{\boldsymbol{\sigma}_s}\right), \boldsymbol{\tau}\right)_{\Omega_s} + \left(\mathcal{A}_\infty\left(\chi^0_{\boldsymbol{\sigma}_f} - \eta^0_{\boldsymbol{\sigma}_f}\right), \boldsymbol{\tau}\right)_{\Omega_f} + \left(\widehat{\boldsymbol{v}_h}^0 - \mathcal{P}_h \boldsymbol{v}^0, \nabla_h \cdot \boldsymbol{\tau}\right)_{\Omega_f} \\ &\quad = -\mathbb{E}_h\left(u^0, \boldsymbol{\tau}\right)_{\Omega_s} - \mathbb{E}_h\left(v^0, \boldsymbol{\tau}\right)_{\Omega_f}. \end{aligned} \tag{4.28}$$

Next take the difference between (4.11b) and the weak form of (3.13a). Then by using the property (4.8) we have

$$-\left(\nabla_h \cdot \left(\chi^0_{\boldsymbol{\sigma}_f}\right), \boldsymbol{\nu}\right)_{\Omega_f} = \left(\boldsymbol{g}_h - \boldsymbol{g}, \boldsymbol{\nu}\right)_{\Omega_f}. \tag{4.29}$$

Take the test functions

$$\boldsymbol{\tau} = \begin{cases} \chi^0_{\boldsymbol{\sigma}_s} & \text{in } \Omega_s, \\ \chi^0_{\boldsymbol{\sigma}_f} & \text{in } \Omega_f \end{cases}$$

and

$$\boldsymbol{\nu} = \begin{cases} \mathbf{0} & \text{in } \Omega_s, \\ \widehat{\boldsymbol{v}_h}^0 - \mathcal{P}_h \boldsymbol{v}^0 & \text{in } \Omega_f, \end{cases}$$

in equations (4.28) and (4.29) and sum them to find

$$\begin{aligned} &\left(\mathcal{A}\left(\chi^0_{\boldsymbol{\sigma}_s} - \eta^0_{\boldsymbol{\sigma}_s}\right), \chi^0_{\boldsymbol{\sigma}_s}\right)_{\Omega_s} + \left(\mathcal{A}_\infty\left(\chi^0_{\boldsymbol{\sigma}_f} - \eta^0_{\boldsymbol{\sigma}_f}\right), \chi^0_{\boldsymbol{\sigma}_f}\right)_{\Omega_f} \\ &\quad = \left(\boldsymbol{g}_h - \boldsymbol{g}, \widehat{\boldsymbol{v}_h}^0 - \mathcal{P}_h \boldsymbol{v}^0\right)_{\Omega_f} - \mathbb{E}_h\left(u^0, \chi^0_{\boldsymbol{\sigma}_s}\right)_{\Omega_s} - \mathbb{E}_h\left(v^0, \chi^0_{\boldsymbol{\sigma}_f}\right)_{\Omega_f}. \end{aligned}$$

Therefore using the Cauchy-Schwarz Inequality and the consistency error bound we find (4.20)

$$\begin{aligned} &\|\chi^0_{\boldsymbol{\sigma}_s}\|^2_{\mathcal{A},\Omega_s} + \|\chi^0_{\boldsymbol{\sigma}_f}\|^2_{\mathcal{A}_\infty,\Omega_f} \\ &\quad = \left(\mathcal{A}\eta^0_{\boldsymbol{\sigma}_s}, \chi^0_{\boldsymbol{\sigma}_s}\right)_{\Omega_s} + \left(\mathcal{A}_\infty \eta^0_{\boldsymbol{\sigma}_f}, \chi^0_{\boldsymbol{\sigma}_f}\right)_{\Omega_f} + \left(\boldsymbol{g}_h - \boldsymbol{g}, \widehat{\boldsymbol{v}_h}^0 - \mathcal{P}_h \boldsymbol{v}^0\right)_{\Omega_f} \\ &\qquad - \mathbb{E}_h\left(\boldsymbol{u}^0, \chi^0_{\boldsymbol{\sigma}_s}\right)_{\Omega_s} - \mathbb{E}_h\left(v^0, \chi^0_{\boldsymbol{\sigma}_f}\right)_{\Omega_f} \\ &\quad \leq I + II + III, \end{aligned} \tag{4.30}$$

with

$$\begin{aligned} I &= \|\eta^0_{\boldsymbol{\sigma}_s}\|_{\mathcal{A},\Omega_s}\|\chi^0_{\boldsymbol{\sigma}_s}\|_{\mathcal{A},\Omega_s} + \|\eta^0_{\boldsymbol{\sigma}_f}\|_{\mathcal{A}_\infty,\Omega_f}\|\chi^0_{\boldsymbol{\sigma}_f}\|_{\mathcal{A}_\infty,\Omega_f}, \\ II &= Ch^k\|\chi^0_{\boldsymbol{\sigma}_s}\|_{\Omega_s}\|\boldsymbol{u}^0\|_{2,\Omega_s} + Ch^k\|\chi^0_{\boldsymbol{\sigma}_f}\|_{\Omega_f}\|\boldsymbol{v}^0\|_{2,\Omega_f}, \\ III &= \|\boldsymbol{g}_h - \boldsymbol{g}\|_{\Omega_f}\|\widehat{\boldsymbol{v}_h}^0 - \mathcal{P}_h\boldsymbol{v}^0\|_{\Omega_f}. \end{aligned}$$

Each of the terms in I is bounded with Young's Inequality with an ϵ chosen so that terms matching the left hand side can be subtracted. For example, consider $\|\eta^0_{\boldsymbol{\sigma}_s}\|_{\mathcal{A},\Omega_s}\|\chi^0_{\boldsymbol{\sigma}_s}\|_{\mathcal{A},\Omega_s}$. Notice that $\|\chi^0_{\boldsymbol{\sigma}_s}\|_{\mathcal{A},\Omega_s}$ appears on the right hand side of (4.30). Therefore, ϵ is chosen so that the coefficient of $\|\chi^0_{\boldsymbol{\sigma}_s}\|_{\mathcal{A},\Omega_s}$ is considerably less than 1. Specifically,

$$\|\eta^0_{\boldsymbol{\sigma}_s}\|_{\mathcal{A},\Omega_s}\|\chi^0_{\boldsymbol{\sigma}_s}\|_{\mathcal{A},\Omega_s} \leq \frac{1}{4}\|\chi^0_{\boldsymbol{\sigma}_s}\|^2_{\mathcal{A},\Omega_s} + C\|\eta^0_{\boldsymbol{\sigma}_s}\|^2_{\mathcal{A},\Omega_s}. \tag{4.31}$$

This is repeated with $\|\eta^0_{\boldsymbol{\sigma}_f}\|_{\mathcal{A}_\infty,\Omega_f}\|\chi^0_{\boldsymbol{\sigma}_f}\|_{\mathcal{A}_\infty,\Omega_f}$. For the terms in II we first use the equivalence of $\|\cdot\|_{\mathcal{A}_\infty,\Omega_f}$ to $\|\cdot\|_{\Omega_f}$ shown in (3.8) and the equivalence of $\|\cdot\|_{\mathcal{A},\Omega_s}$ to $\|\cdot\|_{\Omega_s}$ shown in (2.8), to find

$$II \leq Ch^k\|\chi^0_{\boldsymbol{\sigma}_s}\|_{\mathcal{A},\Omega_s}\|\boldsymbol{u}^0\|_{2,\Omega_s} + Ch^k\|\chi^0_{\boldsymbol{\sigma}_f}\|_{\mathcal{A}_\infty,\Omega_f}\|\boldsymbol{v}^0\|_{2,\Omega_f}, \tag{4.32}$$

for some constant C. Now Young's Inequality is applied to each of terms in (4.32) as described above.

Finally we bound III. First by Young's inequality

$$III \leq C\left(\|\boldsymbol{g}_h - \boldsymbol{g}\|^2_{\Omega_f} + \|\widehat{\boldsymbol{v}_h}^0 - \mathcal{P}_h\boldsymbol{v}^0\|^2_{\Omega_f}\right). \tag{4.33}$$

Since $\boldsymbol{g}_h$ is an approximation to $\boldsymbol{g}$ obtained using a finite element method as described in section 3.2.1, $\|\boldsymbol{g}_h - \boldsymbol{g}\|_{\Omega_f}$ is bounded by (3.19). Choose a finite element space for approximating $\boldsymbol{g}_h$ so that $\|\boldsymbol{g} - \boldsymbol{g}_h\|_{\Omega_f} \leq Ch^{r-1}\|p^0\|_{r,,\Omega_f}$. Also, since $\widehat{\boldsymbol{v}_h}^0$ is the solution to the stationary Stokes problem (3.18), $\|\widehat{\boldsymbol{v}_h}^0 - \mathcal{P}_h\boldsymbol{v}^0\|_{\Omega_f}$ is bounded according to the mixed finite element space chosen. For example, for the conforming Arnold Winther element $\|\widehat{\boldsymbol{v}_h}^0 - \mathcal{P}_h\boldsymbol{v}^0\|_{\Omega_f} \leq Ch^w\|\boldsymbol{v}^0\|_{w+1,\Omega_f}$, with $1 \leq w \leq 2$. On the other hand, when using the nonconforming element, from Theorem 2.3.3, $\|\widehat{\boldsymbol{v}_h}^0 - \mathcal{P}_h\boldsymbol{v}^0\|_{\Omega_f} \leq Ch^w\left(\|\boldsymbol{v}^0\|_{2,\Omega_f} + \|\boldsymbol{\sigma}^0_s\|_{1,\Omega_f}\right)$ with $w = 2$. We use the same mixed finite element space used for approximating $\widehat{\boldsymbol{v}_h}^0$ as the other steps of the method. Then

$$III \leq Ch^{2r}\|p^0\|^2_{r-2,\Omega_f} + h^{2w}q^0,$$

where q^0 represents the norm of the initial solution and w depends on the mixed finite element space chosen. That is, for the conforming case $q^0 = C\|\boldsymbol{v}^0\|^2_{w+1,\Omega_f}$, with $1 \leq w \leq 2$. For the nonconforming case $q^0 = C\left(\|\boldsymbol{v}\|_{2,\Omega_f} + \|\boldsymbol{\sigma}^0_f\|_{1,\Omega_f}\right)^2$ when $w = 2$. So, we chose a finite element method for approximating $\boldsymbol{g}$ so that $2r - 2 \geq \min\{2k, 2m_1\}$. Therefore,

$$\begin{aligned}&\|\chi^0_{\boldsymbol{\sigma}_s}\|^2_{\mathcal{A},\Omega_s} + \|\chi^0_{\boldsymbol{\sigma}_f}\|^2_{\mathcal{A}_\infty,\Omega_f}\\ &\qquad \leq C\left(\|\eta^0_{\boldsymbol{\sigma}_s}\|^2_{\mathcal{A},\Omega_s} + \|\eta^0_{\boldsymbol{\sigma}_f}\|^2_{\mathcal{A}_\infty,\Omega_f} + h^{2k}\|\boldsymbol{u}^0\|^2_{2,\Omega_s} + h^{2k}\|\boldsymbol{v}^0\|^2_{2,\Omega_f} + h^{2r}\|p^0\|^2_{r-2,\Omega_f} + h^{2w}q^0\right).\end{aligned} \tag{4.34}$$

By using the approximation error bounds (4.9a)

$$\begin{aligned}
&\|\chi^0_{\boldsymbol{\sigma}_s}\|^2_{\mathcal{A},\Omega_s} + \|\chi^0_{\boldsymbol{\sigma}_f}\|^2_{\mathcal{A}_\infty,\Omega_f} \\
&\quad \leq C\left(h^{2m_1}\|\boldsymbol{\sigma}^0_s\|^2_{m_1,\Omega_s} + h^{2m_1}\|\boldsymbol{\sigma}^0_f\|^2_{m_1,\Omega_f} + h^{2k}\|\boldsymbol{u}^0\|^2_{2,\Omega_s} + h^{2k}\|\boldsymbol{v}^0\|^2_{2,\Omega_f}\right. \\
&\qquad \left. + h^{2r}\|p^0\|^2_{r-2,\Omega_f} + h^{2w}q^0\right). \qquad (4.35)
\end{aligned}$$

Choosing $2l = \min\{2k, 2m_1, 2r, 2w\}$ in (4.35) the result (4.22) follows.

□

Theorem 4.3.9. *Under the assumptions of Lemma 4.3.8*

$$\|\boldsymbol{u}^0 - \boldsymbol{u}^0_h\|_{\Omega_s} + \|\boldsymbol{v}^0 - \boldsymbol{v}^0_h\|_{\Omega_f} \leq C_a h^{2m_2},$$
$$\|\boldsymbol{\sigma}^0_s - \boldsymbol{\sigma}^0_{s_h}\|^2_{\mathcal{A},\Omega_s} + \|\boldsymbol{\sigma}^0_f - \boldsymbol{\sigma}^0_{f_h}\|^2_{\mathcal{A}_\infty,\Omega_f} \leq C_1 h^{2l} + Ch^{2m_1},$$

with $C_a = C\left(\|\boldsymbol{u}^0\|_{m_2,\Omega_s} + \|\boldsymbol{v}^0\|_{m_2,\Omega_f}\right)$, C_1 *as shown in* (4.23) *and* $C_b = C(\|\boldsymbol{\sigma}^0_s\|_{m_1,\Omega_s}, \|\boldsymbol{\sigma}^0_f\|_{m_1,\Omega_f})$. *Here* m_1 *and* m_2 *are convergence rates determined by the mixed finite element spaces chosen as in* (4.9a) *and* (4.9b) *and* l *is a convergence rate determined by the mixed finite element spaces used as described in Lemma* 4.3.8.

Proof. This follows directly from Lemma 4.3.8 and the Triangle Inequality. □

4.3.4 Error Analysis for the First Time Step

This section will be concerned with the error associated with the terms $(\boldsymbol{\sigma}^1_h, \boldsymbol{\omega}^1_h) \in (\boldsymbol{\Sigma}_h, \mathcal{V}_h)$. We begin by stating and proving some intermediate lemmas which will be useful in the main proof for this section.

Lemma 4.3.10. *Let* $(\boldsymbol{\sigma}(t), \boldsymbol{\omega}(t)) \in (\boldsymbol{\Sigma}, \mathcal{V})$ *be the solution to* (4.4) *and* $(\boldsymbol{\sigma}^1_h, \boldsymbol{\omega}^1_h) \in (\boldsymbol{\Sigma}_h, \mathcal{V}_h)$

be the solution to the system of (4.12a) *and* (4.12b)*. Then,*

$$\rho_s\left(\frac{2}{\Delta t}\partial_t\chi_{\boldsymbol{u}}^{1/2},\boldsymbol{\nu}\right)_{\Omega_s}+\rho_f\left(\partial_t\chi_{\boldsymbol{v}}^{1/2},\boldsymbol{\nu}\right)_{\Omega_f}-\left(\nabla_h\cdot\overline{\chi_{\boldsymbol{\sigma}_s}^{1/2}},\boldsymbol{\nu}\right)_{\Omega_s}-\left(\nabla_h\cdot\overline{\chi_{\boldsymbol{\sigma}_f}^{1/2}},\boldsymbol{\nu}\right)_{\Omega_f}$$
$$=\left(2r_{\boldsymbol{u}}^0,\boldsymbol{\nu}\right)_{\Omega_s}+\left(2r_{\boldsymbol{v}}^0,\boldsymbol{\nu}\right)_{\Omega_f},\qquad \boldsymbol{\nu}\in\mathcal{V}_h, \tag{4.36a}$$

$$\left(\mathcal{A}\partial_t\chi_{\boldsymbol{\sigma}_s}^{1/2},\boldsymbol{\tau}\right)_{\Omega_s}+\left(\mathcal{A}_\infty\overline{\chi_{\boldsymbol{\sigma}_f}^{1/2}},\boldsymbol{\tau}\right)_{\Omega_f}+\left(\partial_t\chi_{\boldsymbol{u}}^{1/2},\nabla_h\cdot\boldsymbol{\tau}\right)_{\Omega_s}+\left(\overline{\chi_{\boldsymbol{v}}^{1/2}},\nabla_h\cdot\boldsymbol{\tau}\right)_{\Omega_f}$$
$$=\left(\mathcal{A}\partial_t\eta_{\boldsymbol{\sigma}_s}^{1/2},\boldsymbol{\tau}\right)_{\Omega_s}+\left(\mathcal{A}_\infty\eta_{\boldsymbol{\sigma}_f}^{1/2},\boldsymbol{\tau}\right)_{\Omega_f}+2I^0+2E^0,\qquad \boldsymbol{\tau}\in\boldsymbol{\Sigma}_h, \tag{4.36b}$$

with

$$r_{\boldsymbol{u}}^0=\frac{\rho_s}{2}\left(\overline{\boldsymbol{u}_{tt}^{1/2}}-\frac{2}{\Delta t}\left(\partial_t\boldsymbol{u}^{1/2}-\boldsymbol{s}_0\right)\right), \tag{4.37}$$

$$r_{\boldsymbol{v}}^0=\frac{\rho_f}{2}\left(\overline{\boldsymbol{v}_t^{1/2}}-\partial_t\boldsymbol{v}^{1/2}\right), \tag{4.38}$$

$$2I^0=-<\overline{\boldsymbol{u}_t^{1/2}},[\boldsymbol{\tau}\cdot\boldsymbol{n}]>_\Gamma+<\overline{\boldsymbol{u}_t^{1/2}}-\partial_t\boldsymbol{u}^{1/2},\boldsymbol{\tau}\boldsymbol{n}_s>_\Gamma, \tag{4.39}$$

$$2E^0=\mathbb{E}_h\left(\overline{\boldsymbol{u}_t^{1/2}}-\partial_t\boldsymbol{u}^{1/2},\boldsymbol{\tau}\right)_{\Omega_s}-\mathbb{E}_h\left(\overline{\boldsymbol{u}_t^{1/2}},\boldsymbol{\tau}\right)_{\Omega_s}-\mathbb{E}_h\left(\overline{\boldsymbol{v}^{1/2}},\boldsymbol{\tau}\right)_{\Omega_f}. \tag{4.40}$$

In (4.36a) there are terms involving $2r_{\boldsymbol{u}}^0$ and $2r_{\boldsymbol{v}}^0$. The definition of $r_{\boldsymbol{u}}^0$ and $r_{\boldsymbol{v}}^0$ can be altered to avoid the factor of 2. However, there is a factor of $\frac{2}{\Delta t}$ in the lead term of (4.36a). In later steps we will multiply by $\frac{\Delta t}{2}$ to make a cancellation. So we keep the current notation for ease later. The factor of 2 in front of I^0 and E^0 in (4.36b) appears for a similar reason. Also note that the definitions $r_{\boldsymbol{u}}^0$, $r_{\boldsymbol{v}}^0$, $2I^0$ and $2E^0$ are special from this first time step.

Proof. Subtracting (4.4d) at the time $t^{1/2}$ from the discrete forms (4.12a)

$$\left(\frac{2\rho_s}{\Delta t}\partial_t\boldsymbol{u}_h^{1/2}-\rho_s\boldsymbol{u}_{tt}^{1/2},\boldsymbol{\nu}\right)_{\Omega_s}+\rho_f\left(\partial_t\boldsymbol{v}_h^{1/2}-\boldsymbol{v}_t^{1/2},\boldsymbol{\nu}\right)_{\Omega_f}-\left(\nabla_h\cdot\overline{\boldsymbol{\sigma}_{s_h}^{1/2}}-\nabla\cdot\boldsymbol{\sigma}_s^{1/2},\boldsymbol{\nu}\right)_{\Omega_s}$$
$$-\left(\nabla_h\cdot\overline{\boldsymbol{\sigma}_{f_h}^{1/2}}-\nabla\cdot\boldsymbol{\sigma}_f^{1/2},\boldsymbol{\nu}\right)_{\Omega_f}$$
$$=\left(\frac{2\rho_s}{\Delta t}\boldsymbol{s}_0,\boldsymbol{\nu}\right)_{\Omega_s}+\left(\overline{\boldsymbol{f}_s^{1/2}}-\boldsymbol{f}_s^{1/2},\boldsymbol{\nu}\right)_{\Omega_s}+\left(\overline{\boldsymbol{f}_f^{1/2}}-\boldsymbol{f}_f^{1/2},\boldsymbol{\nu}\right)_{\Omega_f}. \tag{4.41}$$

We will now re-write this in terms of the auxiliary and projection errors. This is a matter of adding and subtracting the correct terms. For example, consider $\frac{2}{\Delta t}\partial_t \boldsymbol{u}_h^{1/2} - \boldsymbol{u}_{tt}^{1/2}$. This is re-written by adding and subtracting $\frac{2}{\Delta t}\mathcal{P}_h\partial_t \boldsymbol{u}^{1/2}$ and $\frac{2}{\Delta t}\partial_t \boldsymbol{u}^{1/2}$ to give

$$\frac{2}{\Delta t}\partial_t \boldsymbol{u}_h^{1/2} - \boldsymbol{u}_{tt}^{1/2} = \frac{2}{\Delta t}\partial_t \chi_{\boldsymbol{u}}^{1/2} - \frac{2}{\Delta t}\partial_t \eta_{\boldsymbol{u}}^{1/2} + \frac{2}{\Delta t}\partial_t \boldsymbol{u}^{1/2} - \boldsymbol{u}_{tt}^{1/2}.$$

A similar procedure is repeated with every part of (4.41) to obtain

$$\begin{aligned}
&\rho_s\left(\frac{2}{\Delta t}\partial_t \chi_{\boldsymbol{u}}^{1/2}, \boldsymbol{\nu}\right)_{\Omega_s} + \rho_f\left(\partial_t \chi_{\boldsymbol{v}}^{1/2}, \boldsymbol{\nu}\right)_{\Omega_f} - \left(\nabla_h \cdot \overline{\chi_{\boldsymbol{\sigma}_s}^{1/2}}, \boldsymbol{\nu}\right)_{\Omega_s} - \left(\nabla_h \cdot \overline{\chi_{\boldsymbol{\sigma}_f}^{1/2}}, \boldsymbol{\nu}\right)_{\Omega_f} \\
&\quad = \rho_s\left(\boldsymbol{u}_{tt}^{1/2} + \frac{2}{\Delta t}\left(\boldsymbol{s}_0 - \partial_t \boldsymbol{u}^{1/2}\right), \boldsymbol{\nu}\right)_{\Omega_s} + \rho_f\left(\boldsymbol{v}_t^{1/2} - \partial_t \boldsymbol{v}^{1/2}, \boldsymbol{\nu}\right)_{\Omega_f} \\
&\qquad + \left(\nabla \cdot \left(\overline{\boldsymbol{\sigma}_s^{1/2}} - \boldsymbol{\sigma}_s^{1/2}\right), \boldsymbol{\nu}\right)_{\Omega_s} + \left(\nabla \cdot \left(\overline{\boldsymbol{\sigma}_f^{1/2}} - \boldsymbol{\sigma}_f^{1/2}\right), \boldsymbol{\nu}\right)_{\Omega_f} \\
&\qquad + \left(\overline{\boldsymbol{f}_s^{1/2}} - \boldsymbol{f}_s^{1/2}, \boldsymbol{\nu}\right)_{\Omega_s} + \left(\overline{\boldsymbol{f}_f^{1/2}} - \boldsymbol{f}_f^{1/2}, \boldsymbol{\nu}\right)_{\Omega_s}.
\end{aligned} \tag{4.42}$$

Recall that (4.18) is obtained by taking the difference between (4.4d) at $t^{1/2}$ and (4.17a) applied to (4.4d). By rearranging (4.18) we see that

$$\begin{aligned}
&\rho_s\left(\boldsymbol{u}_{tt}^{1/2}, \boldsymbol{\nu}\right)_{\Omega_s} + \rho_f\left(\boldsymbol{v}_t^{1/2}, \boldsymbol{\nu}\right)_{\Omega_f} + \left(\nabla \cdot \left(\overline{\boldsymbol{\sigma}_s^{1/2}} - \boldsymbol{\sigma}_s^{1/2}\right), \boldsymbol{\nu}\right)_{\Omega_s} + \left(\nabla \cdot \left(\overline{\boldsymbol{\sigma}_f^{1/2}} - \boldsymbol{\sigma}_f^{1/2}\right), \boldsymbol{\nu}\right)_{\Omega_f} \\
&\quad + \left(\overline{\boldsymbol{f}_s^{1/2}} - \boldsymbol{f}_s^{1/2}, \boldsymbol{\nu}\right)_{\Omega_s} - \left(\overline{\boldsymbol{f}_f^{1/2}} - \boldsymbol{f}_f^{1/2}, \boldsymbol{\nu}\right)_{\Omega_f} \\
&\quad = \rho_s\left(\overline{\boldsymbol{u}_{tt}^{1/2}}, \boldsymbol{\nu}\right)_{\Omega_s} + \left(\overline{\boldsymbol{v}_t^{1/2}}, \boldsymbol{\nu}\right)_{\Omega_f}
\end{aligned} \tag{4.43}$$

By using (4.43) in (4.42) the result (4.36a) follows.

To prove (4.36b), consider the difference between the weak form (4.19) at the time $t^{1/2}$ and (4.12b)

$$\begin{aligned}
&\left(\mathcal{A}\left(\partial_t \boldsymbol{\sigma}_{s_h}^{1/2} - (\boldsymbol{\sigma}_s)_t^{1/2}\right), \boldsymbol{\tau}\right)_{\Omega_s} + \left(\mathcal{A}_\infty\left(\overline{\boldsymbol{\sigma}_{f_h}^{1/2}} - \boldsymbol{\sigma}_f^{1/2}\right), \boldsymbol{\tau}\right)_{\Omega_f} \\
&\qquad + \left(\partial_t \boldsymbol{u}_h^{1/2} - \boldsymbol{u}_t^{1/2}, \nabla_h \cdot \boldsymbol{\tau}\right)_{\Omega_s} + \left(\overline{\boldsymbol{v}_h^{1/2}} - \boldsymbol{v}^{1/2}, \nabla_h \cdot \boldsymbol{\tau}\right)_{\Omega_f} \\
&\qquad\quad = - < \boldsymbol{u}_t^{1/2}, \boldsymbol{\tau} \cdot \boldsymbol{n}_s >_\Gamma - < \boldsymbol{v}^{1/2}, \boldsymbol{\tau}\boldsymbol{n}_f >_\Gamma - \mathbb{E}_h\left(\boldsymbol{u}_t^{1/2}, \boldsymbol{\tau}\right)_{\Omega_s} \\
&\qquad\qquad - \mathbb{E}_h\left(\boldsymbol{v}^{1/2}, \boldsymbol{\tau}\right)_{\Omega_f}.
\end{aligned} \tag{4.44}$$

By adding and subtracting appropriate projections to each term of (4.44), this can be re-written as

$$\begin{aligned}
&\left(\mathcal{A}\partial_t\chi^{1/2}_{\boldsymbol{\sigma}_s},\boldsymbol{\tau}\right)_{\Omega_s}+\left(\mathcal{A}_\infty\overline{\chi^{1/2}_{\boldsymbol{\sigma}_f}},\boldsymbol{\tau}\right)_{\Omega_f}+\left(\partial_t\chi^{1/2}_{\boldsymbol{u}},\nabla_h\cdot\boldsymbol{\tau}\right)_{\Omega_s}+\left(\overline{\chi^{1/2}_{\boldsymbol{v}}},\nabla_h\cdot\boldsymbol{\tau}\right)_{\Omega_f}\\
&\quad=\left(\mathcal{A}\partial_t\eta^{1/2}_{\boldsymbol{\sigma}_s},\boldsymbol{\tau}\right)_{\Omega_s}+\left(\mathcal{A}\left((\boldsymbol{\sigma}_s)^{1/2}_t-\partial_t\boldsymbol{\sigma}_s^{1/2}\right),\boldsymbol{\tau}\right)_{\Omega_s}+\left(\mathcal{A}_\infty\overline{\eta^{1/2}_{\boldsymbol{\sigma}_f}},\boldsymbol{\tau}\right)_{\Omega_f}\\
&\qquad+\left(\mathcal{A}_\infty\left(\boldsymbol{\sigma}_f^{1/2}-\overline{\boldsymbol{\sigma}_f^{1/2}}\right),\boldsymbol{\tau}\right)_{\Omega_f}+\left(\boldsymbol{u}_t^{1/2}-\partial_t\boldsymbol{u}^{1/2},\nabla_h\cdot\boldsymbol{\tau}\right)_{\Omega_s}+\left(\boldsymbol{v}^{1/2}-\overline{\boldsymbol{v}^{1/2}},\nabla_h\cdot\boldsymbol{\tau}\right)_{\Omega_f}\\
&\qquad-<\boldsymbol{u}_t^{1/2},\boldsymbol{\tau}\boldsymbol{n}_s>_\Gamma-<\boldsymbol{v}^{1/2},\boldsymbol{\tau}\boldsymbol{n}_f>_\Gamma-\mathbb{E}_h\left(\boldsymbol{u}_t^{1/2},\boldsymbol{\tau}\right)_{\Omega_s}-\mathbb{E}_h\left(\boldsymbol{v}^{1/2},\boldsymbol{\tau}\right)_{\Omega_f}.
\end{aligned}\tag{4.45}$$

On the other hand, by taking the difference between (4.19) at $t^{1/2}$ and (4.17a) applied to (4.19) we have

$$\begin{aligned}
&\left(\mathcal{A}\left((\boldsymbol{\sigma}_s)^{1/2}_t-\overline{(\boldsymbol{\sigma}_s)^{1/2}_t}\right),\boldsymbol{\tau}\right)_{\Omega_s}+\left(\mathcal{A}_\infty\left(\boldsymbol{\sigma}_f^{1/2}-\overline{\boldsymbol{\sigma}_f^{1/2}}\right),\boldsymbol{\tau}\right)_{\Omega_f}+\left(\boldsymbol{u}_t^{1/2}-\overline{\boldsymbol{u}_t^{1/2}},\nabla_h\cdot\boldsymbol{\tau}\right)_{\Omega_s}\\
&\quad+\left(\boldsymbol{v}^{1/2}-\overline{\boldsymbol{v}^{1/2}},\nabla_h\cdot\boldsymbol{\tau}\right)_{\Omega_f}\\
&\qquad=<\boldsymbol{u}_t^{1/2}-\overline{\boldsymbol{u}_t^{1/2}},\boldsymbol{\tau}\cdot\boldsymbol{n}_s>_\Gamma+<\boldsymbol{v}^{1/2}-\overline{\boldsymbol{v}^{1/2}},\boldsymbol{\tau}\boldsymbol{n}_f>_\Gamma+\mathbb{E}_h\left(\boldsymbol{u}_t^{1/2}-\overline{\boldsymbol{u}_t^{1/2}},\boldsymbol{\tau}\right)_{\Omega_s}\\
&\qquad\quad+\mathbb{E}_h\left(\boldsymbol{v}^{1/2}-\overline{\boldsymbol{v}^{1/2}},\boldsymbol{\tau}\right)_{\Omega_f}.
\end{aligned}\tag{4.46}$$

See the steps leading to (4.18) for more information about this procedure. Using (4.46) equation (4.45) becomes

$$\begin{aligned}
&\left(\mathcal{A}\partial_t\chi^{1/2}_{\boldsymbol{\sigma}_s},\boldsymbol{\tau}\right)_{\Omega_s}+\left(\mathcal{A}_\infty\overline{\chi^{1/2}_{\boldsymbol{\sigma}_f}},\boldsymbol{\tau}\right)_{\Omega_f}+\left(\partial_t\chi^{1/2}_{\boldsymbol{u}},\nabla_h\cdot\boldsymbol{\tau}\right)_{\Omega_s}+\left(\overline{\chi^{1/2}_{\boldsymbol{v}}},\nabla_h\cdot\boldsymbol{\tau}\right)_{\Omega_f}\\
&\quad=\left(\mathcal{A}\partial_t\eta^{1/2}_{\boldsymbol{\sigma}_s},\boldsymbol{\tau}\right)_{\Omega_s}+\left(\mathcal{A}_\infty\eta^{1/2}_{\boldsymbol{\sigma}_f},\boldsymbol{\tau}\right)_{\Omega_f}+\left(\mathcal{A}\left(\overline{(\boldsymbol{\sigma}_s)^{1/2}_t}-\partial_t\boldsymbol{\sigma}_s^{1/2}\right),\boldsymbol{\tau}\right)_{\Omega_s}+\left(\overline{\boldsymbol{u}_t^{1/2}}-\partial_t u^{1/2},\nabla_h\cdot\boldsymbol{\tau}\right)_{\Omega_s}\\
&\qquad-<\boldsymbol{u}_t^{1/2},\boldsymbol{\tau}\boldsymbol{n}_s>_\Gamma-<\boldsymbol{v}^{1/2},\boldsymbol{\tau}\boldsymbol{n}_f>_\Gamma-\mathbb{E}_h\left(\boldsymbol{u}_t^{1/2},\boldsymbol{\tau}\right)_{\Omega_s}-\mathbb{E}_h\left(\boldsymbol{v}^{1/2},\boldsymbol{\tau}\right)_{\Omega_f}.
\end{aligned}\tag{4.47}$$

Finally, consider the exact solution $\boldsymbol{\sigma}\in H^1(\Omega,\mathbb{S})$ and (4.1b). Take a test function $\boldsymbol{\tau}\in\boldsymbol{\Sigma}_h$, multiply (4.1b) by $\boldsymbol{\tau}$, integrate by parts over each element and sum the results over elements to obtain

$$\left(\mathcal{A}\boldsymbol{\sigma}_s(t),\boldsymbol{\tau}\right)_{\Omega_s}+\left(\boldsymbol{u}(t),\nabla_h\cdot\boldsymbol{\tau}\right)_{\Omega_s}=<\boldsymbol{u}(t),\boldsymbol{\tau}\boldsymbol{n}_s>_\Gamma+\mathbb{E}_h\left(\boldsymbol{u}_t(t),\boldsymbol{\tau}\right)_{\Omega_s}.\tag{4.48}$$

Then by taking the difference between (4.17a)applied to (4.48) and (4.17c) applied to (4.48) we have

$$\begin{aligned}\left(\mathcal{A}\left(\overline{(\boldsymbol{\sigma}_s)_t^{1/2}}-\partial_t\boldsymbol{\sigma}_s^{1/2}\right),\boldsymbol{\tau}\right)_{\Omega_s}+\left(\overline{\boldsymbol{u}_t^{1/2}}-\partial_t\boldsymbol{u}^{1/2},\nabla_h\cdot\boldsymbol{\tau}\right)_{\Omega_s}\\ =<\overline{\boldsymbol{u}_t^{1/2}}-\partial_t\boldsymbol{u}^{1/2},\boldsymbol{\tau}\boldsymbol{n}_s>_\Gamma+\mathbb{E}_h\left(\overline{\boldsymbol{u}_t^{1/2}}-\partial_t\boldsymbol{u}^{1/2},\boldsymbol{\tau}\right)_{\Omega_s}.\end{aligned}\tag{4.49}$$

See the steps leading to (4.18) for more information about this procedure. By using (4.49) in (4.47) the result (4.36b) follows. □

Now we are ready to go about bounding the (4.36a) and (4.36b) for use in the main theorem. Again this will need some preliminary lemmas.

Lemma 4.3.11. *Under the same assumptions as Lemma 4.3.10*

$$\|r_{\boldsymbol{v}}^0\|_{\Omega_f}^2\leq C\Delta t^3\int_0^{t^1}\|\boldsymbol{v}_{ttt}(s)\|_{\Omega_f}^2\,ds.\tag{4.50}$$

Proof. By adding and subtracting $\boldsymbol{v}_t^{1/2}$ from $\|r_{\boldsymbol{v}}^0\|_{\Omega_f}^2$ then applying corollary 4.3.2 we find

$$\|r_{\boldsymbol{v}}^0\|_{\Omega_f}^2\leq\frac{\rho_f^2}{2}\left(\|\overline{\boldsymbol{v}_t^{1/2}}-\boldsymbol{v}_t^{1/2}\|_{\Omega_f}^2+\|\boldsymbol{v}_t^{1/2}-\partial_t\boldsymbol{v}^{1/2}\|_{\Omega_f}^2\right).$$

Now using Lemma 4.3.4 the result follows. □

Note that $\int_0^{t^1}\|\boldsymbol{v}_{ttt}\|_{\Omega_f}^2dt=\|\boldsymbol{v}_{ttt}\|^2_{L^2\left(0,\Delta t;L^2(\Omega_f)\right)}$ and thus (4.50) can be expressed as

$$\|r_{\boldsymbol{v}}^0\|_{\Omega_f}^2\leq C\Delta t^3\|\boldsymbol{v}_{ttt}\|^2_{L^2\left(0,\Delta t;L^2(\Omega_f)\right)}.$$

Lemma 4.3.12. *Under the same assumptions as Lemma 4.3.10*

$$\|r_{\boldsymbol{u}}^0\|_{\Omega_s}^2\leq C\Delta t^2\|\boldsymbol{u}_{ttt}\|^2_{L^\infty_{\Delta t}(L^2(\Omega_s))}.\tag{4.51}$$

Proof. By adding and subtracting $\boldsymbol{u}_{tt}^{1/2}$ to the $r_{\boldsymbol{u}}^0$ and using the Triangle and Young's Inequalities we find

$$\|r_{\boldsymbol{u}}^0\|_{\Omega_s}^2\leq\frac{\rho_s^2}{2}\|\overline{\boldsymbol{u}_{tt}^{1/2}}-\boldsymbol{u}_{tt}^{1/2}\|_{\Omega_s}^2+\|\boldsymbol{u}_{tt}^{1/2}-\frac{2}{\Delta t}\left(\partial_t\boldsymbol{u}^{1/2}-\boldsymbol{s}_0\right)\|_{\Omega_s}^2.$$

From (4.15a), we find

$$\|\overline{\boldsymbol{u}_{tt}^{1/2}} - \boldsymbol{u}_{tt}^{1/2}\|_{\Omega_s}^2 \leq C\Delta t^3 \int_0^{t^1} \|\boldsymbol{u}_{tttt}(s)\|^2 \, ds.$$

So we consider only

$$\boldsymbol{u}_{tt}^{1/2} + \frac{2}{\Delta t}\left(\boldsymbol{s}_0 - \partial_t \boldsymbol{u}^{1/2}\right).$$

Recall that the given initial condition $\boldsymbol{s}_0$ is the solid velocity at time 0, that is, $\boldsymbol{s}_0 = \boldsymbol{u}_t^0$. Then consider the following Taylor expansions:

$$\begin{aligned}
\boldsymbol{u}^1 &= \boldsymbol{u}^{1/2} + \frac{\Delta t}{2}\boldsymbol{u}_t^{1/2} + \frac{\Delta t^2}{8}\boldsymbol{u}_{tt}^{1/2} + \frac{1}{2}\int_{\Delta t/2}^{\Delta t} (\Delta t - s)^2 \boldsymbol{u}_{ttt}(s)\, ds, \\
\boldsymbol{u}^0 &= \boldsymbol{u}^{1/2} - \frac{\Delta t}{2}\boldsymbol{u}_t^{1/2} + \frac{\Delta t^2}{8}\boldsymbol{u}_{tt}^{1/2} + \frac{1}{2}\int_{\Delta t/2}^{0} (-s)^2 \boldsymbol{u}_{ttt}(s)\, ds, \\
\boldsymbol{u}_t^0 &= \boldsymbol{u}_t^{1/2} - \frac{\Delta t}{2}\boldsymbol{u}_{tt}^{1/2} + \int_{\Delta t/2}^{0} (-s)\boldsymbol{u}_{ttt}(s)\, ds.
\end{aligned}$$

Therefore,

$$\frac{-2(\boldsymbol{u}^1 - \boldsymbol{u}^0)}{\Delta t^2} = \frac{-2}{\Delta t}\boldsymbol{u}_t^{1/2} - \frac{1}{\Delta t^2}\int_{\Delta t/2}^{\Delta t} (\Delta t - s)^2 \boldsymbol{u}_{ttt}(s)\, ds - \frac{1}{\Delta t^2}\int_0^{\Delta t/2} (-s)^2 \boldsymbol{u}_{ttt}(s)\, ds.$$

Thus,

$$\begin{aligned}
\boldsymbol{u}_{tt}^{1/2} + \frac{2}{\Delta t}\boldsymbol{u}_t^0 - \frac{2(\boldsymbol{u}^1 - \boldsymbol{u}^0)}{\Delta t^2} &= -\frac{2}{\Delta t}\int_{\Delta t/2}^{0} (-s)\boldsymbol{u}_{ttt}(s)\, ds - \frac{1}{\Delta t^2}\int_{\Delta t/2}^{\Delta t} (\Delta t - s)^2 \boldsymbol{u}_{ttt}(s)\, ds \\
&\quad + \frac{1}{\Delta t^2}\int_0^{\Delta t/2} (-s)^2 u_{ttt}(s)\, ds \\
&\leq \int_0^{\Delta t/2} \mid \boldsymbol{u}_{ttt}(s) \mid \, ds + \frac{1}{4}\int_{\Delta t/2}^{\Delta t} \mid \boldsymbol{u}_{ttt}(s) \mid \, ds + \frac{1}{4}\int_0^{\Delta t/2} \mid \boldsymbol{u}_{ttt}(s) \mid \, ds \\
&\leq 2\int_0^{\Delta t} \mid \boldsymbol{u}_{ttt}(s) \mid \, ds.
\end{aligned}$$

Now by using Hölder's inequality, we have

$$\begin{aligned}
\|\int_0^{\Delta t} \mid \boldsymbol{u}_{ttt}(s) \mid \, ds\|_{\Omega_s}^2 &= \int_\Omega (\int_0^{\Delta t} \mid \boldsymbol{u}_{ttt}(s) \mid \, ds)^2 dx \\
&\leq \int_\Omega (\int_0^{\Delta t} 1^2 \, ds)(\int_0^{\Delta t} \boldsymbol{u}_{ttt}^2(s) \, ds) dx \\
&\leq C\Delta t \int_\Omega \int_0^{\Delta t} \boldsymbol{u}_{ttt}^2(s) \, ds dx \\
&\leq C\Delta t \int_0^{\Delta t} \|\boldsymbol{u}_{ttt}(s)\|_{\Omega_s}^2 \, ds.
\end{aligned}$$

Finally,

$$\begin{aligned}
\|r_{\boldsymbol{u}}^0\|_{\Omega_s}^2 &\leq C\Delta t \int_0^{\Delta t} \|\boldsymbol{u}_{ttt}(s)\|_{\Omega_s}^2 \, ds \\
&\leq C\Delta t \int_0^{\Delta t} \|\boldsymbol{u}_{ttt}(s)\|_{L^\infty_{\Delta t}(L^2(\Omega_s))}^2 ds.
\end{aligned}$$

The result (4.51) follows directly. □

Lemma 4.3.13. *Under the same assumptions as Lemma 4.3.10*

$$\begin{aligned}
&\rho_s \|\partial_t \chi_{\boldsymbol{u}}^{1/2}\|_{\Omega_s}^2 + \rho_f \|\overline{\chi_{\boldsymbol{v}}^{1/2}}\|_{\Omega_f}^2 + \|\overline{\chi_{\boldsymbol{\sigma}_s}^{1/2}}\|_{\mathcal{A},\Omega_s}^2 + \frac{\Delta t}{2} \|\overline{\chi_{\boldsymbol{\sigma}_f}^{1/2}}\|_{\mathcal{A}_\infty,\Omega_f}^2 \\
&\qquad \leq C_2 \left(h^{2l} + \Delta t^4 + h^{2m_1} + + h^{2k}\Delta t + h^{-1}\Delta t^5\right), \qquad (4.52)
\end{aligned}$$

with

$$\begin{aligned}
C_2 = C(&\|\boldsymbol{\sigma}_s^0\|_{m_1,\Omega_s}^2, \|\boldsymbol{\sigma}_f^0\|_{m_1,\Omega_f}^2, \|\boldsymbol{u}^0\|_{2,\Omega_s}^2, \|\boldsymbol{v}^0\|_{2,\Omega_f}^2, \|p^0\|_{r-2,\Omega_f}^2, q^0, \|(\boldsymbol{\sigma}_s^{1/2})_{ttt}\|_{L^2(0,\Delta t;L^2(\Omega_s))}^2, \\
&\|\Pi_h(\boldsymbol{\sigma}_s^{1/2})_{ttt}\|_{L^2(0,\Delta t;L^2(\Omega_s))}^2, \|(\boldsymbol{\sigma}_s^{1/2})_t\|_{m_1}^2, \|\boldsymbol{\sigma}_f^{1/2}\|_{m_1,\Omega_f}, \|\boldsymbol{u}_t^{1/2}\|_{2,\Omega_s}^2, \|\boldsymbol{v}^{1/2}\|_{2,\Omega_f}^2, \\
&\|\boldsymbol{u}_{ttt}\|_{L^\infty_{\Delta t}(L^2(\Omega_s))}^2, \|\boldsymbol{v}_{ttt}\|_{L^2\left(0,\Delta t;L^2(\Omega_f)\right)}^2, \|\boldsymbol{u}_{ttt}\|_{L^2(0,\Delta t;L^2(\Omega_s))}^2, \|\boldsymbol{u}_{ttt}\|_{L^2(0,\Delta t;L^2(\Gamma))}^2\big).
\end{aligned}$$

where m_1 and m_2 are convergence rates determined by the mixed finite element spaces chosen as in (4.9a) *and* (4.9b), *r is determined by the finite element method used to approximate p^0, and q^0 represents the norm of the initial solution, and l is a convergence rate determined by the mixed finite element spaces used as described in Lemma* 4.3.8.

Proof. Let

$$\boldsymbol{\nu} = \begin{cases} \partial_t \chi_{\boldsymbol{u}}^{1/2} & \text{in } \Omega_s, \\ \overline{\chi_{\boldsymbol{v}}^{1/2}} & \text{in } \Omega_f, \end{cases}$$

and

$$\boldsymbol{\tau} = \begin{cases} \overline{\chi_{\boldsymbol{\sigma}_s}^{1/2}} & \text{in } \Omega_s, \\ \overline{\chi_{\boldsymbol{\sigma}_f}^{1/2}} & \text{in } \Omega_f, \end{cases}$$

in (4.36a) and (4.36b). Then we have

$$\begin{aligned}
&\rho_s \left(\frac{2}{\Delta t} \partial_t \chi_{\boldsymbol{u}}^{1/2}, \partial_t \chi_{\boldsymbol{u}}^{1/2} \right)_{\Omega_s} + \rho_f \left(\partial_t \chi_{\boldsymbol{v}}^{1/2}, \overline{\chi_{\boldsymbol{v}}^{1/2}} \right)_{\Omega_f} - \left(\nabla_h \cdot \overline{\chi_{\boldsymbol{\sigma}_s}^{1/2}}, \partial_t \chi_{\boldsymbol{u}}^{1/2} \right)_{\Omega_s} - \left(\nabla_h \cdot \overline{\chi_{\boldsymbol{\sigma}_f}^{1/2}}, \overline{\chi_{\boldsymbol{v}}^{1/2}} \right)_{\Omega_f} \\
&\qquad = \left(2 r_{\boldsymbol{u}}^0, \partial_t \chi_{\boldsymbol{u}}^{1/2} \right)_{\Omega_s} + \left(2 r_{\boldsymbol{v}}^0, \overline{\chi_{\boldsymbol{v}}^{1/2}} \right)_{\Omega_f}, \\
&\left(\mathcal{A} \partial_t \chi_{\boldsymbol{\sigma}_s}^{1/2}, \overline{\chi_{\boldsymbol{\sigma}_s}^{1/2}} \right)_{\Omega_s} + \left(\mathcal{A}_\infty \overline{\chi_{\boldsymbol{\sigma}_f}^{1/2}}, \overline{\chi_{\boldsymbol{\sigma}_f}^{1/2}} \right)_{\Omega_f} + \left(\partial_t \chi_{\boldsymbol{u}}^{1/2}, \nabla_h \cdot \overline{\chi_{\boldsymbol{\sigma}_s}^{1/2}} \right)_{\Omega_s} + \left(\overline{\chi_{\boldsymbol{v}}^{1/2}}, \nabla_h \cdot \overline{\chi_{\boldsymbol{\sigma}_f}^{1/2}} \right)_{\Omega_f} \\
&\qquad = \left(\mathcal{A} \partial_t \eta_{\boldsymbol{\sigma}_s}^{1/2}, \overline{\chi_{\boldsymbol{\sigma}_s}^{1/2}} \right)_{\Omega_s} + \left(\mathcal{A}_\infty \eta_{\boldsymbol{\sigma}_f}^{1/2}, \overline{\chi_{\boldsymbol{\sigma}_f}^{1/2}} \right)_{\Omega_f} + 2I^0 + 2E^0.
\end{aligned}$$

These sum to

$$\begin{aligned}
&\rho_s \frac{2}{\Delta t} \| \partial_t \chi_{\boldsymbol{u}}^{1/2} \|_{\Omega_s}^2 + \rho_f \left(\partial_t \chi_{\boldsymbol{v}}^{1/2}, \overline{\chi_{\boldsymbol{v}}^{1/2}} \right)_{\Omega_f} + \left(\mathcal{A} \partial_t \chi_{\boldsymbol{\sigma}_s}^{1/2}, \overline{\chi_{\boldsymbol{\sigma}_s}^{1/2}} \right)_{\Omega_s} + \| \overline{\chi_{\boldsymbol{\sigma}_f}^{1/2}} \|_{\mathcal{A}_\infty, \Omega_f}^2 \\
&\qquad = \left(\mathcal{A} \partial_t \eta_{\boldsymbol{\sigma}_s}^{1/2}, \overline{\chi_{\boldsymbol{\sigma}_s}^{1/2}} \right)_{\Omega_s} + \left(\mathcal{A}_\infty \eta_{\boldsymbol{\sigma}_f}^{1/2}, \overline{\chi_{\boldsymbol{\sigma}_f}^{1/2}} \right)_{\Omega_f} + \left(2 r_{\boldsymbol{u}}^0, \partial_t \chi_{\boldsymbol{u}}^{1/2} \right)_{\Omega_s} + \left(2 r_{\boldsymbol{v}}^0, \overline{\chi_{\boldsymbol{v}}^{1/2}} \right)_{\Omega_f} + 2I^0 + 2E^0.
\end{aligned} \tag{4.53}$$

We re-write the terms $\left(\partial_t \chi_{\boldsymbol{v}}^{1/2}, \overline{\chi_{\boldsymbol{v}}^{1/2}} \right)_{\Omega_f}$ and $\left(\mathcal{A} \partial_t \chi_{\boldsymbol{\sigma}_s}^{1/2}, \overline{\chi_{\boldsymbol{\sigma}_s}^{1/2}} \right)_{\Omega_s}$ without the discrete derivative terms by adding and subtracting appropriate values. Specifically, to $\left(\partial_t \chi_{\boldsymbol{v}}^{1/2}, \overline{\chi_{\boldsymbol{v}}^{1/2}} \right)_{\Omega_f}$ we add and subtract $\chi_{\boldsymbol{v}}^0$ as follows:

$$\begin{aligned}
\left(\partial_t \chi_{\boldsymbol{v}}^{1/2}, \overline{\chi_{\boldsymbol{v}}^{1/2}} \right)_{\Omega_f} &= \frac{1}{\Delta t} \left(\chi_{\boldsymbol{v}}^1 + \chi_{\boldsymbol{v}}^0 - 2\chi_{\boldsymbol{v}}^0, \overline{\chi_{\boldsymbol{v}}^{1/2}} \right)_{\Omega_f} \\
&= \frac{2}{\Delta t} \| \overline{\chi_{\boldsymbol{v}}^{1/2}} \|_{\Omega_f}^2 - \frac{2}{\Delta t} \left(\chi_{\boldsymbol{v}}^0, \overline{\chi_{\boldsymbol{v}}^{1/2}} \right)_{\Omega_f}.
\end{aligned}$$

A similar procedure is used on the term $\left(\mathcal{A}\partial_t\chi^{1/2}_{\boldsymbol{\sigma}_s}, \overline{\chi^{1/2}_{\boldsymbol{\sigma}_s}}\right)_{\Omega_s}$. Now (4.53) becomes

$$\begin{aligned}\frac{2\rho_s}{\Delta t}\|\partial_t\chi^{1/2}_{\boldsymbol{u}}\|^2_{\Omega_s} + \frac{2\rho_f}{\Delta t}\|\overline{\chi^{1/2}_{\boldsymbol{v}}}\|^2_{\Omega_f} + \frac{2}{\Delta t}\|\overline{\chi^{1/2}_{\boldsymbol{\sigma}_s}}\|^2_{\mathcal{A},\Omega_s} + \|\overline{\chi^{1/2}_{\boldsymbol{\sigma}_f}}\|^2_{\mathcal{A}_\infty,\Omega_f}\\ = \frac{2\rho_f}{\Delta t}\left(\chi^0_{\boldsymbol{v}}, \overline{\chi^{1/2}_{\boldsymbol{v}}}\right)_{\Omega_f} + \frac{2}{\Delta t}\left(\mathcal{A}\chi^0_{\boldsymbol{\sigma}_s}, \overline{\chi^{1/2}_{\boldsymbol{\sigma}_s}}\right)_{\Omega_s} + \left(\mathcal{A}\partial_t\eta^{1/2}_{\boldsymbol{\sigma}_s}, \overline{\chi^{1/2}_{\boldsymbol{\sigma}_s}}\right)_{\Omega_s} + \left(\mathcal{A}_\infty\eta^{1/2}_{\boldsymbol{\sigma}_f}, \overline{\chi^{1/2}_{\boldsymbol{\sigma}_f}}\right)_{\Omega_f}\\ + \left(2r^0_{\boldsymbol{u}}, \partial_t\chi^{1/2}_{\boldsymbol{u}}\right)_{\Omega_s} + \left(2r^0_{\boldsymbol{v}}, \overline{\chi^{1/2}_{\boldsymbol{v}}}\right)_{\Omega_f} + 2I^0 + 2E^0. \qquad (4.54)\end{aligned}$$

Next, we consider the interface integral terms and consistency error terms. First, the consistency error term expands to

$$2E^0 = \mathbb{E}_h\left(\boldsymbol{u}_t^{1/2} - \partial_t\boldsymbol{u}^{1/2}, \overline{\chi^{1/2}_{\boldsymbol{\sigma}_s}}\right)_{\Omega_s} - \mathbb{E}_h\left(\boldsymbol{u}_t^{1/2}, \overline{\chi^{1/2}_{\boldsymbol{\sigma}_s}}\right)_{\Omega_s} - \mathbb{E}_h\left(\boldsymbol{v}^{1/2}, \overline{\chi^{1/2}_{\boldsymbol{\sigma}_f}}\right)_{\Omega_f}.$$

Since $\overline{\chi^{1/2}_{\boldsymbol{\sigma}_s}}, \overline{\chi^{1/2}_{\boldsymbol{\sigma}_f}} \in \boldsymbol{\Sigma}_h$ and $\boldsymbol{u}_t^{1/2}$, $\boldsymbol{v}^{1/2}$, $\partial_t\boldsymbol{u}^{1/2} \in H^2(\Omega, \mathbb{R}^2)$, the bound (4.20) applies to each term of the above statement. Therefore by using (4.20), we find

$$E^0 \leq Ch^k\left(\|\boldsymbol{u}_t^{1/2} - \partial_t\boldsymbol{u}^{1/2}\|_{2,\Omega_s} + \|\boldsymbol{u}_t^{1/2}\|_{2,\Omega_s}\right)\|\overline{\chi^{1/2}_{\boldsymbol{\sigma}_s}}\|_{\Omega_s} + Ch^k\|\boldsymbol{v}^{1/2}\|_{2,\Omega_f}\|\overline{\chi^{1/2}_{\boldsymbol{\sigma}_f}}\|_{\Omega_f}. \qquad (4.55)$$

Note that k is used to denote the power of h in the consistency bound and is determined by the mixed finite element space chosen. Next we turn our attention to the interface integral terms

$$2I^0 = < \boldsymbol{u}_t^{1/2} - \partial_t\boldsymbol{u}^{1/2}, \overline{\chi^{1/2}_{\boldsymbol{\sigma}_s}}\boldsymbol{n}_s >_\Gamma - < \boldsymbol{u}_t^{1/2}, [\overline{\chi^{1/2}_{\boldsymbol{\sigma}_s}}\boldsymbol{n}] >_\Gamma .$$

Consider first the term $< \boldsymbol{u}_t^{1/2}, [\overline{\chi^{1/2}_{\boldsymbol{\sigma}_s}}\boldsymbol{n}] >_\Gamma$. This integral occurs along a specific interior edge. So this can be bounded using the same arguments as when considering consistency error. Since $\overline{\chi^{1/2}_{\boldsymbol{\sigma}_s}} \in \boldsymbol{\Sigma}_h$,

$$\begin{aligned}< \boldsymbol{u}_t^{1/2}, [\overline{\chi^{1/2}_{\boldsymbol{\sigma}_s}}\boldsymbol{n}] >_\Gamma &= \sum_{e\in\Gamma}\int_e [\overline{\chi^{1/2}_{\boldsymbol{\sigma}_s}}\boldsymbol{n}]\boldsymbol{u}_t^{1/2}ds\\ &\leq Ch^k\|\boldsymbol{u}_t^{1/2}\|_{2,\Omega_s}\|\overline{\chi^{1/2}_{\boldsymbol{\sigma}_s}}\|_{\Omega_s}. \qquad (4.56)\end{aligned}$$

However, the other interface term $< \boldsymbol{u}_t^{1/2} - \partial_t^c\boldsymbol{u}^n, \overline{\chi^{1/2}_{\boldsymbol{\sigma}_s}} \cdot \boldsymbol{n}_s >_\Gamma$ does not involve a difference between functions in the test space and therefore cannot be bounded using the same bounds

as the consistency error. Instead, the term is bounded using the Cauchy-Schwarz Inequality, the Trace Theorem 2.3.2 and the Inverse Assumption (2.25) then taking the maximum over time, as follows:

$$< \boldsymbol{u}_t^{1/2} - \partial_t \boldsymbol{u}^{1/2}, \overline{\chi_{\boldsymbol{\sigma}_s}^{1/2}} \cdot \boldsymbol{n}_s >_\Gamma \leq Ch^{-1/2} \|\boldsymbol{u}_t^{1/2} - \partial_t \boldsymbol{u}^{1/2}\|_\Gamma \|\overline{\chi_{\boldsymbol{\sigma}_s}^{1/2}}\|_{\Omega_s}. \tag{4.57}$$

Now, by applying (4.55), (4.56)(4.57) and the Cauchy-Schwarz Inequality to (4.54), multiplying by $\frac{\Delta t}{2}$, and recalling the initial bound (4.21) we find

$$\begin{aligned} &\rho_s \|\partial_t \chi_{\boldsymbol{u}}^{1/2}\|_{\Omega_s}^2 + \rho_f \|\overline{\chi_{\boldsymbol{v}}^{1/2}}\|_{\Omega_f}^2 + \|\overline{\chi_{\boldsymbol{\sigma}_s}^{1/2}}\|_{\mathcal{A},\Omega_s}^2 + \frac{\Delta t}{2} \|\overline{\chi_{\boldsymbol{\sigma}_f}^{1/2}}\|_{\mathcal{A}_\infty,\Omega_f}^2 \\ &\qquad \leq I + II. \end{aligned} \tag{4.58}$$

with

$$\begin{aligned} I = {} & \|\chi_{\boldsymbol{\sigma}_s}^0\|_{\mathcal{A},\Omega_s} \|\overline{\chi_{\boldsymbol{\sigma}_s}^{1/2}}\|_{\mathcal{A},\Omega_s} + \frac{\Delta t}{2} \|\partial_t \eta_{\boldsymbol{\sigma}_s}^{1/2}\|_{\mathcal{A},\Omega_s} \|\overline{\chi_{\boldsymbol{\sigma}_s}^{1/2}}\|_{\mathcal{A},\Omega_s} + \frac{\Delta t}{2} \|\eta_{\boldsymbol{\sigma}_f}^{1/2}\|_{\mathcal{A}_\infty,\Omega_f} \|\overline{\chi_{\boldsymbol{\sigma}_f}^{1/2}}\|_{\mathcal{A}_\infty,\Omega_f} \\ & + \Delta t \|r_{\boldsymbol{u}}^0\|_{\Omega_s} \|\partial_t \chi_{\boldsymbol{u}}^{1/2}\|_{\Omega_s} + \Delta t \|r_{\boldsymbol{v}}^0\|_{\Omega_f} \|\overline{\chi_{\boldsymbol{v}}^{1/2}}\|_{\Omega_f}, \\ II = {} & Ch^k \Delta t \|\boldsymbol{u}_t^{1/2} - \partial_t \boldsymbol{u}^{1/2}\|_{2,\Omega_s} \|\overline{\chi_{\boldsymbol{\sigma}_s}^{1/2}}\|_{\Omega_s} + Ch^k \Delta t \|\boldsymbol{u}_t^{1/2}\|_{2,\Omega_s} \|\overline{\chi_{\boldsymbol{\sigma}_s}^{1/2}}\|_{\Omega_s} \\ & + Ch^k \Delta t \|\boldsymbol{v}^{1/2}\|_{2,\Omega_f} \|\overline{\chi_{\boldsymbol{\sigma}_f}^{1/2}}\|_{\Omega_f} + \Delta t Ch^{-1/2} \|\boldsymbol{u}_t^{1/2} - \partial_t \boldsymbol{u}^{1/2}\|_\Gamma \|\overline{\chi_{\boldsymbol{\sigma}_s}^{1/2}}\|_{\Omega_s}. \end{aligned}$$

We will now follow a procedure similar to that in Lemma 4.3.8. To bound each of the terms in I we directly apply Young's Inequality with an ϵ chosen so that terms matching the left hand side can be subtracted, as described above (4.31). For example, when considering $\frac{\Delta t}{2} \|\partial_t \eta_{\boldsymbol{\sigma}_s}^{1/2}\|_{\mathcal{A},\Omega_s} \|\overline{\chi_{\boldsymbol{\sigma}_s}^{1/2}}\|_{\mathcal{A},\Omega_s}$, we note that $\|\overline{\chi_{\boldsymbol{\sigma}_s}^{1/2}}\|_{\mathcal{A},\Omega_s}^2$ appears on the left hand side of (4.58). Therefore choose $\epsilon = 1$ so that

$$\frac{\Delta t}{2} \|\partial_t \eta_{\boldsymbol{\sigma}_s}^{1/2}\|_{\mathcal{A},\Omega_s} \|\overline{\chi_{\boldsymbol{\sigma}_s}^{1/2}}\|_{\mathcal{A},\Omega_s} \leq \frac{1}{4} \|\overline{\chi_{\boldsymbol{\sigma}_s}^{1/2}}\|_{\mathcal{A},\Omega_s}^2 + \frac{\Delta t^2}{4} \|\partial_t \eta_{\boldsymbol{\sigma}_s}^{1/2}\|_{\mathcal{A},\Omega_s}^2.$$

This is repeated with the other terms of I. For the terms in II we first use the equivalence of $\|\cdot\|_{\mathcal{A}_\infty,\Omega_f}$ to $\|\cdot\|_{\Omega_f}$ shown in (3.8) and the equivalence of $\|\cdot\|_{\mathcal{A},\Omega_s}$ to $\|\cdot\|_{\Omega_s}$ shown in (2.8), to find

$$\begin{aligned} II = {} & Ch^k \Delta t \|\boldsymbol{u}_t^{1/2} - \partial_t \boldsymbol{u}^{1/2}\|_{2,\Omega_s} \|\overline{\chi_{\boldsymbol{\sigma}_s}^{1/2}}\|_{\mathcal{A},\Omega_s} + Ch^k \Delta t \|\boldsymbol{u}_t^{1/2}\|_{2,\Omega_s} \|\overline{\chi_{\boldsymbol{\sigma}_s}^{1/2}}\|_{\mathcal{A},\Omega_s} \\ & + Ch^k \Delta t \|\boldsymbol{v}^{1/2}\|_{2,\Omega_f} \|\overline{\chi_{\boldsymbol{\sigma}_f}^{1/2}}\|_{\mathcal{A}_\infty,\Omega_f} + \Delta t Ch^{-1/2} \|\boldsymbol{u}_t^{1/2} - \partial_t \boldsymbol{u}^{1/2}\|_\Gamma \|\overline{\chi_{\boldsymbol{\sigma}_s}^{1/2}}\|_{\mathcal{A},\Omega_s} \end{aligned} \tag{4.59}$$

for some constant C. Now Young's Inequality is applied to each of terms in (4.59) as described above. Therefore,

$$\begin{aligned}
&\rho_s\|\partial_t\chi_{\boldsymbol{u}}^{1/2}\|_{\Omega_s}^2+\rho_f\|\overline{\chi_{\boldsymbol{v}}^{1/2}}\|_{\Omega_f}^2+\|\overline{\chi_{\boldsymbol{\sigma}_s}^{1/2}}\|_{\mathcal{A},\Omega_s}^2+\frac{\Delta t}{2}\|\overline{\chi_{\boldsymbol{\sigma}_f}^{1/2}}\|_{\mathcal{A}_\infty,\Omega_f}^2\\
&\quad\leq C\Big(\|\chi_{\boldsymbol{\sigma}_s}^0\|_{\mathcal{A},\Omega_s}^2+\Delta t^2\|\partial_t\eta_{\boldsymbol{\sigma}_s}^{1/2}\|_{\mathcal{A},\Omega_s}^2+\Delta t\|\eta_{\boldsymbol{\sigma}_f}^{1/2}\|_{\mathcal{A}_\infty,\Omega_f}^2+\Delta t^2\|r_{\boldsymbol{u}}^0\|_{\Omega_s}^2+\Delta t^2\|r_{\boldsymbol{v}}^0\|_{\Omega_f}^2\\
&\qquad h^{2k}\Delta t^2\|\boldsymbol{u}_t^{1/2}-\partial_t\boldsymbol{u}^{1/2}\|_{2,\Omega_s}^2+h^{2k}\Delta t^2\|\boldsymbol{u}_t^{1/2}\|_{2,\Omega_s}^2+h^{2k}\Delta t^2\|\boldsymbol{v}^{1/2}\|_{2,\Omega_f}^2\\
&\qquad +h^{-1}\Delta t^2\|\boldsymbol{u}_t^{1/2}-\partial_t\boldsymbol{u}^{1/2}\|_{\Gamma}^2\Big).
\end{aligned}\tag{4.60}$$

Note that

$$\|\partial_t\eta_{\boldsymbol{\sigma}_s}^{1/2}\|_{\mathcal{A},\Omega_s}^2\leq C\left(\Delta t^3\|(\boldsymbol{\sigma}_s^{1/2})_{ttt}\|_{L^2(0,\Delta t;L^2(\Omega_s))}^2+\Delta t^3\|\Pi_h(\boldsymbol{\sigma}_s^{1/2})_{ttt}\|_{L^2(0,\Delta t;L^2(\Omega_s))}^2+h^{2m_1}\|(\boldsymbol{\sigma}_s^{1/2})_t\|_{m_1}^2\right).$$

This can be obtained by adding and subtracting $(\eta_{\boldsymbol{\sigma}_s})_t^{1/2}$ inside the norm on the left hand side, then using (4.15a) and (4.9a). Use the equivalence of $\|\cdot\|_{\mathcal{A}_\infty,\Omega_f}$ to $\|\cdot\|_{\Omega_f}$ shown in (3.8) to bound $\|\eta_{\boldsymbol{\sigma}_f}^{1/2}\|_{\mathcal{A}_\infty,\Omega_f}^2$ By noting (4.35), (4.9a), (4.50), (4.51), (4.15b) with (4.60) we find

$$\begin{aligned}
&\rho_s\|\partial_t\chi_{\boldsymbol{u}}^{1/2}\|_{\Omega_s}^2+\rho_f\|\overline{\chi_{\boldsymbol{v}}^{1/2}}\|_{\Omega_f}^2+\|\overline{\chi_{\boldsymbol{\sigma}_s}^{1/2}}\|_{\mathcal{A},\Omega_s}^2+\frac{\Delta t}{2}\|\overline{\chi_{\boldsymbol{\sigma}_f}^{1/2}}\|_{\mathcal{A}_\infty,\Omega_f}^2\\
&\quad\leq C\Big(h^{2m_1}\left(\|\boldsymbol{\sigma}_s^0\|_{m_1,\Omega_s}^2+\|\boldsymbol{\sigma}_f^0\|_{m_1,\Omega_f}^2\right)+h^{2k}\left(\|\boldsymbol{u}^0\|_{2,\Omega_s}^2+\|\boldsymbol{v}^0\|_{2,\Omega_f}^2\right)+h^{2r}\|p^0\|_{r-2,\Omega_f}^2\\
&\qquad +h^{2m}q^0+\Delta t^5\left(\|(\boldsymbol{\sigma}_s^{1/2})_{ttt}\|_{L^2(0,\Delta t;L^2(\Omega_s))}^2+\|\Pi_h(\boldsymbol{\sigma}_s^{1/2})_{ttt}\|_{L^2(0,\Delta t;L^2(\Omega_s))}^2\right)\\
&\qquad +h^{2m_1}\Delta t^2\|(\boldsymbol{\sigma}_s^{1/2})_t\|_{m_1}^2+h^{2m_1}\Delta t\|\boldsymbol{\sigma}_f^{1/2}\|_{m_1,\Omega_f}+\Delta t^4\|\boldsymbol{u}_{ttt}\|_{L_{\Delta t}^\infty(L^2(\Omega_s))}^2\\
&\qquad +\Delta t^5\|\boldsymbol{v}_{ttt}\|_{L^2\left(0,\Delta t;L^2(\Omega_f)\right)}^2+h^{2k}\Delta t^5\|\boldsymbol{u}_{ttt}\|_{L^2(0,\Delta t;L^2(\Omega_s))}^2+h^{2k}\Delta t^2\|\boldsymbol{u}_t^{1/2}\|_{2,\Omega_s}^2\\
&\qquad +h^{2k}\Delta t^2\|\boldsymbol{v}^{1/2}\|_{2,\Omega_f}^2+h^{-1}\Delta t^5\|\boldsymbol{u}_{ttt}\|_{L^2(0,\Delta t;L^2(\Gamma))}^2\Big).
\end{aligned}\tag{4.61}$$

The result (4.52) follows by recalling that $2l=\min\{2k,2m_1,2r,2w\}$ in (4.35). □

Theorem 4.3.14. *Under the same assumptions as Lemma* 4.3.10

$$\begin{aligned}
&\rho_s\|\partial_t\boldsymbol{u}_h^{1/2}-\boldsymbol{u}_t^{1/2}\|_{\Omega_s}^2+\rho_f\|\overline{\boldsymbol{v}_h^{1/2}}-\overline{\boldsymbol{v}^{1/2}}\|_{\Omega_f}^2+\|\overline{\boldsymbol{\sigma}_{s_h}^{1/2}}-\overline{\boldsymbol{\sigma}_s^{1/2}}\|_{\mathcal{A},\Omega_s}^2+\frac{\Delta t}{2}\|\overline{\boldsymbol{\sigma}_{f_h}^{1/2}}-\overline{\boldsymbol{\sigma}_f^{1/2}}\|_{\mathcal{A}_\infty,\Omega_f}^2\\
&\leq C_2\left(h^{2l}+\Delta t^4+h^{2m_1}+h^{2k}\Delta t+h^{-1}\Delta t^5\right)+Ch^{2m_2}
\end{aligned}\tag{4.62}$$

with C_2 as defined in (4.37) *and* $C = C\left(\|\boldsymbol{u}_t^{1/2}\|^2_{m_2,\Omega_s} + \|\boldsymbol{v}^{1/2}\|^2_{m_2,\Omega_f}\right)$. *Here m_1 and m_2 are convergence rates determined by the mixed finite element spaces chosen as in* (4.9a) *and* (4.9b), *k is determined by the consistency error as in* (4.20), *and l is a convergence rate determined by the mixed finite element spaces used as described in Lemma* 4.3.8.

Proof. This follows directly from the Triangle and Young's Inequalities and Lemma 4.3.13. □

We see that that bound in Theorem 4.3.14 contains several problematic bounds. Specifically, $Ch^{-1}\Delta t^5$ is a result of the interface integrals. Additionally, the term $h^{2m_1}\Delta t$ depends on both the time and spacial discretizations. In the next section we will find an error estimate for the later time steps. By the end of this analysis, the error bound (4.62) is improved upon so that the $h^{2m_1}\Delta t$ term does not appear. For the analysis in the next section, (4.58) is altered. Young's Inequality is applied to terms involving the initial step, $\|\chi^0_{\boldsymbol{\sigma}_s}\|_{\mathcal{A},\Omega_s}\|\overline{\chi^{1/2}_{\boldsymbol{\sigma}_s}}\|_{\mathcal{A},\Omega_s}$. Then we take the maximum over time on the right hand side of to find

$$\begin{aligned}\rho_s\|\partial_t\chi^{1/2}_{\boldsymbol{u}}\|^2_{\Omega_s} + \rho_f\|\overline{\chi^{1/2}_{\boldsymbol{v}}}\|^2_{\Omega_f} + \|\overline{\chi^{1/2}_{\boldsymbol{\sigma}_s}}\|^2_{\mathcal{A},\Omega_s} + \frac{\Delta t}{2}\|\overline{\chi^{1/2}_{\boldsymbol{\sigma}_f}}\|^2_{\mathcal{A}_\infty,\Omega_f}\\ \leq I + II\end{aligned} \tag{4.63}$$

with

$$\begin{aligned}I = \|\chi^0_{\boldsymbol{\sigma}_s}\|^2_{\mathcal{A},\Omega_s} + \frac{\Delta t}{2}\|\partial_t\eta^{1/2}_{\boldsymbol{\sigma}_s}\|_{\mathcal{A},\Omega_s}\|\chi_{\boldsymbol{\sigma}_s}\|_{\overline{L^\infty_{\Delta t}}(\mathcal{A},\Omega_s)} + \frac{\Delta t}{2}\|\eta^{1/2}_{\boldsymbol{\sigma}_f}\|_{\mathcal{A}_\infty,\Omega_f}\|\chi_{\boldsymbol{\sigma}_f}\|_{\overline{L^\infty_{\Delta t}}\left(\mathcal{A}_\infty,\Omega_f\right)}\\ + \Delta t\|r^0_{\boldsymbol{u}}\|_{\Omega_s}\|\partial_t\chi_{\boldsymbol{u}}\|_{\overline{L^\infty_{\Delta t}}(L^2(\Omega_s))} + \Delta t\|r^0_{\boldsymbol{v}}\|_{\Omega_f}\|\chi_{\boldsymbol{v}}\|_{\overline{L^\infty_{\Delta t}}\left(L^2(\Omega_f)\right)},\\ II = Ch^k\Delta t\|\boldsymbol{u}_t^{1/2} - \partial_t\boldsymbol{u}^{1/2}\|_{2,\Omega_s}\|\chi_{\boldsymbol{\sigma}_s}\|_{\overline{L^\infty_{\Delta t}}(L^2(\Omega_s))} + Ch^k\Delta t\|\boldsymbol{u}_t\|_{L^\infty_{\Delta t}\left(H^2(\Omega_f)\right)}\|\chi_{\boldsymbol{\sigma}_s}\|_{\overline{L^\infty_{\Delta t}}(L^2(\Omega_s))}\\ + Ch^k\Delta t\|\boldsymbol{v}\|_{L^\infty_{\Delta t}\left(H^2(\Omega_f)\right)}\|\chi_{\boldsymbol{\sigma}_f}\|_{\overline{L^\infty_{\Delta t}}\left(L^2(\Omega_f)\right)} + Ch^k\Delta t\|\boldsymbol{u}_t\|_{L^\infty_{\Delta t}\left(H^2(\Omega_f)\right)}\|\chi_{\boldsymbol{\sigma}_s}\|_{\overline{L^\infty_{\Delta t}}(L^2(\Omega_s))}\\ + \Delta tCh^{-1/2}\|\boldsymbol{u}_t^{1/2} - \partial_t\boldsymbol{u}^{1/2}\|_\Gamma\|\chi_{\boldsymbol{\sigma}_s}\|_{\overline{L^\infty_{\Delta t}}(L^2(\Omega_s))}.\end{aligned}$$

4.3.5 Error Analysis for time steps $n \geq 1$

Next, we seek to find an error bound over all time steps. We will consider the difference between equations (4.10) and (4.4) for $n \geq 1$.

Lemma 4.3.15. *Let* $(\boldsymbol{\sigma}(t), \boldsymbol{\omega}(t)) \in (\boldsymbol{\Sigma}, \mathcal{V})$ *be the solution to* (4.4) *and* $(\boldsymbol{\sigma}^{n+1}\boldsymbol{\omega}_h^{n+1}) \in (\boldsymbol{\Sigma}_h, \mathcal{V}_h)$ *be the solution to* (4.10)*. Then,*

$$\begin{aligned}
&\rho_s \left(\partial_t^2 \chi_{\boldsymbol{u}}^n, \boldsymbol{\nu}\right)_{\Omega_s} + \rho_f \left(\partial_t^c \chi_{\boldsymbol{v}}^n, \boldsymbol{\nu}\right)_{\Omega_f} - \left(\nabla_h \cdot \widetilde{\chi_{\boldsymbol{\sigma}_s}^n}, \boldsymbol{\nu}\right)_{\Omega_s} - \left(\nabla_h \cdot \widetilde{\chi_{\boldsymbol{\sigma}_f}^n}, \boldsymbol{\nu}\right)_{\Omega_f} \\
&\qquad = \left(r_{\boldsymbol{u}}^n, \boldsymbol{\nu}\right)_{\Omega_s} + \left(r_{\boldsymbol{v}}^n, \boldsymbol{\nu}\right)_{\Omega_f}, \qquad \boldsymbol{\nu} \in \mathcal{V}_h, \qquad (4.64a) \\
&\left(\mathcal{A}\partial_t^c \chi_{\boldsymbol{\sigma}_s}^n, \boldsymbol{\tau}\right)_{\Omega_s} + \left(\mathcal{A}_\infty \widetilde{\chi_{\boldsymbol{\sigma}_f}^n}, \boldsymbol{\tau}\right)_{\Omega_f} + \left(\partial_t^c \chi_{\boldsymbol{u}}^n, \nabla_h \cdot \boldsymbol{\tau}\right)_{\Omega_s} + \left(\widetilde{\chi_{\boldsymbol{v}}^n}, \nabla_h \cdot \boldsymbol{\tau}\right)_{\Omega_f} \\
&\qquad = \left(\mathcal{A}\partial_t^c \eta_{\boldsymbol{\sigma}_s}^n, \boldsymbol{\tau}\right)_{\Omega_s} + \left(\mathcal{A}_\infty \widetilde{\eta_{\boldsymbol{\sigma}_f}^n}, \boldsymbol{\tau}\right)_{\Omega_f} + I^n + E^n(\boldsymbol{\tau}), \qquad \boldsymbol{\tau} \in \boldsymbol{\Sigma}_h \qquad (4.64b)
\end{aligned}$$

with

$$\begin{aligned}
r_{\boldsymbol{u}}^n &= \rho_s \left(\widetilde{\boldsymbol{u}_{tt}^n} - \partial_t^2 \boldsymbol{u}^n\right), \\
r_{\boldsymbol{v}}^n &= \rho_f \left(\widetilde{\boldsymbol{v}_t^n} - \partial_t^c \boldsymbol{v}^n\right), \\
I^n &= < \widetilde{\boldsymbol{u}_t^n} - \partial_t^c \boldsymbol{u}^n, \boldsymbol{\tau}\boldsymbol{n}_s >_\Gamma - < \widetilde{\boldsymbol{u}_t^n}, [\boldsymbol{\tau} \cdot n] >_\Gamma, \\
E^n(\boldsymbol{\tau}) &= \mathbb{E}_h \left(\widetilde{\boldsymbol{u}_t^n} - \partial_t^c \boldsymbol{u}^n, \boldsymbol{\tau}\right)_{\Omega_s} - \mathbb{E}_h \left(\widetilde{\boldsymbol{u}_t^n}, \boldsymbol{\tau}\right)_{\Omega_s} - \mathbb{E}_h \left(\widetilde{\boldsymbol{v}^n}, \boldsymbol{\tau}\right)_{\Omega_f}.
\end{aligned}$$

Proof. Subtracting (4.4d) from (4.10a) we find

$$\begin{aligned}
&\rho_s \left(\partial_t^2 {\boldsymbol{u}_h}^n - u_{tt}^n, \boldsymbol{\nu}\right)_{\Omega_s} + \rho_f \left(\partial_t^c \boldsymbol{v}_h^n - v_t^n, \boldsymbol{\nu}\right)_{\Omega_f} - \left(\nabla_h \cdot \widetilde{\boldsymbol{\sigma}_{s_h}^n} - \nabla \cdot \boldsymbol{\sigma}_s^n, \boldsymbol{\nu}\right)_{\Omega_s} \\
&\quad - \left(\nabla_h \cdot \widetilde{\boldsymbol{\sigma}_{f_h}^n} - \nabla \cdot \boldsymbol{\sigma}_f^n, \boldsymbol{\nu}\right)_{\Omega_f} = \left(\widetilde{\boldsymbol{f}_s^n} - \boldsymbol{f}_s^n, \boldsymbol{\nu}\right)_{\Omega_s} + \left(\widetilde{\boldsymbol{f}_f^n} - \boldsymbol{f}_f^n, \boldsymbol{\nu}\right)_{\Omega_f}. \qquad (4.65)
\end{aligned}$$

To write this in terms of auxiliary and projection errors, we add and subtract appropriate quantities. For example, to $\partial_t^2 {\boldsymbol{u}_h}^n - u_{tt}^n$ we add and subtract $\partial_t^2 \mathcal{P}_h u^n$, $\partial_t^2 \boldsymbol{u}^n$ and $\widetilde{\boldsymbol{u}_{tt}^n}$ to find that

$$\partial_t^2 {\boldsymbol{u}_h}^n - u_{tt}^n = \partial_t^2 \chi_{\boldsymbol{u}}^n - \partial_t^2 \eta_{\boldsymbol{u}}^n + \partial_t^2 \boldsymbol{u}^n - \widetilde{\boldsymbol{u}_{tt}^n} + \widetilde{\boldsymbol{u}_{tt}^n} - u_{tt}^n.$$

Similar additions and subtractions are made to the other right hand side terms and (4.65) becomes

$$\begin{aligned}
&\rho_s \left(\partial_t^2 \chi_{\boldsymbol{u}}^n, \boldsymbol{\nu}\right)_{\Omega_s} + \rho_f \left(\partial_t^c \chi_{\boldsymbol{v}}^n, \boldsymbol{\nu}\right)_{\Omega_f} - \left(\nabla_h \cdot \widetilde{\chi_{\boldsymbol{\sigma}_s}^n}, \boldsymbol{\nu}\right)_{\Omega_s} - \left(\nabla_h \cdot \widetilde{\chi_{\boldsymbol{\sigma}_f}^n}, \boldsymbol{\nu}\right)_{\Omega_f} \\
&\quad = \rho_s \left(\widetilde{\boldsymbol{u}_{tt}^n} - \partial_t^2 \boldsymbol{u}^n, \boldsymbol{\nu}\right)_{\Omega_s} + \rho_s \left(\boldsymbol{u}_{tt}^n - \widetilde{\boldsymbol{u}_{tt}^n}, \boldsymbol{\nu}\right)_{\Omega_s} + \rho_f \left(\widetilde{\boldsymbol{v}_t^n} - \partial_t^c \boldsymbol{v}^n, \boldsymbol{\nu}\right)_{\Omega_f} \\
&\qquad + \rho_f \left(\boldsymbol{v}_t^n - \widetilde{\boldsymbol{v}_t^n}, \boldsymbol{\nu}\right)_{\Omega_f} - \left(\nabla \cdot \boldsymbol{\sigma}_s^n - \nabla_h \cdot \widetilde{\boldsymbol{\sigma}_s^n}, \boldsymbol{\nu}\right)_{\Omega_s} - \left(\nabla \cdot \boldsymbol{\sigma}_f^n - \nabla_h \cdot \widetilde{\boldsymbol{\sigma}_f^n}, \boldsymbol{\nu}\right)_{\Omega_f} \\
&\qquad - \left(\boldsymbol{f}_s^n - \widetilde{\boldsymbol{f}_s^n}, \boldsymbol{\nu}\right)_{\Omega_s} - \left(\boldsymbol{f}_f^n - \widetilde{\boldsymbol{f}_f^n}, \boldsymbol{\nu}\right)_{\Omega_f}. \qquad (4.66)
\end{aligned}$$

By subtracting (4.17b) to (4.4d) and (4.4d) at time t^n we find

$$\begin{aligned}
&\rho_s \left(\boldsymbol{u}_{tt}^2 - \widetilde{\boldsymbol{u}_{tt}^n}, \boldsymbol{\nu}\right)_{\Omega_s} + \rho_f \left(\boldsymbol{v}_t^n - \widetilde{\boldsymbol{v}_t^n}, \boldsymbol{\nu}\right)_{\Omega_f} - \left(\nabla \cdot \left(\boldsymbol{\sigma}_s^n - \widetilde{\boldsymbol{\sigma}_s^n}\right), \boldsymbol{\nu}\right)_{\Omega_s} - \left(\nabla \cdot \left(\boldsymbol{\sigma}_f^n - \widetilde{\boldsymbol{\sigma}_f^n}\right), \boldsymbol{\nu}\right)_{\Omega_f} \\
&\quad = \left(\boldsymbol{f}_s^n - \widetilde{\boldsymbol{f}_s^n}, \boldsymbol{\nu}\right)_{\Omega_s} + \left(\boldsymbol{f}_f^n - \widetilde{\boldsymbol{f}_f^n}, \boldsymbol{\nu}\right)_{\Omega_f}.
\end{aligned}$$

By using the above statement with (4.66), we find

$$\begin{aligned}
&\rho_s \left(\partial_t^2 \chi_{\boldsymbol{u}}^n, \boldsymbol{\nu}\right)_{\Omega_s} + \rho_f \left(\partial_t^c \chi_{\boldsymbol{v}}^n, \boldsymbol{\nu}\right)_{\Omega_f} - \left(\nabla_h \cdot \widetilde{\chi_{\boldsymbol{\sigma}_s}^n}, \boldsymbol{\nu}\right)_{\Omega_s} - \left(\nabla_h \cdot \widetilde{\chi_{\boldsymbol{\sigma}_f}^n}, \boldsymbol{\nu}\right)_{\Omega_f} \\
&\quad = \rho_s \left(\widetilde{\boldsymbol{u}_{tt}^n} - \partial_t^2 \boldsymbol{u}^n, \boldsymbol{\nu}\right)_{\Omega_s} + \rho_f \left(\widetilde{\boldsymbol{v}_t^n} - \partial_t^c \boldsymbol{v}^n, \boldsymbol{\nu}\right)_{\Omega_f} \\
&\qquad - \left(\nabla \cdot \widetilde{\boldsymbol{\sigma}_s^n} - \nabla_h \cdot \widetilde{\boldsymbol{\sigma}_s^n}, \boldsymbol{\nu}\right)_{\Omega_s} - \left(\nabla \cdot \widetilde{\boldsymbol{\sigma}_f^n} - \nabla_h \cdot \widetilde{\boldsymbol{\sigma}_f^n}, \boldsymbol{\nu}\right)_{\Omega_f}. \qquad (4.67)
\end{aligned}$$

Note that for the continuous functions $\boldsymbol{\sigma}_s$ and $\boldsymbol{\sigma}_f$

$$\begin{aligned}
\left(\nabla \cdot \widetilde{\boldsymbol{\sigma}_s^n} - \nabla_h \cdot \widetilde{\boldsymbol{\sigma}_s^n}, \boldsymbol{\nu}\right)_{\Omega_s} &= 0, \\
\left(\nabla \cdot \widetilde{\boldsymbol{\sigma}_f^n} - \nabla_h \cdot \widetilde{\boldsymbol{\sigma}_f^n}, \boldsymbol{\nu}\right)_{\Omega_f} &= 0.
\end{aligned}$$

Therefore (4.64a) follows directly from (4.67).

To prove (4.64b), consider the difference between (4.10b) and (4.19)

$$\begin{aligned}
&\left(\mathcal{A}\left(\partial_t^c \boldsymbol{\sigma}_{s_h}^n - (\boldsymbol{\sigma}_s)_t^n\right), \boldsymbol{\tau}\right)_{\Omega_s} + \left(\mathcal{A}_\infty \left(\widetilde{\boldsymbol{\sigma}_{f_h}^n} - \boldsymbol{\sigma}_f^n\right), \boldsymbol{\tau}\right)_{\Omega_f} + \left(\partial_t^c \boldsymbol{u}_h^n - u_t^n, \nabla_h \cdot \boldsymbol{\tau}\right)_{\Omega_s} \\
&\quad + \left(\widetilde{\boldsymbol{v}_h^n} - \boldsymbol{v}^n, \nabla_h \cdot \boldsymbol{\tau}\right)_{\Omega_f} \\
&\qquad = - < \boldsymbol{u}_t(t_n), \boldsymbol{\tau}\boldsymbol{n}_s >_\Gamma - < \boldsymbol{v}(t_n), \boldsymbol{\tau}\boldsymbol{n}_f >_\Gamma - \mathbb{E}_h\left(\boldsymbol{u}_t^n, \boldsymbol{\tau}\right)_{\Omega_s} - \mathbb{E}_h\left(\boldsymbol{v}^n, \boldsymbol{\tau}\right)_{\Omega_f}. \qquad (4.68)
\end{aligned}$$

We re-write this in terms of discrete and projection errors by adding and subtracting appropriate terms so (4.68) becomes

$$\begin{aligned}
&\left(\mathcal{A}\partial_t^c\chi_{\boldsymbol{\sigma}_s}^n,\boldsymbol{\tau}\right)_{\Omega_s}+\left(\mathcal{A}_\infty\widetilde{\chi_{\boldsymbol{\sigma}_f}^n},\boldsymbol{\tau}\right)_{\Omega_f}+\left(\partial_t^c\chi_{\boldsymbol{u}}^n,\nabla_h\cdot\boldsymbol{\tau}\right)_{\Omega_s}+\left(\widetilde{\chi_{\boldsymbol{v}}^n},\nabla_h\cdot\boldsymbol{\tau}\right)_{\Omega_f}\\
&\quad=\left(\mathcal{A}\partial_t^c\eta_{\boldsymbol{\sigma}_s}^n,\boldsymbol{\tau}\right)_{\Omega_s}+\left(\mathcal{A}\left(\widetilde{(\boldsymbol{\sigma}_s)_t^n}-\partial_t^c\boldsymbol{\sigma}_s^n\right),\boldsymbol{\tau}\right)_{\Omega_s}+\left(\mathcal{A}\left((\boldsymbol{\sigma}_s)_t^n-\widetilde{(\boldsymbol{\sigma}_s)_t^n}\right),\boldsymbol{\tau}\right)_{\Omega_s}\\
&\qquad+\left(\mathcal{A}_\infty\widetilde{\eta_{\boldsymbol{\sigma}_f}^n},\boldsymbol{\tau}\right)_{\Omega_f}+\left(\mathcal{A}_\infty\left(\boldsymbol{\sigma}_f^n-\widetilde{\boldsymbol{\sigma}_f^n}\right),\boldsymbol{\tau}\right)_{\Omega_f}+\left(\widetilde{\boldsymbol{u}_t^n}-\partial_t^c\boldsymbol{u}^n,\nabla_h\cdot\boldsymbol{\tau}\right)_{\Omega_s}\\
&\qquad+\left(u_t^n-\widetilde{\boldsymbol{u}_t^n},\nabla_h\cdot\boldsymbol{\tau}\right)_{\Omega_s}+\left(\boldsymbol{v}^n-\widetilde{v^n},\nabla_h\cdot\boldsymbol{\tau}\right)_{\Omega_f}\\
&\qquad-<\boldsymbol{u}_t^n,\boldsymbol{\tau}\boldsymbol{n}_s>_\Gamma-<\boldsymbol{v}^n,\boldsymbol{\tau}\boldsymbol{n}_f>_\Gamma-\mathbb{E}_h\left(\boldsymbol{u}_t^n,\boldsymbol{\tau}\right)_{\Omega_s}-\mathbb{E}_h\left(\boldsymbol{v}^n,\boldsymbol{\tau}\right)_{\Omega_f}.
\end{aligned}\tag{4.69}$$

Using the result from applying (4.17b) to (4.4e) and subtracting it from (4.4e) at t^n, (4.69) becomes

$$\begin{aligned}
&\left(\mathcal{A}\partial_t^c\chi_{\boldsymbol{\sigma}_s}^n,\boldsymbol{\tau}\right)_{\Omega_s}+\left(\mathcal{A}_\infty\widetilde{\chi_{\boldsymbol{\sigma}_f}^n},\boldsymbol{\tau}\right)_{\Omega_f}+\left(\partial_t^c\widetilde{\chi_{\boldsymbol{u}}^n},\nabla_h\cdot\boldsymbol{\tau}\right)_{\Omega_s}+\left(\chi_{\boldsymbol{v}}^n,\nabla_h\cdot\boldsymbol{\tau}\right)_{\Omega_f}\\
&\quad=\left(\mathcal{A}\partial_t^c\eta_{\boldsymbol{\sigma}_s}^n,\boldsymbol{\tau}\right)_{\Omega_s}+\left(\mathcal{A}\left(\widetilde{(\boldsymbol{\sigma}_s)_t^n}-\partial_t^c\boldsymbol{\sigma}_s^n\right),\boldsymbol{\tau}\right)_{\Omega_s}+\left(\mathcal{A}_\infty\widetilde{\eta_{\boldsymbol{\sigma}_f}^n},\boldsymbol{\tau}\right)_{\Omega_f}+\left(\widetilde{\boldsymbol{u}_t^n}-\partial_t^c\boldsymbol{u}^n,\nabla_h\cdot\boldsymbol{\tau}\right)_{\Omega_s}\\
&\qquad-<\widetilde{\boldsymbol{u}_t^n},\boldsymbol{\tau}\boldsymbol{n}_s>_\Gamma-<\widetilde{\boldsymbol{v}^n},\boldsymbol{\tau}\boldsymbol{n}_f>_\Gamma-\mathbb{E}_h\left(\widetilde{\boldsymbol{u}_t^n},\boldsymbol{\tau}\right)_{\Omega_s}-\mathbb{E}_h\left(\widetilde{\boldsymbol{v}^n},\boldsymbol{\tau}\right)_{\Omega_f}.
\end{aligned}$$

See the steps leading to (4.18) for a similar procedure. Then by using the result of taking the difference between (4.17b) applied to (4.48) and (4.17d) applied to (4.48) this is re-written as

$$\begin{aligned}
&\left(\mathcal{A}\partial_t^c\chi_{\boldsymbol{\sigma}_s}^n,\boldsymbol{\tau}\right)_{\Omega_s}+\left(\mathcal{A}_\infty\widetilde{\chi_{\boldsymbol{\sigma}_f}^n},\boldsymbol{\tau}\right)_{\Omega_f}+\left(\partial_t^c\widetilde{\chi_{\boldsymbol{u}}^n},\nabla_h\cdot\boldsymbol{\tau}\right)_{\Omega_s}+\left(\chi_{\boldsymbol{v}}^n,\nabla_h\cdot\boldsymbol{\tau}\right)_{\Omega_f}\\
&\quad=\left(\mathcal{A}\partial_t^c\eta_{\boldsymbol{\sigma}_s}^n,\boldsymbol{\tau}\right)_{\Omega_s}+\left(\mathcal{A}_\infty\widetilde{\eta_{\boldsymbol{\sigma}_f}^n},\boldsymbol{\tau}\right)_{\Omega_f}+<\widetilde{\boldsymbol{u}_t^n}-\partial_t^c\boldsymbol{u}^n,\boldsymbol{\tau}\boldsymbol{n}_s>_\Gamma-<\widetilde{\boldsymbol{u}_t^n},\boldsymbol{\tau}\boldsymbol{n}_s>_\Gamma\\
&\qquad-<\widetilde{\boldsymbol{v}^n},\boldsymbol{\tau}\boldsymbol{n}_f>_\Gamma+\mathbb{E}_h\left(\widetilde{\boldsymbol{u}_t^n}-\partial_t^c\boldsymbol{u}^n,\boldsymbol{\tau}\right)_{\Omega_s}-\mathbb{E}_h\left(\widetilde{\boldsymbol{u}_t^n},\boldsymbol{\tau}\right)_{\Omega_s}-\mathbb{E}_h\left(\widetilde{\boldsymbol{v}^n},\boldsymbol{\tau}\right)_{\Omega_f}.
\end{aligned}\tag{4.70}$$

A similar procedure is used in the proof of Lemma 4.3.10.

Next, we note that the terms $-<\widetilde{\boldsymbol{u}_t^n},\boldsymbol{\tau}\boldsymbol{n}_s>_\Gamma-<\widetilde{\boldsymbol{v}^n},\boldsymbol{\tau}\boldsymbol{n}_f>_\Gamma$ can be re-written in a form similar to the consistency errors. This is done using the interface condition $\boldsymbol{u}_t=\boldsymbol{v}$

on the interface Γ. Therefore,

$$\begin{aligned} - < \widetilde{\boldsymbol{u}_t^n}, \boldsymbol{\tau}\boldsymbol{n}_s >_\Gamma - < \widetilde{\boldsymbol{v}^n}, \boldsymbol{\tau}\boldsymbol{n}_f >_\Gamma &= - < \widetilde{\boldsymbol{u}_t^n}, \boldsymbol{\tau}\boldsymbol{n}_s + \boldsymbol{\tau}\boldsymbol{n}_f >_\Gamma \\ &=< \widetilde{\boldsymbol{u}_t^n}, [\boldsymbol{\tau}\cdot n] >_\Gamma . \end{aligned}$$

Now let

$$I^n =< \widetilde{\boldsymbol{u}_t^n} - \partial_t^c \boldsymbol{u}^n, \boldsymbol{\tau}\boldsymbol{n}_s >_\Gamma - < \widetilde{\boldsymbol{u}_t^n}, [\boldsymbol{\tau}\cdot n] >_\Gamma .$$

The result (4.64b) follows directly from (4.70). □

We expect that there should be no restriction on the step size Δt with this method. Therefore we expect the terms involving divergence to cancel, removing the need for an inverse assumption. With this motivation, we are ready to state and prove the following lemma to bound the projection errors and theorem to bound the error.

Lemma 4.3.16. *Let* $(\boldsymbol{\sigma}(t), \boldsymbol{\omega}(t)) \in (\boldsymbol{\Sigma}, \mathcal{V})$ *be the solution to* (4.4) *and* $(\boldsymbol{\sigma}^{n+1}, \boldsymbol{\omega}_h^{n+1}) \in (\boldsymbol{\Sigma}_h, \mathcal{V}_h)$ *be the solution to* (4.10). *Then,*

$$\begin{aligned} &\|\partial_t \chi_{\boldsymbol{u}}\|^2_{\overline{L^\infty_{\Delta t}}(L^2(\Omega_s))} + \|\chi_{\boldsymbol{v}}\|^2_{\overline{L^\infty_{\Delta t}}\left(L^2(\Omega_f)\right)} + \|\chi_{\boldsymbol{\sigma}_s}\|^2_{\overline{L^\infty_{\Delta t}}(L^2(\Omega_s))} + \Delta t \sum_{i=1}^{N} \|\widetilde{\chi^i_{\boldsymbol{\sigma}_f}}\|^2_{\mathcal{A}_\infty,\Omega_f} \\ &\qquad \le C_3 \left(\Delta t^4 + h^{2m_1} + h^{2k}\Delta t^4 + h^{-1}\Delta t^4 + h^{2k} + h^{2l}\right) \end{aligned} \tag{4.71}$$

with

$$\begin{aligned} C_3 = C \Big(&\|\boldsymbol{u}_{ttt}\|^2_{L^\infty_{\Delta t}(L^2(\Omega_s))}, \|\boldsymbol{u}_{tttt}\|^2_{L^2(0,T;L^2(\Omega_s))}, \|\boldsymbol{v}_{ttt}\|^2_{L^2\left(0,T;L^2(\Omega_f)\right)}, \|\boldsymbol{u}_{ttt}\|^2_{L^2(0,T;H^2(\Omega_s))}, \\ &\|\boldsymbol{u}_{ttt}\|^2_{L^2(0,T;L^2(\partial\Omega_s))}, \|(\boldsymbol{\sigma}_s)_{ttt}\|^2_{L^2(0,T;L^2(\Omega_s))}, \|\Pi_h(\boldsymbol{\sigma}_s)_{ttt}\|^2_{L^2(0,T;L^2(\Omega_s))}, \|(\boldsymbol{\sigma}_s)_t\|^2_{L^2(0,T;H^{m_1}(\Omega_s))} \\ &\|\boldsymbol{\sigma}_f\|^2_{L^2\left(0,T;H^{m_1}(\Omega_f)\right)}, \|\boldsymbol{v}\|^2_{L^\infty_{\Delta t}\left(H^2(\Omega_f)\right)}, \|\boldsymbol{u}_t\|^2_{L^\infty_{\Delta t}\left(H^2(\Omega_f)\right)}, \|\boldsymbol{\sigma}_s^0\|^2_{m_1,\Omega_s}, \\ &\|\boldsymbol{\sigma}_f^0\|^2_{m_1,\Omega_f}, \|\boldsymbol{u}^0\|^2_{2,\Omega_s}\|\boldsymbol{v}^0\|^2_{2,\Omega_f}, \|p^0\|^2_{r-2,\Omega_f}, q^0 \Big) \end{aligned} \tag{4.72}$$

where m_1 *and* m_2 *are convergence rates determined by the mixed finite element spaces chosen as in* (4.9a) *and* (4.9b), k *is determined by the consistency error as in* (4.20), r *is determined by the finite element method used to approximate* p^0, *and* q^0 *represents the norm*

of the initial solution, and l is a convergence rate determined by the mixed finite element spaces used.

Proof. Letting

$$\boldsymbol{\nu} = \begin{cases} \partial_t^c \chi_{\boldsymbol{u}}^n & \text{in } \Omega_s, \\ \widetilde{\chi_{\boldsymbol{v}}^n} & \text{in } \Omega_f, \end{cases}$$

and

$$\boldsymbol{\tau} = \begin{cases} \widetilde{\chi_{\boldsymbol{\sigma}_s}^n} & \text{in } \Omega_s, \\ \widetilde{\chi_{\boldsymbol{\sigma}_f}^n} & \text{in } \Omega_f, \end{cases}$$

in (4.64), we find

$$\begin{aligned} &\rho_s \left(\partial_t^2 \chi_{\boldsymbol{u}}^n, \partial_t^c \chi_{\boldsymbol{u}}^n\right)_{\Omega_s} + \rho_f \left(\partial_t^c \chi_{\boldsymbol{v}}^n, \widetilde{\chi_{\boldsymbol{v}}^n}\right)_{\Omega_f} - \left(\nabla_h \cdot \widetilde{\chi_{\boldsymbol{\sigma}_s}^n}, \partial_t^c \chi_{\boldsymbol{u}}^n\right)_{\Omega_s} - \left(\nabla_h \cdot \widetilde{\chi_{\boldsymbol{\sigma}_f}^n}, \widetilde{\chi_{\boldsymbol{v}}^n}\right)_{\Omega_f} \\ &\qquad = \left(r_{\boldsymbol{u}}^n, \partial_t^c \chi_{\boldsymbol{u}}^n\right)_{\Omega_s} + \left(r_{\boldsymbol{v}}^n, \widetilde{\chi_{\boldsymbol{v}}^n}\right)_{\Omega_f}, \\ &\left(\mathcal{A}\partial_t^c \chi_{\boldsymbol{\sigma}_s}^n, \widetilde{\chi_{\boldsymbol{\sigma}_s}^n}\right)_{\Omega_s} + \left(\mathcal{A}_\infty \widetilde{\chi_{\boldsymbol{\sigma}_f}^n}, \widetilde{\chi_{\boldsymbol{\sigma}_f}^n}\right)_{\Omega_f} + \left(\partial_t^c \chi_{\boldsymbol{u}}^n, \nabla_h \cdot \widetilde{\chi_{\boldsymbol{\sigma}_s}^n}\right)_{\Omega_s} + \left(\widetilde{\chi_{\boldsymbol{v}}^n}, \nabla_h \cdot \widetilde{\chi_{\boldsymbol{\sigma}_f}^n}\right)_{\Omega_f} \\ &\qquad = \left(\mathcal{A}\partial_t^c \eta_{\boldsymbol{\sigma}_s}^n, \widetilde{\chi_{\boldsymbol{\sigma}_s}^n}\right)_{\Omega_s} + \left(\mathcal{A}_\infty \widetilde{\eta_{\boldsymbol{\sigma}_f}^n}, \widetilde{\chi_{\boldsymbol{\sigma}_f}^n}\right)_{\Omega_f} + I^n + E^n. \end{aligned}$$

Adding these equations gives

$$\begin{aligned} &\rho_s \left(\partial_t^2 \chi_{\boldsymbol{u}}^n, \partial_t^c \chi_{\boldsymbol{u}}^n\right)_{\Omega_s} + \rho_f \left(\partial_t^c \chi_{\boldsymbol{v}}^n, \widetilde{\chi_{\boldsymbol{v}}^n}\right)_{\Omega_f} + \left(\mathcal{A}\partial_t^c \chi_{\boldsymbol{\sigma}_s}^n, \widetilde{\chi_{\boldsymbol{\sigma}_s}^n}\right)_{\Omega_s} + \left(\mathcal{A}_\infty \widetilde{\chi_{\boldsymbol{\sigma}_f}^n}, \widetilde{\chi_{\boldsymbol{\sigma}_f}^n}\right)_{\Omega_f} \\ &\qquad = \left(\mathcal{A}\partial_t^c \eta_{\boldsymbol{\sigma}_s}^n, \widetilde{\chi_{\boldsymbol{\sigma}_s}^n}\right)_{\Omega_s} + \left(\mathcal{A}_\infty \widetilde{\eta_{\boldsymbol{\sigma}_f}^n}, \widetilde{\chi_{\boldsymbol{\sigma}_f}^n}\right)_{\Omega_f} + \left(r_{\boldsymbol{u}}^n, \partial_t^c \chi_{\boldsymbol{u}}^n\right)_{\Omega_s} + \left(r_{\boldsymbol{v}}^n, \widetilde{\chi_{\boldsymbol{v}}^n}\right)_{\Omega_f} + \\ &\qquad\qquad + I^n + E^n. \end{aligned} \tag{4.73}$$

To get the desired result, we will be summing (4.73) over all time steps. Therefore we wish to write each of the left hand side terms as differences which will then become telescoping series when summed. For example, for the term $\left(\partial_t^2 \chi_{\boldsymbol{u}}^n, \partial_t^c \chi_{\boldsymbol{u}}^n\right)_{\Omega_s}$ recall (2.45) which states that $\partial_t^2 \chi_{\boldsymbol{u}}^n$ can be written as the difference of discrete first derivatives. Therefore using (2.45) and (2.44) we find

$$\left(\partial_t^2 \chi_{\boldsymbol{u}}^n, \partial_t^c \chi_{\boldsymbol{u}}^n\right)_{\Omega_s} = \frac{1}{2\Delta t} \left(\|\partial_t \chi_{\boldsymbol{u}}^{n+1/2}\|_{\Omega_s}^2 - \|\partial_t \chi_{\boldsymbol{u}}^{n-1/2}\|_{\Omega_s}^2\right).$$

Similar procedures can be used on the remaining terms by noting that for some function q

$$\begin{aligned}\partial_t^c q^n &= \frac{\frac{q^{n+1}-q^n}{\Delta t} + \frac{q^n - q^{n-1}}{\Delta t}}{2} \\ &= \frac{1}{\Delta t}\left(\overline{q^{n+1/2}} - \overline{q^{n-1/2}}\right).\end{aligned}$$

Therefore (4.73) becomes

$$\begin{aligned}&\frac{\rho_s}{2\Delta t}\left(\|\partial_t \chi_{\boldsymbol{u}}^{n+1/2}\|_{\Omega_s}^2 - \|\partial_t \chi_{\boldsymbol{u}}^{n-1/2}\|_{\Omega_s}^2\right) + \frac{\rho_f}{2\Delta t}\left(\|\overline{\chi_{\boldsymbol{v}}^{n+1/2}}\|_{\Omega_f}^2 - \|\overline{\chi_{\boldsymbol{v}}^{n-1/2}}\|_{\Omega_f}^2\right) \\ &\quad + \frac{1}{2\Delta t}\left(\|\chi_{\boldsymbol{\sigma}_s}^{n+1/2}\|_{\mathcal{A},\Omega_s}^2 - \|\chi_{\boldsymbol{\sigma}_s}^{n-1/2}\|_{\mathcal{A},\Omega_s}^2\right) + \|\widetilde{\chi_{\boldsymbol{\sigma}_f}^n}\|_{\mathcal{A}_\infty,\Omega_f}^2 \\ &\qquad = \left(\mathcal{A}\partial_t^c \eta_{\boldsymbol{\sigma}_s}^n, \widetilde{\chi_{\boldsymbol{\sigma}_s}^n}\right)_{\Omega_s} + \left(\mathcal{A}_\infty \widetilde{\eta_{\boldsymbol{\sigma}_f}^n}, \widetilde{\chi_{\boldsymbol{\sigma}_f}^n}\right)_{\Omega_f} + \left(r_{\boldsymbol{u}}^n, \partial_t^c \chi_{\boldsymbol{u}}^n\right)_{\Omega_s} + \left(r_{\boldsymbol{v}}^n, \widetilde{\chi_{\boldsymbol{v}}^n}\right)_{\Omega_f} \\ &\qquad\quad + I^n + E^n. \end{aligned} \tag{4.74}$$

Consider the right hand side of (4.74). With the use of the Cauchy-Schwarz Inequality, the definitions (2.47), and the inequalities (4.14), we can bound the right hand side with

$$\begin{aligned}R.H.S. &\le \|\mathcal{A}\partial_t^c \eta_{\boldsymbol{\sigma}_s}^n\|_{\Omega_s}\|\widetilde{\chi_{\boldsymbol{\sigma}_s}^n}\|_{\Omega_s} + \|\widetilde{\eta_{\boldsymbol{\sigma}_f}^n}\|_{\mathcal{A}_\infty,\Omega_f}\|\widetilde{\chi_{\boldsymbol{\sigma}_f}^n}\|_{\mathcal{A}_\infty,\Omega_f} + \|r_{\boldsymbol{u}}^n\|_{\Omega_s}\|\partial_t^c \chi_{\boldsymbol{u}}^n\|_{\Omega_s} + \|r_{\boldsymbol{v}}^n\|_{\Omega_f}\|\widetilde{\chi_{\boldsymbol{v}}^n}\|_{\Omega_f} \\ &\quad + I^n + E^n \\ &\le C\|\partial_t^c \eta_{\boldsymbol{\sigma}_s}^n\|_{\Omega_s}\|\chi_{\boldsymbol{\sigma}_s}\|_{\widetilde{L_{\Delta t}^\infty}(L^2(\Omega_s))} + \|\widetilde{\eta_{\boldsymbol{\sigma}_f}^n}\|_{\mathcal{A}_\infty,\Omega_f}\|\widetilde{\chi_{\boldsymbol{\sigma}_f}^n}\|_{\mathcal{A}_\infty,\Omega_f} + \|r_{\boldsymbol{u}}^n\|_{\Omega_s}\|\partial_t^c \chi_{\boldsymbol{u}}\|_{L_{\Delta t}^\infty(L^2(\Omega_s))} \\ &\quad + \|r_{\boldsymbol{v}}^n\|_{\Omega_f}\|\chi_{\boldsymbol{v}}\|_{\widetilde{L_{\Delta t}^\infty}\left(L^2(\Omega_f)\right)} + I^n + E^n \\ &\le C\|\partial_t^c \eta_{\boldsymbol{\sigma}_s}^n\|_{\Omega_s}\|\chi_{\boldsymbol{\sigma}_s}\|_{\overline{L_{\Delta t}^\infty}(L^2(\Omega_s))} + \|\widetilde{\eta_{\boldsymbol{\sigma}_f}^n}\|_{\mathcal{A}_\infty,\Omega_f}\|\widetilde{\chi_{\boldsymbol{\sigma}_f}^n}\|_{\mathcal{A}_\infty,\Omega_f} + \|r_{\boldsymbol{u}}^n\|_{\Omega_s}\|\partial_t \chi_{\boldsymbol{u}}\|_{\overline{L_{\Delta t}^\infty}(L^2(\Omega_s))} \\ &\quad + \|r_{\boldsymbol{v}}^n\|_{\Omega_f}\|\chi_{\boldsymbol{v}}\|_{\overline{L_{\Delta t}^\infty}\left(L^2(\Omega_f)\right)} + I^n + E^n.\end{aligned}$$

Next we will consider the consistency error and interface integral terms. These terms are similar to those appearing in Lemma 4.3.13 and are bound similarly. First consider the consistency error terms

$$E^n = \mathbb{E}_h\left(\widetilde{\boldsymbol{u}_t^n} - \partial_t^c \boldsymbol{u}^n, \widetilde{\chi_{\boldsymbol{\sigma}_s}^n}\right)_{\Omega_s} - \mathbb{E}_h\left(\widetilde{\boldsymbol{u}_t^n}, \widetilde{\chi_{\boldsymbol{\sigma}_s}^n}\right)_{\Omega_s} - \mathbb{E}_h\left(\widetilde{\boldsymbol{v}^n}, \widetilde{\chi_{\boldsymbol{\sigma}_f}^n}\right)_{\Omega_f}.$$

Since $\widetilde{\chi^n_{\boldsymbol{\sigma}_s}}, \widetilde{\chi^n_{\boldsymbol{\sigma}_f}} \in \boldsymbol{\Sigma}_h$ and $\widetilde{\boldsymbol{u}^n_t}$, $\widetilde{\boldsymbol{v}^n}$, $\partial^c_t \boldsymbol{u}^n \in H^2(\Omega, \mathbb{R}^2)$ for each value of n, the bound (2.19) applies to each term of the above statement. Therefore, as in Lemma 4.3.13, by applying (2.19), taking the maximum in time, and noting the relationship (4.14c), we find

$$\begin{aligned} E^n \leq Ch^k \left(\|\widetilde{\boldsymbol{u}^n_t} - \partial^c_t \boldsymbol{u}^n\|_{2,\Omega_s} + \|\boldsymbol{u}_t\|_{L^\infty_{\Delta t}(H^2(\Omega_s))} \right) \|\chi_{\boldsymbol{\sigma}_s}\|_{\widetilde{L^\infty_{\Delta t}}(L^2(\Omega_s))} \\ + Ch^k \|\boldsymbol{v}\|_{L^\infty_{\Delta t}\left(H^2(\Omega_f)\right)} \|\chi_{\boldsymbol{\sigma}_f}\|_{\widetilde{L^\infty_{\Delta t}}\left(L^2(\Omega_f)\right)}. \end{aligned} \tag{4.75}$$

We turn our attention to the interface integral terms

$$I^n = < \widetilde{\boldsymbol{u}^n_t} - \partial^c_t \boldsymbol{u}^n, \widetilde{\chi^n_{\boldsymbol{\sigma}_s}} \cdot \boldsymbol{n}_s >_\Gamma - < \widetilde{\boldsymbol{u}^n_t}, [\widetilde{\chi^n_{\boldsymbol{\sigma}_s}} \cdot n] >_\Gamma .$$

Again as in Lemma 4.3.13, the term $< \widetilde{\boldsymbol{u}^n_t}, [\widetilde{\chi^n_{\boldsymbol{\sigma}_s}} \cdot n] >_\Gamma$ can be bounded using the same arguments as when considering consistency error and by taking the maximum over time. Therefore

$$< \widetilde{\boldsymbol{u}^n_t}, [\widetilde{\chi^n_{\boldsymbol{\sigma}_s}} \boldsymbol{n}] >_\Gamma \leq Ch^k \|\boldsymbol{u}_t\|_{L^\infty_{\Delta t}(H^2(\Omega_s))} \|\chi_{\boldsymbol{\sigma}_s}\|_{\widetilde{L^\infty_{\Delta t}}(L^2(\Omega_s))}.$$

The other interface integral term $< \widetilde{\boldsymbol{u}^n_t} - \partial^c_t \boldsymbol{u}^n, \widetilde{\chi^n_{\boldsymbol{\sigma}_s}} \boldsymbol{n}_s >_\Gamma$ does not involve a difference between functions in the test space and is bounded using the Cauchy-Schwarz Inequality, the Trace Theorem 2.3.2, and the inverse assumption (2.25). Similar to the bound on the initial interface term bound in Lemma 4.3.13, we find

$$< \widetilde{\boldsymbol{u}^n_t} - \partial^c_t \boldsymbol{u}^n, \widetilde{\chi^n_{\boldsymbol{\sigma}_s}} \cdot \boldsymbol{n}_s >_\Gamma \leq Ch^{-1/2} \|\widetilde{\boldsymbol{u}^n_t} - \partial^c_t \boldsymbol{u}^n\|_\Gamma \|\chi_{\boldsymbol{\sigma}_s}\|_{\widetilde{L^\infty_{\Delta t}}(L^2(\Omega_s))}.$$

Therefore,

$$I^n \leq C \left(h^k \|\boldsymbol{u}_t\|_{L^\infty_{\Delta t}(H^2(\Omega_s))} + h^{-1/2} \|\widetilde{\boldsymbol{u}^n_t} - \partial^c_t \boldsymbol{u}^n\|_\Gamma \right) \|\chi_{\boldsymbol{\sigma}_s}\|_{\widetilde{L^\infty_{\Delta t}}(L^2(\Omega_s))}. \tag{4.76}$$

Combining (4.75), (4.76) and Young's Inequality with (4.74), we find

$$\begin{aligned}
&\frac{\rho_s}{2\Delta t}\left(\|\partial_t\chi_{\boldsymbol{u}}^{n+1/2}\|_{\Omega_s}^2-\|\partial_t\chi_{\boldsymbol{u}}^{n-1/2}\|_{\Omega_s}^2\right)+\frac{\rho_f}{2\Delta t}\left(\|\overline{\chi_{\boldsymbol{v}}^{n+1/2}}\|_{\Omega_f}^2-\|\overline{\chi_{\boldsymbol{v}}^{n-1/2}}\|_{\Omega_f}^2\right)\\
&\quad+\frac{1}{2\Delta t}\left(\|\chi_{\boldsymbol{\sigma}_s}^{n+1/2}\|_{\mathcal{A},\Omega_s}^2-\|\chi_{\boldsymbol{\sigma}_s}^{n-1/2}\|_{\mathcal{A},\Omega_s}^2\right)+\|\widetilde{\chi_{\boldsymbol{\sigma}_f}^n}\|_{\mathcal{A}_\infty,\Omega_f}^2\\
&\qquad\le\|r_{\boldsymbol{u}}^n\|_{\Omega_s}\|\partial_t\chi_{\boldsymbol{u}}\|_{\overline{L^\infty_{\Delta t}}(L^2(\Omega_s))}+C\|r_{\boldsymbol{v}}^n\|_{\Omega_f}\|\chi_{\boldsymbol{v}}\|_{\overline{L^\infty_{\Delta t}}\left(L^2(\Omega_f)\right)}\\
&\qquad\quad+Ch^k\|\boldsymbol{v}\|_{L^\infty_{\Delta t}\left(H^2(\Omega_f)\right)}\|\chi_{\boldsymbol{\sigma}_f}\|_{\widetilde{L^\infty_{\Delta t}}\left(L^2(\Omega_f)\right)}\\
&\qquad\quad+C\left(\|\partial_t^c\eta_{\boldsymbol{\sigma}_s}^n\|_{\Omega_s}+h^k\|\widetilde{\boldsymbol{u}_t^n}-\partial_t^c\boldsymbol{u}^n\|_{2,\Omega_s}+h^k\|\boldsymbol{u}_t\|_{L^\infty_{\Delta t}(H^2(\Omega_s))}\right)\|\chi_{\boldsymbol{\sigma}_s}\|_{\overline{L^\infty_{\Delta t}}(L^2(\Omega_s))}\\
&\qquad\quad+Ch^{-1/2}\|\widetilde{\boldsymbol{u}_t^n}-\partial_t^c\boldsymbol{u}^n\|_\Gamma\|\chi_{\boldsymbol{\sigma}_s}\|_{\overline{L^\infty_{\Delta t}}(L^2(\Omega_s))}+\frac{1}{2}\|\widetilde{\eta_{\boldsymbol{\sigma}_f}^n}\|_{\mathcal{A}_\infty,\Omega_f}^2+\frac{1}{2}\|\widetilde{\chi_{\boldsymbol{\sigma}_f}^n}\|_{\mathcal{A}_\infty,\Omega_f}^2.
\end{aligned}$$

The term $\frac{1}{2}\|\widetilde{\chi_{\boldsymbol{\sigma}_f}^n}\|_{\mathcal{A}_\infty,\Omega_f}^2$ is moved from the right hand side to the left hand side. We now multiply by $2\Delta t$ and sum from time step 1 to n, where $1\le n<N-1$ and the final time is $N\Delta t$ to find

$$\begin{aligned}
&\rho_s\left(\|\partial_t\chi_{\boldsymbol{u}}^{n+1/2}\|_{\Omega_s}^2-\|\partial_t\chi_{\boldsymbol{u}}^{1/2}\|_{\Omega_s}^2\right)+\rho_f\left(\|\overline{\chi_{\boldsymbol{v}}^{n+1/2}}\|_{\Omega_f}^2-\|\overline{\chi_{\boldsymbol{v}}^{1/2}}\|_{\Omega_f}^2\right)+\|\chi_{\boldsymbol{\sigma}_s}^{n+1/2}\|_{\mathcal{A},\Omega_s}^2-\|\overline{\chi_{\boldsymbol{\sigma}_s}^{1/2}}\|_{\mathcal{A},\Omega_s}^2\\
&\quad+\Delta t\sum_{i=1}^n\|\widetilde{\chi_{\boldsymbol{\sigma}_f}^i}\|_{\mathcal{A}_\infty,\Omega_f}^2\\
&\qquad\le 2\Delta t\sum_{i=1}^n\Big(\|r_{\boldsymbol{u}}^i\|_{\Omega_s}\|\partial_t\chi_{\boldsymbol{u}}\|_{\overline{L^\infty_{\Delta t}}(L^2(\Omega_s))}+C\|r_{\boldsymbol{v}}^i\|_{\Omega_f}\|\chi_{\boldsymbol{v}}\|_{\overline{L^\infty_{\Delta t}}\left(L^2(\Omega_f)\right)}\\
&\qquad\quad+C\left(\|\partial_t^c\eta_{\boldsymbol{\sigma}_s}^i\|_{\Omega_s}+h^k\|\widetilde{\boldsymbol{u}_t^i}-\partial_t^c\boldsymbol{u}^i\|_{2,\Omega_s}+2h^k\|\boldsymbol{u}_t\|_{L^\infty_{\Delta t}(H^2(\Omega_s))}\right)\|\chi_{\boldsymbol{\sigma}_s}\|_{\overline{L^\infty_{\Delta t}}(L^2(\Omega_s))}\\
&\qquad\quad+Ch^{-1/2}\|\widetilde{\boldsymbol{u}_t^i}-\partial_t^c\boldsymbol{u}^i\|_\Gamma\|\chi_{\boldsymbol{\sigma}_s}\|_{\overline{L^\infty_{\Delta t}}(L^2(\Omega_s))}+Ch^k\|\boldsymbol{v}\|_{L^\infty_{\Delta t}\left(H^2(\Omega_f)\right)}\|\chi_{\boldsymbol{\sigma}_f}\|_{\widetilde{L^\infty_{\Delta t}}\left(L^2(\Omega_f)\right)}\\
&\qquad\quad+\frac{1}{2}\|\widetilde{\eta_{\boldsymbol{\sigma}_f}^n}\|_{\mathcal{A}_\infty,\Omega_f}^2\Big).
\end{aligned}$$

Any negative terms on the left hand side are moved to the right hand side. Now, since this inequality is true for any time step n, we take the maximum over time steps

$1 \le n \le N-1$ on the left hand side

$$\rho_s\|\partial_t\chi_{\boldsymbol{u}}\|^2_{\overline{L^\infty_{\Delta t}}(L^2(\Omega_s))} + \rho_f\|\chi_{\boldsymbol{v}}\|^2_{\overline{L^\infty_{\Delta t}}\left(L^2(\Omega_f)\right)} + \|\chi_{\boldsymbol{\sigma}_s}\|^2_{\overline{L^\infty_{\Delta t}}(L^2(\Omega_s))} + \Delta t\sum_{i=1}^{N-1}\|\widetilde{\chi^i_{\boldsymbol{\sigma}_f}}\|^2_{\mathcal{A}_\infty,\Omega_f}$$

$$\le 2\Delta t\sum_{i=1}^{N-1}\Big(\|r^i_{\boldsymbol{u}}\|_{\Omega_s}\|\partial_t\chi_{\boldsymbol{u}}\|_{\overline{L^\infty_{\Delta t}}(L^2(\Omega_s))} + C\|r^i_{\boldsymbol{v}}\|_{\Omega_f}\|\chi_{\boldsymbol{v}}\|_{\overline{L^\infty_{\Delta t}}\left(L^2(\Omega_f)\right)}$$

$$+C\left(\|\partial^c_t\eta^i_{\boldsymbol{\sigma}_s}\|_{\Omega_s} + h^k\|\widetilde{\boldsymbol{u}^i_t} - \partial^c_t\boldsymbol{u}^i\|_{2,\Omega_s} + 2h^k\|\boldsymbol{u}_t\|_{L^\infty_{\Delta t}(H^2(\Omega_s))}\right)\|\chi_{\boldsymbol{\sigma}_s}\|_{\overline{L^\infty_{\Delta t}}(L^2(\Omega_s))}$$

$$+Ch^{-1/2}\|\widetilde{\boldsymbol{u}^i_t} - \partial^c_t\boldsymbol{u}^i\|_\Gamma\|\chi_{\boldsymbol{\sigma}_s}\|_{\overline{L^\infty_{\Delta t}}(L^2(\Omega_s))} + Ch^k\|\boldsymbol{v}\|_{L^\infty_{\Delta t}\left(H^2(\Omega_f)\right)}\|\chi_{\boldsymbol{\sigma}_f}\|_{\widetilde{L^\infty_{\Delta t}}\left(L^2(\Omega_f)\right)}$$

$$+\frac{1}{2}\|\widetilde{\eta^i_{\boldsymbol{\sigma}_f}}\|^2_{\mathcal{A}_\infty,\Omega_f}\Big) + \rho_s\|\partial_t\chi^{1/2}_{\boldsymbol{u}}\|^2_{\Omega_s} + \rho_f\|\overline{\chi^{1/2}_{\boldsymbol{v}}}\|^2_{\Omega_f} + \|\overline{\chi^{1/2}_{\boldsymbol{\sigma}_s}}\|^2_{\mathcal{A},\Omega_s}. \tag{4.77}$$

Next we consider the initial conditions, specifically, the terms with an exponent of $n = 1/2$. We note intuitively that

$$\rho_s\|\partial_t\chi^{1/2}_{\boldsymbol{u}}\|^2_{\Omega_s} + \rho_f\|\overline{\chi^{1/2}_{\boldsymbol{v}}}\|^2_{\Omega_f} + \|\overline{\chi^{1/2}_{\boldsymbol{\sigma}_s}}\|^2_{\mathcal{A},\Omega_s}$$

$$\le \rho_s\|\partial_t\chi^{1/2}_{\boldsymbol{u}}\|^2_{\Omega_s} + \rho_f\|\overline{\chi^{1/2}_{\boldsymbol{v}}}\|^2_{\Omega_f} + \|\overline{\chi^{1/2}_{\boldsymbol{\sigma}_s}}\|^2_{\mathcal{A},\Omega_s} + \frac{\Delta t}{2}\|\overline{\chi^{1/2}_{\boldsymbol{\sigma}_f}}\|^2_{\mathcal{A}_\infty,\Omega_f}$$

and (4.63) can be used to bound the initial terms appearing on the right hand side of (4.77).

Therefore, by adding $\frac{\Delta t}{2}\|\overline{\chi^{1/2}_{\boldsymbol{\sigma}_f}}\|^2_{\mathcal{A}_\infty,\Omega_f}$ to both sides of (4.77) we find

$$\rho_s\|\partial_t\chi_{\boldsymbol{u}}\|^2_{\overline{L^\infty_{\Delta t}}(L^2(\Omega_s))} + \rho_f\|\chi_{\boldsymbol{v}}\|^2_{\overline{L^\infty_{\Delta t}}\left(L^2(\Omega_f)\right)} + \|\chi_{\boldsymbol{\sigma}_s}\|^2_{\overline{L^\infty_{\Delta t}}(L^2(\Omega_s))}$$

$$+\Delta t\sum_{i=1}^{N-1}\|\widetilde{\chi^i_{\boldsymbol{\sigma}_f}}\|^2_{\mathcal{A}_\infty,\Omega_f} + \frac{\Delta t}{2}\|\overline{\chi^{1/2}_{\boldsymbol{\sigma}_f}}\|^2_{\mathcal{A}_\infty,\Omega_f}$$

$$\le I + II + III + IV + V + VI + VII + VIII + IX$$

with

$$
\begin{aligned}
I &= 2C\Delta t \sum_{i=0}^{N-1} \|r_{\boldsymbol{v}}^i\|_{\Omega_f} \|\chi_{\boldsymbol{v}}\|_{\overline{L^\infty_{\Delta t}}\left(L^2(\Omega_f)\right)}, \\
II &= 2C\Delta t \sum_{i=0}^{N-1} \|\partial_t^c \eta_{\boldsymbol{\sigma}_s}^i\|_{\Omega_s} \|\chi_{\boldsymbol{\sigma}_s}\|_{\overline{L^\infty_{\Delta t}}(L^2(\Omega_s))}, \\
III &= 2Ch^k\Delta t \sum_{i=0}^{N-1} \|\widetilde{\boldsymbol{u}_t^i} - \partial_t^c \boldsymbol{u}^i\|_{2,\Omega_s} \|\chi_{\boldsymbol{\sigma}_s}\|_{\overline{L^\infty_{\Delta t}}(L^2(\Omega_s))}, \\
IV &= 2Ch^{-1/2}\Delta t \sum_{i=0}^{N-1} \|\widetilde{\boldsymbol{u}_t^i} - \partial_t^c \boldsymbol{u}^i\|_{\Gamma} \|\chi_{\boldsymbol{\sigma}_s}\|_{\overline{L^\infty_{\Delta t}}(L^2(\Omega_s))}, \\
V &= 2\Delta t \sum_{i=0}^{N-1} \|r_{\boldsymbol{u}}^i\|_{\Omega_s} \|\partial_t \chi_{\boldsymbol{u}}\|_{\overline{L^\infty_{\Delta t}}(L^2(\Omega_s))}, \\
VI &= 2Ch^k\Delta t \sum_{i=0}^{N-1} \|\boldsymbol{u}_t\|_{L^\infty_{\Delta t}(H^2(\Omega_s))} \|\chi_{\boldsymbol{\sigma}_s}\|_{\overline{L^\infty_{\Delta t}}(L^2(\Omega_s))}, \\
VII &= 2Ch^k\Delta t \sum_{i=0}^{N-1} \|\boldsymbol{v}\|_{L^\infty_{\Delta t}\left(H^2(\Omega_f)\right)} \|\chi_{\boldsymbol{\sigma}_f}\|_{\widetilde{L^\infty_{\Delta t}}\left(L^2(\Omega_f)\right)}, \\
VIII &= \Delta t \sum_{i=0}^{N-1} \|\widetilde{\eta_{\boldsymbol{\sigma}_f}^i}\|^2_{\mathcal{A}_\infty,\Omega_f}, \\
IX &= \|\chi_{\boldsymbol{\sigma}_s}^0\|^2_{\mathcal{A},\Omega_s}.
\end{aligned}
$$

by noting the special definitions (2.46).

For each of the terms I, II, III and IV on the right hand side, we will apply Lemma 4.3.6. The constant ϵ is taken large enough so that when a term on the right hand side matches one on the left hand side, the coefficient on the right hand side is small enough that we can combine like terms on the left hand side and have a positive result. For example, consider I. This terms contains a factor $\|\chi_{\boldsymbol{v}}\|_{\overline{L^\infty_{\Delta t}}\left(L^2(\Omega_f)\right)}$ and on the left hand side the similar term is $\rho_f \|\chi_{\boldsymbol{v}}\|^2_{\overline{L^\infty_{\Delta t}}\left(L^2(\Omega_f)\right)}$. Therefore we choose ϵ large enough so that the coefficient of $\|\partial_t \chi_{\boldsymbol{u}}\|^2_{\overline{L^\infty_{\Delta t}}(L^2(\Omega_s))}$ is less than $\frac{\rho_s}{2}$ when the Lemma is applied. Specifically, let $a_i = \Delta t \|r_{\boldsymbol{v}}^i\|_{\Omega_f}$, $b = \|\chi_{\boldsymbol{v}}\|_{\overline{L^\infty_{\Delta t}}\left(L^2(\Omega_f)\right)}$ and choose $\epsilon > \frac{2C}{\rho_f}$. Then

$$I \leq C\Delta t \sum_{i=0}^{N-1} \|r_{\boldsymbol{v}}^i\|_{\Omega_f}^2 + \frac{\rho_f}{2}\|\chi_{\boldsymbol{v}}\|^2_{\overline{L^\infty_{\Delta t}}\left(L^2(\Omega_f)\right)} \tag{4.78}$$

where C is some new but still unknown constant.

The next term V is handled in a very similar way, except that the first term of the summation must be handled separately. This is due to the bound on $\|r_{\boldsymbol{u}}^0\|_{\Omega_s}^2$ found in 4.3.12. Specifically, rewrite

$$V = 2\Delta t\|r_{\boldsymbol{u}}^0\|_{\Omega_s}\|\partial_t\chi_{\boldsymbol{u}}\|_{\overline{L^\infty_{\Delta t}}(L^2(\Omega_s))} + 2\Delta t\sum_{i=1}^{N-1}\|r_{\boldsymbol{u}}^i\|_{\Omega_s}\|\partial_t\chi_{\boldsymbol{u}}\|_{\overline{L^\infty_{\Delta t}}(L^2(\Omega_s))}.$$

For the first term we use Young's Inequality and for the second we use Lemma 4.3.6 as described above. Let ϵ_1 be the chosen value for the Young's Inequality while ϵ_2 is used in Lemma 4.3.6 to find

$$V \leq C\epsilon_1\Delta t^2\|r_{\boldsymbol{u}}^0\|_{\Omega_s}^2 + \frac{C}{\epsilon_1}\|\partial_t\chi_{\boldsymbol{u}}\|^2_{\overline{L^\infty_{\Delta t}}(L^2(\Omega_s))} + C\Delta t\sum_{i=1}^{N-1}\|r_{\boldsymbol{u}}^i\|_{\Omega_s}^2 + \frac{C}{\epsilon_2}\|\partial_t\chi_{\boldsymbol{u}}\|^2_{\overline{L^\infty_{\Delta t}}(L^2(\Omega_s))}.$$

Now ϵ_1 and ϵ_2 must be chosen so that $\frac{C}{\epsilon_1} + \frac{C}{\epsilon_2} < \rho_s$. Choose $\epsilon_1, \epsilon_2 > \frac{4C}{\rho_s}$.

For the next two terms, VI and VII, we see that these are sums of constants. So we just note that $\Delta t\sum_{i=0}^{N-1} 1 = T_f$ which is a constant and apply Young's Inequality. For example, consider VII, to find

$$VII \leq 2CT_f h^k\|\boldsymbol{v}\|_{L^\infty_{\Delta t}\left(H^2(\Omega_f)\right)}\|\chi_{\boldsymbol{\sigma}_f}\|_{\overline{L^\infty_{\Delta t}}\left(L^2(\Omega_f)\right)}.$$

Let $a = h^k\|\boldsymbol{v}\|_{L^\infty_{\Delta t}\left(H^2(\Omega_f)\right)}$, $b = \|\chi_{\boldsymbol{\sigma}_f}\|_{\overline{L^\infty_{\Delta t}}\left(L^2(\Omega_f)\right)}$ and choose $\epsilon > \frac{4CT_F}{\rho_f}$, where C is the current constant, in Young's Inequality. Then

$$VII \leq Ch^{2k}\|\boldsymbol{v}\|^2_{L^\infty_{\Delta t}\left(H^2(\Omega_f)\right)} + \frac{\rho_f}{4}\|\chi_{\boldsymbol{\sigma}_f}\|^2_{\overline{L^\infty_{\Delta t}}\left(L^2(\Omega_f)\right)}. \tag{4.79}$$

Therefore, using the bound on $I - VII$ we find

$$\begin{aligned}\|\partial_t\chi_{\boldsymbol{u}}\|^2_{\overline{L^\infty_{\Delta t}}(L^2(\Omega_s))} + \|\chi_{\boldsymbol{v}}\|^2_{\overline{L^\infty_{\Delta t}}\left(L^2(\Omega_f)\right)} + \|\chi_{\boldsymbol{\sigma}_s}\|^2_{\overline{L^\infty_{\Delta t}}(L^2(\Omega_s))} + \Delta t\sum_{i=0}^{N-1}\|\widetilde{\chi^i_{\boldsymbol{\sigma}_f}}\|^2_{\mathcal{A}_\infty,\Omega_f} \\ \leq I + II + III + IV \end{aligned} \tag{4.80}$$

$$
\begin{aligned}
I &= C\left(\Delta t^2\|r_{\boldsymbol{u}}^0\|_{\Omega_s}^2 + \Delta t\sum_{i=1}^{N-1}\|r_{\boldsymbol{u}}^i\|_{\Omega_s}^2 + \Delta t\sum_{i=0}^{N-1}\|r_{\boldsymbol{v}}^i\|_{\Omega_f}^2\right),\\
II &= C\Delta t\sum_{i=0}^{N-1} h^{2k}\|\widetilde{\boldsymbol{u}_t^i} - \partial_t^c\boldsymbol{u}^i\|_{2,\Omega_s}^2 + h^{-1}\|\widetilde{\boldsymbol{u}_t^i} - \partial_t^c\boldsymbol{u}^i\|_{\Gamma}^2,\\
III &= C\Delta t\sum_{i=0}^{N-1}\|\partial_t^c\eta_{\boldsymbol{\sigma}_s}^i\|_{\Omega_s}^2 + \|\widetilde{\eta_{\boldsymbol{\sigma}_f}^i}\|_{\mathcal{A}_\infty,\Omega_f}^2,\\
IV &= C\left(h^{2k}\|\boldsymbol{v}\|_{L_{\Delta t}^\infty\left(H^2(\Omega_f)\right)}^2 + h^{2k}\|\boldsymbol{u}_t\|_{L_{\Delta t}^\infty\left(H^2(\Omega_f)\right)}^2\right),\\
V &= C\rho_s\|\chi_{\boldsymbol{\sigma}_s}^0\|_{\mathcal{A},\Omega_s}^2.
\end{aligned}
$$

The terms in I are bounded by Lemma 4.3.12, (4.16c), Lemma 4.3.11 and (4.16b) as

$$
I \leq C\Delta t^4\left(\|\boldsymbol{u}_{ttt}\|_{L_{\Delta t}^\infty(L^2(\Omega_s))}^2 + \|\boldsymbol{u}_{tttt}\|_{L^2(0,T;L^2(\Omega_s))}^2 + \|\boldsymbol{v}_{ttt}\|_{L^2\left(0,T;L^2(\Omega_f)\right)}^2\right).
$$

The terms in II are similarly bounded by (4.16b). Similarly III is bounded by the approximation properties (4.9a). The terms in IV depend only on the regularity of the weak solution. The terms in V are discussed in a previous section in (4.22). From (4.80) we find

$$
\begin{aligned}
&\|\partial_t\chi_{\boldsymbol{u}}\|_{\overline{L_{\Delta t}^\infty}(L^2(\Omega_s))}^2 + \|\chi_{\boldsymbol{v}}\|_{\overline{L_{\Delta t}^\infty}\left(L^2(\Omega_f)\right)}^2 + \|\chi_{\boldsymbol{\sigma}_s}\|_{\overline{L_{\Delta t}^\infty}(L^2(\Omega_s))}^2 + \Delta t\sum_{i=1}^{N}\|\widetilde{\chi_{\boldsymbol{\sigma}_f}^i}\|_{\mathcal{A}_\infty,\Omega_f}^2\\
&\quad\leq C\Big(\Delta t^4\left(\|\boldsymbol{u}_{ttt}\|_{L_{\Delta t}^\infty(L^2(\Omega_s))}^2 + \|\boldsymbol{u}_{tttt}\|_{L^2(0,T;L^2(\Omega_s))}^2 + \|\boldsymbol{v}_{ttt}\|_{L^2\left(0,T;L^2(\Omega_f)\right)}^2\right)\\
&\qquad + h^{2k}\Delta t^4\|\boldsymbol{u}_{ttt}\|_{L^2(0,T;H^2(\Omega_s))}^2 + h^{-1}\Delta t^4\|\boldsymbol{u}_{ttt}\|_{L^2(0,T;L^2(\partial\Omega_s))}^2 + \Delta t^4\|(\boldsymbol{\sigma}_s)_{ttt}\|_{L^2(0,T;L^2(\Omega_s))}^2\\
&\qquad + \Delta t^4\|\Pi_h(\boldsymbol{\sigma}_s)_{ttt}\|_{L^2(0,T;L^2(\Omega_s))}^2 + h^{2m_1}\|(\boldsymbol{\sigma}_s)_t\|_{L^2(0,T;H^{m_1}(\Omega_s))}^2\\
&\qquad + \Delta t h^{2m_1}\|\boldsymbol{\sigma}_f\|_{L^2\left(0,T;H^{m_1}(\Omega_f)\right)}^2 + h^{2k}\|\boldsymbol{v}\|_{L_{\Delta t}^\infty\left(H^2(\Omega_f)\right)}^2\\
&\qquad + h^{2k}\|\boldsymbol{u}_t\|_{L_{\Delta t}^\infty\left(H^2(\Omega_f)\right)}^2 + h^{2m_1}\|\boldsymbol{\sigma}_s^0\|_{m_1,\Omega_s}^2 + h^{2m_1}\|\boldsymbol{\sigma}_f^0\|_{m_1,\Omega_f}^2 + h^{2k}\|\boldsymbol{u}^0\|_{2,\Omega_s}^2\\
&\qquad + h^{2k}\|\boldsymbol{v}^0\|_{2,\Omega_f}^2 + h^{2r}\|p^0\|_{r-2,\Omega_f}^2 + h^{2w}q^0\Big).
\end{aligned}
\tag{4.81}
$$

The result (4.71) follow directly by noting l was chosen in Lemma 4.3.8. □

Theorem 4.3.17. *Under the assumptions of Lemma 4.3.16,*

$$\begin{aligned}\|\partial_t(\boldsymbol{u}-\boldsymbol{u}_h)\|^2_{\overline{L^\infty_{\Delta t}}(L^2(\Omega_s))} + \|\boldsymbol{v}-\boldsymbol{v}_h\|^2_{\overline{L^\infty_{\Delta t}}\left(L^2(\Omega_f)\right)} + \|\boldsymbol{\sigma}_s-\boldsymbol{\sigma}_{s_h}\|^2_{\overline{L^\infty_{\Delta t}}(L^2(\Omega_s))} \\ + \Delta t\sum_{i=1}^{N}\|\boldsymbol{\sigma}_f-\boldsymbol{\sigma}_{f_h}\|^2_{\mathcal{A}_\infty,\Omega_f} \\ \leq C_3\left(\Delta t^4 + h^{2m_1} + h^{2k}\Delta t^4 + h^{-1}\Delta t^4 + h^{2k} + h^{2l}\right) + Ch^{2m_2}\end{aligned}$$

with C_3 as defined in (4.72) *and* $C = C\left(\|\boldsymbol{u}_t\|^2_{\overline{L^\infty_{\Delta t}}(H^{m_2}(\Omega_s))}, \|\boldsymbol{v}\|^2_{\overline{L^\infty_{\Delta t}}\left(H^{m_2}(\Omega_f)\right)}\right)$. *Here m_1 and m_2 are convergence rates determined by the mixed finite element spaces chosen as in* (4.9a) *and* (4.9b), *k is determined by the consistency error as in* (4.20), *and l is a convergence rate determined by the mixed finite element spaces used.*

Proof. This follows directly from Lemma 4.3.16 and the Triangle Inequality. □

Note that the values of m_1, m_2, k, and l are chosen in accordance with the solution regularity. We now have a bound on the error in fluid velocity and stress and solid stress. However, we only have an error bound for the discrete derivative for displacement, but not for the displacement itself.

4.4 Improved Error Estimate for Displacement

We would like to have an error bound for displacement instead of an error bound for the discrete derivative of displacement. This will require two summations in time. To this end, we define a notation and some useful properties of it. Let $q = \chi_{\boldsymbol{\sigma}_s}, \chi_{\boldsymbol{\sigma}_f}, \chi_{\boldsymbol{u}}$. Then following notation will simplify calculations :

$$\Phi_q^0 = 0, \quad \Phi_q^n = \Delta t\sum_{i=0}^{n-1} q^{i+1/2}, \quad n \geq 1. \tag{4.82}$$

Lemma 4.4.1. *For the notation defined in* (4.82)

$$\Phi_q^{1/2} = \frac{\Delta t}{2} q^{1/2}, \tag{4.83}$$

$$\Phi_q^{n+1/2} - \Phi_q^{1/2} = \Delta t \sum_{i=1}^{n} \widetilde{q^i}, \tag{4.84}$$

$$\partial_t \Phi_q^{n+1/2} = q^{n+1/2}. \tag{4.85}$$

Proof. All of these equations are proved by direct computation. Both (4.83) and (4.85) follow directly from definitions so we prove only (4.84). This is done with the following calculations:

$$\begin{aligned}
\Phi_q^{n+1/2} &= \frac{1}{2}\Phi_q^{n+1} + \frac{1}{2}\Phi_q^{n} \\
&= \frac{\Delta t}{2}\left(\sum_{i=0}^{n} q^{i+1/2} + \sum_{i=0}^{n-1} q^{i+1/2}\right) \\
&= \frac{\Delta t}{2}\left(\sum_{i=0}^{n} q^{i+1/2} + \sum_{i=1}^{n} q^{i-1/2}\right) \\
&= \Delta t\left(\frac{q^{1/2}}{2} + \sum_{i=1}^{n} \frac{q^{i+1/2} + q^{i-1/2}}{2}\right) \\
&= \Phi_q^{1/2} + \Delta t \sum_{i=1}^{n} \widetilde{q^i}.
\end{aligned}$$

Therefore (4.84) follows. □

For simplicity we also use the following notation when $q = \boldsymbol{u}, \boldsymbol{v}$:

$$R_q^N = \Delta t \sum_{i=0}^{N} r_q. \tag{4.86}$$

Lemma 4.4.2. *Under the same assumptions as Lemma 4.3.15*

$$\begin{aligned}
&\rho_s \left(\partial_t \chi_{\boldsymbol{u}}^{n+1/2}, \boldsymbol{\nu}\right)_{\Omega_s} + \rho_f \left(\partial_t \Phi_{\chi_{\boldsymbol{v}}}^{n+1/2}, \boldsymbol{\nu}\right)_{\Omega_f} - \left(\nabla_h \cdot \left(\Phi_{\chi_{\boldsymbol{\sigma}_s}}^{n+1/2}\right), \boldsymbol{\nu}\right)_{\Omega_s} - \left(\nabla_h \cdot \left(\Phi_{\chi_{\boldsymbol{\sigma}_f}}^{n+1/2}\right), \boldsymbol{\nu}\right)_{\Omega_f} \\
&\qquad = \left(R_{\boldsymbol{u}}^n, \boldsymbol{\nu}\right)_{\Omega_s} + \left(R_{\boldsymbol{v}}^n, \boldsymbol{\nu}\right)_{\Omega_f} + \rho_f \left(\chi_{\boldsymbol{v}}^0, \boldsymbol{\nu}\right)_{\Omega_f}, \qquad \boldsymbol{\nu} \in \mathcal{V}_h,
\end{aligned} \tag{4.87a}$$

$$\begin{aligned}
&\left(\mathcal{A}\partial_t \Phi_{\chi_{\boldsymbol{\sigma}_s}}^{n+1/2}, \boldsymbol{\tau}\right)_{\Omega_s} + \left(\mathcal{A}_\infty \Phi_{\chi_{\boldsymbol{\sigma}_f}}^{n+1/2}, \boldsymbol{\tau}\right)_{\Omega_f} + \left(\chi_{\boldsymbol{u}}^{n+1/2}, \nabla_h \cdot \boldsymbol{\tau}\right)_{\Omega_s} + \left(\Phi_{\chi_{\boldsymbol{v}}}^{n+1/2}, \nabla_h \cdot \boldsymbol{\tau}\right)_{\Omega_f} \\
&\qquad = \left(\mathcal{A}\left(\eta_{\boldsymbol{\sigma}_s}^{n+1/2} - \eta_{\boldsymbol{\sigma}_s}^0\right), \boldsymbol{\tau}\right)_{\Omega_s} + \left(\mathcal{A}_\infty \Phi_{\eta_{\boldsymbol{\sigma}_f}}^{n+1/2}, \boldsymbol{\tau}\right)_{\Omega_f} + \Delta t \sum_{i=0}^{n} I^i + E^i, \qquad \boldsymbol{\tau} \in \boldsymbol{\Sigma}_h.
\end{aligned} \tag{4.87b}$$

Proof. This proof largely follows the work of [35]. We begin by summing the error equations (4.64) over all time steps. To do this we would like to start by writing the equations (4.64) using differences so that when summed over time there will be a telescoping effect. Therefore recall the definition of ∂_t^2 stated in (2.45) which expresses the discrete second derivative as the difference of discrete first derivatives. Furthermore, the discrete first derivative (2.44) can be re-written as the difference of averages as follows:

$$\partial_t^c \phi^n = \frac{1}{\Delta t}\left(\overline{\phi^{n+1/2}} - \overline{\phi^{n-1/2}}\right).$$

This can be verified by direct calculation. Therefore (4.64a) can be written as

$$\begin{aligned}
&\frac{\rho_s}{\Delta t}\left(\left(\partial_t \chi_{\boldsymbol{u}}^{n+1/2} - \partial_t \chi_{\boldsymbol{u}}^{n-1/2}\right), \boldsymbol{\nu}\right)_{\Omega_s} + \frac{\rho_f}{\Delta t}\left(\left(\overline{\chi_{\boldsymbol{v}}^{n+1/2}} - \overline{\chi_{\boldsymbol{v}}^{n-1/2}}\right), \boldsymbol{\nu}\right)_{\Omega_f} - \left(\nabla_h \cdot \widetilde{\chi_{\boldsymbol{\sigma}_s}^n}, \boldsymbol{\nu}\right)_{\Omega_s} \\
&\qquad - \left(\nabla_h \cdot \widetilde{\chi_{\boldsymbol{\sigma}_f}^n}, \boldsymbol{\nu}\right)_{\Omega_f} \\
&\qquad\qquad = \left(r_{\boldsymbol{u}}^n, \boldsymbol{\nu}\right)_{\Omega_s} + \left(r_{\boldsymbol{v}}^n, \boldsymbol{\nu}\right)_{\Omega_f}.
\end{aligned}$$

Multiplying by Δt and summing from time step 1 to n, where $1 \leq n < N-1$ and the final

time is $N\Delta t$ we find

$$\rho_s\left(\left(\partial_t\chi_{\boldsymbol{u}}^{n+1/2}-\partial_t\chi_{\boldsymbol{u}}^{1/2}\right),\boldsymbol{\nu}\right)_{\Omega_s}+\rho_f\left(\left(\overline{\chi_{\boldsymbol{v}}^{n+1/2}}-\overline{\chi_{\boldsymbol{v}}^{1/2}}\right),\boldsymbol{\nu}\right)_{\Omega_f}-\Delta t\sum_{i=1}^{n}\left(\nabla_h\cdot\widetilde{\chi_{\boldsymbol{\sigma}_s}^{i}},\boldsymbol{\nu}\right)_{\Omega_s}$$
$$-\Delta t\sum_{i=1}^{n}\left(\nabla_h\cdot\widetilde{\chi_{\boldsymbol{\sigma}_f}^{i}},\boldsymbol{\nu}\right)_{\Omega_f}$$
$$=\Delta t\sum_{i=1}^{n}\left(r_{\boldsymbol{u}}^{i},\boldsymbol{\nu}\right)_{\Omega_s}+\Delta t\sum_{i=1}^{n}\left(r_{\boldsymbol{v}}^{i},\boldsymbol{\nu}\right)_{\Omega_f}. \tag{4.88}$$

Using (4.85), (4.84), and (4.86) with (4.88) we find

$$\rho_s\left(\partial_t\chi_{\boldsymbol{u}}^{n+1/2}-\partial_t\chi_{\boldsymbol{u}}^{1/2},\boldsymbol{\nu}\right)_{\Omega_s}+\rho_f\left(\partial_t\Phi_{\chi\boldsymbol{v}}^{n+1/2}-\overline{\chi_{\boldsymbol{v}}^{1/2}},\boldsymbol{\nu}\right)_{\Omega_f}-\left(\nabla_h\cdot\left(\Phi_{\chi\boldsymbol{\sigma}_s}^{n+1/2}-\Phi_{\chi\boldsymbol{\sigma}_s}^{1/2}\right),\boldsymbol{\nu}\right)_{\Omega_s}$$
$$-\left(\nabla_h\cdot\left(\Phi_{\chi\boldsymbol{\sigma}_f}^{n+1/2}-\Phi_{\chi\boldsymbol{\sigma}_f}^{1/2}\right),\boldsymbol{\nu}\right)_{\Omega_f}$$
$$=\left(R_{\boldsymbol{u}}^{n}-\Delta t\,r_{\boldsymbol{u}}^{0},\boldsymbol{\nu}\right)_{\Omega_s}+\left(R_{\boldsymbol{v}}^{n}-\Delta t\,r_{\boldsymbol{v}}^{0},\boldsymbol{\nu}\right)_{\Omega_f}. \tag{4.89}$$

Next, recall the initial condition (4.36a). By multiplying by $\frac{\Delta t}{2}$ and using the relationship

$$\frac{\Delta t}{2}\partial_t\chi_{\boldsymbol{v}}^{1/2}=\frac{\chi_{\boldsymbol{v}}^{1}-\chi_{\boldsymbol{v}}^{0}}{2}+\frac{\chi_{\boldsymbol{v}}^{0}}{2}-\frac{\chi_{\boldsymbol{v}}^{0}}{2}$$
$$=\overline{\chi_{\boldsymbol{v}}^{1/2}}-\chi_{\boldsymbol{v}}^{0},$$

the initial condition is written as

$$\rho_s\left(\partial_t\chi_{\boldsymbol{u}}^{1/2},\boldsymbol{\nu}\right)_{\Omega_s}+\rho_f\left(\overline{\chi_{\boldsymbol{v}}^{1/2}}-\chi_{\boldsymbol{v}}^{0},\boldsymbol{\nu}\right)_{\Omega_f}-\left(\nabla_h\cdot\Phi_{\chi\boldsymbol{\sigma}_s}^{1/2},\boldsymbol{\nu}\right)_{\Omega_s}-\left(\nabla_h\cdot\Phi_{\chi\boldsymbol{\sigma}_f}^{1/2},\boldsymbol{\nu}\right)_{\Omega_f}$$
$$=\Delta t\left(r_{\boldsymbol{u}}^{0},\boldsymbol{\nu}\right)_{\Omega_s}+\Delta t\left(r_{\boldsymbol{v}}^{0},\boldsymbol{\nu}\right)_{\Omega_f}. \tag{4.90}$$

Now (4.90) can be used with (4.89) to find

$$\rho_s\left(\partial_t\chi_{\boldsymbol{u}}^{n+1/2},\boldsymbol{\nu}\right)_{\Omega_s}+\rho_f\left(\partial_t\Phi_{\chi\boldsymbol{v}}^{n+1/2},\boldsymbol{\nu}\right)_{\Omega_f}-\left(\nabla_h\cdot\left(\Phi_{\chi\boldsymbol{\sigma}_s}^{n+1/2}\right),\boldsymbol{\nu}\right)_{\Omega_s}-\left(\nabla_h\cdot\left(\Phi_{\chi\boldsymbol{\sigma}_f}^{n+1/2}\right),\boldsymbol{\nu}\right)_{\Omega_f}$$
$$=\left(R_{\boldsymbol{u}}^{n},\boldsymbol{\nu}\right)_{\Omega_s}+\left(R_{\boldsymbol{v}}^{n},\boldsymbol{\nu}\right)_{\Omega_f}+\rho_f\left(\chi_{\boldsymbol{v}}^{0},\boldsymbol{\nu}\right)_{\Omega_f}.$$

To prove (4.87b), we similarly re-write (4.64b) as

$$\frac{1}{\Delta t}\left(\mathcal{A}\left(\chi_{\boldsymbol{\sigma}_s}^{n+1/2}-\chi_{\boldsymbol{\sigma}_s}^{n-1/2}\right),\boldsymbol{\tau}\right)_{\Omega_s}+\left(\mathcal{A}_\infty\widetilde{\chi_{\boldsymbol{\sigma}_f}^{n}},\boldsymbol{\tau}\right)_{\Omega_f}+\frac{1}{\Delta t}\left(\left(\chi_{\boldsymbol{u}}^{n+1/2}-\chi_{\boldsymbol{u}}^{n-1/2}\right),\nabla_h\cdot\boldsymbol{\tau}\right)_{\Omega_s}$$
$$+\left(\widetilde{\chi_{\boldsymbol{v}}^{n}},\nabla_h\cdot\boldsymbol{\tau}\right)_{\Omega_f}$$
$$=\frac{1}{\Delta t}\left(\mathcal{A}\left(\eta_{\boldsymbol{\sigma}_s}^{n+1/2}-\eta_{\boldsymbol{\sigma}_s}^{n-1/2}\right),\boldsymbol{\tau}\right)_{\Omega_s}+\left(\mathcal{A}_\infty\widetilde{\eta_{\boldsymbol{\sigma}_f}^{n}},\boldsymbol{\tau}\right)_{\Omega_f}+I^n+E^n.$$

Multiplying by Δt and summing from time step 1 to n, where $1 \leq n < N-1$ and the final time is $N\Delta t$ we find

$$\begin{aligned}\left(\mathcal{A}\left(\chi_{\boldsymbol{\sigma}_s}^{n+1/2} - \overline{\chi_{\boldsymbol{\sigma}_s}^{1/2}}\right), \boldsymbol{\tau}\right)_{\Omega_s} + \Delta t \sum_{i=1}^{n} \left(\mathcal{A}_\infty \widetilde{\chi_{\boldsymbol{\sigma}_f}^i}, \boldsymbol{\tau}\right)_{\Omega_f} + \left(\left(\chi_{\boldsymbol{u}}^{n+1/2} - \chi_{\boldsymbol{u}}^{1/2}\right), \nabla_h \cdot \boldsymbol{\tau}\right)_{\Omega_s} \\ + \Delta t \sum_{i=1}^{n} \left(\widetilde{\chi_{\boldsymbol{v}}^i}, \nabla_h \cdot \boldsymbol{\tau}\right)_{\Omega_f} \\ = \left(\mathcal{A}\left(\eta_{\boldsymbol{\sigma}_s}^{n+1/2} - \eta_{\boldsymbol{\sigma}_s}^{1/2}\right), \boldsymbol{\tau}\right)_{\Omega_s} + \Delta t \sum_{i=1}^{n} \left(\mathcal{A}_\infty \widetilde{\eta_{\boldsymbol{\sigma}_f}^i}, \boldsymbol{\tau}\right)_{\Omega_f} + \Delta t \sum_{i=1}^{n} \left(I^i + E^i\right).\end{aligned} \tag{4.91}$$

Again using (4.85) and (4.84) we re-write (4.91) as

$$\begin{aligned}\left(\mathcal{A}\left(\partial_t \Phi_{\chi_{\boldsymbol{\sigma}_s}}^{n+1/2} - \overline{\chi_{\boldsymbol{\sigma}_s}^{1/2}}\right), \boldsymbol{\tau}\right)_{\Omega_s} + \left(\mathcal{A}_\infty \Phi_{\chi_{\boldsymbol{\sigma}_f}}^{n+1/2} - \Phi_{\chi_{\boldsymbol{\sigma}_f}}^{1/2}, \boldsymbol{\tau}\right)_{\Omega_f} + \left(\left(\chi_{\boldsymbol{u}}^{n+1/2} - \chi_{\boldsymbol{u}}^{1/2}\right), \nabla_h \cdot \boldsymbol{\tau}\right)_{\Omega_s} \\ + \left(\Phi_{\chi_{\boldsymbol{v}}}^{n+1/2} - \Phi_{\chi_{\boldsymbol{v}}}^{1/2}, \nabla_h \cdot \boldsymbol{\tau}\right)_{\Omega_f} \\ = \left(\mathcal{A}\left(\eta_{\boldsymbol{\sigma}_s}^{n+1/2} - \eta_{\boldsymbol{\sigma}_s}^{1/2}\right), \boldsymbol{\tau}\right)_{\Omega_s} + \Delta t \sum_{i=1}^{n} \left(\mathcal{A}_\infty \widetilde{\eta_{\boldsymbol{\sigma}_f}^i}, \boldsymbol{\tau}\right)_{\Omega_f} + \Delta t \sum_{i=1}^{n} \left(I^i + E^i\right).\end{aligned}$$

Next we recall and rewrite the initial condition (4.36b) as above to find

$$\begin{aligned}\left(\mathcal{A}\left(\overline{\chi_{\boldsymbol{\sigma}_s}^{1/2}} - \chi_{\boldsymbol{\sigma}_s}^0\right), \boldsymbol{\tau}\right)_{\Omega_s} + \left(\mathcal{A}_\infty \Phi_{\chi_{\boldsymbol{\sigma}_f}}^{1/2}, \boldsymbol{\tau}\right)_{\Omega_f} + \left(\chi_{\boldsymbol{u}}^{1/2} - \chi_{\boldsymbol{u}}^0, \nabla_h \cdot \boldsymbol{\tau}\right)_{\Omega_s} + \left(\Phi_{\chi_{\boldsymbol{v}}}^{1/2}, \nabla_h \cdot \boldsymbol{\tau}\right)_{\Omega_f} \\ = \left(\mathcal{A}\left(\eta_{\boldsymbol{\sigma}_s}^{1/2} - \eta_{\boldsymbol{\sigma}_s}^0\right), \boldsymbol{\tau}\right)_{\Omega_s} + \frac{\Delta t}{2}\left(\mathcal{A}_\infty \eta_{\boldsymbol{\sigma}_f}^{1/2}, \boldsymbol{\tau}\right)_{\Omega_f} + \Delta t I^0 + \Delta t E^0.\end{aligned}$$

Finally we note that

$$\Delta t \sum_{i=1}^{n} \left(\mathcal{A}_\infty \widetilde{\eta_{\boldsymbol{\sigma}_f}^i}, \boldsymbol{\tau}\right)_{\Omega_f} + \frac{\Delta t}{2}\left(\mathcal{A}_\infty \eta_{\boldsymbol{\sigma}_f}^{1/2}, \boldsymbol{\tau}\right)_{\Omega_f} = \left(\Phi_{\eta_{\boldsymbol{\sigma}_f}}^{n+1/2}, \boldsymbol{\tau}\right)_{\Omega_f}$$

and the result (4.91) follows directly. □

Lemma 4.4.3. *Under the same assumptions as Lemma 4.4.2*

$$\|\chi_{\boldsymbol{u}}\|_{L^\infty_{\Delta t}(L^2(\Omega_s))}^2 \leq C\left(\Delta t^4 + h^{2m_1}\Delta t^4 + h^{-1}\Delta t^4 + h^{2k} + h^{2l}\right), \tag{4.92}$$

with

$$C_4 = C\Big(\|\boldsymbol{v}_{ttt}\|^2_{L^2\left(0,T;L^2(\Omega_f)\right)}, \|\boldsymbol{u}_{ttt}\|^2_{L^1(0,T;L^2(\Omega_s))}, \|\boldsymbol{u}_{tttt}\|^2_{L^1(0,T;L^2(\Omega_s))}, \|\boldsymbol{\sigma}_s\|^2_{L^\infty_{\Delta t}(H^{m_1}(\Omega_s))},$$
$$\|\boldsymbol{\sigma}_f\|^2_{L^\infty_{\Delta t}\left(H^{m_1}(\Omega_f)\right)}, \|\boldsymbol{u}_t\|^2_{L^\infty_{\Delta t}(H^2(\Omega_s))}, \|\boldsymbol{v}\|^2_{L^\infty_{\Delta t}\left(H^2(\Omega_f)\right)}, \|\boldsymbol{v}\|^2_{L^\infty_{\Delta t}\left(H^2(\Omega_f)\right)}, \|\boldsymbol{u}_{ttt}\|^2_{L^2(0,T;H^2(\Omega_s))}$$
$$\|\boldsymbol{u}_{ttt}\|^2_{L^2(0,T;H^2(\Gamma))}, \|\boldsymbol{\sigma}_s^0\|_{m_1}\Big) \tag{4.93}$$

where m_1 and m_2 are convergence rates determined by the mixed finite element spaces chosen as in (4.9a) *and* (4.9b)*, k is determined by the consistency error as in* (4.20)*, and l is a convergence rate determined by the mixed finite element spaces used as described in Lemma* 4.3.8.

Proof. Choose the test functions

$$\boldsymbol{\nu} = \begin{cases} \chi_{\boldsymbol{u}}^{n+1/2} & \text{in } \Omega_s, \\ \Phi_{\chi_{\boldsymbol{v}}}^{n+1/2} & \text{in } \Omega_f \end{cases}$$

and

$$\boldsymbol{\tau} = \begin{cases} \Phi_{\chi_{\boldsymbol{\sigma}_s}}^{n+1/2} & \text{in } \Omega_s, \\ \Phi_{\chi_{\boldsymbol{\sigma}_f}}^{n+1/2} & \text{in } \Omega_f. \end{cases}$$

Plugging in these test functions and adding the equations (4.87a) and (4.87b) gives

$$\begin{aligned} &\rho_s\left(\partial_t\chi_{\boldsymbol{u}}^{n+1/2}, \chi_{\boldsymbol{u}}^{n+1/2}\right)_{\Omega_s} + \rho_f\left(\partial_t\Phi_{\chi_{\boldsymbol{v}}}^{n+1/2}, \Phi_{\chi_{\boldsymbol{v}}}^{n+1/2}\right)_{\Omega_f} + \left(\mathcal{A}\partial_t\Phi_{\chi_{\boldsymbol{\sigma}_s}}^{n+1/2}, \Phi_{\chi_{\boldsymbol{\sigma}_s}}^{n+1/2}\right)_{\Omega_s} \\ &\quad + \left(\mathcal{A}_\infty\Phi_{\chi_{\boldsymbol{\sigma}_f}}^{n+1/2}, \Phi_{\chi_{\boldsymbol{\sigma}_f}}^{n+1/2}\right)_{\Omega_f} \\ &\qquad = \left(R_{\boldsymbol{u}}^n, \chi_{\boldsymbol{u}}^{n+1/2}\right)_{\Omega_s} + \left(R_{\boldsymbol{v}}^n, \Phi_{\chi_{\boldsymbol{v}}}^{n+1/2}\right)_{\Omega_f} + \rho_f\left(\chi_{\boldsymbol{v}}^0, \Phi_{\chi_{\boldsymbol{v}}}^{n+1/2}\right)_{\Omega_f} \\ &\qquad\quad + \left(\mathcal{A}\left(\eta_{\boldsymbol{\sigma}_s}^{n+1/2} - \eta_{\boldsymbol{\sigma}_s}^0\right), \Phi_{\chi_{\boldsymbol{\sigma}_s}}^{n+1/2}\right)_{\Omega_s} + \left(\mathcal{A}_\infty\Phi_{\eta_{\boldsymbol{\sigma}_f}}^{n+1/2}, \Phi_{\chi_{\boldsymbol{\sigma}_f}}^{n+1/2}\right)_{\Omega_f} \\ &\qquad\quad + \Delta t\sum_{i=0}^{n}\left(I^i + E^i\right). \end{aligned} \tag{4.94}$$

Next, we apply the Cauchy-Schwarz Inequality, the equivalence of $\|\cdot\|_{\mathcal{A}_\infty,\Omega_f}$ to $\|\cdot\|_{\Omega_f}$ shown in 3.8, the equivalence of $\|\cdot\|_{\mathcal{A},\Omega_s}$ to $\|\cdot\|_{\Omega_s}$ shown in 2.8, the norm relations (4.14),

and the initial error bound (4.21), on the left hand side of (4.94) to find

$$\begin{aligned}
&\rho_s \left(\partial_t \chi_{\boldsymbol{u}}^{n+1/2}, \chi_{\boldsymbol{u}}^{n+1/2}\right)_{\Omega_s} + \rho_f \left(\partial_t \Phi_{\chi_{\boldsymbol{v}}}^{n+1/2}, \Phi_{\chi_{\boldsymbol{v}}}^{n+1/2}\right)_{\Omega_f} + \left(\mathcal{A}\partial_t \Phi_{\chi_{\boldsymbol{\sigma}_s}}^{n+1/2}, \Phi_{\chi_{\boldsymbol{\sigma}_s}}^{n+1/2}\right)_{\Omega_s} \\
&\quad + \left(\mathcal{A}_\infty \Phi_{\chi_{\boldsymbol{\sigma}_f}}^{n+1/2}, \Phi_{\chi_{\boldsymbol{\sigma}_f}}^{n+1/2}\right)_{\Omega_f} \\
&\qquad \leq \|R_{\boldsymbol{u}}^n\|_{\Omega_s} \|\chi_{\boldsymbol{u}}\|_{L^\infty_{\Delta t}(L^2(\Omega_s))} + \|R_{\boldsymbol{v}}^n\|_{\Omega_f} \|\Phi_{\chi_{\boldsymbol{v}}}\|_{L^\infty_{\Delta t}\left(L^2(\Omega_f)\right)} + \rho_f \|\chi_{\boldsymbol{v}}^0\|_{\Omega_f} \|\Phi_{\chi_{\boldsymbol{v}}}\|_{L^\infty_{\Delta t}\left(L^2(\Omega_f)\right)} \\
&\qquad\quad + C\left(\|\eta_{\boldsymbol{\sigma}_s}^{n+1/2}\|_{\Omega_s} + \|\eta_{\boldsymbol{\sigma}_s}^0\|_{\Omega_s}\right) \|\Phi_{\chi_{\boldsymbol{\sigma}_s}}\|_{L^\infty_{\Delta t}(L^2(\Omega_s))} + \|\Phi_{\eta_{\boldsymbol{\sigma}_f}}^{j+1/2}\|_{\mathcal{A}_\infty,\Omega_f} \|\Phi_{\chi_{\boldsymbol{\sigma}_f}}^{j+1/2}\|_{\mathcal{A}_\infty,\Omega_f} \\
&\qquad\quad + \Delta t \sum_{i=0}^{n} I^i + E^i.
\end{aligned}$$

We will once again sum this equation over time steps. We take advantage of telescoping by noting that for $q = \chi_{\boldsymbol{u}}, \Phi_{\chi_{\boldsymbol{v}}}, \Phi_{\chi_{\boldsymbol{\sigma}_s}}$

$$(\partial_t q^{n+1/2}, q) = \frac{1}{2\Delta t}\left(\|q^{n+1}\|^2 - \|q^n\|^2\right).$$

We will again sum (4.94) over the time steps. Recall that $\Phi_q^0 = 0$. Therefore, the left hand side of (4.94) is

$$\begin{aligned}
&\frac{\rho_s}{2\Delta t}\left(\|\chi_{\boldsymbol{u}}^n\|_{\Omega_s}^2 - \|\chi_{\boldsymbol{u}}^0\|_{\Omega_s}^2\right) + \frac{\rho_f}{2\Delta t}\left(\|\Phi_{\chi_{\boldsymbol{v}}}^n\|_{\Omega_f}^2 - \|\Phi_{\chi_{\boldsymbol{v}}}^0\|_{\Omega_f}^2\right) + \frac{1}{2\Delta t}\left(\|\Phi_{\chi_{\boldsymbol{\sigma}_s}}^n\|_{\mathcal{A},\Omega_s}^2 - \|\Phi_{\chi_{\boldsymbol{\sigma}_s}}^0\|_{\mathcal{A},\Omega_s}^2\right) \\
&\quad + \sum_{j=0}^{n} \|\Phi_{\chi_{\boldsymbol{\sigma}_f}}^{j+1/2}\|_{\mathcal{A}_\infty,\Omega_f}^2 \\
&\qquad = \frac{\rho_s}{2\Delta t}\|\chi_{\boldsymbol{u}}^n\|_{\Omega_s}^2 + \frac{\rho_f}{2\Delta t}\|\Phi_{\chi_{\boldsymbol{v}}}^n\|_{\Omega_f}^2 + \frac{1}{2\Delta t}\|\Phi_{\chi_{\boldsymbol{\sigma}_s}}^n\|_{\mathcal{A},\Omega_s}^2 + \sum_{j=0}^{n} \|\Phi_{\chi_{\boldsymbol{\sigma}_f}}^{j+1/2}\|_{\mathcal{A}_\infty,\Omega_f}^2
\end{aligned}$$

and we find

$$\begin{aligned}
&\frac{\rho_s}{2\Delta t}\|\chi_{\boldsymbol{u}}^n\|_{\Omega_s}^2 + \frac{\rho_f}{2\Delta t}\|\Phi_{\chi_{\boldsymbol{v}}}^n\|_{\Omega_f}^2 + \frac{1}{2\Delta t}\|\Phi_{\chi_{\boldsymbol{\sigma}_s}}^n\|_{\mathcal{A},\Omega_s}^2 + \sum_{j=0}^{n} \|\Phi_{\chi_{\boldsymbol{\sigma}_f}}^{j+1/2}\|_{\mathcal{A}_\infty,\Omega_f}^2 \\
&\quad \leq \sum_{j=0}^{n} \Bigg(\|R_{\boldsymbol{u}}^j\|_{\Omega_s} \|\chi_{\boldsymbol{u}}\|_{L^\infty_{\Delta t}(L^2(\Omega_s))} + \|R_{\boldsymbol{v}}^j\|_{\Omega_f} \|\Phi_{\chi_{\boldsymbol{v}}}\|_{L^\infty_{\Delta t}\left(L^2(\Omega_f)\right)} \\
&\qquad + C\left(\|\eta_{\boldsymbol{\sigma}_s}^{j+1/2}\|_{\Omega_s} + \|\eta_{\boldsymbol{\sigma}_s}^0\|_{\Omega_s}\right) \|\Phi_{\chi_{\boldsymbol{\sigma}_s}}\|_{L^\infty_{\Delta t}(L^2(\Omega_s))} + \|\Phi_{\eta_{\boldsymbol{\sigma}_f}}^{j+1/2}\|_{\mathcal{A}_\infty,\Omega_f} \|\Phi_{\chi_{\boldsymbol{\sigma}_f}}^{j+1/2}\|_{\mathcal{A}_\infty,\Omega_f} \\
&\qquad + \Delta t \sum_{i=0}^{N} \left(I^i + E^i\right) \Bigg).
\end{aligned}$$

The remaining steps are similar to those used in Lemma 4.3.16. We again note that this equation is true for all time steps so we take the maximum on the left hand side to achieve

$$\rho_s\|\chi_{\boldsymbol{u}}\|^2_{L^\infty_{\Delta t}(L^2(\Omega_s))} + \rho_f\|\Phi_{\chi_{\boldsymbol{v}}}\|^2_{L^\infty_{\Delta t}\left(L^2(\Omega_f)\right)} + \|\Phi_{\chi_{\boldsymbol{\sigma}_s}}\|^2_{L^\infty_{\Delta t}(L^2(\Omega_s))} + 2\Delta t\sum_{j=0}^{N}\|\Phi^{i+1/2}_{\chi_{\boldsymbol{\sigma}_f}}\|^2_{\mathcal{A}_\infty,\Omega_f}$$
$$\leq I + II + III + IV + V + VI + VII$$

where

$$I = 2\Delta t\sum_{j=0}^{N-1}\|R^j_{\boldsymbol{v}}\|_{\Omega_f}\|\Phi_{\chi_{\boldsymbol{v}}}\|_{L^\infty_{\Delta t}\left(L^2(\Omega_f)\right)},$$
$$II = 2C\Delta t\sum_{j=0}^{N-1}\|\eta^{j+1/2}_{\boldsymbol{\sigma}_s}\|_{\Omega_s}\|\Phi_{\chi_{\boldsymbol{\sigma}_s}}\|_{L^\infty_{\Delta t}(L^2(\Omega_s))},$$
$$III = 2\Delta t\sum_{j=0}^{N-1}\|R^j_{\boldsymbol{u}}\|_{\Omega_s}\|\chi_{\boldsymbol{u}}\|_{L^\infty_{\Delta t}(L^2(\Omega_s))},$$
$$IV = 2C\Delta t\sum_{j=0}^{N-1}\|\eta^0_{\boldsymbol{\sigma}_s}\|_{\Omega_s}\|\Phi_{\chi_{\boldsymbol{\sigma}_s}}\|_{L^\infty_{\Delta t}(L^2(\Omega_s))},$$
$$V = 2C\Delta t\sum_{j=0}^{N-1}\|\Phi^{j+1/2}_{\eta_{\boldsymbol{\sigma}_f}}\|_{\mathcal{A}_\infty,\Omega_f}\|\Phi^{j+1/2}_{\chi_{\boldsymbol{\sigma}_f}}\|_{\mathcal{A}_\infty,\Omega_f},$$
$$VI = 2T_f\Delta t\sum_{i=0}^{N-1}\left(I^i + E^i\right).$$

For each of the terms I and II we will apply Lemma 4.3.6 with ϵ chosen to ensure positive terms on the right hand side as in Lemma 4.3.16. See (4.78) for an example. To bound III, we use Young's Inequality with the value of ϵ chosen in same way as above to find

$$III \leq C\left(\Delta t\sum_{j=0}^{N-1}\|R^j_{\boldsymbol{u}}\|_{\Omega_s}\right)^2 + \frac{\rho_s}{2}\|\chi_{\boldsymbol{u}}\|^2_{L^\infty_{\Delta t}(L^2(\Omega_s))}.$$

As sums of constants with respect to j the terms IV is bounded with Young's Inequality with appropriate ϵ. See (4.79) for an example.

For V, using Young's Inequality we find

$$V \leq \Delta t \sum_{j=0}^{N-1} \|\Phi_{\eta_{\boldsymbol{\sigma}_f}}^{j+1/2}\|_{\mathcal{A}_\infty,\Omega_f}^2 + \Delta t \sum_{j=0}^{N-1} \|\Phi_{\chi_{\boldsymbol{\sigma}_f}}^{j+1/2}\|_{\mathcal{A}_\infty,\Omega_f}^2.$$

Finally for VI we recall the bound (4.76) from the previous Lemma and apply Lemma 4.3.6 and Young's Inequality as needed. Specifically, for I^i we have

$$I^n \leq C\left(h^k \|\boldsymbol{u}_t\|_{L^\infty_{\Delta t}(H^2(\Omega_s))} + h^{-1/2}\|\widetilde{\boldsymbol{u}_t^n} - \partial_t^c \boldsymbol{u}^n\|_\Gamma\right) \|\Phi_{\chi_{\boldsymbol{\sigma}_s}}\|_{L^\infty_{\Delta t}(L^2(\Omega_s))}.$$

from (4.76). Therefore we choose the appropriate ϵ in Lemma 4.3.6 and Young's Inequality to find

$$2T_f\Delta t \sum_{i=0}^{N-1} I^i \leq Ch^{2k}\Delta t \sum_{i=0}^{N-1} \|\boldsymbol{u}_t\|^2_{L^\infty_{\Delta t}(H^2(\Omega_s))} + Ch^{-1}\Delta t \sum_{i=0}^{N-1} \|\widetilde{\boldsymbol{u}_t^i} - \partial_t^c \boldsymbol{u}^i\|_\Gamma^2 + \frac{1}{8}\|\Phi_{\chi_{\boldsymbol{\sigma}_s}}\|^2_{\overline{L^\infty_{\Delta t}}(L^2(\Omega_s))}.$$

A similar procedure is repeated on $2T_f\Delta t \sum_{i=0}^{N-1} E^i$ by recalling (4.75). Using these bounds on $I - VI$, the initial bound (4.21), and combining like terms on the left hand side, we find

$$\begin{aligned}
&\|\chi_{\boldsymbol{u}}\|^2_{L^\infty_{\Delta t}(L^2(\Omega_s))} + \|\Phi_{\chi_{\boldsymbol{v}}}\|^2_{L^\infty_{\Delta t}\left(L^2(\Omega_f)\right)} + \|\Phi_{\chi_{\boldsymbol{\sigma}_s}}\|^2_{L^\infty_{\Delta t}(L^2(\Omega_s))} + \Delta t \sum_{j=0}^{N-1} \|\Phi_{\chi_{\boldsymbol{\sigma}_f}}^{j+1/2}\|^2_{\mathcal{A}_\infty,\Omega_f} \\
&\qquad \leq I + II + III + IV + V + VI
\end{aligned}$$

where

$$\begin{aligned}
I &= C\Delta t \sum_{j=0}^{N-1} \|R_{\boldsymbol{v}}^j\|^2_{\Omega_f}, \\
II &= C\left(\Delta t \sum_{j=0}^{N-1} \|R_{\boldsymbol{u}}^j\|_{\Omega_s}\right)^2, \\
III &= C\Delta t \sum_{j=0}^{N-1} \|\eta_{\boldsymbol{\sigma}_s}^{j+1/2}\|^2_{\Omega_s} + \|\Phi_{\eta_{\boldsymbol{\sigma}_f}}^{j+1/2}\|^2_{\Omega_f}, \\
IV &= Ch^{2k}\left(\|\boldsymbol{u}_t\|^2_{L^\infty_{\Delta t}(H^2(\Omega_s))} + \|\boldsymbol{v}\|^2_{L^\infty_{\Delta t}\left(H^2(\Omega_f)\right)}\right), \\
V &= C\Delta t \sum_{i=0}^{N-1} \left(h^{2k}\|\widetilde{\boldsymbol{u}_t^i} - \partial_t^c \boldsymbol{u}^i\|_{2,\Omega_s} + h^{-1}\|\widetilde{\boldsymbol{u}_t^i} - \partial_t^c \boldsymbol{u}^i\|^2_\Gamma\right) \\
VI &= \|\eta_{\boldsymbol{\sigma}_s}^0\|^2_{\Omega_s}.
\end{aligned}$$

To bound I we first note the following relationship which is obtained by use of the Triangle Inequality:

$$\|R_{\boldsymbol{v}}^j\|_{\Omega_f} \leq \Delta t \sum_{j=0}^{N-1} \|r_{\boldsymbol{v}}^j\|_{\Omega_f}.$$

Therefore, by using Hölder's inequality, Lemma 4.3.11 and (4.16b) we find

$$\begin{aligned}\|R_{\boldsymbol{v}}^j\|_{\Omega_s}^2 &\leq C\Delta t \sum_{j=0}^{N} \|r_{\boldsymbol{v}}^j\|_{\Omega_s}^2 \\ &\leq C\Delta t^4 \|\boldsymbol{v}_{ttt}\|^2_{L^2\left(0,T;L^2(\Omega_f)\right)}.\end{aligned}$$

To bound II, we follow the work of [35] and note that

$$\begin{aligned}\|R_{\boldsymbol{u}}^j\|_{\Omega_s} &\leq C\Delta t \sum_{j=0}^{N} \|r_{\boldsymbol{u}}^j\|_{\Omega_s} \\ &\leq C\Delta t^2 \left(\|\boldsymbol{u}_{ttt}\|_{L^1(0,T;L^2(\Omega_s))} + \|\boldsymbol{u}_{tttt}\|_{L^1(0,T;L^2(\Omega_s))}\right)\end{aligned}$$

and therefore

$$II \leq C\Delta t^4 \left(\|\boldsymbol{u}_{ttt}\|^2_{L^1\left(0,T;L^2(\Omega_f)\right)} + \|\boldsymbol{u}_{tttt}\|^2_{L^1\left(0,T;L^2(\Omega_f)\right)}\right).$$

The next two terms in III are bounded using the Triangle Inequality and the approximation property (4.9a). The terms in IV depend only on the regularity of the weak solutions. The terms in V are bounded by noting (4.16b). Note that this term also appeared in and was bounded in the previous Lemma 4.3.16, see (4.80)

Finally the terms of VI are bounded by (4.21). Thus we obtain

$$\begin{aligned}&\|\chi_{\boldsymbol{u}}\|^2_{L^\infty_{\Delta t}(L^2(\Omega_s))} + \|\Phi_{\chi_{\boldsymbol{v}}}\|^2_{L^\infty_{\Delta t}\left(L^2(\Omega_f)\right)} + \|\Phi_{\chi_{\boldsymbol{\sigma}_s}}\|^2_{L^\infty_{\Delta t}(L^2(\Omega_s))} + \Delta t \sum_{j=0}^{N-1} \|\Phi^{i+1/2}_{\chi_{\boldsymbol{\sigma}_f}}\|^2_{\mathcal{A}_\infty,\Omega_f} \\ &\quad\leq C\Big(\Delta t^4 \|\boldsymbol{v}_{ttt}\|^2_{L^2\left(0,T;L^2(\Omega_f)\right)} + \Delta t^4 \left(\|\boldsymbol{u}_{ttt}\|^2_{L^1(0,T;L^2(\Omega_s))} + \|\boldsymbol{u}_{tttt}\|^2_{L^1(0,T;L^2(\Omega_s))}\right) \\ &\qquad + h^{2m_1}\|\boldsymbol{\sigma}_s\|^2_{L^\infty_{\Delta t}(H^{m_1}(\Omega_s))} + h^{2m_1}\|\boldsymbol{\sigma}_f\|^2_{L^\infty_{\Delta t}\left(H^{m_1}(\Omega_f)\right)} + h^{2k}\|\boldsymbol{u}_t\|^2_{L^\infty_{\Delta t}(H^2(\Omega_s))} \\ &\qquad + \|\boldsymbol{v}\|^2_{L^\infty_{\Delta t}\left(H^2(\Omega_f)\right)} + h^{2k}\|\boldsymbol{v}\|^2_{L^\infty_{\Delta t}\left(H^2(\Omega_f)\right)} + \Delta t^4 \|\boldsymbol{u}_{ttt}\|^2_{L^2(0,T;H^2(\Omega_s))} \\ &\qquad + h^{-1}\Delta t^4 \|\boldsymbol{u}_{ttt}\|^2_{L^2(0,T;H^2(\Gamma))} + h^{2m_1}\|\boldsymbol{\sigma}_s^0\|_{m_1}\Big)\end{aligned} \tag{4.95}$$

□

Theorem 4.4.4. *Under the assumptions of Lemma 4.4.3*

$$\|\boldsymbol{u} - \boldsymbol{u}_h\|^2_{L^\infty_{\Delta t}(L^2(\Omega_s))} \leq C_4 \left(\Delta t^4 + h^{2m_1} + + h^{-1}\Delta t^4 + h^{2k} + h^{2l}\right) + Ch^{2m_2} \tag{4.96}$$

with C_4 as defined in (4.93) *and $C = C(\|\boldsymbol{u}\|^2_{L^\infty_{\Delta t}(H^{m_2}(\Omega_s))})$. Here m_1 and m_2 are convergence rates determined by the mixed finite element spaces chosen as in* (4.9a) *and* (4.9b), *k is determined by the consistency error as in* (4.20), *and l is a convergence rate determined by the mixed finite element spaces used as described in Lemma* 4.3.8.

Proof. This follows directly of Lemma 4.4.3 and the Triangle Inequality. Note that the value of C depends on the function norms in (4.95) □

4.5 Numerical Results

In this section, we will present numerical results using the conforming and nonconforming Arnold-Winther mixed finite elements described for the linear elasticity problem in Sections 2.3.3 and 2.3.4. Recall that the conforming method enforces continuity of the stress at vertices, which is a condition not required by the mixed variational formulation and may be undesirable [7]. In an effort to confirm the expected convergence rates when studying the solid or fluid domains separately, we have used problems with analytic solutions. However, these analytic solutions have been continuous and we have observed expected convergence rates when using the conforming mixed finite elements.

For the FSI problem, we again test problems with analytic solutions. First, we test a constructed problem with an analytic solution that is continuous at the interface between the solid and fluid. This test problem has been constructed to preserve this continuity and not in accordance with a realistic physical problem. Its value is only as a test problem with an analytic solution. Secondly, we test a problem found in [67] which is designed with the interaction between fluids and solids of similar density in mind. This problem is based on

one originally present in [9]. Only the normal component of stress is continuous across the interface in this test problem.

Before presenting numerical results using these test cases, we describe the expected convergence rate using the conforming and nonconforming cases. For the conforming case, we expect that there is no consistency error, thus terms involving the consistency error bound h^{2k} do not effect the expected convergence. In the case of the conforming element we expect $m_1 = 3$, $m_2 = 2$ and $l = 2$ provided that a finite element space with sufficient accuracy is used in approximating the fluid pressure as described in section 3.2.1. Assuming there is sufficient regularity in the solutions $\boldsymbol{\omega}$ and $\boldsymbol{\sigma}$, by Theorem 4.3.17,

$$\begin{aligned}\|\partial_t(\boldsymbol{u}-\boldsymbol{u}_h)\|^2_{\overline{L^\infty_{\Delta t}}(L^2(\Omega_s))} + \|\boldsymbol{v}-\boldsymbol{v}_h\|^2_{\overline{L^\infty_{\Delta t}}\left(L^2(\Omega_f)\right)} + \|\boldsymbol{\sigma}_s-\boldsymbol{\sigma}_{s_h}\|^2_{\overline{L^\infty_{\Delta t}}(L^2(\Omega_s))} \\ + \Delta t\sum_{i=1}^{N}\|\boldsymbol{\sigma}_f-\boldsymbol{\sigma}_{f_h}\|^2_{\mathcal{A}_\infty,\Omega_f} \\ \leq C\left(\Delta t^4 + h^4 + h^{-1}\Delta t^4\right).\end{aligned} \tag{4.97}$$

Additionally from Theorem 4.4.4

$$\|\boldsymbol{u}-\boldsymbol{u}_h\|^2_{L^\infty_{\Delta t}(L^2(\Omega_s))} \leq C\left(\Delta t^4 + h^4 + h^{-1}\Delta t^4\right). \tag{4.98}$$

On the other hand, in the case of the nonconforming element we expect $m_1 = 1$, $m_2 = 1$, $k = 1$, and $l = 1$ in Theorem 4.3.17 giving

$$\begin{aligned}\|\partial_t(\boldsymbol{u}-\boldsymbol{u}_h)\|^2_{\overline{L^\infty_{\Delta t}}(L^2(\Omega_s))} + \|\boldsymbol{v}-\boldsymbol{v}_h\|^2_{\overline{L^\infty_{\Delta t}}\left(L^2(\Omega_f)\right)} + \|\boldsymbol{\sigma}_s-\boldsymbol{\sigma}_{s_h}\|^2_{\overline{L^\infty_{\Delta t}}(L^2(\Omega_s))} \\ + \Delta t\sum_{i=1}^{N}\|\boldsymbol{\sigma}_f-\boldsymbol{\sigma}_{f_h}\|^2_{\mathcal{A}_\infty,\Omega_f} \\ \leq C\left(\Delta t^4 + h^2 + h^{-1}\Delta t^4\right)\end{aligned} \tag{4.99}$$

and, from Theorem 4.4.4,

$$\|\boldsymbol{u}-\boldsymbol{u}_h\|^2_{L^\infty_{\Delta t}(L^2(\Omega_s))} \leq C\left(\Delta t^4 + h^2 + h^{-1}\Delta t^4\right). \tag{4.100}$$

We see that in both the conforming and nonconforming case the effect of the interface integral terms is seen in the $h^{-1}\Delta t^4$ term. From this, we may expect an increase in error as

the grid is refined spatially. However if we make the restriction that h and Δt are reduced at the same rate, that is $h \sim \Delta t$, then this factor becomes Δt^3.

In the case of the conforming mixed finite element space, (4.97) and(4.98) are now

$$\begin{aligned}
&\|\partial_t (\boldsymbol{u} - \boldsymbol{u}_h)\|^2_{\overline{L^\infty_{\Delta t}}(L^2(\Omega_s))} + \|\boldsymbol{v} - \boldsymbol{v}_h\|^2_{\overline{L^\infty_{\Delta t}}\left(L^2(\Omega_f)\right)} + \|\boldsymbol{\sigma}_s - \boldsymbol{\sigma}_{s_h}\|^2_{\overline{L^\infty_{\Delta t}}(L^2(\Omega_s))} \\
&\quad + \Delta t \sum_{i=1}^{N} \|\boldsymbol{\sigma}_f - \boldsymbol{\sigma}_{f_h}\|^2_{\mathcal{A}_\infty,\Omega_f} \\
&\quad \leq C\left(\Delta t^3 + h^4\right)
\end{aligned}$$

and

$$\|\boldsymbol{u} - \boldsymbol{u}_h\|^2_{L^\infty_{\Delta t}(L^2(\Omega_s))} \leq C\left(\Delta t^3 + h^4\right)$$

respectively. This is lower than the second order convergence rate in time observed for the solid and fluid subdomains. However in the nonconforming case (4.99) and (4.100) become

$$\begin{aligned}
&\|\partial_t (\boldsymbol{u} - \boldsymbol{u}_h)\|^2_{\overline{L^\infty_{\Delta t}}(L^2(\Omega_s))} + \|\boldsymbol{v} - \boldsymbol{v}_h\|^2_{\overline{L^\infty_{\Delta t}}\left(L^2(\Omega_f)\right)} + \|\boldsymbol{\sigma}_s - \boldsymbol{\sigma}_{s_h}\|^2_{\overline{L^\infty_{\Delta t}}(L^2(\Omega_s))} \\
&\quad + \Delta t \sum_{i=1}^{N} \|\boldsymbol{\sigma}_f - \boldsymbol{\sigma}_{f_h}\|^2_{\mathcal{A}_\infty,\Omega_f} \\
&\quad \leq C\left(\Delta t^3 + h^2\right)
\end{aligned}$$

and

$$\|\boldsymbol{u} - \boldsymbol{u}_h\|^2_{L^\infty_{\Delta t}(L^2(\Omega_s))} \leq C\left(\Delta t^3 + h^2\right).$$

Although this shows a degraded rate in terms of time, as both time and spatial are being reduced simultaneously, the overall observed rate is limited by the h^2. That is, we expect only first order convergence when considering the L^∞-norm of each variable. Therefore the effect of the interface integral terms may not be observed.

FSI Example 1

To verify these experimental results numerically, we attempt use the model to find an approximation in the rare case where the analytic solution is known. Consider the domain

$\Omega = [0,1] \times [0,1]$ divided into fluid and structure subdomains $\Omega_f = [0,1] \times [0,.5]$ and $\Omega_s = [0,1] \times [.5,1]$. Then consider the test problem with the analytic solution

$$\boldsymbol{u} = \begin{bmatrix} e^t \sin(x)\sin(y) \\ e^t \cos(x)\cos(y) \end{bmatrix}, \quad \boldsymbol{v} = \begin{bmatrix} e^t \sin(x)\sin(y) \\ e^t \cos(x)\cos(y) \end{bmatrix}.$$

The other variables $\boldsymbol{\sigma}_s$ and $\boldsymbol{f}_s$ are constructed from this result.

$$\boldsymbol{f}_s = \begin{bmatrix} e^t(\rho_s - 2\mu)\sin(x)\sin(y) \\ e^t(\rho_s - 2\mu)\cos(x)\cos(y) \end{bmatrix}, \quad \boldsymbol{f}_f = \begin{bmatrix} e^t(\rho_s - 2\mu)\sin(x)\sin(y) \\ e^t(\rho_s - 2\mu)\cos(x)\cos(y) \end{bmatrix}$$

where $\mu_s = \mu_f = \mu$ and $\rho_s = \rho_f$ which is not realistic physically. By construction $\boldsymbol{u}_t = \boldsymbol{v}$ over the entire region so the interface condition (4.3a) is satisfied no matter where the interface falls in the domain. Furthermore for this particular system $\boldsymbol{\sigma}_s = \boldsymbol{\sigma}_f$ in the entire domain, satisfying the interface condition (4.3b). The interface in this case falls along the line $y = 0.5$. However this solution is formed just as an academic example. It has little or no physical meaning and is used solely for verification purposes. The parameters $\mu = 3.57 \times 10^4, \lambda = 1.43 \times 10^5$, and $rhoS = \rho_f = 1$ have been used here.

In Figure 4.2 we show a example graphs for the variable $\boldsymbol{\omega}_1$. and in Figure 4.3 there is a example graphs for $\boldsymbol{\sigma}_{11}$. We see that results obtained using both the conforming and nonconforming elements, shown in the top row of the figures, yield graphs that are nearly indistinguishable from the analytic solution, show in the bottom row.

In Table 4.1 and Figure 4.4, we show the results of a convergence study using this FSI example 1. We see a better than expected second order convergence for both the stress $\boldsymbol{\sigma}$ and displacement/ velocity $\boldsymbol{\omega}$. This may be due the fact that the interface is artificial since $\boldsymbol{\sigma}_s = \boldsymbol{\sigma}_f$. In Table 4.2 and Figure 4.5, we show the results of a convergence study using the nonconforming element instead. In this case we observe an unexpected drop in convergence rate in the last step of refinement. For a possible explanation, we note the unrealistic nature of the problem. As noted in the introduction, in some cases, such as when the density of the fluid and the solid are comparable, convergence issues have been observed [79]. Explanations of the causes of these instabilities,called added mass effects, can be found in [30, 44]. Setting $\rho_s = \rho_f$ may cause convergence issues in this case.

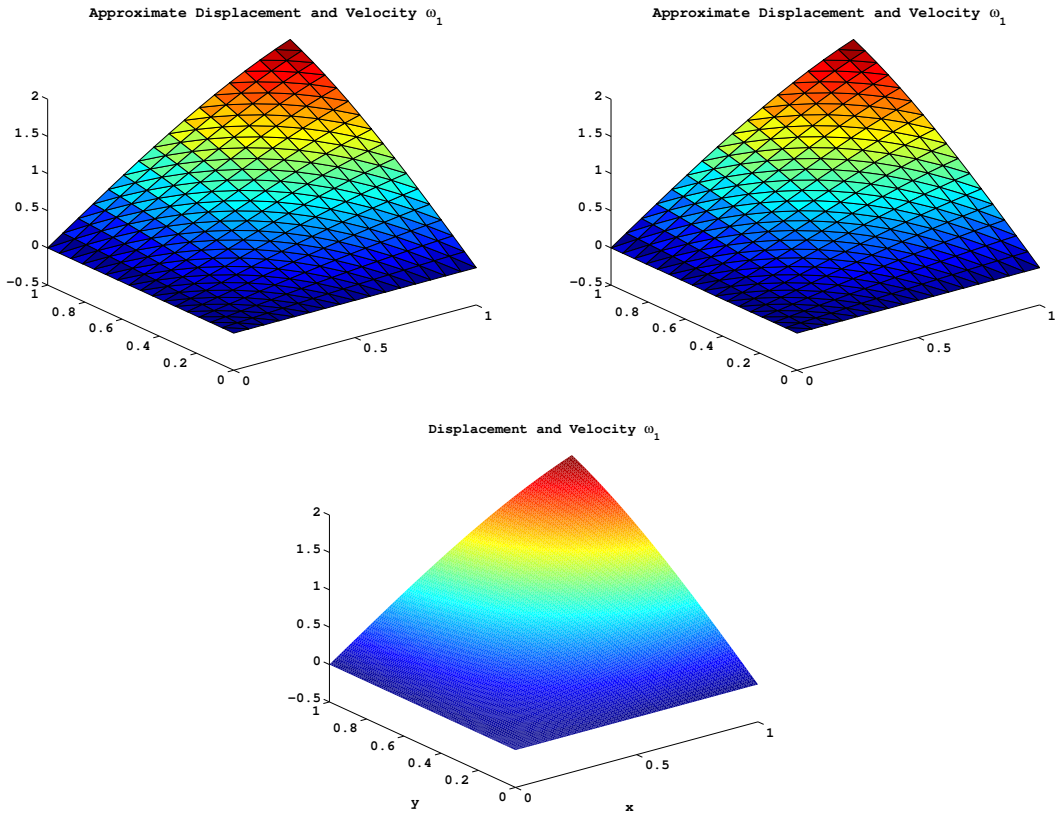

Figure 4.2: Solution graphs for the first component of displacement, $\boldsymbol{\omega}_1$ for the FSI example 1 at $T_f = 1$ with $h = \frac{1}{16}$ and $\Delta t = 1.25 \times 10^{-2}$: using the conforming element (left), using the nonconforming element (right), and the exact analytic solution (bottom).

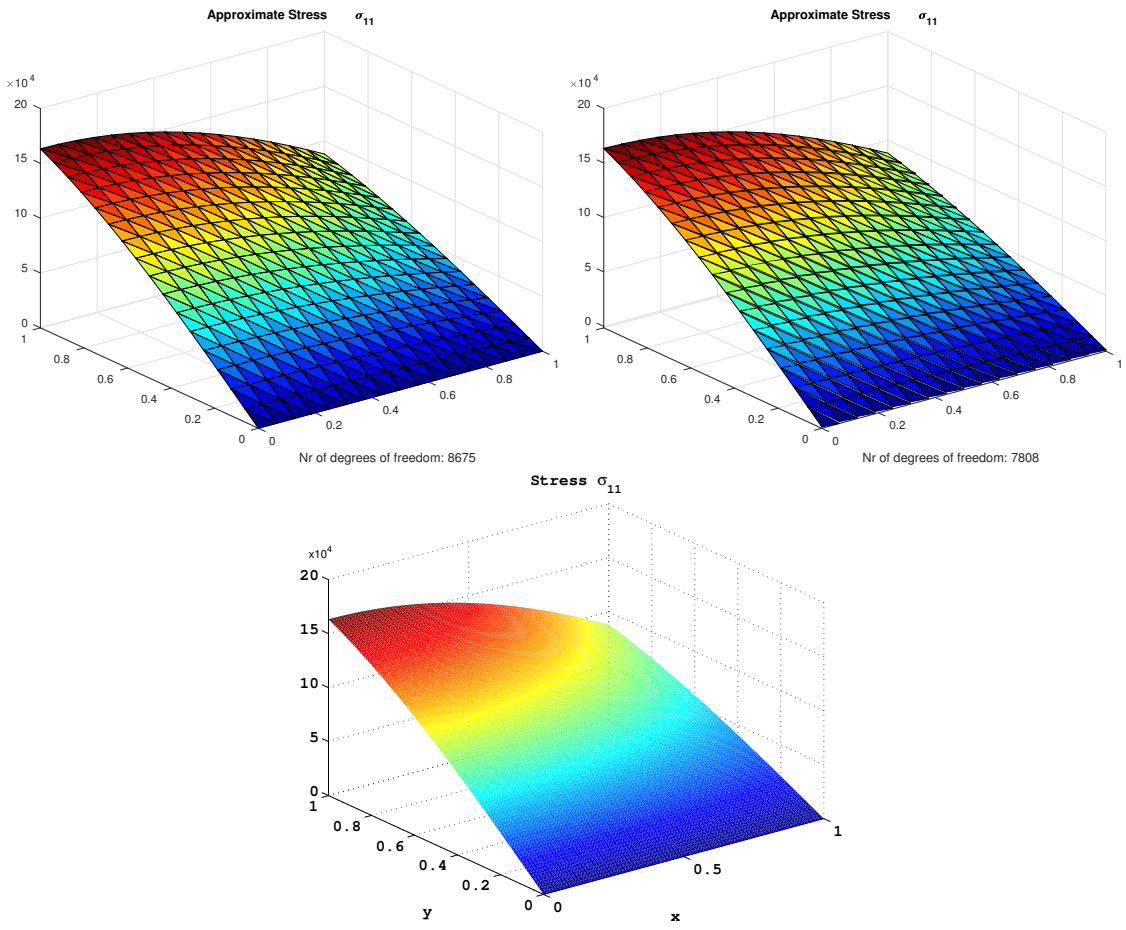

Figure 4.3: Solution graphs for the first component of stress, $\boldsymbol{\sigma}_{11}$ for the FSI example 1 at $T_f = 1$ with $h = \frac{1}{16}$ and $\Delta t = 1.25 \times 10^{-2}$: using the conforming element (left), using the nonconforming element (right), and the exact analytic solution (bottom).

Table 4.1: Convergence study results for FSI Example 1 with the conforming element

h	Δt	$\|\boldsymbol{\omega} - \boldsymbol{\omega}_h\|_{L^\infty_{\Delta t}(\Omega)}$	Order	$\|\boldsymbol{\sigma} - \boldsymbol{\sigma}_h\|_{L^\infty_{\Delta t}(\Omega)}$	Order
$\frac{1}{2}$	1.000E-01	3.952E-02	—	3.623E+02	—
$\frac{1}{4}$	5.000E-02	9.844E-03	2.01	6.742E+01	2.43
$\frac{1}{8}$	2.500E-02	2.459E-03	2.00	1.513E+01	2.16
$\frac{1}{16}$	1.250E-02	6.146E-04	2.00	3.664E+00	2.05
$\frac{1}{32}$	6.250E-03	1.537E-04	2.00	9.069E-01	2.01
$\frac{1}{64}$	3.125E-03	3.841E-05	2.00	2.269E-01	2.00

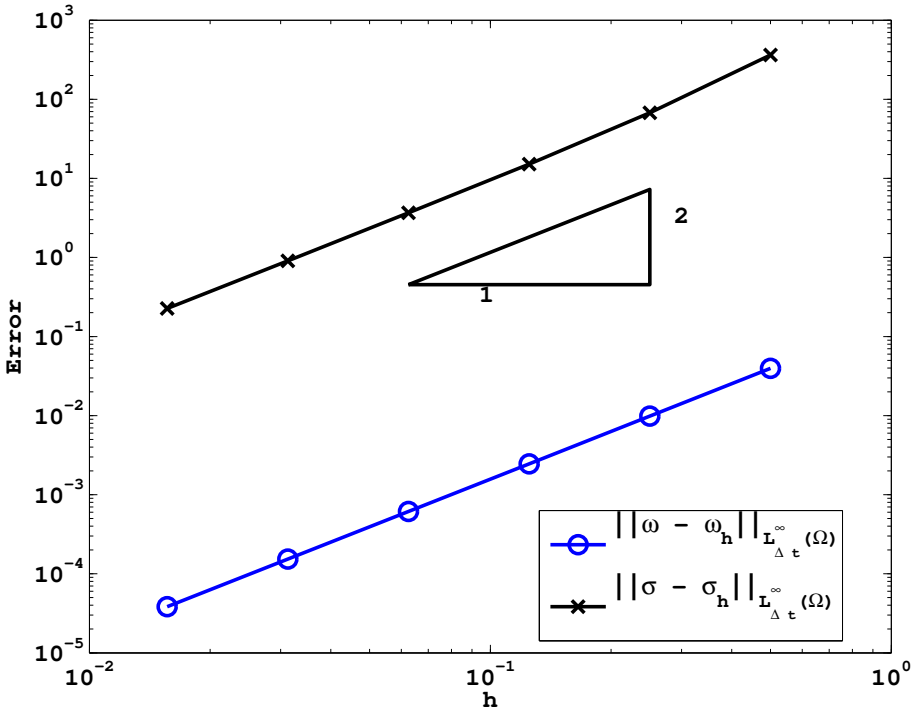

Figure 4.4: Graphical representation of the convergence study results for FSI Example 1 with the conforming element

Table 4.2: Convergence study results for FSI example 1 with the nonconforming element

h	Δt	$\|\boldsymbol{\omega} - \boldsymbol{\omega}_h\|_{L^\infty_{\Delta t}(\Omega)}$	Order	$\|\boldsymbol{\sigma} - \boldsymbol{\sigma}_h\|_{L^\infty_{\Delta t}(\Omega)}$	Order
$\frac{1}{2}$	1.000E-01	3.967E-02	—	5.100E+03	—
$\frac{1}{4}$	5.000E-02	9.912E-03	2.00	2.629E+03	0.96
$\frac{1}{8}$	2.500E-02	2.615E-03	1.92	1.351E+03	0.96
$\frac{1}{16}$	1.250E-02	1.042E-03	1.33	6.981E+02	0.95
$\frac{1}{32}$	6.250E-03	4.373E-04	1.25	3.425E+02	1.03
$\frac{1}{64}$	3.125E-03	3.165E-04	0.47	1.807E+02	0.92

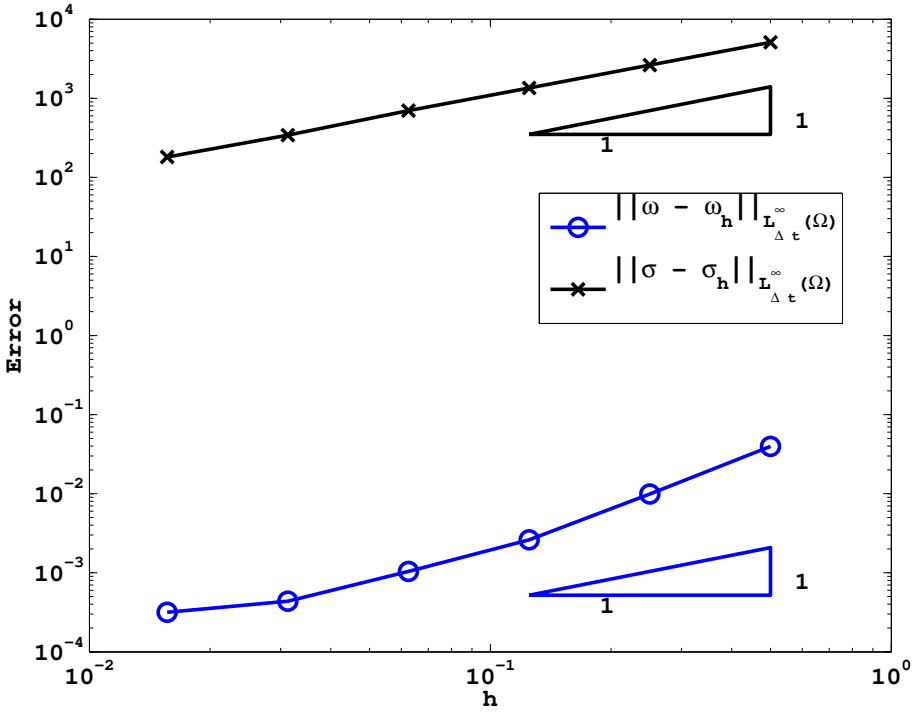

Figure 4.5: Graphical representation of the convergence study results for FSI Example 1 with the nonconforming element

Additionally, when using the nonconforming element, we have observed that the condition numbers linear system solved for this example are quite large. For example, when $h = \frac{1}{2}$ and $\Delta t = 0.1$ the condition numbers are approximately 1×10^8 and when $h = \frac{1}{4}$ and $\Delta t = 0.05$ the condition numbers are approximately 1×10^9. We have attempted to reduce this large condition number by implementing a preconditioned version of the FGMRES iterative method using the incomplete LU decomposition [87, 88]. This is used as a black box and does not converge in 1000 iterations per time step.

We have observed smaller condition numbers when $\lambda = \mu = 1$. Results of a convergence study with this change are shown in Table 4.3 and Figure 4.6. For this case, we no longer see the unexpected drop in convergence rate. The convergence rate in $\boldsymbol{\sigma}$ is roughly the expected first order rate by the last refinement and the convergence rate in $\boldsymbol{\omega}$ is higher than expected at 2.

Finally, recall that we have used the method described in Section 3.2.1 to find an approximation to $\boldsymbol{\sigma}$ at $t = 0$. Here we have found an approximation to the pressure p at $t = 0$ and used it to form and solve a linear system to find $\boldsymbol{\sigma}_{f_h}^0$. However, we may have alternatively used the definition of fluid stress (3.2) at $t = 0$ and approximation to the pressure p at $t = 0$ to find a different approximation to fluid stress. Results of a convergence study using this different initial condition are shown in Table 4.4 and 4.7. When looking at the the convergence rates of $\boldsymbol{\omega}$ we observe declining rates of convergence up to the point when $h = \frac{1}{32}$. However, in the last refinement, the rate increase above the expected rate of 1. A similar pattern may occur for our original problem show in Table 4.2, however, we are unable to refine this further due to computing resource and computing time restraints.

FSI Example 2

Next, consider the example problem studied in [69]. Again, consider the domain $\Omega = [0, 1] \times [0, 1]$ divided into fluid and structure subdomains $\Omega_f = [0, 1] \times [0, .5]$ and $\Omega_s = [0, 1] \times [.5, 1]$.

Table 4.3: Convergence study results for FSI example 1 with the nonconforming element with $\lambda = \mu = 1$

h	Δt	$\|\boldsymbol{\omega} - \boldsymbol{\omega}_h\|_{L^\infty_{\Delta t}(\Omega)}$	Order	$\|\boldsymbol{\sigma} - \boldsymbol{\sigma}_h\|_{L^\infty_{\Delta t}(\Omega)}$	Order
$\frac{1}{2}$	1.000E-01	3.988E-02	—	1.413E-01	—
$\frac{1}{4}$	5.000E-02	9.918E-03	2.01	7.229E-02	0.97
$\frac{1}{8}$	2.500E-02	2.476E-03	2.00	3.672E-02	0.98
$\frac{1}{16}$	1.250E-02	6.185E-04	2.00	1.850E-02	0.99
$\frac{1}{32}$	6.250E-03	1.551E-04	2.00	9.677E-03	0.93
$\frac{1}{64}$	3.125E-03	3.888E-05	2.00	4.731E-03	1.03

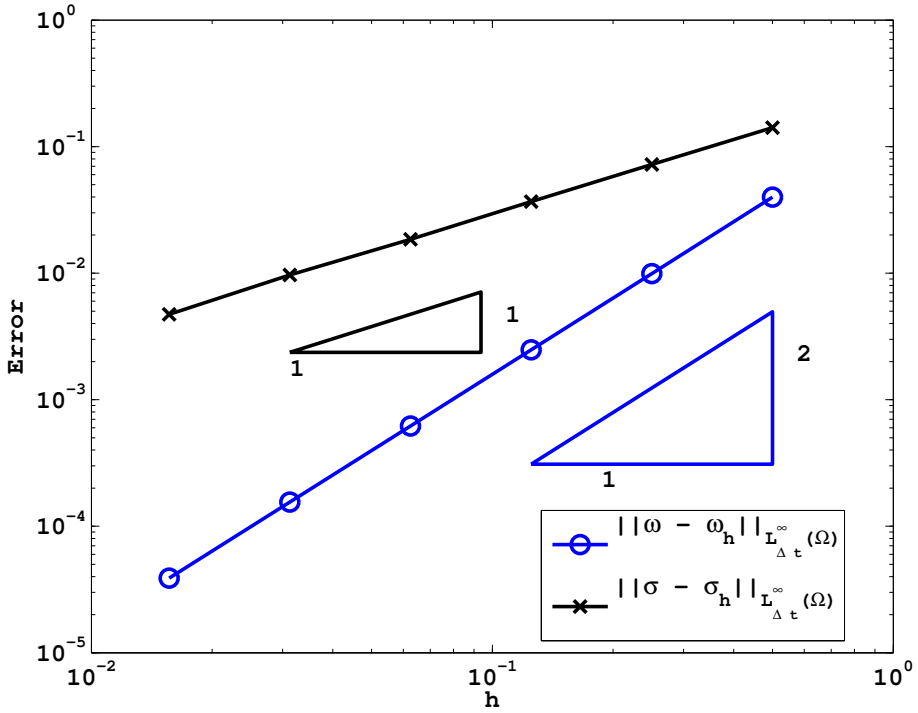

Figure 4.6: Graphical representation of the convergence study results for FSI Example 1 with the nonconforming element with $\lambda = \mu = 1$.

Table 4.4: Convergence study results for FSI example 1 with the nonconforming element with change initial condition

h	Δt	$\|\boldsymbol{\omega} - \boldsymbol{\omega}_h\|_{L^\infty_{\Delta t}(\Omega)}$	Order	$\|\boldsymbol{\sigma} - \boldsymbol{\sigma}_h\|_{L^\infty_{\Delta t}(\Omega)}$	Order
$\frac{1}{2}$	1.000E-01	3.976E-02	—	5.828E+03	—
$\frac{1}{4}$	5.000E-02	1.009E-02	1.98	2.969E+03	0.97
$\frac{1}{8}$	2.500E-02	3.238E-03	1.64	1.539E+03	0.95
$\frac{1}{16}$	1.250E-02	2.104E-03	0.62	8.344E+02	0.88
$\frac{1}{32}$	6.250E-03	1.164E-03	0.85	4.154E+02	1.01
$\frac{1}{64}$	3.125E-03	4.883E-04	1.25	1.891E+02	1.14

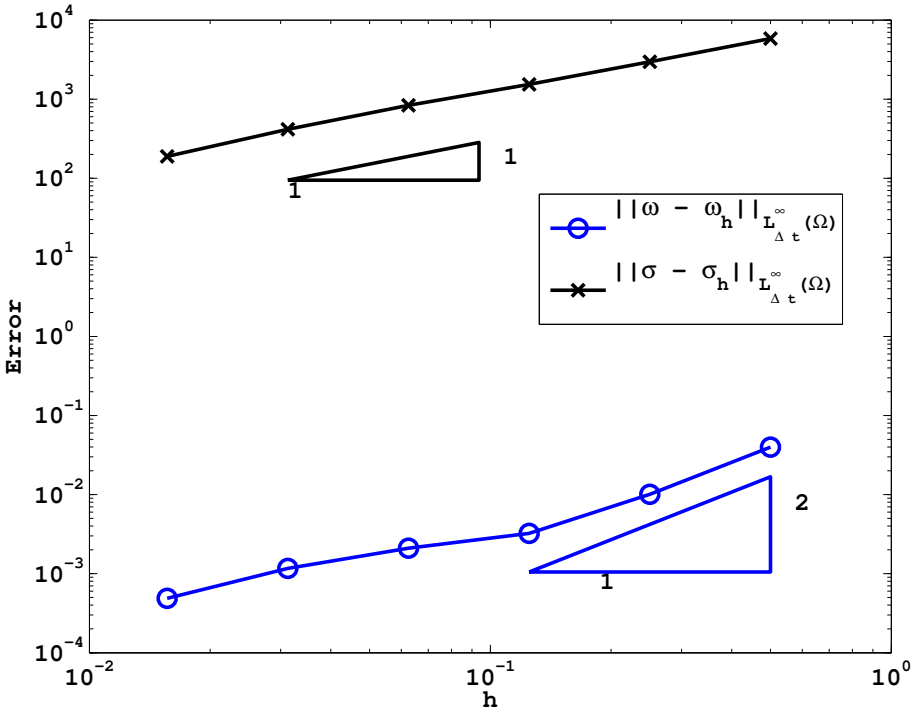

Figure 4.7: Graphical representation of the convergence study results for FSI Example 1 with the nonconforming element with changed initial condition

The analytic solution is given as

$$\boldsymbol{u} = \begin{bmatrix} \sin(x+t)\sin(y+t) \\ \cos(x+t)\cos(y+t) \end{bmatrix},$$

$$\boldsymbol{v} = \begin{bmatrix} \cos(x+t)\sin(y+t) + \sin(x+t)\cos(y+t) \\ -\sin(x+t)\cos(y+t) - \cos(x+t)\sin(y+t) \end{bmatrix},$$

$$p = 2\mu_f\left(\sin(x+t)\sin(y+t) - \cos(x+t)\cos(y+t)\right) + 2\mu_s\cos(x+t)\sin(y+t)$$

where p is the fluid pressure. These expressions are used to find an analytic expression for stress. For this case, the following parameters are used: $\rho_s = 1.9\,\frac{\text{g}}{\text{cm}^3}, \mu_s = 3\,\frac{\text{dyne}}{\text{cm}^2}, \lambda = 4.5\,\frac{\text{dyne}}{\text{cm}^2}, \rho_f = 1\,\frac{\text{g}}{\text{cm}^3}$, and $\mu_f = .0013\,\frac{\text{g}}{\text{cm}\cdot\text{s}}$. Although the interface condition (4.3a) on displacement and velocity is satisfied throughout the region, the condition on the stress (4.3b) is only satisfied in some locations in the domain. In particular, it is satisfied if the interface is horizontal (i.e. $\boldsymbol{n} = (0,1)^T$).

Table 4.5 shows the results of a a convergence study with this example 2 using the conforming element and refining both the spatial grid and reducing the time step simultaneously. For both variables, $\boldsymbol{\sigma}$ and $\boldsymbol{\omega}$, we see a convergence rate lower than the expect rate of 1.5. Specifically, by the final refinement, for $\boldsymbol{\sigma}$ the observed convergence rate is approximately .67 and for $\boldsymbol{\omega}$ is approximately .37. This may be due to the fact the conforming element forces continuity of the stress at vertices. Enforcing a condition that is not true of the analytic solution may result in the reduced convergence rates.

Table 4.6 shows the results of a convergence study with this example 2 using the nonconforming elements and refining both the spatial grid and reducing the time step simultaneously. For the displacement/velocity variable $\boldsymbol{\omega}$, we observe a faster a convergence rate of 2.92 for the final refinement, despite the expected first order convergence. Although a similar phenomena is observed for the elasticity only or fluid only problem in the previous sections, the rate of convergence here is faster than the observed rates for the separated problems. However the convergence rate for the stress variable is close to the expected rate of 1.

Table 4.5: Convergence study results for FSI Example 2 with the conforming element

h	Δt	$\|\boldsymbol{\omega} - \boldsymbol{\omega}_h\|_{L^\infty_{\Delta t}(\Omega)}$	Order	$\|\boldsymbol{\sigma} - \boldsymbol{\sigma}_h\|_{L^\infty_{\Delta t}(\Omega)}$	Order
$\frac{1}{2}$	1.000E-01	2.044E-01	—	1.321E+00	—
$\frac{1}{4}$	5.000E-02	4.975E-02	2.04	9.610E-01	0.46
$\frac{1}{8}$	2.500E-02	3.232E-02	0.62	6.715E-01	0.52
$\frac{1}{16}$	1.250E-02	2.276E-02	0.51	5.259E-01	0.35
$\frac{1}{32}$	6.250E-03	1.523E-02	0.58	4.143E-01	0.34
$\frac{1}{64}$	3.125E-03	9.599E-03	0.67	3.202E-01	0.37

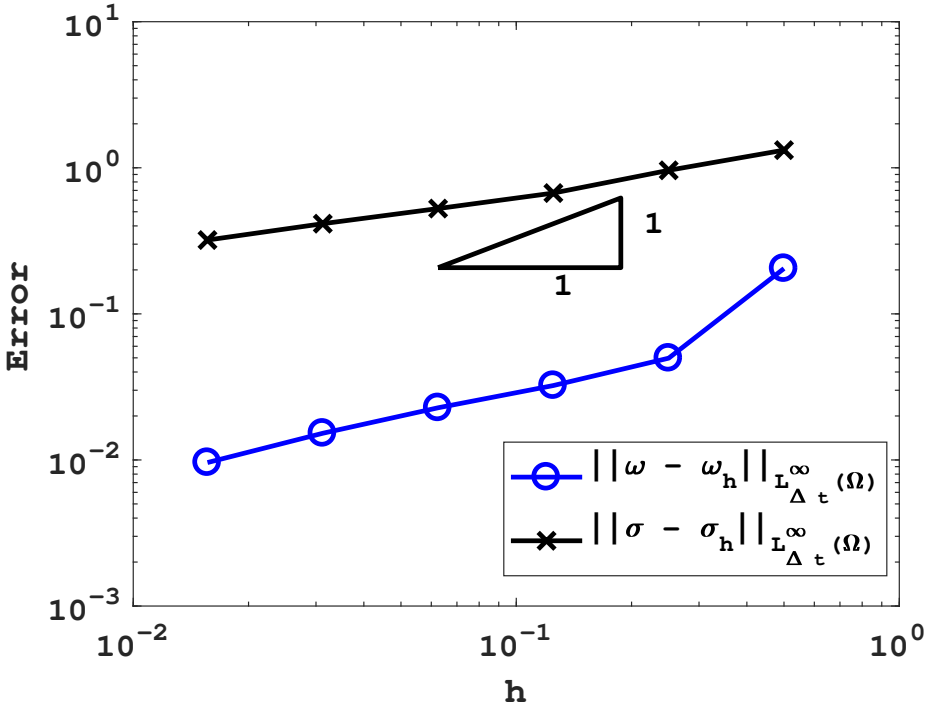

Figure 4.8: Graphical representation of the convergence study results for FSI Example 2 with the conforming element

Table 4.6: Convergence study results for FSI Example 2 with the nonconforming element

h	Δt	$\|\boldsymbol{\omega} - \boldsymbol{\omega}_h\|_{L^\infty_{\Delta t}(\Omega)}$	Order	$\|\boldsymbol{\sigma} - \boldsymbol{\sigma}_h\|_{L^\infty_{\Delta t}(\Omega)}$	Order
$\frac{1}{2}$	1.000E-01	3.087E-01	—	1.573E-01	—
$\frac{1}{4}$	5.000E-02	9.687E-02	1.67	6.087E-02	1.37
$\frac{1}{8}$	2.500E-02	3.110E-02	1.64	3.400E-02	0.84
$\frac{1}{16}$	1.250E-02	6.748E-03	2.20	1.891E-02	0.85
$\frac{1}{32}$	6.250E-03	1.013E-03	2.74	9.148E-03	1.05
$\frac{1}{64}$	3.125E-03	1.337E-04	2.92	4.555E-03	1.01

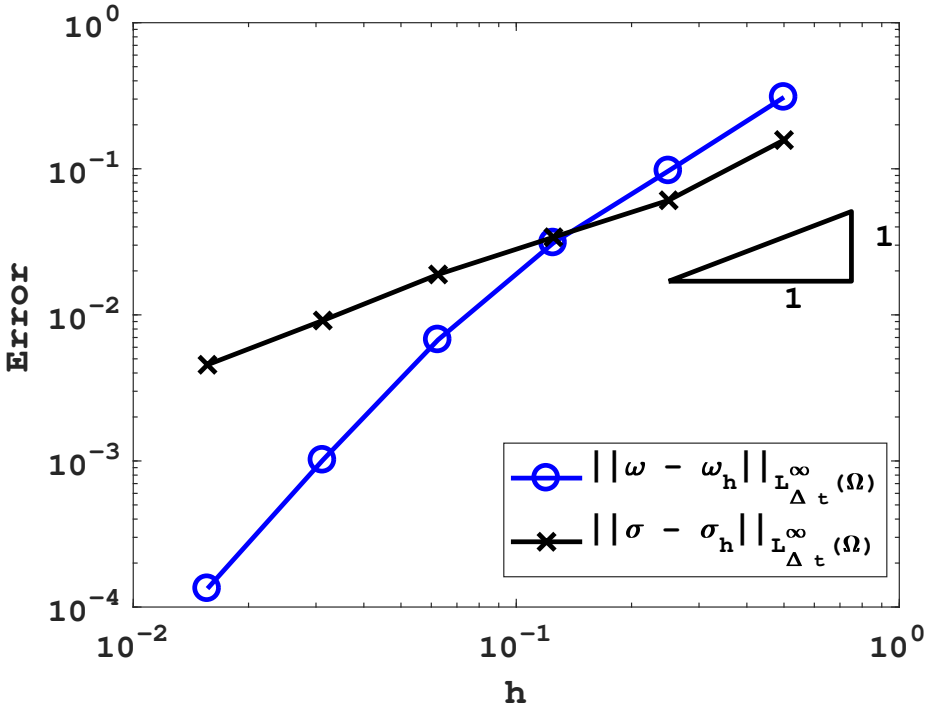

Figure 4.9: Graphical representation of the convergence study results for FSI Example 2 with the conforming element

For this example we provide some example graphs in Figure 4.10 and 4.11. Recall that for both the conforming and nonconforming elements, the finite element space for the vector quantity is not subject to global continuity conditions. Figure 4.10 shows an example graph for the variable $\boldsymbol{\omega}_1$. On the left, the graph of the approximation $\boldsymbol{\omega}_1$ using the conforming method is shown. In this graph, we see that the elements near the interface show some oscillations. These oscillations are not clearly visible in when the nonconforming element is used, see the right side of Figure 4.10. Furthermore, in the graphs for the approximate stress using the conforming MFEM, shown on the left side of Figure 4.11, we see that this approximation is continuous across the interface. The graph of the analytic solution for $\boldsymbol{\sigma}_{11}$ on the bottom of Figure 4.11, shows that this continuity is not required. The approximation $\boldsymbol{\sigma}_{11}$ using the nonconforming MFEM, shown on the right side of Figure 4.11, more closely resembles the analytic solution.

FSI Example 3

As it is known that the added mass effect can cause convergence issues when the density of the fluid and the solid are of similar densities, we study the convergence results again using the example problem studied in [69] and FSI example 2. However, different parameters are set. First, to test the case of differing densities, the following parameters are used: $\rho_s = 4\,\frac{\text{g}}{\text{cm}^3}, \mu_s = 3\,\frac{\text{dyne}}{\text{cm}^2}, \lambda = 4.5\,\frac{\text{dyne}}{\text{cm}^2}, \rho_f = 1\,\frac{\text{g}}{\text{cm}^3}$, and $\mu_f = .0013\,\frac{\text{g}}{\text{cm}\cdot\text{s}}$. This is referred to as parameter case A.

Tables 4.7 and 4.8 show the results of a convergence study. These convergence results are similar to those observed in FSI example 2. Specifically, for the conforming case in Table 4.7 for both variables, $\boldsymbol{\sigma}$ and $\boldsymbol{\omega}$, we see a convergence rate lower than the expected rate of 1.5. By the final refinement, for $\boldsymbol{\sigma}$ the observed convergence rate is approximately 0.67 and for $\boldsymbol{\omega}$ is approximately 0.34. When using the nonconforming element, for the displacement and velocity variable, we again observe convergence rate of 2.92 for the final refinement, despite the expected first order convergence. The convergence rate for the stress variable is close to the expected rate of 1.

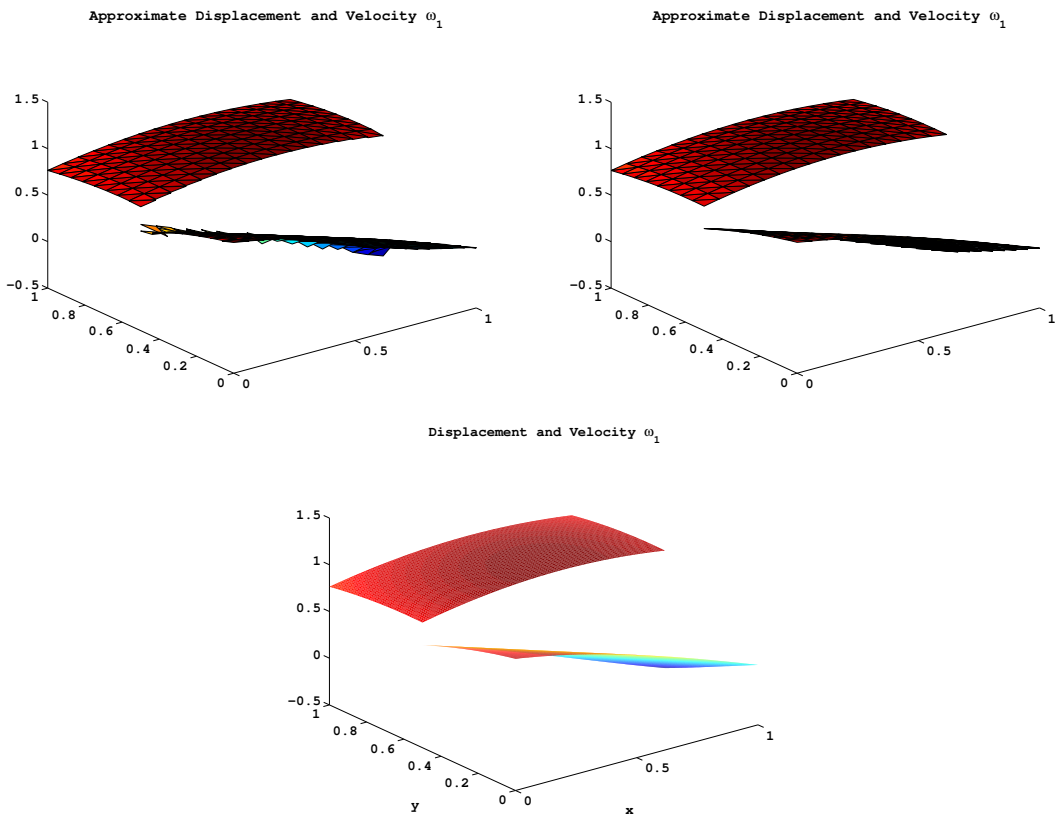

Figure 4.10: Solution graphs for the first component of displacement, $\boldsymbol{\omega}_1$ for the FSI example 2 at $T_f = 1$ with $h = \frac{1}{16}$ and $\Delta t = 1.25 \times 10^{-2}$: using the conforming element (left), using the nonconforming element (right), and the exact analytic solution (bottom).

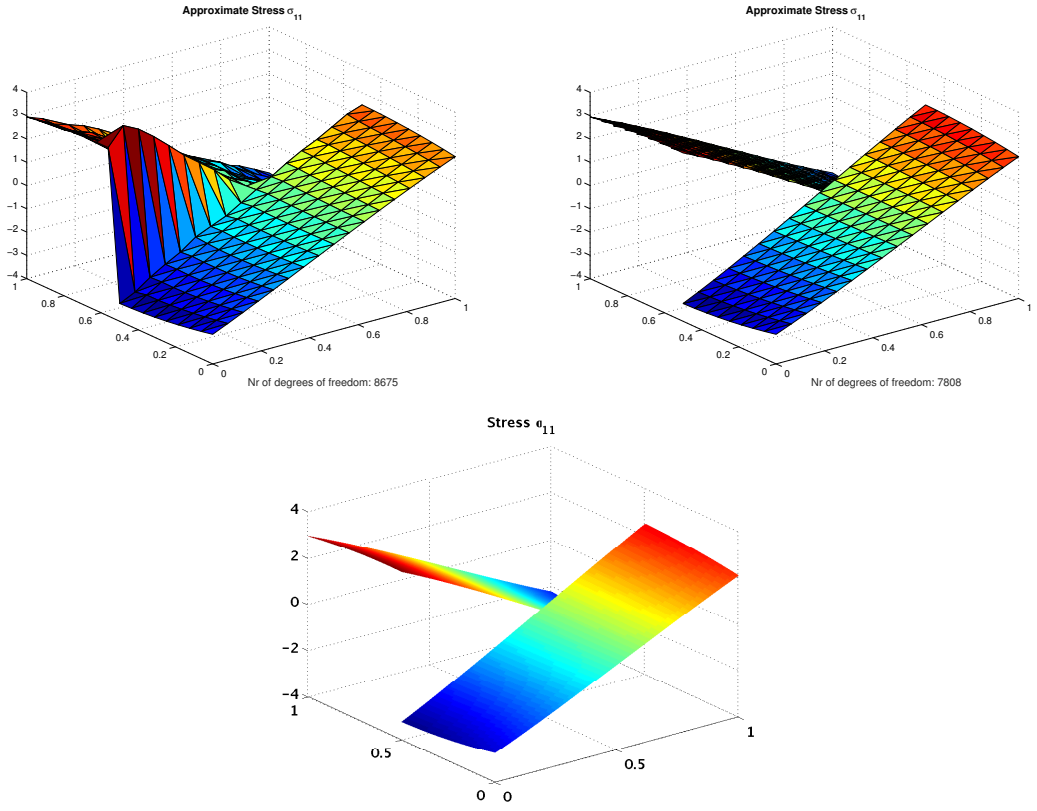

Figure 4.11: Solution graphs for the first component of stress, $\boldsymbol{\sigma}_{11}$ for the FSI example 2 at $T_f = 1$ with $h = \frac{1}{16}$ and $\Delta t = 1.25 \times 10^{-2}$: using the conforming element (left), using the nonconforming element (right), and the exact analytic solution (bottom).

Table 4.7: Convergence study results for FSI Example 3 parameter case A with the conforming element

h	Δt	$\|\boldsymbol{\omega} - \boldsymbol{\omega}_h\|_{L^\infty_{\Delta t}(\Omega)}$	Order	$\|\boldsymbol{\sigma} - \boldsymbol{\sigma}_h\|_{L^\infty_{\Delta t}(\Omega)}$	Order
$\frac{1}{2}$	1.000E-01	2.065E-01	—	1.348E+00	—
$\frac{1}{4}$	5.000E-02	4.392E-02	2.23	9.919E-01	0.44
$\frac{1}{8}$	2.500E-02	2.857E-02	0.62	7.065E-01	0.49
$\frac{1}{16}$	1.250E-02	1.849E-02	0.63	5.008E-01	0.50
$\frac{1}{32}$	6.250E-03	1.184E-02	0.64	3.855E-01	0.38
$\frac{1}{64}$	3.125E-03	7.453E-03	0.67	3.054E-01	0.34

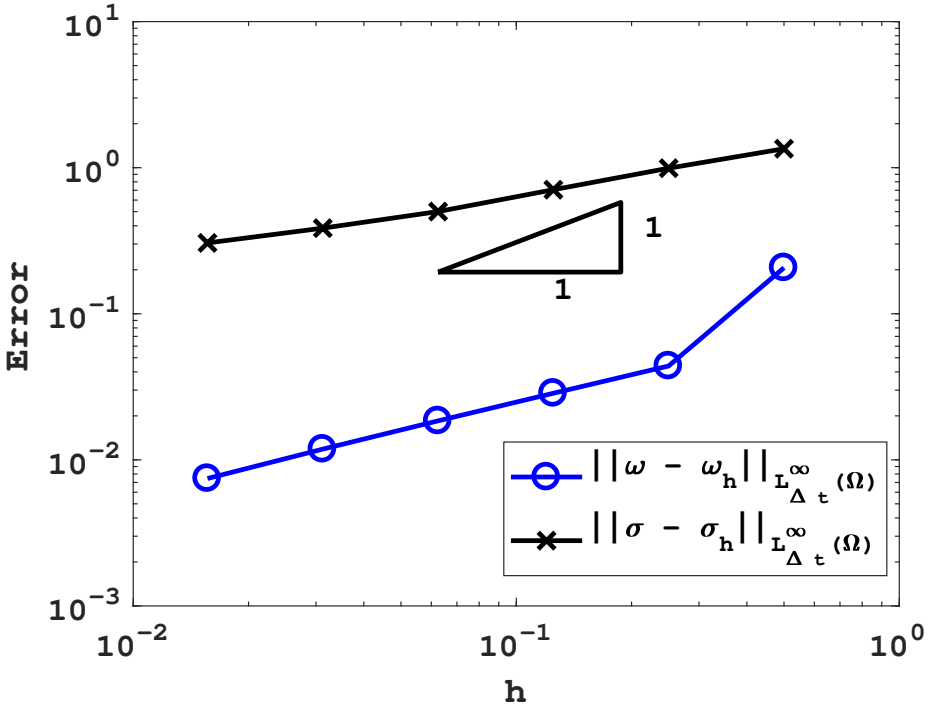

Figure 4.12: Graphical representation of the convergence study results for FSI Example 3 parameter case A with the conforming element

Table 4.8: Convergence study results for FSI Example 3 parameter case A with the nonconforming element

h	Δt	$\|\boldsymbol{\omega} - \boldsymbol{\omega}_h\|_{L^\infty_{\Delta t}(\Omega)}$	Order	$\|\boldsymbol{\sigma} - \boldsymbol{\sigma}_h\|_{L^\infty_{\Delta t}(\Omega)}$	Order
$\frac{1}{2}$	1.000E-01	3.086E-01	—	1.555E-01	—
$\frac{1}{4}$	5.000E-02	9.684E-02	1.67	6.299E-02	1.30
$\frac{1}{8}$	2.500E-02	3.108E-02	1.64	3.444E-02	0.87
$\frac{1}{16}$	1.250E-02	6.748E-03	2.20	2.082E-02	0.73
$\frac{1}{32}$	6.250E-03	1.014E-03	2.73	9.532E-03	1.13
$\frac{1}{64}$	3.125E-03	1.338E-04	2.92	4.727E-03	1.01

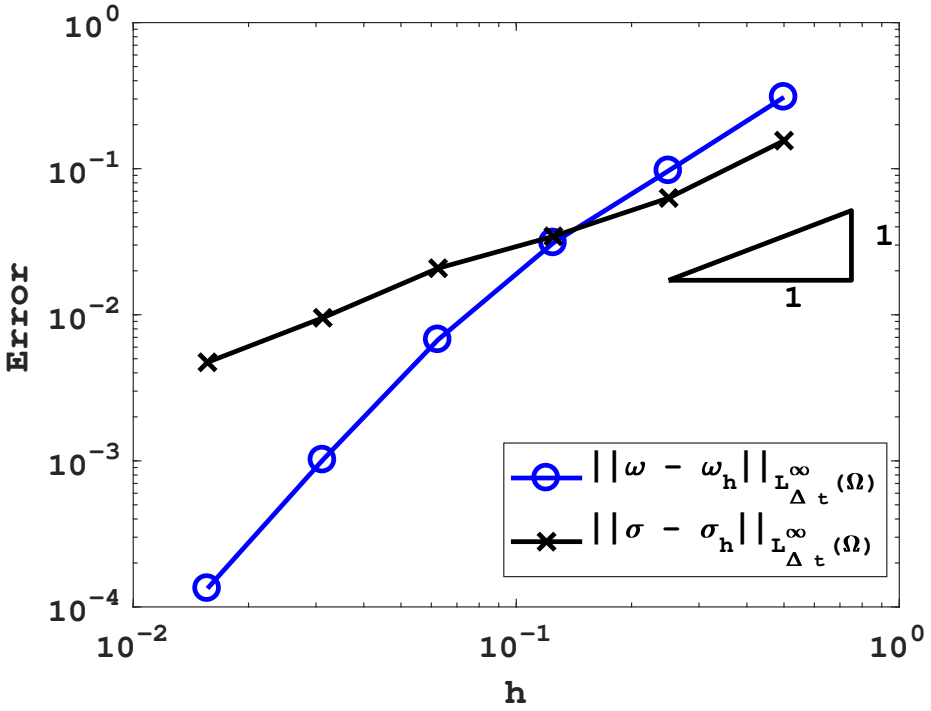

Figure 4.13: Graphical representation of the convergence study results for FSI Example 3 parameter case A with the nonconforming element

Finally, we set all parameters equal to 1. This provides a mathematical test despite not being physically realistic. Specifically, use: $\rho_s = 1, \mu_s = 1\, \lambda = 1$, $\rho_f = 1$, and $\mu_f = 1$. This is referred to a parameter case B.

Table 4.9 shows the result of a convergence study for parameter case B using the conforming elements. For both variables, $\boldsymbol{\sigma}$ and $\boldsymbol{\omega}$, we see again see convergence rates lower than the expect rate of 1.5. However the convergence rates are higher in this case. By the final refinement, the observed convergence rate for $\boldsymbol{\sigma}$ is approximately 1.02 and for $\boldsymbol{\omega}$ it is approximately 0.51. When using the nonconforming element, results are shown in 4.10, for the displacement and velocity variable, we observe a convergence rate of 1.89 for the final refinement, despite the expected first order convergence and the convergence rate for the stress variable is slightly under the expected rate of 1 at 0.95. We clearly see that the parameters effect convergence rates.

4.6 Conclusions and Future Work

In this dissertation, we have modeled the interaction between a linearly elastic solid and the time-dependent Stokes flow of a fluid. The model equations are expressed in terms of displacement and stress for the solid and velocity and stress for the fluid. Approximations for stress obtained using mixed finite element methods with these primary variables are more accurate than those obtained by using finite element methods and post processing. Although this these types of problems have been studied separately, to our knowledge, an FSI problem has not been studied using these models. Using these primary variables has the additional benefit that the conditions at the interface are in terms of the primary variables. We have developed a fully discrete model that does not explicitly include any interface integrals. The motivation for this has been discussed.

For the linear elasticity problem, we show an improved error estimate when using the nonconforming Arnold Winther element used with the elastostatic problem. Some numerical results are shown to confirm this error estimate. Some numerical results are show using

Table 4.9: Convergence study for FSI example 3 parameter case B with the conforming element

h	Δt	$\|\boldsymbol{\omega} - \boldsymbol{\omega}_h\|_{L^\infty_{\Delta t}(\Omega)}$	Order	$\|\boldsymbol{\sigma} - \boldsymbol{\sigma}_h\|_{L^\infty_{\Delta t}(\Omega)}$	Order
$\frac{1}{2}$	1.000E-01	2.419E-02	—	6.809E-01	—
$\frac{1}{4}$	5.000E-02	6.461E-03	1.90	4.288E-01	0.67
$\frac{1}{8}$	2.500E-02	2.527E-03	1.35	2.761E-01	0.64
$\frac{1}{16}$	1.250E-02	1.095E-03	1.21	1.875E-01	0.56
$\frac{1}{32}$	6.250E-03	5.393E-04	1.02	1.293E-01	0.54
$\frac{1}{64}$	3.125E-03	2.657E-04	1.02	9.071E-02	0.51

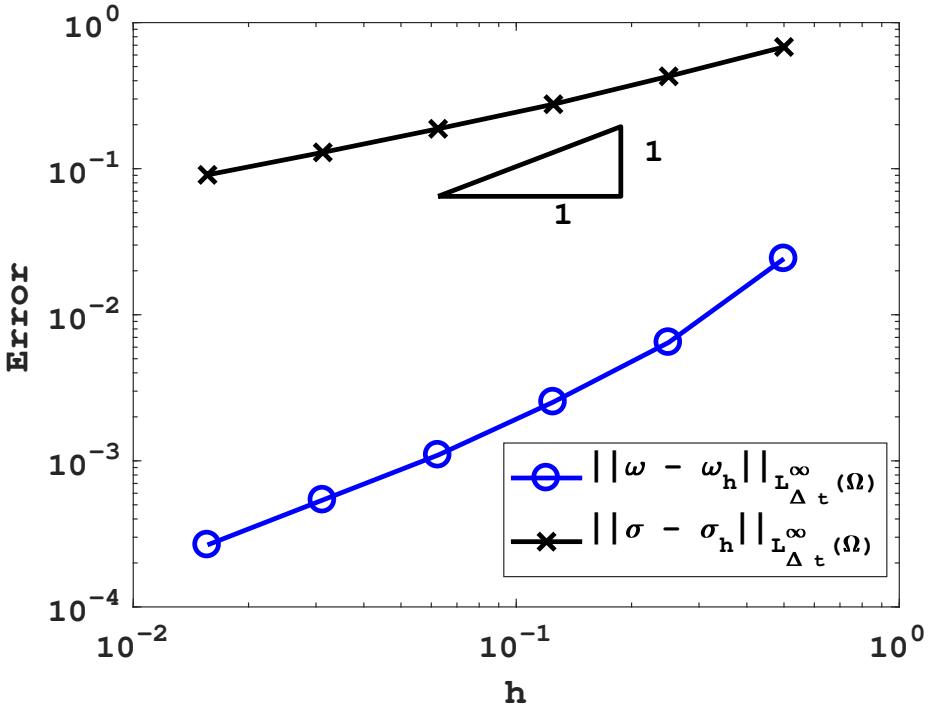

Figure 4.14: Graphical representation of the convergence study results for FSI Example 3 parameter case A with the conforming element

Table 4.10: Convergence study for FSI example 3 parameter case B with the nonconforming element

h	Δt	$\|\boldsymbol{\omega} - \boldsymbol{\omega}_h\|_{L^\infty_{\Delta t}(\Omega)}$	Order	$\|\boldsymbol{\sigma} - \boldsymbol{\sigma}_h\|_{L^\infty_{\Delta t}(\Omega)}$	Order
$\frac{1}{2}$	1.000E-01	1.303E-02	—	6.805E-02	—
$\frac{1}{4}$	5.000E-02	3.337E-03	1.97	3.399E-02	1.00
$\frac{1}{8}$	2.500E-02	8.544E-04	1.97	1.725E-02	0.98
$\frac{1}{16}$	1.250E-02	2.225E-04	1.94	8.967E-03	0.94
$\frac{1}{32}$	6.250E-03	5.798E-05	1.94	4.626E-03	0.95
$\frac{1}{64}$	3.125E-03	1.564E-05	1.89	2.400E-03	0.95

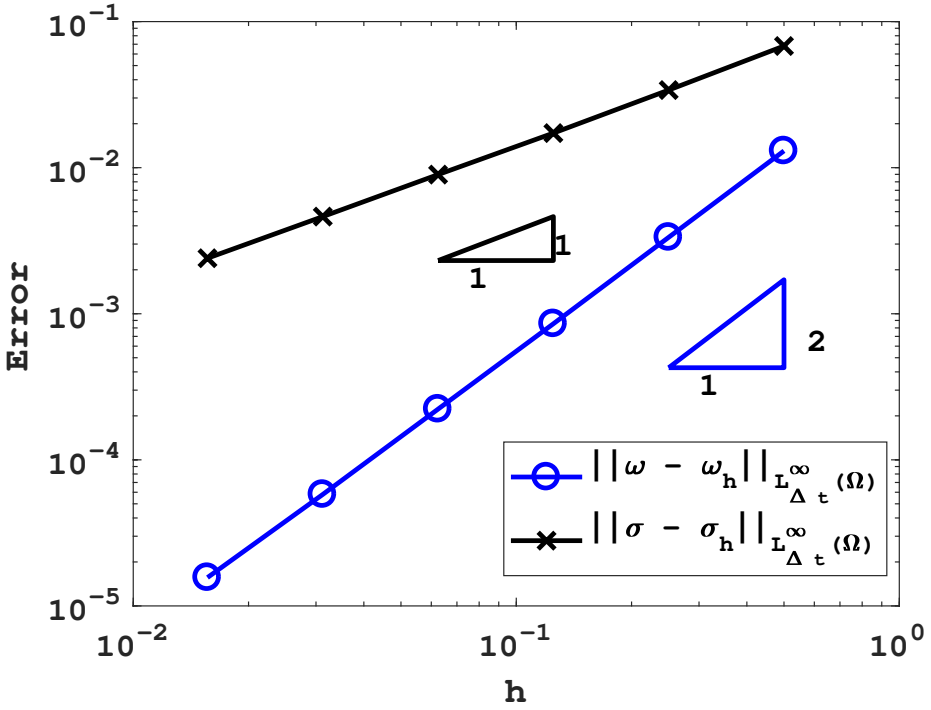

Figure 4.15: Graphical representation of the convergence study results for FSI Example 3 parameter case B with the nonconforming element

both the conforming and nonconforming Arnold Winther elements in both the static and dynamic cases.

For the Stokes fluid flow problem, when the model equations are expressed in terms of fluid stress and velocity, the same MFEMs are used to approximate the solution in the fluid domain and the solid domain. Although this has been studied in the static case [27], we extend to the nonstationary case. However, this requires careful treatment of the initial conditions to find an approximation to the fluid stress at the initial time. In this work, we have used a second finite element method to find an approximate fluid pressure at the initial time. As long as this pressure is found with enough accuracy, the stress at the initial time can be found with enough accuracy. However, it may be desirable to devote future work to finding an approximation to stress at the initial time step that does not require these complications.

The models for elasticity and fluid flow have then been combined to study the fluid-structure interaction problem. From the a priori analysis presented, we see that the presence of an interface is negatively impacting the expected error bounds. Depending on the specific mixed finite element method chosen, this impact may not be seen. For example, consider the nonconforming elements proposed by Arnold and Winther [7]. In this case, the consistency error associated with these elements limits the expected convergence rate more than the interface integral terms. Therefore, the convergence rate is not impacted by the interface. Numerical results showing this impact have been included and discussed in the previous section. However, to use a mixed finite element space where the consistency error does not limit the expected convergence rate more than the interface integral terms, it may be useful to impose the interface conditions differently or by adding stabilization terms. More work is required on this topic.

Furthermore, we have tested this numerical model using the conforming mixed finite element space proposed by Arnold and Winther [6]. Recall that when using this space, the approximation to stress is continuous at the mesh vertices, which is not required by the FSI model. We have observed a sub optimal convergence rate when attempting to

approximate a discontinuous stress. Although it is known that the continuity of stress at the mesh vertices is unavoidable, future work may be done to enforce the interface conditions differently. For example additional terms may be added to the model along the interface. This may improve convergence rates.

Alternatively, a partitioned method may be more suitable when using conforming mixed finite element spaces. When a partitioned method is used a separate mesh is used for the solid and fluid subdomains. Therefore the continuity of stress at the mesh vertices will not be enforced at the interface. However, different convergence issues will arise. Many partitioned methods have been proposed that may extend to the case where stress, displacement and velocity are primary variables. Further study is required on this topic.

Finally, in this dissertation, a fixed reference domain for both the fluid and solid subdomains has been used. Although this simplification is reasonable for some cases, more work is required to extend this model for use in general cases. This may be done by using the so called Arbitrary Lagrangian-Eulerian method. Then the interface will be allowed to move.

References

[1] M. Amara and J. M. Thomas. Equilibrium finite elements for the linear elastic problem. *Numer. Math.*, 33(4):367–383, 1979.

[2] D. N. Arnold and G. Awanou. Rectangular mixed finite elements for elasticity. *Math. Models Methods Appl. Sci.*, 15(9):1417–1429, 2005.

[3] D. N. Arnold, F. Brezzi, and J. Douglas, Jr. PEERS: a new mixed finite element for plane elasticity. *Japan J. Appl. Math.*, 1(2):347–367, 1984.

[4] D. N. Arnold, J. Douglas, Jr., and C. P. Gupta. A family of higher order mixed finite element methods for plane elasticity. *Numer. Math.*, 45(1):1–22, 1984.

[5] D. N. Arnold and R. S. Falk. Well-posedness of the fundamental boundary value problems for constrained anisotropic elastic materials. *Archive for Rational Mech. and Analysis*, 98(2):143–165, Jun 1987.

[6] D. N. Arnold and R. Winther. Mixed finite elements for elasticity. *Numer. Math.*, 92(3):401–419, 2002.

[7] D. N. Arnold and R. Winther. Mixed finite elements for elasticity in the stress-displacement formulation. In *Current trends in scientific computing (Xi'an, 2002)*, volume 329 of *Contemp. Math.*, pages 33–42. Amer. Math. Soc., Providence, RI, 2003.

[8] D. N. Arnold and R. Winther. Nonconforming mixed elements for elasticity. *Math. Models Methods Appl. Sci.*, 13(3):295–307, 2003. Dedicated to Jim Douglas, Jr. on the occasion of his 75th birthday.

[9] M. Astorino and C. Grandmont. Convergence analysis of a projection semi-implicit coupling scheme for fluid–structure interaction problems. *Numer. Math.*, 116(4):721–767, 2010.

[10] G. Awanou. A rotated nonconforming rectangular mixed element for elasticity. *Calcolo*, 46(1):49–60, 2009.

[11] L. Baffico and T. Sassi. Existence result for a fluid structure interaction problem with friction type slip boundary condition. *J. Appl. Math and Mech*, 95(8):831–844.

[12] J. W. Banks, W. D. Henshaw, and D. W Schwendeman. An analysis of a new stable partitioned algorithm for fsi problems. part i: Incompressible flow and elastic solids. *J. Comput. Phys.*, 269:108–137, 2014.

[13] J. R. Barber. *Elasticity.* Solid mechanics and its applications: v. 172. Dordrecht ; New York : Springer Verlag c2010., 2010.

[14] Y. Bazilevs, M.-C. Hsu, Y. Zhang, W. Wang, X. Liang, T. Kvamsdal, R. Brekken, and J. G. Isaksen. A fully-coupled fluid-structure interaction simulation of cerebral aneurysms. *Comput. Mech.*, 46(1):3–16, Jun 2010.

[15] R. Bhaskaran. Big ideas: Fluid dynamics. `https://confluence.cornell.edu/display/SIMULATION/Big+Ideas%3A+Fluid+Dynamics`, 2017. [Online; accessed 1-October-2018].

[16] F. J. Blom. A monolithical fluid-structure interaction algorithm applied to the piston problem. *Comput. Methods Appl. Mech. Engrg.*, 167(3-4):369–391, 1998.

[17] S. Brenner and L. Ridgway Scott. *The mathematical theory of finite element methods*, volume 15. Springer Science & Business Media, 2007.

[18] F. Brezzi. On the existence, uniqueness and approximation of saddle-point problems arising from Lagrangian multipliers. *Rev. Française Automat. Informat. Recherche Opérationnelle Sér. Rouge*, 8(R-2):129–151, 1974.

[19] F. Brezzi and M. Fortin. *Mixed and hybrid finite element methods.* Springer, 1991.

[20] M. Bukac, I. Yotov, R. Zakerzadeh, and P. Zunino. *Effects of Poroelasticity on Fluid-Structure Interaction in Arteries: a Computational Sensitivity Study*, pages 197–220. Springer International Publishing, Cham, 2015.

[21] M. Bukac, I. Yotov, R. Zakerzadeh, and P. Zunino. Partitioning strategies for the interaction of a fluid with a poroelastic material based on a Nitsche's coupling approach. *Comput. Methods Appl. Mech. Engrg.*, 292:138–170, 2015.

[22] H.-J. Bungartz and M.l Schäfer. *Fluid-structure interaction: modelling, simulation, optimisation*, volume 53. Springer Science & Business Media, 2006.

[23] E. Burman and M. A. Fernández. Stabilization of explicit coupling in fluid-structure interaction involving fluid incompressibility. *Comput. Methods Appl. Mech. Engrg.*, 198(5-8):766–784, 2009.

[24] Gedicke D. Günther D. Reininhaus J. Byfut, A. and S. Wiedemann. *F_FW Documentation.*

[25] Z. Cai and X. Ye. A mixed nonconforming finite element for linear elasticity. *Numer. Methods Partial Differential Equations*, 21(6):1043–1051, 2005.

[26] C. Carstensen, M. Eigel, and J. Gedicke. Computational competition of symmetric mixed FEM in linear elasticity. *Comput. Methods Appl. Mech. Engrg.*, 200(41-44):2903–2915, 2011.

[27] C. Carstensen, J. Gedicke, and E.-J. Park. Numerical experiments for the Arnold-Winther mixed finite elements for the Stokes problem. *SIAM J. Sci. Comput.*, 34(4):A2267–A2287, 2012.

[28] C. Carstensen, D. Günther, J. Reininghaus, and J. Thiele. The Arnold-Winther mixed FEM in linear elasticity. I. Implementation and numerical verification. *Comput. Methods Appl. Mech. Engrg.*, 197(33-40):3014–3023, 2008.

[29] L. Cattabriga. Su un problema al contorno relativo al sistema di equazioni di stokes. *Rendiconti del Seminario Matematico della Università di Padova*, 31:308–340, 1961.

[30] P. Causin, J.F. Gerbeau, and F. Nobile. Added-mass effect in the design of partitioned algorithms for fluidstructure problems. *Comput. Methods Appl. Mech. Engrg.*, 194(42):4506 – 4527, 2005.

[31] K. Chen. *Matrix Preconditioning Techniques and Applications*. Number 19. Cambridge University Press, 2005.

[32] S.-C. Chen and Y.-N. Wang. Conforming rectangular mixed finite elements for elasticity. *J. Sci. Comput.*, 47(1):93–108, 2011.

[33] B. Cockburn, J. Gopalakrishnan, and J. Guzmán. A new elasticity element made for enforcing weak stress symmetry. *Math. Comp.*, 79(271):1331–1349, 2010.

[34] A. Constantinescu and A. Korsunsky. *Elasticity with Mathematica : an introduction to continuum mechanics and linear elasticity.* Cambridge : New York : Cambridge University Press, 2007., 2007.

[35] L. C. Cowsar, T. F. Dupont, and M. F. Wheeler. A priori estimates for mixed finite element approximations of second-order hyperbolic equations with absorbing boundary conditions. *SIAM J. Numer. Anal.*, 33(2):492–504, 1996.

[36] J. Douglas, Jr. and C. P. Gupta. Superconvergence and interior estimates for a mixed finite element method for elastic waves in a planar domain. *Mat. Apl. Comput.*, 7(2):75–99, 1988.

[37] K. Dumont, J. Vierendeels, R. Kaminsky, G. Van Nooten, P.l Verdonck, and D. Bluestein. Comparison of the hemodynamic and thrombogenic performance of two bileaflet mechanical heart valves using a cfd/fsi model.

[38] T. Dupont. L^2-estimates for Galerkin methods for second order hyperbolic equations. *SIAM J. Numer. Anal.*, 10:880–889, 1973.

[39] Z. M. Fairuz, M. Z. Abdullah, H. Yusoff, and M. K. Abdullah. Fluid structure interaction of unsteady aerodynamics of flapping wing at low reynolds number. *Eng. Appl. of Comput. Fluid Mech.*, 7(1):144–158, 2013.

[40] R. S. Falk. Nonconforming finite element methods for the equations of linear elasticity. *Math. Comp.*, 57(196):529–550, 1991.

[41] C. Farhat, K. G. van der Zee, and P. Geuzaine. Provably second-order time-accurate loosely-coupled solution algorithms for transient nonlinear computational aeroelasticity. *Comput. Methods Appl. Mech. Engrg.*, 195(17-18):1973–2001, 2006.

[42] M. A Fernández and J.-F. Gerbeau. Algorithms for fluid-structure interaction problems. In *Cardiovascular mathematics*, pages 307–346. Springer, 2009.

[43] L. Formaggia, K. Perktold, and A. Quarteroni. *Basic mathematical models and motivations*, pages 47–75. Springer Milan, Milano, 2009.

[44] C. Förster, W. A. Wall, and E. Ramm. Artificial added mass instabilities in sequential staggered coupling of nonlinear structures and incompressible viscous flows. *Comput. Methods Appl. Mech. Engrg.*, 196(7):1278–1293, 2007.

[45] V. Girault and P. A. Raviart. Finite element approximation of the navier-stokes equations, vol. 749 of lecture notes in mathematics. *Springer-Verlag, Berlin*, 4:12, 1979.

[46] M. S Gockenbach. *Understanding and implementing the finite element method*, volume 97. Siam, 2006.

[47] J. Gopalakrishnan and J. Guzmán. Symmetric nonconforming mixed finite elements for linear elasticity. *SIAM J. Numer. Anal.*, 49(4):1504–1520, 2011.

[48] J. Guzmán. A unified analysis of several mixed methods for elasticity with weak stress symmetry. *J. Sci. Comput.*, 44(2):156–169, 2010.

[49] S. Hamdi, W. E. Schiesser, and G. W Griffiths. Method of lines. *Scholarpedia*, 2(7):2859, 2007. revision #124335.

[50] Edward J Haug. *Intermediate dynamics*. Prentice Hall, 1992.

[51] Y. He. Two-level method based on finite element and Crank-Nicolson extrapolation for the time-dependent Navier-Stokes equations. *SIAM J. Numer. Anal.*, 41(4):1263–1285, 2003.

[52] Y. He and W. Sun. Stability and convergence of the Crank-Nicolson/Adams-Bashforth scheme for the time-dependent Navier-Stokes equations. *SIAM J. Numer. Anal.*, 45(2):837–869, 2007.

[53] E. Hellinger. Die allgemeinen ansätze der mechanik der kontinua. enc. d. math. *Encyklopädie der mathematischen Wissenschaften*, 30:602–694, 1914.

[54] J. G. Heywood and R. Rannacher. Finite element approximation of the nonstationary Navier-Stokes problem. I. Regularity of solutions and second-order error estimates for spatial discretization. *SIAM J. Numer. Anal.*, 19(2):275–311, 1982.

[55] J. G. Heywood and R. Rannacher. Finite-element approximation of the nonstationary Navier-Stokes problem. IV. Error analysis for second-order time discretization. *SIAM J. Numer. Anal.*, 27(2):353–384, 1990.

[56] G. Hou, J. Wang, and A. Layton. Numerical methods for fluid-structure interaction—a review. *Commun. Comput. Phys.*, 12(2):337–377, 2012.

[57] J. Hron and M. Mádlí k. Fluid-structure interaction with applications in biomechanics. *Nonlinear Anal. Real World Appl.*, 8(5):1431–1458, 2007.

[58] J. Hu and Z. Shi. Lower order rectangular nonconforming mixed finite elements for plane elasticity. *SIAM J. Numer. Anal.*, 46(1):88–102, 2008.

[59] P. Huang, X. Feng, and D. Liu. A stabilized finite element method for the time-dependent Stokes equations based on Crank-Nicolson scheme. *Appl. Math. Model.*, 37(4):1910–1919, 2013.

[60] A. Jain, N. P. Jones, and Scanian R. H. Coupled flutter and buffeting analysis of long-span bridges. *J. of Struct. Eng.*, 122(7):716–725, 1996.

[61] E. W. Jenkins, B. Rivière, and M. F. Wheeler. A priori error estimates for mixed finite element approximations of the acoustic wave equation. *SIAM J. Numer. Anal.*, 40(5):1698–1715, 2002.

[62] C. Johnson and B. Mercier. Some equilibrium finite element methods for two-dimensional problems in continuum mechanics. In *Energy methods in finite element analysis*, pages 213–224. Wiley, Chichester, 1979.

[63] H. Johnston and J.-G. Liu. Accurate, stable and efficient navierstokes solvers based on explicit treatment of the pressure term. *J. Comput. Phys.*, 199(1):221 – 259, 2004.

[64] S. Karaa. Finite element θ-schemes for the acoustic wave equation. *Adv. Appl. Math. Mech.*, 3(2):181–203, 2011.

[65] F. C. Karal and S. N. Karp. The elastic-field behavior in the neighborhood of a crack of arbitrary angle. *Communications on Pure and Applied Mathematics*, 15(4):413–421, 1962.

[66] P. A. Kelly. Mechanics lecture notes: An introduction to solid mechanics. `http://homepages.engineering.auckland.ac.nz/~pkel015/SolidMechanicsBooks/Part_I/`, 2015. [Online; accessed 1-October-2018].

[67] P. Kuberry and H. Lee. A decoupling algorithm for fluid-structure interaction problems based on optimization. *Comput. Methods Appl. Mech. Engrg.*, 267:594–605, 2013.

[68] V. Kumar and V. Udoewa. Fluid-structure interaction techniques for parachute. In *Fluid Dynamics, Computational Modeling and Applications*. InTech, 2012.

[69] J. Lee. *Mixed methods with weak symmetry for time dependent problems of elasticity and viscoelasticity*. University of Minnesota, 2012.

[70] C. LeRoux and A. Tani. Steady solutions of the navierstokes equations with threshold slip boundary conditions. *Math Methods Appl. Sci.*, 30(5):595–624.

[71] J. Li and Y. T. Chen. *Computational partial differential equations using MATLAB*, volume 17. Chapman & Hall/CRC, 2008.

[72] C. G. Makridakis. On mixed finite element methods for linear elastodynamics. *Numer. Math.*, 61(2):235–260, 1992.

[73] C. Michler, S. J. Hulshoff, and R. van Brummelen, E. H.and de Borst. A monolithic approach to fluidstructure interaction. *Computers & Fluids*, 33(5):839 – 848, 2004. Applied Mathematics for Industrial Flow Problems.

[74] P. J Mucha, S.-Y. Tee, D. A. Weitz, B. I. Shraiman, and M. P. Brenner. A model for velocity fluctuations in sedimentation. *J. of Fluid Mech.*, 501:71–104, 2004.

[75] MIT Department of Ocean Engineering. Marine hydrodynamics : Lecture 4. `http://web.mit.edu/fluids-modules/www/potential_flows/LecturesHTML/lec04/lecture4.html`, 2003. [Online; accessed 1-October-2018].

[76] Washington Department of Public Safety. Tacoma Narrows bridge : "Galloping Gertie" collapses november 7, 1940. `http://www.wsdot.wa.gov/tnbhistory/connections/connections3.htm`, 2005. [Online; accessed 1-October-2018].

[77] A. Quaini. Algorithms for fluid-structure interaction problems arising in hemodynamics. page 207, 2009.

[78] P.-A. Raviart and J.-M. Thomas. A mixed finite element method for 2-nd order elliptic problems. In *Mathematical aspects of finite element methods*, pages 292–315. Springer, 1977.

[79] S. Rugonyi and K. J. Bathe. On finite element analysis of fluid flows fully coupled with structural interactions. *CMES- Computer Modeling in Engineering and Sciences*, 2(2):195–212, 2001.

[80] M. H. Sadd. *Elasticity : Theory, Applications, and Numerics.* Burlington : Elsevier, 2009., 2009.

[81] R. L. Sani, J. Shen, O. Pironneau, and P. M. Gresho. Pressure boundary condition for the time-dependent incompressible Navier-Stokes equations. *Internat. J. Numer. Methods Fluids*, 50(6):673–682, 2006.

[82] W. E Schiesser. *The numerical method of lines: integration of partial differential equations.* Elsevier, 2012.

[83] J. Schöberl and A. Sinwel. Tangential-displacement and normal-normal-stress continuous mixed finite elements for elasticity. *Ricam Report*, 10, 2007.

[84] I. H. Shames and F. A. Cozzarelli. *Elastic and Inelastic Stress Analysis.* Prentic Hall, 1992.

[85] R. Stenberg. A family of mixed finite elements for the elasticity problem. *Numer. Math.*, 53(5):513–538, 1988.

[86] The University of Texas at Austin Texas Advanced Computing Center (TACC).

[87] Inc. The MathWorks. Generalized minimum residual method. `https://www.mathworks.com/help/matlab/ref/gmres.htmll`, 1994-2018. [Online; accessed 3-December-2018].

[88] Inc. The MathWorks. Incomplete lu factorization. `https://www.mathworks.com/help/matlab/ref/ilu.html`, 1994-2018. [Online; accessed 3-December-2018].

[89] F. Tone. Error analysis for a second order scheme for the Navier-Stokes equations. *Appl. Numer. Math.*, 50(1):93–119, 2004.

[90] A.-K. Tornberg and M. J. Shelley. Simulating the dynamics and interactions of flexible fibers in stokes flows. *J. Comput. Phys.*, 196(1):8–40, 2004.

[91] T. Valent. *Boundary value problems of finite elasticity.* Springer-Verlag, New York, 1988.

[92] R. Van Loon, P. D. Anderson, F. N. Van de Vosse, and S. J. Sherwin. Comparison of various fluid–structure interaction methods for deformable bodies. *Computers & structures*, 85(11-14):833–843, 2007.

[93] Z. Weng, X. Feng, and P. Huang. A new mixed finite element method based on the Crank-Nicolson scheme for the parabolic problems. *Appl. Math. Model.*, 36(10):5068–5079, 2012.

[94] G. D. Weymouth, D. G. Dommermuth, K. Hendrickson, and D. K.-P. Yue. Advancements in cartesian-grid methods for computational ship hydrodynamics. *26th Symposium on Naval Hydrodynamics, Rome, Italy, 17-22 September 2006.*

[95] T. Wick. Solving monolithic fluid-structure interaction problems in arbitrary lagrangian eulerian coordinates with the deal. ii library. 2011.

[96] M. L. Williams. Stress singularities resulting from various boundary conditions in angular corners of plates in extension. *J. Appl. Mech.*, 19(4):526–528, 1952.

[97] J. N. Yang, A. K. Agrawal, B. Samali, and J.-C. Wu. Benchmark problem for response control of wind-excited tall buildings. *J. of Eng. Mech.*, 130(4):437–446, 2004.

[98] S.-Y. Yi. Nonconforming mixed finite element methods for linear elasticity using rectangular elements in two and three dimensions. *Calcolo*, 42(2):115–133, 2005.

[99] S.-Y. Yi. A new nonconforming mixed finite element method for linear elasticity. *Math. Models Methods Appl. Sci.*, 16(07):979–999, 2006.

[100] S.-Y. Yi and M. L. Bean. Iteratively coupled solution strategies for a four-field mixed finite element method for poroelasticity. *Inter. J. Numer. Anal. Methods in Geomech.*, 41(2):159–179, FEB 10 2017.

[101] O. C. Zienkiewicz. Displacement and equilibrium models in the finite element method by B. Fraeijs de Veubeke, Chapter 9, pages $145-197$ of Stress Analysis, edited by O. C. Zienkiewicz and G. S. Holister, published by John Wiley & Sons, 1965. *Internat. J. Numer. Methods Engrg.*, 52(3):287–342, 2001.

Curriculum Vita

Maranda Lee Bean is a Doctoral Candidate in the Computational Science program at The University of Texas at El Paso (UTEP). In the spring of 2007, she earned a Bachelor of Science degree in Physics from The New Mexico Institute of Mining and Technology. After spending several years working as an online tutor. She entered Graduate School at UTEP, in the fall of 2010. She became a teaching assistant for the Mathematics department in January of 2011. In the fall of 2012, she earned a Master of Science degree in Mathematics. Then in the Spring of 2013, she entered the Computational Science PhD program at UTEP as a research assistant supported a National Science Foundation Grant (DMS 1217123). She earned a Master of Science degree in Computational Science from UTEP in 2014.

With her mentor, Dr. Son-Young Yi, she published An Immersed Interface Method for a 1D Poroelasticity Problem with Discontinuous Coefficients in the Journal of Computational and Applied Mathematics in 2014. In 2017, the pair published Iteratively Coupled Solution Strategies for a Four-Field Mixed Finite Element Method for Poroelasticity in the International Journal for Numerical and Analytical Methods in Geomechanics. Also in 2017, she published A Block Preconditioner for a Four-Field Mixed Finite Element Method for Biot's Equations in Applied Numerical Mathematics, with Drs. Yi and Lipnikov.

Contact Email: mlbean@miners.utep.edu